# COMPUTATIONAL AND ANALYTICAL STUDIES OF LIQUID DYNAMICS IN WEIGHTLESSNESS

**Wei Yan**

A Thesis

in

The Department

of

Mechanical Engineering

Presented in Partial Fulfillment of the Requirements

for the Degree of Doctor of Philosophy at

Concordia University

Montreal, Quebec, Canada

November 1995

National Library
of Canada

Acquisitions and
Bibliographic Services Branch

395 Wellington Street
Ottawa, Ontario
K1A 0N4

Bibliothèque nationale
du Canada

Direction des acquisitions et
des services bibliographiques

395, rue Wellington
Ottawa (Ontario)
K1A 0N4

Your file Votre référence

Our file Notre référence



ISBN 0-612-10916-X

Canada

# ABSTRACT

## Computational and Analytical Studies of Liquid Dynamics in Weightlessness

**Wei Yan, Ph.D.**

**Concordia University, 1995**

Computational and analytical studies with respect to liquid dynamics in a liquid-vapor-solid system in weightlessness are presented. Computational simulations are used to describe the dynamic behavior of liquid motion during the transition from terrestrial gravitation (1-g) to zero-gravity (0-g) and liquid draining in a spacecraft in rectangular and cylindrical tanks. The use of approximate solutions to solve complicated equations for a time-dependent transient, incompressible free surface flow where the surface tension forces are dominant, provides accurate physical information and reduces the number of experiments performed in space. Moreover, it overcomes the difficulty arising from very limited periods of microgravity time by Earthbound experiments.

The numerical results show that the time required for the liquid-vapor interface to reach 0-g equilibrium configuration increases with the decrease of the viscous forces, however, during outflow, the liquid-vapor interface can be greatly influenced by the outflow velocity and outlet location. Liquid residuals are affected by fluid properties, geometry of the tank and other physical parameters. They are found to be a function of the Weber number, the initial

liquid height and the contact angle where tank geometry and draining start time are initially defined. The liquid residuals vary with draining start time. The outlet location from the center to the edge of the tank decreases the liquid residuals. The corner location of outlet can be considered as a potential method of reducing or even eliminating liquid residuals. The liquid-vapor interface configuration at the zero-gravity equilibrium state is also predicted.

Analytical results show conclusively that the liquid-vapor interface configuration under 0-g condition is dependent on tank geometry, initial liquid height and contact angle. The critical, minimum and maximum heights can be used to determine a configuration. Hysteresis phenomena are presented during draining and filling of a liquid through an infinitesimal slow process. The configuration during draining may be different from the one during filling while other physical parameters are held constant. The computational and analytical results compare favorably to the published data. The results can be used for guidance and aid to design liquid management systems.

# ACKNOWLEDGEMENTS

My sincerest gratitude goes out to my thesis advisor, Dr. G.H. Vatistas for his help, guidance and encouragement.

I wish to thank the Quebec government and Concordia University for FCAR Fellowship and the Graduate Fellowship, respectively. I also wish to thank the Canadian and Quebec governments for the financial support through NSERC and FCAR grants to Dr. G.H. Vatistas and Dr. T.S. Sankar, respectively.

The thesis could not have been created without the encouragement from my parents, Xu Shi Yan and Liu Qin Zhuang. I wish to extend my thanks to my friends. I would like to thank my wife, Xiu Tao Zhang for her support, patience and understanding.

# TABLE OF CONTENTS

# LIST OF FIGURES

# NOMENCLATURE

| | |
|---|---|
| $A$ | surface area |
| a | constant |
| b | constant |
| c | constant |
| D | discrepancy of a cell |
| $D_o$ | width or diameter of outlet |
| d | constant |
| E | energy |
| $E_i$ | energy in configurations i, i = 1 or 2 |
| $\Delta E$ | energy difference between configuration 1 and 2 |
| F | function of the fractional volume of fluid |
| $F_m$ | force |
| $f_n$ | function symbol |
| $G_x$ | body acceleration at x-direction |
| $G_y$ | body acceleration at y-direction |
| g | the universal constant of the terrestrial gravity in y-direction |
| H | height of a tank |
| $H_l$ | liquid height at the central line under 1-g gravity |
| $H_{lcr}$ | critical liquid height at the central line under 1-g gravity |
| $H_{lmin}$ | minimum liquid height at the central line under 1-g gravity |
| $H_{lmax}$ | maximum liquid height at the central line under 1-g gravity |
| $H_a$ | liquid wetting length on a side of a tank wall |

| | |
|---|---|
| $H_c$ | liquid depth which is the interface height from the bottom of a tank at the central line under 0-g gravity |
| $H_{c,max}$ | maximum liquid depth at the central line under 0-g gravity |
| $H_I$ | initial liquid height |
| $\Delta H$ | liquid height distance between lower plane and higher plane |
| $\vec{i}$ | unit vector |
| $\vec{j}$ | unit vector |
| K | curvature |
| k | parameter of interface |
| L | half width or radius of a tank |
| $L_o$ | length of outlet |
| l | tube length |
| m | constant |
| n | constant |
| p | pressure |
| $p_l$ | pressure in the phase on concave side of liquid-vapor interface |
| $P_n$ | pressure inside the fluid |
| $P_s$ | surface pressure |
| $p_v$ | pressure in the phase on convex side of liquid-vapor interface |
| $\Delta p$ | pressure change |
| $\vec{q}$ | velocity vector |
| R | radius of curvature of a spherical surface |
| $R_1$ | principal radius of curvature in x-y plane |
| $R_2$ | principal radius of curvature in azimuthal direction |
| $R_d$ | distance between tank center and outlet center |
| Re | Reynolds number |
| $R_o$ | half width or radius of the outlet pipe |

| | |
|---|---|
| $R_t$ | radius of a tube |
| $r$ | radial coordinate |
| $r_1$ | principal radius of curvature |
| $r_2$ | principal radius of curvature |
| $\vec{r}$ | fixed points in space |
| $t$ | time |
| $t_d$ | draining time |
| $t_o$ | characteristic time |
| $t_s$ | draining starting time |
| $t_{0.1}$ | time required for the liquid-vapor interface oscillations to decay to 0.1% of their original amplitude |
| $\Delta t$ | time increment |
| $u$ | velocity component in x-direction or r-direction |
| $u_{av}$ | average velocity |
| $V_m$ | volume |
| $V_I$ | initial liquid volume |
| $V_R$ | liquid residual volume |
| $v$ | velocity component in y-direction or z-direction |
| $v_c$ | characteristic velocity |
| $v_o$ | outlet velocity |
| $v_t$ | mean outflow velocity of a tank |
| $We$ | Weber number |
| $w$ | work |
| $X(y)$ | liquid-vapor interface function of y |
| $x$ | coordinate in the horizontal direction |
| $x_2$ | distance parameter in configuration 2 |
| $\Delta x$ | cell width |

| | |
|---|---|
| $Y(x)$ | liquid-vapor interface function of x |
| $y$ | coordinate in the vertical direction |
| $\Delta y$ | cell height |
| $z$ | axial coordinate |

Greek Letters

| | |
|---|---|
| $\alpha$ | contact angle |
| $\alpha_d$ | dynamic contact angle |
| $\beta$ | angle |
| $\delta$ | distance of the vertex at the central line at 0-g from the original level at 1-g |
| $\varepsilon$ | coordinate index, $\varepsilon = 0$ or 1 for Cartesian or cylindrical coordinate, respectively |
| $\zeta$ | distance parameter |
| $\eta$ | distance parameter |
| $\eta_2$ | function of angle |
| $\lambda$ | small number |
| $\mu$ | viscosity |
| $\nu$ | kinematic viscosity |
| $\xi$ | distance parameter |
| $\xi_1$ | distance parameter |
| $\pi_2$ | dimensionless parameter |
| $\rho$ | density of liquid |
| $\sigma$ | surface tension |
| $\tau$ | interface formation time, equal to $t_{0\,1}/t_o$ |

| | |
|---|---|
| $\varphi$ | angle parameter |
| $\psi$ | coefficient of donor-cell or centered-difference approximations |
| $\Omega$ | vapor-liquid-solid contact line |
| $\omega$ | over-relaxation factor |

Superscripts

| | |
|---|---|
| – | dimensionless |
| n+1 | a quantity evaluated at time $(n+1)\Delta t$ |

Subscripts

| | |
|---|---|
| i | number of cell in x-direction |
| j | number of cell in y-direction |
| l | liquid |
| v | vapor |
| lv | liquid-vapor interface |
| vs | vapor-solid interface |
| ls | liquid-solid interface |
| 1 | configuration 1 |
| 2 | configuration 2 |

# CHAPTER 1

# INTRODUCTION

## 1.1 Background

The dynamic behavior and static conditions of liquids in spacecrafts is a subject that has attracted the serious attention of researchers in the past decade. Since the operation of the space shuttle, the microgravity research has rapidly expanded into many fundamental areas of science and technology. The International Space Station will soon become operational, utilizing a permanently manned, multi-facility microgravity laboratory in low-Earth orbit to provide a long-lasting, stable microgravity environment. The need to handle large quantities of liquids to be used for propulsion and life support have intensified research activities in microgravity fluid science. For instance the fluid dynamics and transport phenomena was one of the six disciplines included in the Microgravity Science and Application program of the National Aeronautics and Space Administration, U.S.A. (Crouch et al, 1991; Halpern, 1986). The EEC countries, Russia, China and Japan have similar research and application programs (Seibert, 1993; Walter, 1992; Ishida, 92; Avduyevsky, 1991; Rath, 1992; Davis, 1987). The Canadian Space Agency has supported microgravity research projects related to fluid physics since 1986 (Saghir et al, 1991).

The management of large amount of liquids is required for various activities (Gluck et al, 1965; Otto, 1966; Ostrach, 1982). When all the external forces are removed, fluid mass undergoes a dynamic transition with the aim to establish a new equilibrium state. The forces generated, during and after the dynamic phase, might affect dramatically all liquid management systems and in extreme cases the stability and control of a spacecraft.

The current available constitutive correlations developed for applications on Earth are inadequate in zero-gravity, consequently, there is need for analyzing fluid flow in zero-gravity. The present study solves the problems associated with fluid dynamic behavior in spacecrafts while exposed to weightlessness.

## 1.2 Liquid Problems in Weightlessness

Liquid transportation and storage in a spacecraft are essential requirement as liquid propellant, water and other types of liquids stored in experiments and industrial processes are widely used. It is particularly important for deployment and docking of orbit transfer vehicles with large quantities of liquids in the near future. Research and engineering in the management of liquids, such as water in space cabins, is an important part in sending humans to outer space. A human being must be supplied with an environment similar to the one that is accustomed on Earth. Thus, a moderately comfortable environment suitable for the existence and function of space crews must be provided. The liquid management systems which are able to operate at zero-gravity condition can be adopted for manned

spacecrafts and space platform station. Equipment design for space missions must conform to the most efficient liquid management systems.

There are many problems related to liquid behavior under low-gravity conditions. A typical example can be found in a propellant tank of a spacecraft. Liquid propellant rocket engines are used for boost and auxiliary propulsion. They are also used for space rendezvous, docking maneuvers and instrument orientation. The liquid fuel, oxidizer and other chemical compounds are consumed in the rocket engines. A supply of a vapor-free propellant in sufficient quantity is the basic prerequisite of any liquid transfer system for storable propellants to assure proper engine operation. The requirements of advanced spacecraft missions have created new challenges for the designer of propellant-transfer systems. The motions of spacecrafts during weightless phases of the coast mission may cause part or all of the propellant in the tank-outlet region to be displaced by vapor. The oscillations of spacecrafts in flight may cause sloshing of propellant which can also uncover the tank outlet. If vapor or a mixture of vapor and liquid reaches the engine through the tank outlet pipe, it can adversely change propellant flow rates and mixture ratios and cause combustion instability and thrust degradation.

A sudden thrust reversal on a spacecraft during maneuvering or docking in a low-gravity environment and thrust termination in the atmosphere may produce an alteration of liquid in tanks. Thus high forces can be imposed on the tanks and thus on the vehicle by sloshing motions of the liquid and by sudden changes in position of liquid mass in a partly

emptied tank. The forces may cause structural damage, and will result in concomitant attitude-control difficulties and flight instability.

The efficiency of liquid expulsion of a tank is another important factor to be considered. Liquid tanks can be difficult to empty through forced outflow during low-gravity flight. The residual liquid remaining in the tank, such as the propellant, is not available for combustion and must be treated as an inert mass, causing the effective vehicle mass ratio to decrease. An effort must be made to minimize the liquid residuals in the design of tanks. Although the liquid and vapor could be positioned by means of acceleration fields such as accelerating or spinning the tank, these methods may require considerably high energy levels and additional loads, particularly for large vehicles.

The shape of liquid-vapor surface plays a key role in the design and management of a liquid tank of a spacecraft. A problem under study, as shown in Fig.1.2.1, is of a cylinder partially filled with a wetting liquid exposed to one and zero-gravity environment. This diagram illustrates that on Earth, in relatively large tanks, the capillary effects are suppressed thus resulting in a flat, free liquid surface. In the zero-gravity environment, the equilibrium configuration of liquid-vapor interface will be different from the one on Earth since the external forces are almost absent, resulting in the change of the liquid position. This dramatic change can cause many problems, as mentioned previously.

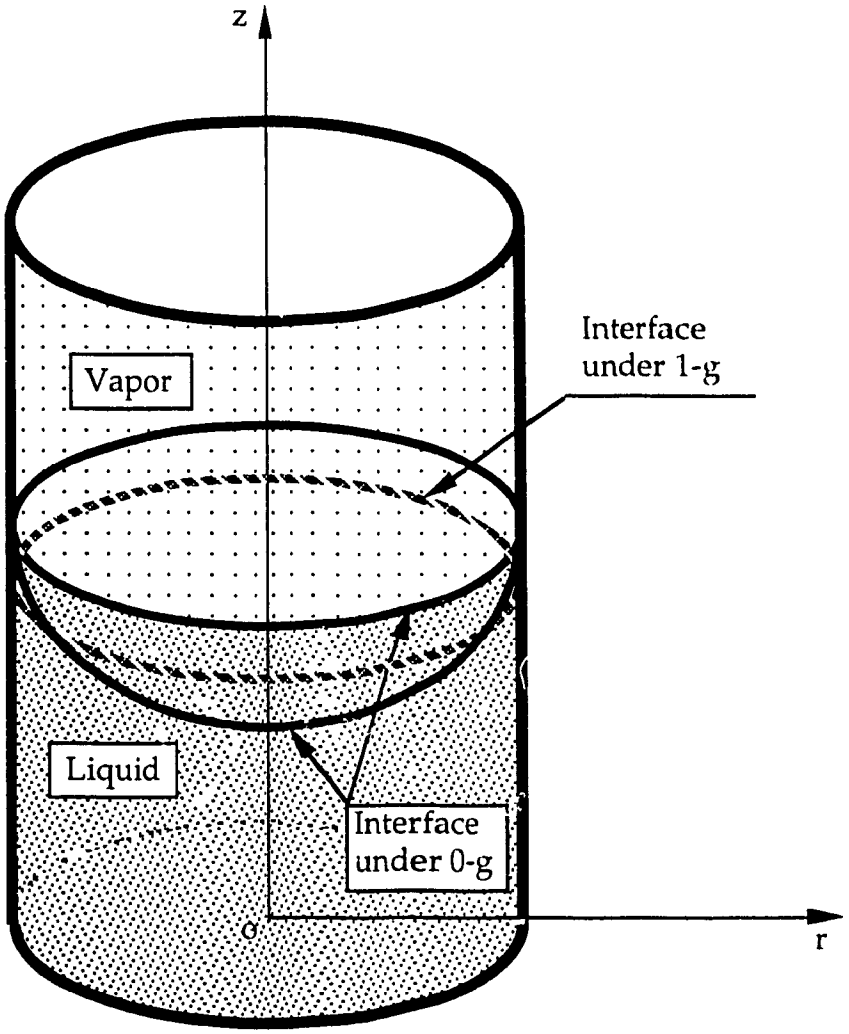


Fig.1.2.1 Wetting liquid in a cylindrical tank in zero-gravity environment

The liquid dynamic behavior during outflow in a zero-gravity environment is another problem, as shown in Fig.1.2.2. For example, this problem is often encountered in a propellant tank during the restart sequence of the engines. The engine starting flow causes liquid-vapor interface distortion. The distortion may cause vapor to enter the outlet line leaving the tank with a considerable amount of liquid residuals. A time history of the transient period of the liquid dynamic behavior is needed to design the system that avoids vapors entering the outlet while efficiently expelling liquids.

Hence, liquid management systems, stability and control of a spacecraft might be dramatically affected by the liquid behavior in a liquid-vapor-solid system. The proper employment of the system through the use of suitable tank geometry offers the possibility of a liquid management system that does not require expenditure of energy with effective tank volume and effective liquid storage. The knowledge of the motion of a liquid during a dynamic transition from terrestrial gravitation to weightlessness and during liquid draining, the time required for the system to reach the 0-g equilibrium configuration, the liquid-vapor interface equilibrium configuration, the liquid residuals and the stability of the system, is therefore required in order to solve many of the problems encountered in design and operation of spacecrafts and experiment.

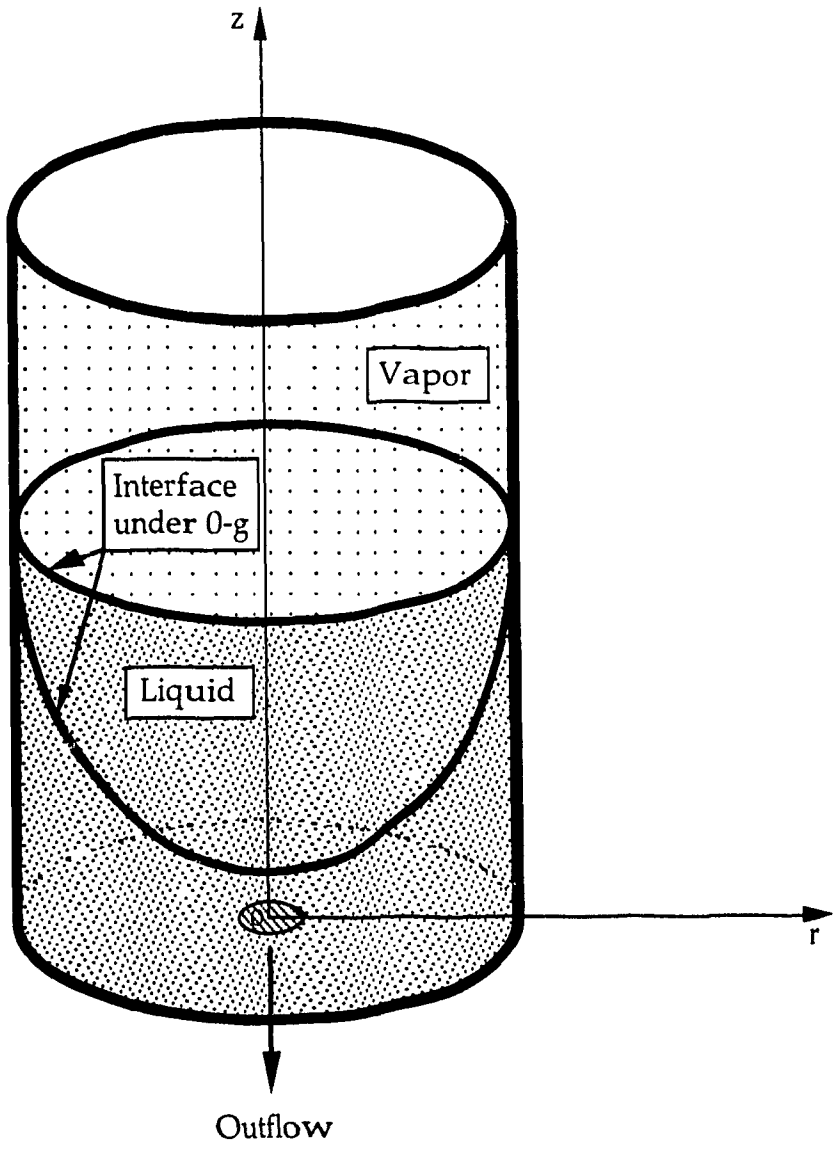


Fig.1.2.2 Wetting liquid in a cylindrical tank during draining in zero-gravity environment

## 1.3 Previous Work

### *1.3.1 General*

Studies on capillary-dominated fluid flows started early in the 19th century. Extensive studies of liquid setting and interface dynamics as related to liquid storage and management in spacecrafts under microgravity conditions began in the late 1950s and early 1960s with the rapid development of space activities. Extensive research was carried out during that period. The status of zero-gravity technology at that time was surveyed by Unterberg et al (1962) and Otto (1966). Research on liquids in partially empty tank was stimulated in the 1970s due to propellant requirements of the Apollo lunar landing program. The recent comprehensive survey was present by Krotiuk et al (1990) and Myshkis (1992).

Mechanical effects of fluid presented on Earth might be altered if gravity is removed. A liquid is under the influence of inertial and intermolecular forces that are represented in the form of surface tension forces. On Earth, gravitational forces dominate much of the liquid behavior. For example, the weight of the liquid, the shaping of liquids in tanks and the hydrostatic pressure of liquid columns are the effects of predominant inertial forces while the surface tension force effects are occasionally observable such as in the capillary rise. The gravitational forces are negligibly small and consequently do not influence the behavior of liquid in a spacecraft while surface tension forces, which are minor on Earth, exert a greater effect. Myshkis (1987) estimated the magnitude of all forces in space. Surface tension forces and aerodynamic deceleration are most pronounced in the orbit with an altitude of 240 km. The surface tension forces play dominant role at

altitudes of greater than 500 km. A liquid on board of a spacecraft in free flight is exposed to zero-gravity environment, thus is subjected to surface tension forces. These forces are predominant in determining the liquid dynamics and the equilibrium configurations.

An appropriate macroscopic representation of capillary phenomena can be defined by surface tension forces and contact angle. A schematic diagram illustrating how these surface tension forces act at the solid-liquid-vapor interfaces in a capillary dominated environment is presented in Fig.1.2.3. A liquid and a vapor contained in a solid vessel are in contact with each other and are separated by an interface that behaves as though it consists of two homogeneous fluids separated by a uniformly stretched membrane of infinitesimal thickness (Young, 1805). The surface tension of a liquid is defined as the surface potential energy per unit area of surface. The free surface energies at the solid-liquid-vapor interfaces may be visualized in the form of surface tension forces $\sigma$ acting in the direction of the surface. The surface tension is a monotonically decreasing function of temperature for a given interface.

Wetting phenomena may be observed depending on the affinity of a liquid for the contacting surface of a solid. For example, if the liquid is water contacting to the hydrophobic surface, no wetting is expected. Conversely, wetting by water will take place on hydrophilic surfaces. Between these two extremes there is a range of intermediate situations, where an equilibrium state is reached. The liquid-vapor interface meets the liquid-solid at an angle

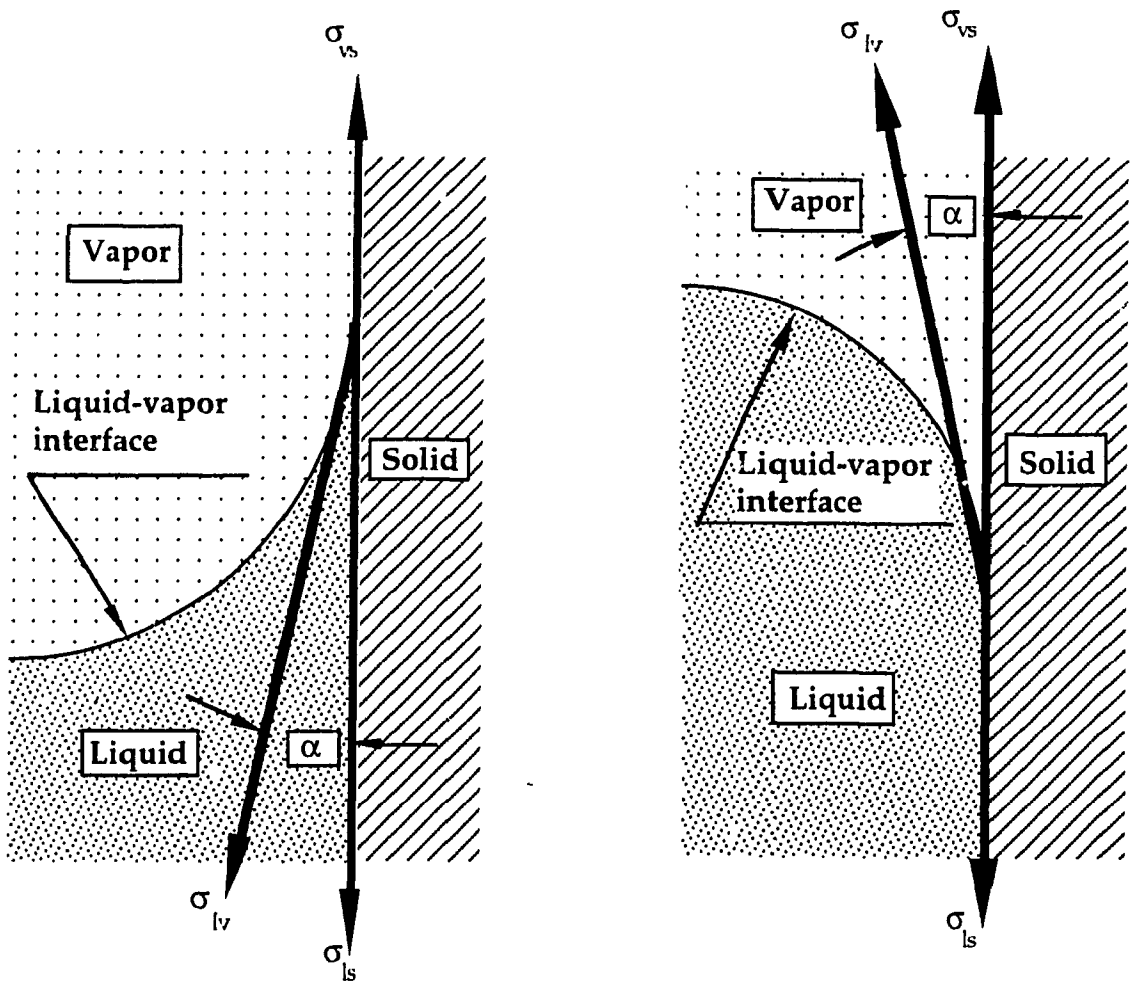


Wetting liquid

Non-wetting liquid

Fig.1.2.3 Surface tensions and contact angle of liquid in zero-gravity

$\alpha$, the contact angle which can be taken as a measure of the relative hydrophilicity or hydrophobicity of the solid. The contact angle $\alpha$ is the angle between the tangential planes to the liquid-solid and liquid-vapor interfaces at the line of contact with the solid. A wetting liquid is the one with the contact angles lying between $0^o$ and $90^o$. Most propellants to be considered are wetting liquids. Non-wetting liquids form contact angles between $90^o$ and $180^o$. The contact angle is a relatively variant property of the interface while the surface tension is not. Sensitivity to surface and environmental conditions makes reproduction of the contact angle measurement difficult resulting in uncertainty to some extent in prediction of capillary phenomena.

### *1.3.2 Research Means*

Liquid dynamics in zero-gravity environment have been studied by means of analytical solutions, experimental tests and numerical simulations (Agafonov et al, 1992; Eckhart et al, 1982; Hedgepeth, 1961; Halpern, 1986; Ostrach, 1982). In order to obtain analytical solutions, through classical methods, drastic simplifications with respect to the physics of the problem must be employed, and therefore the applications of the results are limited.

Experiments seek to provide observations of complex phenomenon and precision enhanced measurements of physical attributes due to the low-gravity space environment. Experimental data are needed to support the analytical and computational efforts by providing the basis for new constitutive models and correlations. The results are used to challenge and validate contemporary scientific theories.

Experimental data can be obtained from microgravity facilities, including drop towers and tubes, aircraft, rockets, balloons, magnetic levitation and space shuttle. Earthbound experimental facilities such as drop towers and aircraft have been developed to obtain new knowledge and the starting blocks for experimental research in space. They can provide a low-gravity condition for a short period of time during which experiments are done with monitoring and measuring instruments.

In drop towers or tubes an experimental package is allowed to undergo a free fall from an elevated position. During the period of free fall, the test fluid will be in almost true weightlessness. The short period of microgravity time is a severe constraint (2 to 5s). Airplanes flying in parabolic Keplerian trajectories between two altitudes can accommodate large payloads during about 20 to 25 seconds microgravity time. It is able to provide relatively high g field level; however, it is difficult to maintain at a steady value. In addition, an acceleration of about 2 g is experienced before the free fall maneuvers. This acceleration may perturb flow in the test loop, increasing the time required to establish steady state once low-gravity is achieved. Thus, the period for obtaining valid data may be shorter than the free fall time.

Earthbound experiments using drop towers or aircraft suffer from limited low periods of microgravity time that is insufficient to examine the fluid dynamic response. Experiments in orbit, such as the space shuttle enabling the conduct of experiments in very low gravity for up to 7 days, provide excellent means to evaluate low-gravity fluid dynamic behavior. However, these experiments are very expensive, provide very limited space

and payloads, and long scheduling lead time. It is generally desirable that sufficient knowledge and experience through earthbound research must be gained prior to undertaking a space research project in order to ensure it to be effective.

The issue associated with zero-gravity experimentation are extremely complex. Severe constraints exist on the capability and availability of proper facilities, time and funding levels which are incommensurate to the immense task of developing a complete understanding of liquid behavior in weightlessness. The scale of the experiment also limits the application of the results. Therefore, the experiments and acquired data have been limited to a few variables and considerably narrow range of applications, yielding insufficient and inaccurate information. Thus, the usefulness of these past experiments to the analysis and design of fluid managing components is marginal and new experiments will be required. Due to limited information, the best approach for obtaining zero-gravity results would be best suited to a design engineer and computer code researcher.

Collection of data on liquid behavior in microgravity by experimental means represents a complex and arduous task. Testing components under normal and transient operating conditions can prove to be very difficult to attain. However, numerical simulation can prove to be an effective tool in liquid behavior study. With the advent of super computers, the development of computational methods has made simulations of the fluid dynamics such as liquid-vapor interfaces possible. Mathematical modeling using the detailed computer codes can expand the performance data over the steady-state and transient range.

Computer codes represent an important tool for designing a complicated fluid management system. The use of approximate solutions to solve complicated equations in fluid dynamics provides sufficiently accurate information concerning the physics of problems and reduces the number of experiments that have to be performed in space. Analysis and design of the fluid system in a spacecraft might require the computational codes to be modified in order to accommodate various operating conditions. As a result, the computational method must be verified by other means such as experimental study.

### *1.3.3 Liquid Behavior in 0-g Equilibrium*

The liquid-vapor interface configuration under zero-gravity conditions was previously investigated by analytical means. Exact solutions for the configuration of the interface between parallel plates as a function of the gravity field were calculated by Reynolds (1961) and Benedikt (1961). Li (1961, 1962) predicted the interface configuration in many geometries by applying the minimum energy principle. The primary dependence of the interface configuration is indicated in all these studies. Their analytical approach was valid in predicting the cases of steady state with large liquid heights. The liquid-vapor interface equilibrium configuration in a zero-gravity environment was investigated by Yan et al (1993) and Vatistas et al (1994). The interface configuration in rectangular and cylindrical tanks with high and low liquid height can be predicted by the interface configuration ratio and the liquid critical depth. Multiple configurations exist at the low initial liquid

height. The results of numerical simulations also confirm the preferable equilibrium configuration prediction (Yan et al, 1994). These results agree favorably with the previous experimental data.

A number of experiments investigating the configuration of the liquid-vapor interface when the gravity is removed have been carried out in drop towers. Reynolds (1959) photographically examined wetting and non-wetting liquid placed in a transparent tank with different ullage during a 1-second free-fall. The results indicate that wetting liquids in spherical tanks will crawl around the tank walls leaving a vapor pocket in the center. Coalesced of non-wetting fluids resulted in a globe at the center of the tank surrounded by a vapor blanket. The behavior of liquids in spherical tanks was studied by Petrash et al (1962). Experimental results for simulation of weightlessness were obtained in the 100-foot zero-gravity drop tower facility at the Lewis Research Center of NASA, U.S.A. The actual free-fall distance of the drop tower is 85 feet, yielding a 2.3-second period of zero-gravity time. Further investigation of the microgravity equilibrium configuration of the liquid-vapor interface with liquids with three different contact angles in various geometries at three different liquid fillings were conducted using the same facility by Petrash et al (October 1963). The contact angle remained unchanged from its 1-g value but in 0-g, the liquid-vapor interface tended towards a configuration of constant surface curvature meeting the tank walls at the contact angle. The experimental work was confirmed and extended by Clodfelter (1963) who reported on end boundary effects in flat-bottom cylinders at the 1.85 second drop facility.

The other study was conducted by Petrash et al (January, 1963) on the effect of the acceleration disturbances encounter in the MA-7 spacecraft on the liquid-vapor interface in a baffled spherical tank. The zero-gravity steady-state configuration of the liquid-vapor interface observed in previous drop towers was identical to that observed in the spacecraft test. The intention of a liquid-vapor-solid system at 0-g is towards the minimum surface energy configuration. This was verified by a study into the capillary rise in tubes (Petrash et al, January 1963). The hydrostatic stability characteristics of the liquid-vapor interface when subjected to acceleration disturbances were also investigated (Masica et al, 1964).

### *1.3.4 Liquid Dynamic Behavior during Gravity Change and Draining*

The time required for the liquid-vapor-solid system to reach 0-g equilibrium configuration after the system has switched from 1-g to 0-g was previously studied. Analyses were conducted to determine the time response of a deformed liquid drop under the action of surface forces. Paynter (1964) presented an analytical method to predict the time required for a liquid-vapor system to deform from a gravity-dominated environment to that of a zero-gravity equilibrium state. However, liquid-vapor systems at 0-g are more important to a spacecraft designer. Benedikt (1959, 1961) studied the hydrostatic behavior of liquids in a microgravity environment taking into account the liquid deformations due to surface tension forces. It was indicated that there is a transition period between time entering the zero-gravity environment and time when an equilibrium is established. A functional expression for the transient time period was also derived. A free-fall

experimental study was conducted by Siegert (1964) to determine the time required for the liquid-vapor interface to reach equilibrium in spherical, cylindrical, and annular tanks. The dependence of the time to reach equilibrium as a function of the pertinent liquid parameters and system dimensions was obtained.

The liquid behavior in a rectangular and cylindrical tanks during the entire time period of a dynamic transition from terrestrial gravitation to weightlessness has been numerically studied by Vatistas et al (1994) and Yan et al (1994). The results show that in all cases the zero-gravity equilibrium state is attained asymptotically as the transient effects diminish. The interface formation time increases with the increase of contact angle and the decrease of the viscous forces.

In a microgravity environment, the surface tension forces are so influential on the draining characteristics of a tank that a residual amount of fluid can be trapped due to surface tension alone (Berenyi et al, 1970). Studies of these flows are therefore important in order to comprehend the extent of the residual volume of propellant in the fuel tanks and the amount of additional payload to a spacecraft that the residual volume implies. Further studies of mechanisms to reduce the residual volumes can aid in the design of propellant tanks thus reducing or eliminating the additional payload.

The results of a photographic study of outflow from cylindrical tanks, conducted by Nussle et al (1965) in a 2.3-second drop tower indicated that significant distortion of the interface occurred as the outflow velocity was increased. The experiment was limited to one test liquid in a cylindrical tank,

and outflow velocities of 2.91 m/s and 14.08 m/s. The outflow was initiated at 0.25 second after the beginning of the free fall. The 0.25-second delay was for the liquid-vapor interface to assume its zero-gravity configuration. However, this amount of time is generally not sufficient to ensure the complete absence of oscillatory interface motion.

The distortion of the liquid-vapor interface during the draining process in weightlessness was examined (Derdul et al, 1966; Berenyi et al, 1969). The magnitude of the distortion was dependent on the outflow Weber number and the initial liquid height and independent of the shape of the tank bottom for the cylindrical tanks with inverted elliptical hemispherical and flat bottom tested. The liquid residuals, critical and vapor ingestion heights in both normal-gravity and zero-gravity for flat bottom cylindrical tanks and hemispherical bottom tanks were determined by Abdalla et al (1969) and Berenyi et al (1970), respectively. The vapor ingestion and critical heights were found to be correlated with the Froude number in one-gravity and the Weber number in weightlessness, respectively. Gluck et al (1966) experimentally investigated interface distortion during outflow of liquid from small flat-bottomed tanks under standard gravity conditions. Grubb et al (1967) conducted an experimental investigation of interfacial behavior following termination of outflow in weightlessness. An axial geyser was found to occur that can transfer a small amount of liquid to the inlet of the tank.

Various methods which might be used to reduce the quantity of liquid residuals were investigated in later studies. Baffling of the incoming pressurized vapor to avoid direct impingement on the interface and of the

outlet to retard vapor ingestion can minimize interface distortion and maximize the total amount of liquid drained from the tanks (Nussle et al, 1965). Installing baffles over the outlet line in cylindrical tanks with flat and hemispherical bottoms were examined by Berenyi (1970) and Symons (1972). The uses of a single-step throttling of the outflow rate in a flat bottom cylindrical tank and contoured outlets for hemispherical-bottomed cylindrical tanks during weightlessness were tested (Symons, 1974; 1979).

A large portion of the zero-gravity experimental research work has focused on liquid dynamic behavior during a limited time period. However, little work has been devoted to study the effects of outflow or gravity change on the liquid covering the entire range.

Computational studies of the liquid dynamic characteristics during draining in weightlessness were presented by Yan et al (1995). The interface configuration can be affected by outflow velocity, location of outlet and draining start time. Liquid residuals decrease with decreasing outflow velocity. Outflow from corner outlet presents less severe interface distortion and liquid residuals. Draining start time has significant influence on liquid residuals.

## 1.4 Methods

The present work focuses on numerical and analytical investigations with the aim to study aspects of the mechanics of liquids in a liquid-vapor-solid system while it is exposed to weightlessness. Both analytical solutions

and the numerical results that will be presented here have been developed to predict liquid characteristics for general conditions.

Numerical investigations are conducted to examine the dynamic behavior of the fluids during transient period of outflow and gravity change in cylindrical and rectangular tanks. A practical numerical method has been developed resulting in a powerful means for analysis of the fluid dynamics in a microgravity environment. The dynamic responses of the system during weightlessness under the influence of various physical and geometric conditions are simulated using the modified version of a transient numerical solution, SOLA-VOF, previously developed by Hirt and Nichols (1981, 1980). This numerical algorithm is for a time-dependent transient incompressible flow involving free surfaces where surface tension forces exert the effects. This solution algorithm uses the fractional volume of fluid scheme to track the liquid-vapor interface. Simulations concerning the liquid dynamics are accomplished solving simultaneously fluid dynamic equations. The present studies contain several improvements over the original SOLA-VOF code.

The analytical component deals with the liquid-vapor interface characterization under hydrostatic conditions in a zero-gravity environment. The analysis of liquid behavior in a zero-gravity environment proceeds from an investigation of equilibrium configurations the liquid may assume. The analytical approach is based on the minimum potential energy principle and physics of a liquid. Experimental data from previous studies are used for validation of the numerical and analytical results.

## 1.5 Outline

The studies of fluids in the liquid management tanks during weightlessness are conducted. They deal with problems related to liquids at the zero-gravity equilibrium state, and their dynamic responses to the external disturbance. The following items are covered in this thesis:

(i) the liquid-vapor interface configuration at 0-g equilibrium;

(ii) the stable state of a liquid-vapor-solid system;

(iii) the dynamic motion of a liquid during the transition from 1-g to 0-g;

(iv) the interface formation time during the transition from 1-g to 0-g;

(v) the interfacial behavior during liquid outflow in weightlessness;

(vi) the liquid residuals during outflow in weightlessness;

(vii) the dynamic motion of a liquid under the transient conditions of outflows and the gravity change;

(viii) verification for the analytic solution, the computational method and the experimental data.

The purpose of this thesis is to present the results of analytical and numerical investigations into the behavior of liquids in zero-gravity environment. The results will lead to guidance and aid to design liquid management devices without the need of extensive experimental verifications or reducing the number of experiments significantly. Fluid management systems in spacecrafts would most likely benefit by efficient and predictable fluid supply.

This chapter introduces the fluid problems encountered in a microgravity environment, the previous work, the methods employed to

solve the problems and the scope of the thesis. Chapter 2 deals in detail with the liquid-vapor interface configuration and the stability at the zero-gravity equilibrium state by the analytical method. In Chapter 3 the numerical solution algorithm is introduced. The results concerning the dynamic behavior of liquids during the transition of gravity field level change from the terrestrial to weightless conditions is presented in Chapter 4. Chapter 5 and 6 show results of the dynamic behavior of liquids during outflow and the liquid residuals during draining in weightlessness, respectively. Finally in Chapter 7 the results are summarized.

# CHAPTER 2

# LIQUIDS AT ZERO-G EQUILIBRIUM STATE

## 2.1 Liquids in Equilibrium

The purpose of the analytical work is to determine a liquid-vapor interface configuration at a zero-gravity equilibrium state and the stability of a liquid-vapor-solid system. The location of the liquid and vapor, and the factors of influencing the configuration under the conditions of no external disturbances to the system are also investigated. The optimum shape for liquid tanks is spherical resulting in less weight. Unfortunately, spheres are not very efficient shapes in terms of occupying space of vehicles flying in the atmosphere. Liquid tanks are integral part of the vehicle fuselage or wing and can be irregular in shape. Thus, two dimensional rectangular and cylindrical geometries are considered in the present studies.

Capillarity deals with the macroscopic and statistical behavior of interface rather than with the details of their molecular structure. The interfacial tension acts in any interface, trying to minimize the free-surface area. For liquid-liquid or liquid-vapor interfaces, the action of the interfacial tension manifests itself in the shape that the interface assumes. For boundaries involving solid, the presence of an interfacial tension can only be indirectly established. The tension in surface layers is the result of the attraction of the bulk material for the surface layer which tends to reduce the

number of molecules in the surface region resulting in an increase in intermolecular distance. This increase requires work to be done, and returns work to the system upon a return to normal configuration. The surface energy is proportional to its surface area. Surface tension strives to make the surface as small as possible. Thus the surface tends to have minimum potential energy which is the condition for stable equilibrium. The magnitude of the surface tension is dependent on the physical properties of the materials in contact. As the temperature is raised, the kinetic energy of the molecules increases, and the attraction between molecules is partially overcome. Thus, the surface tension is a monotonically decreasing function of temperature on the liquid-vapor interface. A decrease in surface tension is accompanying with increasing pressure.

The conditions concerning the system in equilibrium must be investigated for the analysis of the configuration when the system is exposed to a zero-gravity environment. Consider the conditions of equilibrium for a liquid-vapor-solid system. The physical nature of a liquid and vapor placed in a solid tank may be described in terms of regions: two homogeneous bulk phases and a region of space between them whose properties are different from those of the bulk phases, but which merge into them at the extremities of the surface layer. A curved surface of liquid-vapor is described by two principal radii of curvature. A small section of an arbitrarily curved surface is chosen. The two principal radii of curvature $r_1$ and $r_2$ of the section are considered as positive if they are drawn into the vapor phase. The radii of curvature (where both are of the same sign) lie on that side of the interface experiencing the greater pressure.

The surface is assumed to be displaced isothermally an infinitesimal distance $d\eta$ towards the liquid phase while keeping the physical content of the system unaltered. The distance $d\eta$ is taken as positive, the elements of length $d\xi$ and $d\zeta$ on the surface in their principal radii increase $\left(\frac{d\eta}{r_1}\right)d\xi$ and $\left(\frac{d\eta}{r_2}\right)d\zeta$. After the displacement, the surface element $d\xi d\zeta$ becomes $\left(1+\frac{d\eta}{r_1}+\frac{d\eta}{r_2}\right)d\xi\, d\zeta$. Thus the increment of the surface for the element surround by the vapor and liquid is

$$dA_{lv} = \left(\frac{1}{r_1}+\frac{1}{r_2}\right)d\eta d\xi d\zeta \tag{2.1.1}$$

The change of the surface area contacting to the solid is $dA_{lv,\Omega} = \cos\alpha\, d\eta d\Omega$ The total variation of the liquid-vapor surface area is

$$\delta A_{lv} = \int_{lv}\left(\frac{1}{r_1}+\frac{1}{r_2}\right)d\eta d\xi d\zeta - \int_{lv,\Omega}\cos\alpha\, d\eta d\Omega \tag{2.1.2}$$

Since the surface of the tank is unchanged:

$$A_c = A_{ls} + A_{vs} \tag{2.1.3}$$

The increase of the vapor-solid surface will be at the expense of the liquid-solid surface. Thus the changes of the surface areas of vapor-solid and liquid-solid are

$$\delta A_{vs} = -\delta A_{ls} = \int_{lv,\Omega} d\eta d\Omega \tag{2.1.4}$$

The total work done in forming this additional amount of surface area is concerned with situations in which mechanical and surface work are simultaneously involved. Therefore, the total work done at constant temperature, pressure and composition is

$$\delta w = \delta\left(\sum_k \sigma_k A_k\right) + \delta\int_{V_m} F_m \, dV_m \tag{2.1.5}$$

where the subscript k with lv, ls and vs corresponding to the interfaces of the liquid-vapor, liquid-solid and vapor-solid, respectively. $F_m$ is the force and $V_m$ is the volume. The surface tensions are considered as constant under the given conditions, consequently, one needs only to calculate the interfacial areas. Thus Equation (2.1.5) becomes

$$\delta w = \sigma_{lv}\,\delta A_{lv} + \sigma_{ls}\,\delta A_{ls} + \sigma_{vs}\,\delta A_{vs} + \delta\int_{V_m} F_m \, dV_m \tag{2.1.6}$$

The surface change due to displacement is subjected to the condition that liquid volume remains unchanged,

$$\int_{V_l} dV_l = \text{constant} \tag{2.1.7}$$

Therefore, the total work done is only due to the change in interface energy. Making use of Equations (2.1.2) and (2.1.4)

$$\delta w = \sigma_{lv}\left\{\int_{lv}\left(\frac{1}{r_1}+\frac{1}{r_2}\right)d\eta d\xi d\zeta - \int_{lv,\Omega}\cos\alpha\, d\eta d\Omega\right\} + \sigma_{vs}\int_{lv,c} d\eta d\Omega$$
$$- \sigma_{ls}\int_{lv,\Omega} d\eta d\Omega - \int_{lv}(p_v - p_l)\, d\eta d\xi d\zeta \qquad (2.1.8)$$

where $p_v$ is the pressure in the phase on the convex side of the liquid-vapor surface while $p_l$ is the pressure in the phase on the concave side. $\alpha$ denotes the contact angle, the angle between the tangential planes to the solid-liquid and liquid-vapor interfaces at the line of contact with the solid. Rearrange Equation (2.1.8)

$$\delta w = \int_{lv}\left\{\sigma_{lv}\left(\frac{1}{r_1}+\frac{1}{r_2}\right) - (p_v - p_l)\right\} d\eta d\xi d\zeta + \int_{lv,\Omega}\left(\sigma_{vs} - \sigma_{ls} - \sigma_{lv}\cos\alpha\right) d\eta d\Omega \qquad (2.1.9)$$

Since the process is an infinitesimal change in an equilibrium system the total work done is zero. Thus the expression in the braces of the first term in Equation (2.1.9) becomes

$$\sigma_{lv}\left(\frac{1}{r_1}+\frac{1}{r_2}\right) = p_v - p_l \qquad (2.1.10)$$

which is the familiar equation of Young and Laplace (Adamson, 1982). Equation (2.1.10) presents the values of pressures, radii and surface tensions at a point in the surface and does not involve an assumption regarding the variation of the pressures $p_v$ and $p_l$ with the height. For the presence of the effects of gravitational acceleration, the pressures $p_v$ and $p_l$ vary with the height of the point considered. If the effect of gravity is neglected, for example,

zero-gravity environment, the pressure is constant in each phase. Thus the equation of Young and Laplace is valid in any gravitational field.

If both radii are equal, a spherical surface of radius of curvature maintains equilibrium between two phases at pressure difference of $p_v - p_l$. Equation (2.1.10) then reduces to

$$\frac{2\sigma_{lv}}{r_1} = p_v - p_l \tag{2.1.11}$$

The pressure in either liquid or vapor phase is kept constant when the system exposed to zero-gravity environment

$$\frac{\sigma_{lv}}{r_1} = \text{constant} \tag{2.1.12}$$

The sum of the curvature over the liquid-vapor interface is constant.

The shape of the surface can be determined in Cartesian and cylindrical coordinates:

$$\sigma_{lv}\left\{\frac{d}{dx}\left[\frac{\frac{dy}{dx}}{\sqrt{1+\left(\frac{dy}{dx}\right)^2}}\right]+\frac{\varepsilon}{x}\left[\frac{\frac{dy}{dx}}{\sqrt{1+\left(\frac{dy}{dx}\right)^2}}\right]\right\} = \text{constant} \tag{2.1.13}$$

where $\varepsilon$ =0 or 1 indicates Cartesian or cylindrical coordinate, respectively, and y=y(x) is the height of the interface. Hence, in a weightless environment, the

equilibrium liquid configuration will deform until it forms the liquid-vapor interface with a constant curvature.

The condition of the equilibrium also requires the second term of the Equation (2.1.9) to be zero, which will be satisfied if

$$\sigma_{lv} \cos\alpha = \sigma_{vs} - \sigma_{ls} \tag{2.1.14}$$

which is Young-Dupre equation. The surface tensions of the liquid-vapor, vapor-solid and liquid-solid are related through the contact angle. The absence of the gravitational term in the Equation (2.1.14) indicates that the contact angle is independent on gravity. Both contact angle and surface tensions are dependent only on the nature of the solid-liquid-vapor interfacial surfaces and are not affected by the gravitational forces because the intermolecular forces are assumed to be independent of the level of the gravitational field. An experimental investigation conducted by Petrash et al (1963) verified the contention that the contact angle of the liquid at the solid-liquid-vapor interface observed at 1-g is preserved in 0-g environment.

The energy of the liquid-vapor-solid system takes the following form

$$E = \sum_{k=lv,ls,vs} E_k + \int_{V_m} F_m \, dV_m \tag{2.1.15}$$

Under the constraint condition, the liquid volume must remain constant and the total energy must be at its minimum value in equilibrium.

## 2.2 Wetting Liquid Configurations

A wetting liquid in a rectangular tank is selected to illustrate the method of solving problems. The analysis and results can also be analogous to a non-wetting liquid and a cylindrical tank. Two configuration systems at the zero-gravity equilibrium state will be discussed. One of them is under the condition that the liquid volume is sufficient to cover the base of the containing tank at all times, called configuration system 1. The other is the volume of a liquid may not be enough to cover the base of the tank at all times, called configuration system 2.

Configuration system 1 in a rectangular tank partially filled with a wetting liquid while exposed to weightlessness is shown in Fig.2.2.1. When the liquid wets the walls of the tank, the liquid surface is thereby constrained to lie parallel with the walls resulting in a concave surface. The y axis of the tank points upward and the gravitational force acts downward. The meniscus of the configuration system 1 is approximately hemispherical. The contact angle requirement necessitates that:

$$\left.\frac{dy}{dx}\right|_{(x=L)} = \cot(\alpha) \qquad (2.2.1)$$

The surface radius is then

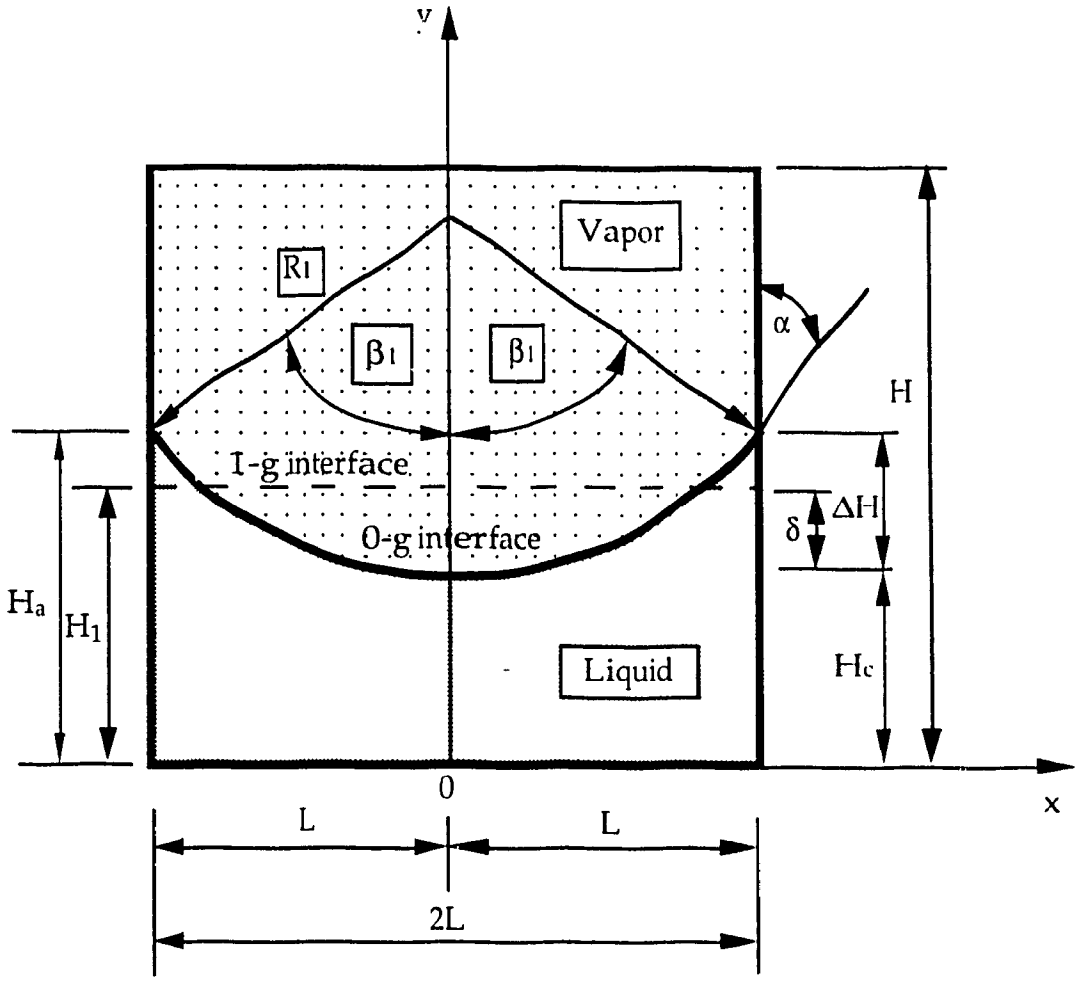


Fig.2.2.1 Wetting liquid configuration system 1 in a rectangular tank $(0^{o} \leq \alpha \leq 90^{o})$

$$R_1 = \frac{L}{\cos(\alpha)} \tag{2.2.2}$$

In the equilibrium state the liquid-vapor interface curve passes through the point (0, $H_c$), the height of the interface is given by

$$y = R_1 + H_c - \sqrt{R_1^2 - x^2} \tag{2.2.3}$$

The liquid height in 1-g field is

$$H_1 = H_c + \delta \tag{2.2.4}$$

where $H_c$ denotes the height of the meniscus above the bottom of the tank and

$$\delta = \Delta H - \frac{\beta_1 L}{2\cos^2\alpha} + \frac{L}{2}\tan\alpha \tag{2.2.5}$$

where

$$\beta_1 = \frac{\pi}{2} - \alpha \tag{2.2.6}$$

and $\Delta H$ is a liquid height distance between lower and higher plane, given by:

$$\Delta H = R_1 - \sqrt{R_1^2 - L^2} \tag{2.2.7}$$

Configuration system 2 is another most likely configuration that also obeys the conditions, as shown in Figs.2.2.2 and 2.2.3 for contact angle less than and greater than 45 degrees. The surface radius is defined as

$$R_2 = \frac{\sqrt{2}}{2\sin\beta_2} H_a \tag{2.2.8}$$

where

$$\beta_2 = \left| \frac{\pi}{4} - \alpha \right| \tag{2.2 9}$$

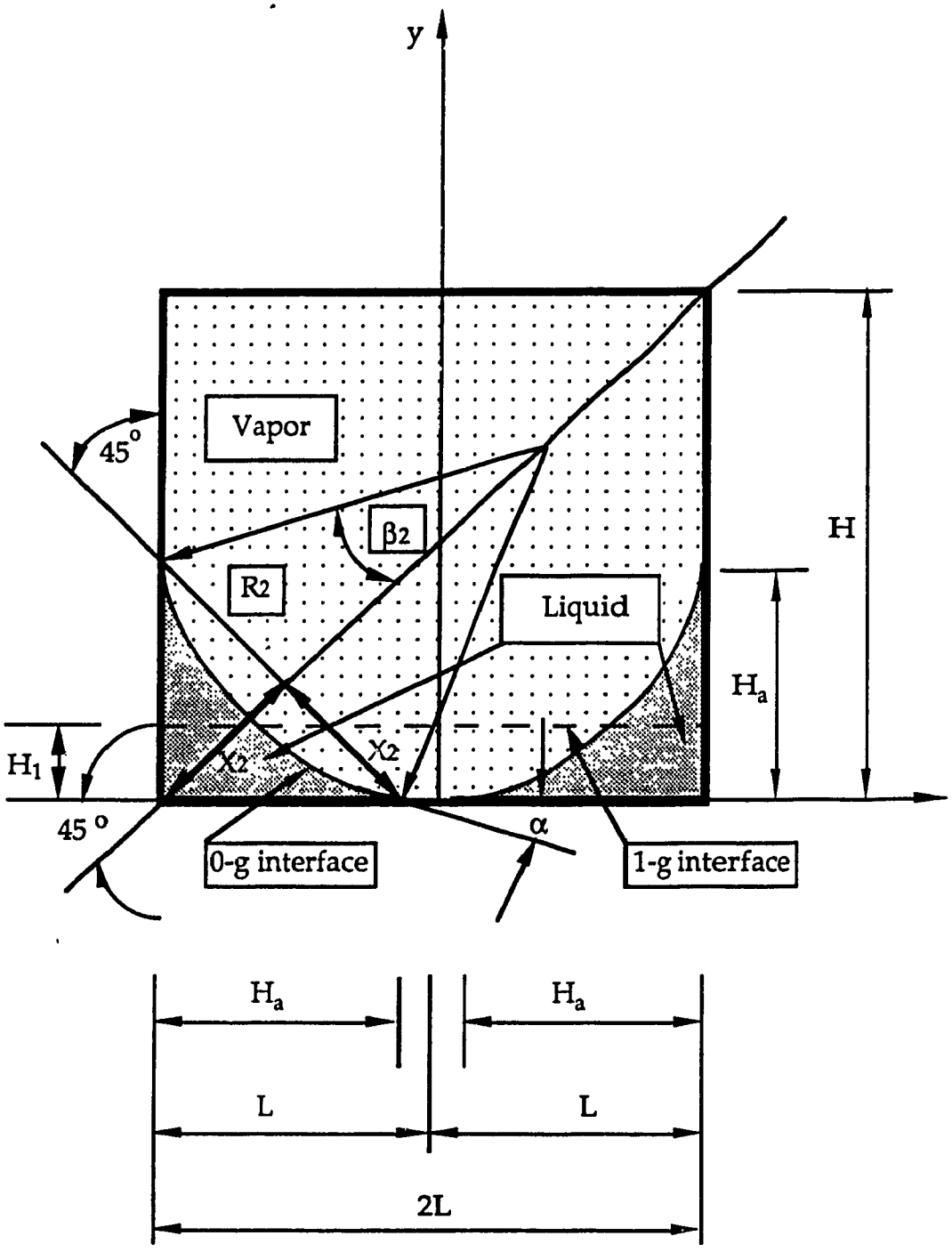


Fig.2.2.2 Wetting liquid configuration system 2 in a rectangular tank

$(0° \leq \alpha \leq 45°)$

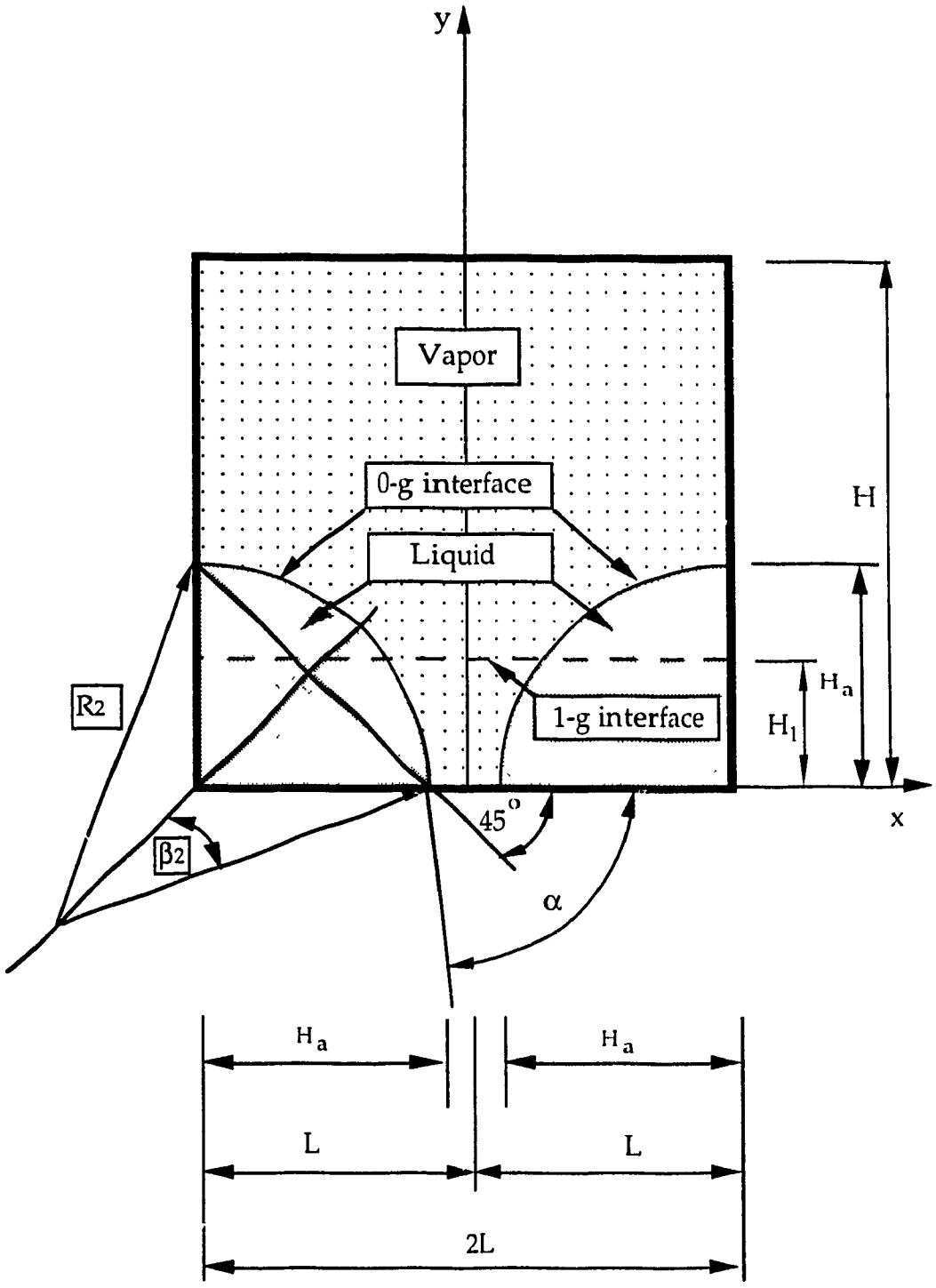


Fig.2.2.3 Wetting liquid configuration system 2 in a rectangular tank $(45^o \le \alpha \le 90^o)$

## 2.3 Energy in Configuration Systems

### *2.3.1 Minimum Energy Principle*

Equation (2.1.15) is recalled for the energy of the liquid-vapor-solid system.

$$E = \sum_{k=lv,ls,vs} E_k + \int_{V_m} F_m \, dV_m \qquad (2.1.15)$$

If the system experiences zero-gravity, the energy consists of the surface energy:

$$E = \sigma_{lv} |A_{lv}| + \sigma_{ls} |A_{ls}| + \sigma_{vs} |A_{vs}| \qquad (2.3.1.1)$$

The configuration having smaller surface energy is more stable and more likely to be formed for certain amounts of liquid while maintaining the same contact angle. If the interface area is not initially at the minimum, then it reaches the minimum through a dynamic process. On the other hand, if it is at a local minimum state then given a disturbance in an appropriate magnitude, the interface area might degenerate to the next minimum state. In certain situations the liquid-vapor interface might have several configurations that satisfy the requirements of the Laplace's equation, the contact angle and the mass conservation. These might be considered the system at a number of different metastable states for which small perturbations in configuration result in potential energy increase. If a sufficiently large disturbance is imposed, the system will pass to the next more stable state or to the most stable state.

It is assumed that both configurations 1 and 2 are at the zero-gravity equilibrium state. The energy difference is then given by:

$$\Delta E = E_2 - E_1 = \sigma_{lv}\,\Delta|A_{lv}| + \sigma_{ls}\,\Delta|A_{ls}| + \sigma_{vs}\,\Delta|A_{vs}| \qquad (2.3.1.2)$$

The system is subjected to the Young-Dupre's condition and the constant surface area of the tank. Then

$$\Delta E = \sigma_{lv}\{\Delta|A_{lv}| - \cos(\alpha)\,\Delta|A_{ls}|\} \qquad (2.3.1.3)$$

Let

$$\Delta\bar{E} = \frac{\Delta E}{L^2\sigma_{lv}} \qquad (2.3.1.4)$$

which may be called as the dimensionless energy difference. Equation (2.3.1.3) can be rewritten,

$$\Delta\bar{E} = \Delta|\bar{A}_{lv}| - \cos(\alpha)\,\Delta|\bar{A}_{ls}| \qquad (2.3.1.5)$$

The configuration with the least energy may be determined by the sign of $\Delta\bar{E}$ value in Equation (2.3.1.5). If the value of $\Delta\bar{E}$ is negative, which means that

$$\Delta\bar{E} < 0$$

it indicates $\bar{E}_2 < \bar{E}_1$, and configuration 2 has less energy than configuration 1. Thus configuration 2 is more stable than configuration 1. On the other hand, if the value of $\Delta\bar{E}$ is positive, configuration 1 is more stable than configuration 2.

For a given tank, the surface energy of a system is dependent on interface areas. To determine a possible configuration in zero-gravity condition, the interfacial areas must be calculated.

### 2.3.2 (a) *Interface Areas of Configuration System 1 ($0^\circ \leq \alpha < 90^\circ$)*

From Fig.2.2.1, for a unit depth (in the z-direction perpendicular to the x-y plan), the liquid-vapor interface area in configuration 1 for contact angle between 0 and 90 degrees may be calculated by integration. Let the area be normalized by the half width of the tank, L, then, the dimensionless liquid-vapor interface area is

$$\bar{A}_{lv,1} = \frac{\pi - 2\alpha}{\cos\alpha} \qquad (2.3.2.1)$$

The dimensionless liquid-solid interface area is easily expressed by

$$\bar{A}_{ls,1} = 2\left(1 + \bar{H}_c + \Delta\bar{H}\right) \qquad (2.3.2.2)$$

where

$$\overline{H}_c = \overline{H}_1 - \frac{1-\sin\alpha}{\cos\alpha} + \frac{\beta_1}{2\cos^2\alpha} - \frac{\tan\alpha}{2} \qquad (2.3.2.3)$$

$$\Delta\overline{H} = \frac{1-\sin\alpha}{\cos\alpha} \qquad (2.3.2.4)$$

Equation (2.3.2.2) may also be written as,

$$\overline{A}_{ls,1} = 2 + 2\,\overline{H}_1 + \frac{\pi - 2\alpha}{2\cos^2\alpha} - \tan\alpha \qquad (2.3.2.5)$$

In the equilibrium state, the area of the liquid-vapor interface is a function of contact angle only, while the area of liquid-solid interface varies with the contact angle and the liquid height.

### 2.3.2 (b) *Interface Areas of Configuration System 1 ($\alpha = 90^o$)*

A contact angle of 90 degrees is the limiting case of configuration 1. Consider the Equations (2.3.2.1) and (2.3.2.5).

$$\overline{A}_{lv,1} = \frac{\pi - 2\alpha}{\cos\alpha} \qquad (2.3.2.1)$$

$$\overline{A}_{ls,1} = 2 + 2\,\overline{H}_1 + \frac{\pi - 2\alpha}{2\cos^2\alpha} - \tan\alpha \qquad (2.3.2.5)$$

As the result of $\alpha$ approaching 90°, cos $\alpha$ towards 0. To solve this problem, L' Hopital's rule is used (details see Section A.4 in Appendix). The interface areas are calculated, respectively, as:

$$\bar{A}_{lv,1} = 2 \tag{2.3.2.6}$$

$$\bar{A}_{ls,1} = 2 + 2\bar{H}_1 \tag{2.3.2.7}$$

### 2.3.2 (c) *Interface Areas of Configuration System 2 ($0° \le \alpha < 45°$)*

From Fig.2.2.2, for a unit depth, the liquid-vapor interface area $A_{lv,2}$ is

$$A_{lv,2} = 4\,\beta_2\,R_2 \tag{2.3.2.8}$$

where

$$\beta_2 = \frac{\pi}{4} - \alpha \tag{2.3.2.9}$$

Making use of Equation (2.2.8)

$$A_{lv,2} = 2\sqrt{2}\left(\frac{\pi}{4} - \alpha\right)\frac{H_a}{\sin\beta_2} \tag{2.3.2.10}$$

The height $H_a$ can be obtained from the conservation of the liquid volume (see A.2 in Appendix).

$$H_a = \sqrt{\frac{2\,L\,H_1}{\eta_2}}\,\sin\beta_2 \qquad (2.3.2.11)$$

where

$$\eta_2 = \sin^2\beta_2 + \sin\beta_2\cos\beta_2 - \beta_2 \qquad (2.3.2.12)$$

Thus

$$\overline{A}_{lv,2} = (\pi - 4\,\alpha)\sqrt{\frac{\overline{\overline{H}}_1}{\eta_2}} \qquad (2.3.2.13)$$

The liquid-solid interface area $A_{ls,2}$ is

$$A_{ls,2} = 4\,H_a \qquad (2.3.2.14)$$

Similarly, the liquid-solid interface area $\overline{A}_{ls,2}$ can be calculated

$$\overline{A}_{ls,2} = \sqrt{\frac{32\,\overline{\overline{H}}_1}{\eta_2}}\,\sin\beta_2 \qquad (2.3.2.15)$$

The difference of the liquid-vapor and liquid-solid interface areas between configurations 1 and 2 can be calculated, respectively.

$$\Delta\left|\overline{A}_{lv}\right| = \frac{\Delta\left|A_{lv}\right|}{L} = 4\left(\frac{\pi}{4} - \alpha\right)\sqrt{\frac{\overline{\overline{H}}_1}{\eta_2}} - \frac{\pi - 2\,\alpha}{\cos\alpha} \qquad (2.3.2.16)$$

$$\Delta\left|\overline{A}_{ls}\right| = \frac{\Delta\left|A_{ls}\right|}{L} = \sqrt{\frac{32\,\overline{\overline{H}}_1}{\eta_2}}\,\sin\beta_2 - 2\left(1 + \overline{H}_1 + \frac{\beta_1}{2\cos^2\alpha} - \frac{\tan\alpha}{2}\right) \qquad (2.3.2.17)$$

### 2.3.2 (d) *Interface Areas of Configuration System 2 ($45^{o} < \alpha \leq 90^{o}$)*

The equation of liquid-vapor interface area $\overline{A}_{ls,2}$ of the configuration system 2 for the contact angles from 45 to 90 degrees, as shown in Fig.2.2.3, has similar form as one for the contact angles from 0 to 45 degrees.

$$\overline{A}_{lv,2} = (4\,\alpha - \pi)\sqrt{\frac{\overline{\overline{H}}_1}{\eta_2}} \tag{2.3.2.18}$$

where

$$\eta_2 = \sin^2\beta_2 - \sin\beta_2\cos\beta_2 + \beta_2 \tag{2.3.2.19}$$

$$\beta_2 = \alpha - \frac{\pi}{4} \tag{2.3.2.20}$$

The liquid-solid interface area is

$$\overline{A}_{ls,2} = \sqrt{\frac{32\,\overline{\overline{H}}_1}{\eta_2}}\,\sin\beta_2 \tag{2.3.2.21}$$

The differences of the liquid-vapor and liquid-solid areas between configurations 1 and 2 can be respectively expressed as:

$$\Delta|\overline{A}_{lv}| = \frac{\Delta|A_{lv}|}{L} = 4\left(\alpha - \frac{\pi}{4}\right)\sqrt{\frac{\overline{\overline{H}}_1}{\eta_2}} - \frac{\pi - 2\,\alpha}{\cos\alpha} \tag{2.3.2.22}$$

and

$$\Delta\left|\overline{A}_{ls}\right| = \frac{\Delta\left|A_{ls}\right|}{L} = \sqrt{\frac{32\,\overline{H}_1}{\eta_2}}\,\sin\beta_2 - 2\left(1 + \overline{H}_1 + \frac{\beta_1}{2\cos^2\alpha} - \frac{\tan\alpha}{2}\right) \qquad (2.3.2.23)$$

### 2.3.2 (e) *Interface Areas of Configuration System 2 ($\alpha = 45^o$)*

Consider the Equations (2.3.2.18) and (2.3.2.21) at the contact angle of 45 degrees. As $\alpha$ approaches $45^o$, $\beta_2$ tends to be 0. Consequently, $\eta_2$ is also approaching zero. The radius $\overline{R}_2$ is going to be infinite so that the interface would become flat. This difficulty can be overcome by applying L' Hopital's rule to the Equation twice. One obtains the liquid-vapor and liquid-solid interface areas at the contact angle of 45 degrees, respectively.

$$\overline{A}_{lv,2} = 4\sqrt{\overline{H}_1} \qquad (2.3.2.24)$$

$$\overline{A}_{ls,2} = \sqrt{32\,\overline{H}_1} \qquad (2.3.2.25)$$

### 2.3.3 *Energy Difference between configurations 1 and 2*

### 2.3.3 (a) *($0^o \le \alpha < 45^o$)*

The systems with contact angle between 0 and 45 degrees are considered. Substituting the expressions for $\Delta\left|\overline{A}_{lv}\right|$ and $\Delta\left|\overline{A}_{ls}\right|$ in Equation (2.3.1.5) by Equations (2.3.2.16) and (2.3.2.17), the energy difference between configurations 1 and 2 is then calculated.

$$\Delta\bar{E} = 4\left(\frac{\pi}{4} - \alpha\right)\sqrt{\frac{\bar{H}_1}{\eta_2}} - \frac{\pi - 2\alpha}{\cos\alpha} - \cos\alpha\left\{\sqrt{\frac{32\,\bar{H}_1}{\eta_2}}\,\sin\beta_2 - 2\left(1 + \bar{H}_1 + \frac{\pi - 2\alpha}{4\cos^2\alpha} - \frac{\tan\alpha}{2}\right)\right\} \tag{2.3.3.1}$$

Equation (2.3.3.1) can be used to predict the most likely configuration. Figure 2.3.1 shows the relationship between liquid-vapor interface area and energy at contact angle of 9°. This shows that the smaller the normalized liquid-vapor interface area, the smaller the surface energy when $\Delta\bar{E} \leq 0$. This type of configuration is more stable and more likely to be formed for certain amounts of liquid while sustaining the same contact angles. These stable interface configurations are expected when no kinetic energy exists in the liquid. The equilibrium configurations are conditions of minimum surface energy. Any disturbance, causing some other shape of the interface, results in an increase in surface energy at the expense of kinetic energy. This implies that the state with the smallest liquid-vapor interface is the one with the absolute minimum energy provided the energy difference being less zero. The interface area will reach the minimum through a dynamic process if the initial interface area is not at the minimum. If it is at the local minimum then given an appropriate disturbance it might degenerate to the absolute minimum state. The system will tend to be the configuration with the absolute minimum energy.

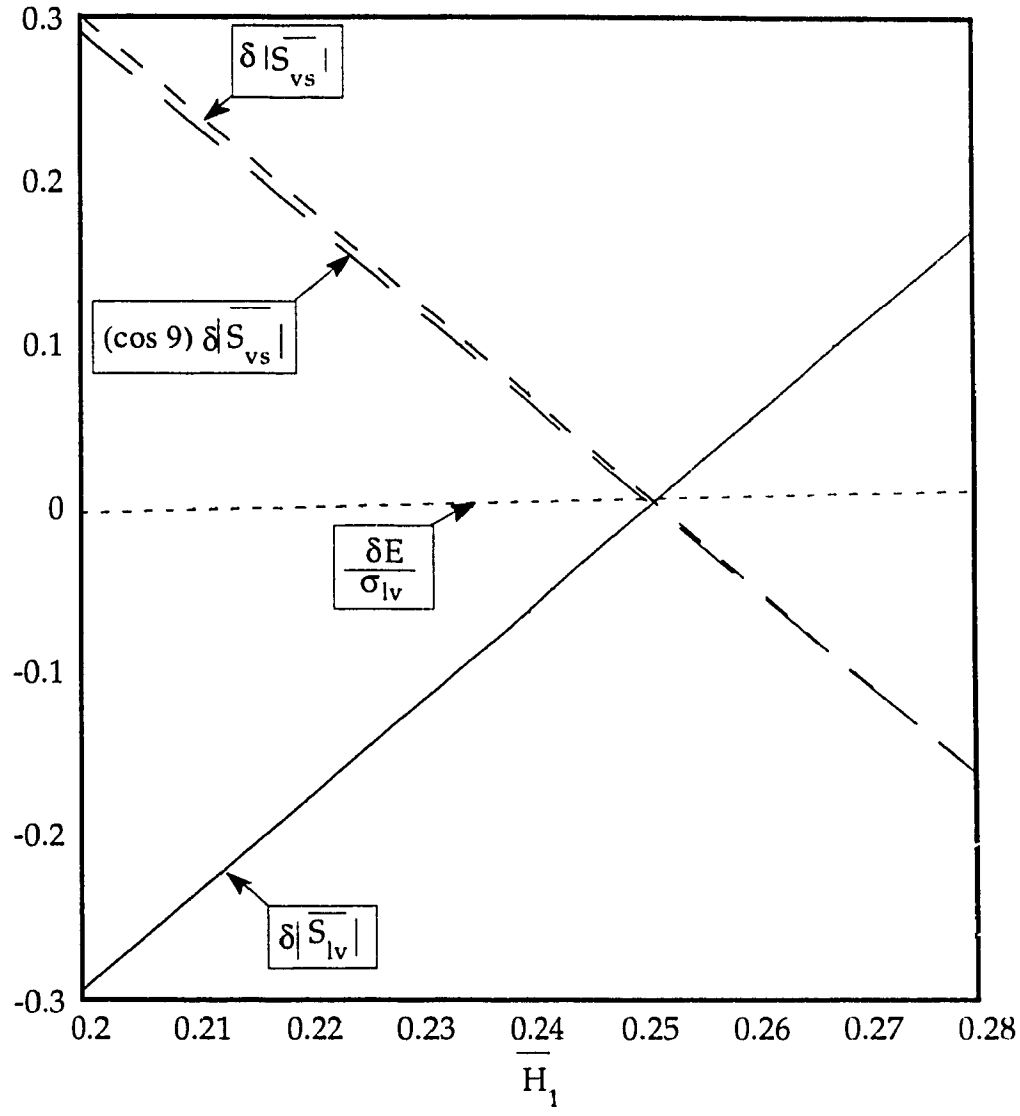


Fig.2.3.1 The relationship between liquid-vapor interface area and energy difference at $\alpha = 9^o$

The energy difference distribution with different contact angles is shown in Fig.2.3.2. All the curves intersect at point B where liquid height $\overline{H}_1$ is about 0.248. $\Delta\overline{E}$ is increasing with the increase of liquid height if the value of $\overline{H}_1$ is beyond point B. The value of $\Delta\overline{E}$ is increasing with the contact angle for the same liquid height. However, positive $\Delta\overline{E}$ for a number of contact angles when $\overline{H}_1$ is less than the value at point B is not a real solution since there will not be enough liquid to maintain configuration 1 (see Section 2.4). The energy differences with contact angle are shown in Fig.2.3.3. The energy difference is always positive for the contact angle between 0 to 45 degrees if the liquid height is above the height of 0.3, indicating that configuration 1 is preferred. The difference in energy $\Delta\overline{E}$ also increases with the contact angle. For the liquid height lower than 0.3, the $\Delta\overline{E}$ may be positive or negative depending on the contact angle.

*2.3.3 (b)* $(\alpha = 45^\circ)$

The energy difference at 45 degrees can be expressed (detail calculation see A.4 in Appendix) as follows:

$$\Delta\overline{E}_{45^\circ} = 4\sqrt{\overline{H}_1} - \frac{2\left(\frac{\pi}{2}-\frac{\pi}{4}\right)}{\sin 45^\circ} - \cos 45^\circ\left[\sqrt{32\,\overline{H}_1} - 2\left(1+\overline{H}_1+\frac{\frac{\pi}{2}-\frac{\pi}{4}}{2\cos^2 45^\circ}-\frac{\tan 45^\circ}{2}\right)\right] \qquad (2.3.3.2)$$

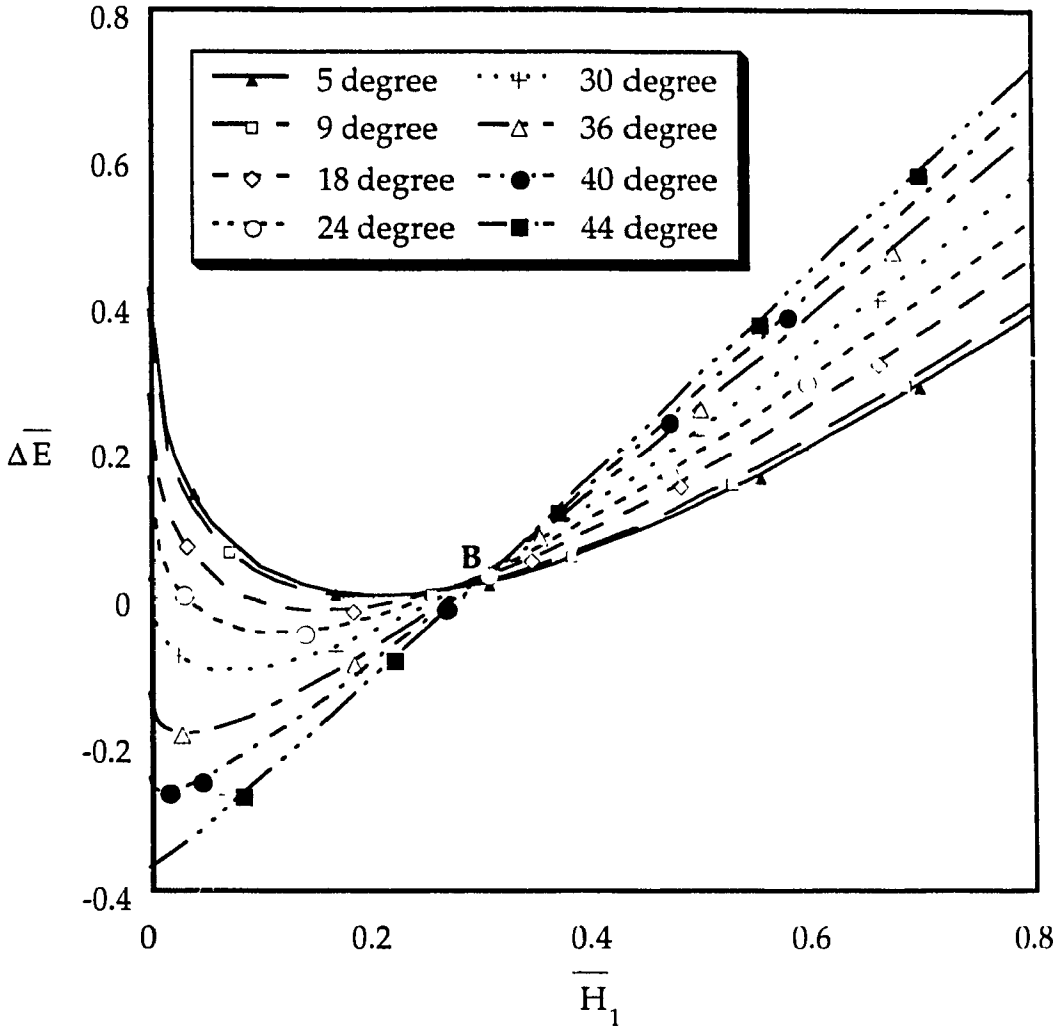


Fig.2.3.2 Distribution of energy differences versus liquid height

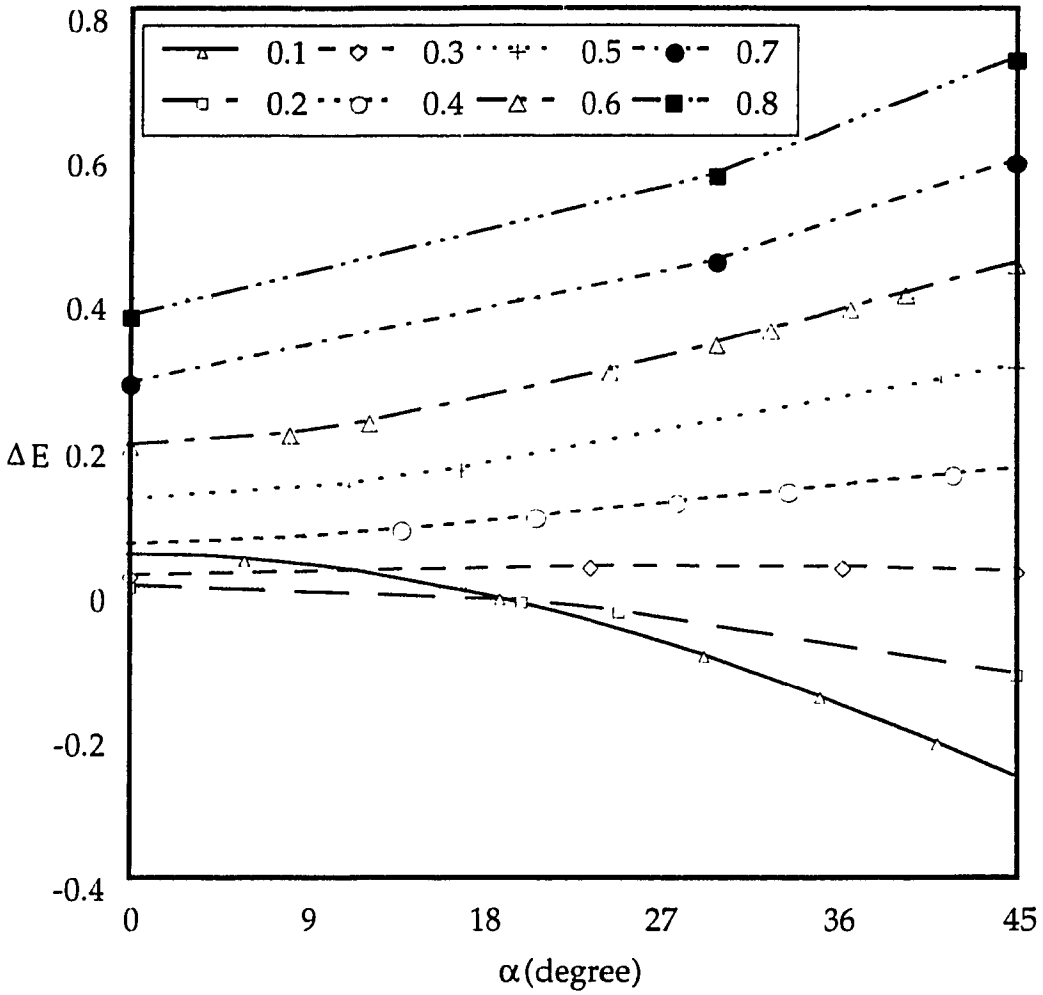


Fig.2.3.3 The energy differences versus contact angle

At the limit case, the above Equation can be simplified as

$$\Delta\overline{E}_{45^o} = \sqrt{2}\ \overline{H}_1 + \sqrt{2}\left(\frac{1}{2} - \frac{\pi}{4}\right) \tag{2.3.3.3}$$

*2.3.3 (c)* *($45^o < \alpha \leq 90^o$)*

Similar to the analysis presented in Section 2.3.3 (a), the energy difference for the contact angle between 45 and 90 degrees is

$$\begin{aligned}\Delta\overline{E} = {} & 4\left(\alpha - \frac{\pi}{4}\right)\sqrt{\frac{\overline{H}_1}{\eta_2}} - \frac{\pi - 2\alpha}{\cos\alpha} \\ & - \cos\alpha\left\{\sqrt{\frac{32\,\overline{H}_1}{\eta_2}}\sin\beta_2 - 2\left(1 + \overline{H}_1 + \frac{\pi - 2\alpha}{4\cos^2\alpha} - \frac{\tan\alpha}{2}\right)\right\}\end{aligned} \tag{2.3.3.4}$$

where

$$\eta_2 = \sin^2\beta_2 - \sin\beta_2\cos\beta_2 + \beta_2 \tag{2.3.3.5}$$

$$\beta_2 = \alpha - \frac{\pi}{4} \tag{2.3.3.6}$$

*2.3.3 (d)* $(\alpha = 90^o)$

The energy difference at 90 degrees can be expressed (detail see A.4 in Appendix) as follows:

$$\Delta\bar{E}_{90^o} = 2\sqrt{\pi \bar{H}_1} - 2 \qquad (2.3.3.7)$$

## 2.4 Limit Conditions of Configuration

### *2.4.1 Minimum Liquid Height $H_{1min}$ ($0 \le \alpha < 90^{o}$)*

The equilibrium condition requires that the system satisfies Young's equation. Initially, the system is at configuration 1, as shown in Fig.2.2.1. If a liquid-vapor interface at centerline in 0-g equilibrium state reaches the bottom of the tank, or $\overline{H}_c$ equals zero, the liquid will be separated into two parts staying at the lower corners of the tank. Configuration 2 becomes the only possible configuration and configuration 1 does not exist any longer since there is no sufficient liquid to maintain. The minimum liquid volume is defined as the volume required to maintain configuration 1 possible. The minimum volume requirement may be expressed by the minimum liquid height at the 1-g field, $H_{1min}$, which can be determined by the conservation of liquid volume since it remains unchanged at any gravitational field. Consider configuration 1, as shown in Fig.2.2.1, for a unit thickness in z-direction which is perpendicular to x-y plan, the liquid volume of configuration system 1, $V_1$, in zero-gravity environment is

$$V_1 = 2\,L\,H_c + 2\,L^2\left(\frac{1-\sin\alpha}{\cos\alpha} - \frac{\beta_1}{2\cos^2\alpha} + \frac{\tan\alpha}{2}\right) \qquad (2.4.1.1)$$

The liquid volume $V_1$ under gravitational condition is

$$V_1 = 2LH_1 \qquad (2.4.1.2)$$

where $H_1$ is the liquid height in 1-g condition, which may be used as the representation of the liquid volume in the tank. Length parameters are normalized by the half width of the tank L. By the previous assumption of conservation of mass, the liquid volume $V_1$ in 1-g condition is the same as in 0-g environment. The dimensionless liquid height $\overline{H}_1$, is thus obtained by equating Equations (2.4.1.1) and (2.4.1.2).

$$\overline{H}_1 = \overline{H}_c + \frac{1}{2\cos^2\alpha}\left\{\cos\alpha(2-\sin\alpha) - \left(\frac{\pi}{2}-\alpha\right)\right\} \qquad (2.4.1.3)$$

Applying the criterion of the minimum liquid height, the minimum liquid height $\overline{H}_{1min}$, is

$$\overline{H}_{1min} = \frac{1-\sin\alpha}{\cos\alpha} - \frac{\pi-2\alpha}{4\cos^2\alpha} + \frac{\tan\alpha}{2} \qquad (2.4.1.4)$$

The minimum liquid volume is a criterion for determination of the lower limit of a possible configuration 1. The configuration can be determined by comparing the liquid height to the minimum value. If the liquid height is less than the minimum liquid height, then configuration 2 is the solution.

### 2.4.2 *Maximum Liquid Height $H_{1max}$*

#### 2.4 2 *(a)* $(0 \le \alpha < 45^\circ)$

The liquid from both parts in configuration 2 will meet each other to form configuration 1 if the liquid volume is larger than certain amount. Configuration 2 will disappear. Configuration 1 becomes the only possible

configuration. The certain amount of liquid volume, which may be called as the maximum liquid volume, is required to make configuration 2 possible. The maximum volume requirement may be expressed by the maximum liquid height at the 1-g field, $H_{1max}$, which can be determined by the unchanged liquid volume condition. For a unit thickness in z-direction which is perpendicular to x-y plan, as shown in Fig.2.2.2, the total liquid volume of configuration 2 in zero-gravity environment, $V_2$ is the sum of the left and right parts. Mathematically,

$$V_2 = \frac{\eta_2 H_a^2}{\sin^2\beta_2} \tag{2.4.2.1}$$

where

$$\eta_2 = \sin^2\beta_2 + \sin\beta_2 \cos\beta_2 - \beta_2 \tag{2.4.2.2}$$

$$\beta_2 = \frac{\pi}{4} - \alpha \tag{2.4.2.3}$$

The liquid volume $V_2$ in 1-g condition is $V_2 = 2LH_1$. The liquid volume remains unchanged at any gravity level. The liquid height in 1-g environment $H_1$ is, therefore, determined

$$H_1 = \frac{H_a^2}{2L \sin^2\beta_2}\eta_2 \tag{2.4.2.4}$$

If $H_a \rightarrow L$, the result is

$$V_2 = \frac{\eta_2 L^2}{\sin^2\beta_2} \tag{2.4.2.5}$$

which is the liquid volume for configuration 2 to be maximum. If the liquid volume is larger than the maximum value, the liquid from both parts will meet each other to form configuration system 1. Therefore, the maximum value of dimensionless liquid height $\overline{H}_1$ is defined by:

$$\overline{H}_{1max} = \frac{\eta_2}{2\sin^2\beta_2} \tag{2.4.2.6}$$

*2.4.2 (b)* *(45 $^o$< $\alpha$ < 90$^o$)*

Following the same procedure to obtain the maximum liquid height used for the contact angle between 0 and 45 degrees, the maximum value of dimensionless $H_1$ may be written as:

$$\overline{H}_{1max} = \frac{\eta_2}{2\sin^2\beta_2} \tag{2.4.2.7}$$

where

$$\eta_2 = \sin^2\beta_2 - \sin\beta_2\cos\beta_2 + \beta_2 \tag{2.4.2.8}$$

$$\beta_2 = \alpha - \frac{\pi}{4} \tag{2.4.2.9}$$

### 2.4.2 (c) *Maximum Liquid Height $H_{1max}$ ($\alpha = 45^{o}$)*

Rearrange the Equation (2.4.2.4)

$$H_a = \sqrt{\frac{2\,L\,H_1}{\eta_2}}\,\sin\beta_2 \qquad (2.4.2.10)$$

Combining the above Equation with the Equation (2.2.8), yields

$$\overline{R}_2 = \sqrt{\frac{\overline{H}_1}{\eta_2}} \qquad (2.4.2.11)$$

Consider the limit of the Equations (2.4.2.2), (2.4.2.3) and (2.4.2.11). As $\alpha$ approaches 45°, $\beta_2$ goes to zero resulting in $\eta_2$ approaching zero. As a result, $\overline{R}_2$ is thereby going to be infinite and the interface would become flat which is unrealistic. To overcome the difficulty of obtaining the maximum height at 45°, L' Hopital's rule is applied (see A.4 in Appendix). The maximum height limit for configuration 2 is:

$$\overline{H}_{1max,\,45^{o}} = \frac{1}{2} \qquad (2.4.2.12)$$

## 2.5 Critical Liquid Height

*2.5 (a)* $(0 \le \alpha < 45^{o})$

If the energy difference between configurations 1 and 2 is equal to zero, a system can take either configuration 1 or 2. When the energy difference is positive, configuration 1 has less energy than the configuration 2. Configuration 1 has more energy than the configuration 2 if the energy difference is negative. The sign of the energy difference can be served to determined which one is more stable. Based on the concept, the liquid height $H_1$ corresponding to the zero value of $\Delta\bar{E}$ is defined as the critical liquid height, $H_{1cr}$. At the critical liquid height, the energy difference equals zero in Equation (2.3.3.1). One can write

$$\overline{H}_{1cr} + \left\{ \frac{(\pi - 4\alpha)}{2\cos\alpha} \sqrt{\frac{1}{\eta_2}} - \sin\beta_2 \sqrt{\frac{8}{\eta_2}} \right\} \sqrt{\overline{H}_{1cr}} + 1 - \frac{\pi - 2\alpha}{4\cos^2\alpha} - \frac{\tan\alpha}{2} = 0 \quad (2.5.1)$$

The critical liquid height is obtained from Equation (2.5.1) (see A.3 in Appendix),

$$\overline{H}_{1cr} = \left\{ \frac{\left( \sqrt{2}\sin\beta_2 - \frac{\beta_2}{\cos\alpha} \right) \frac{1}{\sqrt{\eta_2}} + }{\sqrt{\left[ \frac{\beta_2}{\cos\alpha} - \sqrt{2}\sin\beta_2 \right]^2 \frac{1}{\eta} - \left( 1 - \frac{\pi - 2\alpha}{4\cos^2\alpha} - \frac{\tan\alpha}{2} \right)}} \right\}^2 \quad (2.5.2)$$

where

$$\beta_2 = \frac{\pi}{4} - \alpha \tag{2.5.3}$$

$$\eta_2 = \sin^2\beta_2 + \sin\beta_2 \cos\beta_2 - \beta_2 \tag{2.5.4}$$

*2.5 (b)* *($45^o < \alpha \leq 90^o$)*

Following the same procedure as for the contact angle of 45 to 90 degrees, the critical liquid height has the following expression:

$$\overline{H}_{1cr} = \left\{ \left( \sqrt{2}\sin\beta_2 - \frac{(4\alpha - \pi)}{4\cos\alpha} \right) \frac{1}{\sqrt{\eta_2}} + \sqrt{\left[ \frac{(4\alpha - \pi)}{4\cos\alpha} - \sqrt{2}\sin\beta_2 \right]^2 \frac{1}{\eta} - \left( 1 - \frac{\pi - 2\alpha}{4\cos^2\alpha} - \frac{\tan\alpha}{2} \right)} \right\}^2 \tag{2.5.5}$$

where

$$\eta_2 = \sin^2\beta_2 - \sin\beta_2 \cos\beta_2 + \beta_2 \tag{2.5.6}$$

$$\beta_2 = \alpha - \frac{\pi}{4} \tag{2.5.7}$$

*2.5 (c)* $(\alpha = 45^{o})$

Equation (2.5.2) reduces to the following:

$$\overline{H}_{1cr,\ 45^{o}} = \frac{\pi}{4} - \frac{1}{2} \tag{2.5.8}$$

*(d)* $(\alpha = 90^{o})$

Equation (2.5.5) can be reduced to:

$$\overline{H}_{1cr,\ 90^{o}} = \frac{1}{\pi} \tag{2.5.9}$$

## 2.6 Configuration and Stability Prediction

The critical height combined with the limit conditions analyzed in Section 2.4 can be used for predicting the possible liquid-vapor interface configuration. The configuration is subjected to the tank geometry, the liquid height and the contact angle taking into account the maximum, minimum and critical heights. It is a function of the initial 1-g liquid height and the contact angle if the tank shape is given. This correlation is clearly shown in Figs.2.6.1 and 2.6.2 for contact angles less or greater than 45 degrees, respectively. After plotting Equations of these heights, there are four zones corresponding to different configuration systems due to contact angles and liquid heights. Schematic diagrams presented in Fig.2.6.3 show configurations in these zones.

In Zone I, where the liquid height $H_l$ is higher than the maximum height for the given contact angle, configuration 1 is the only possible solution due to the contact angle requirement. A schematic diagram of configuration 1 is shown in frame (a) of Fig.2.6.3.

If the liquid height is less than the $\overline{H}_{1min}$, configuration 1 will not exist since there is not sufficient liquid to maintain it. The only possible solution in Zone II is configuration 2, see frame (b) of Fig.2.6.3.

For the liquid heights between $\overline{H}_{1min}$ and $\overline{H}_{1max}$ there is a multi-configuration region, where these two configurations could co-exist. If the intersect point of a given liquid height and contact angle lies in the Zone III where configuration system 1 will most likely be present since configuration

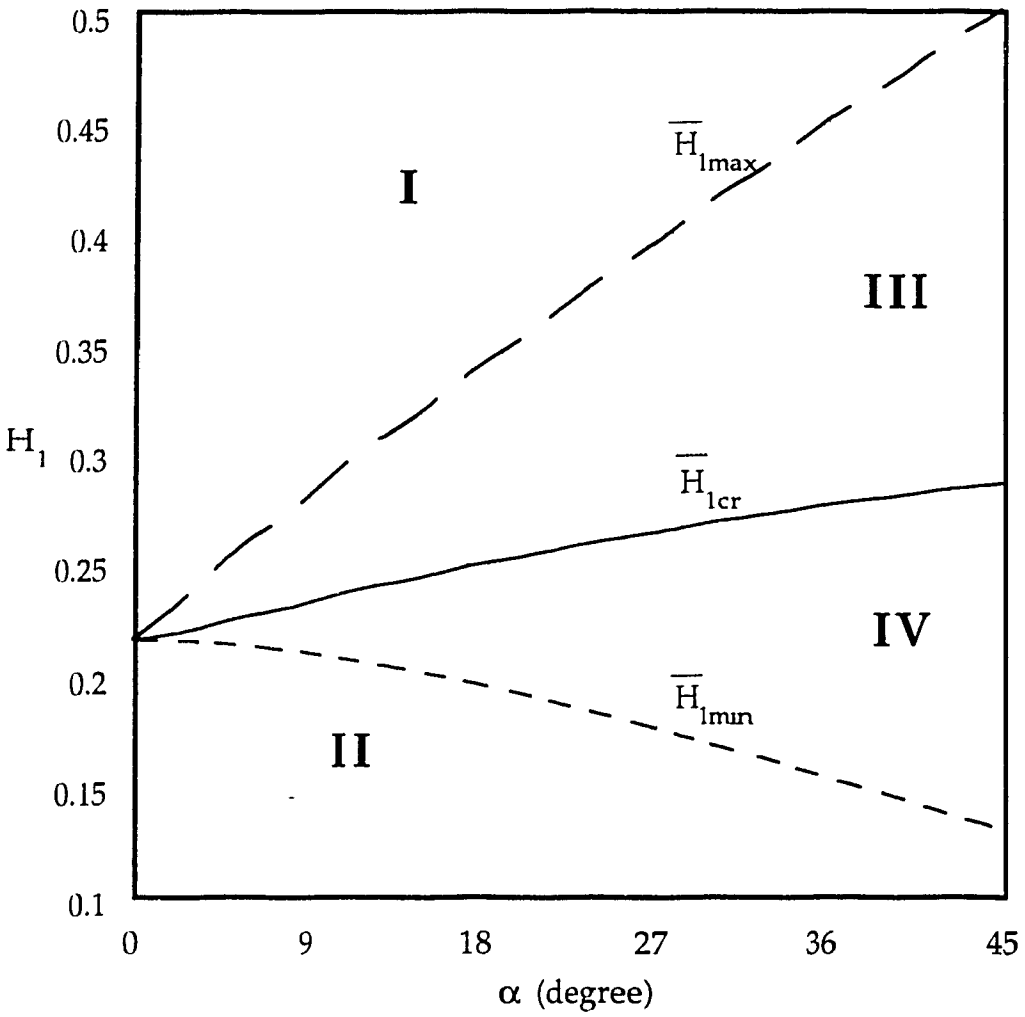


Fig.2.6.1 Liquid height versus contact angle ($0 \leq \alpha \leq 45^{\circ}$)

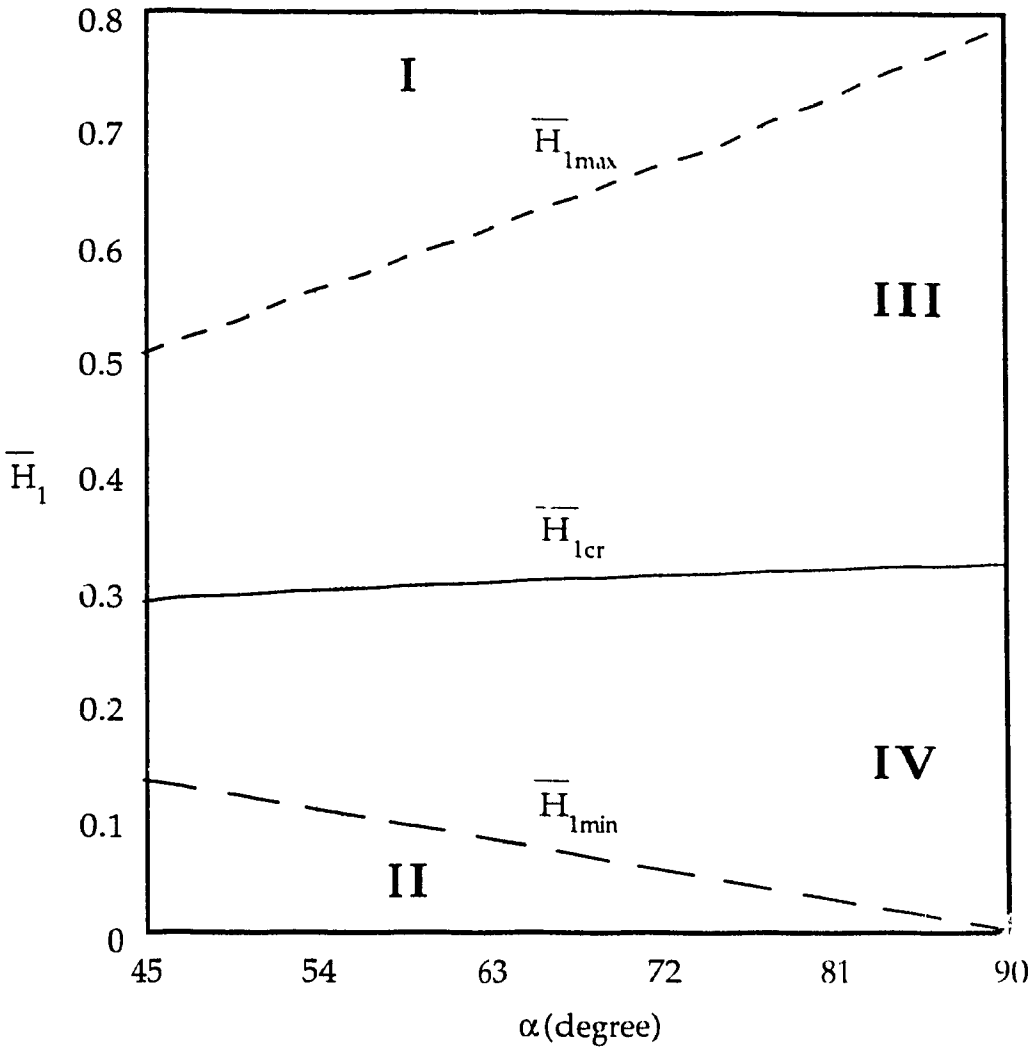


Fig.2.6.2 Liquid height versus contact angle ($45^o \leq \alpha \leq 90^o$)

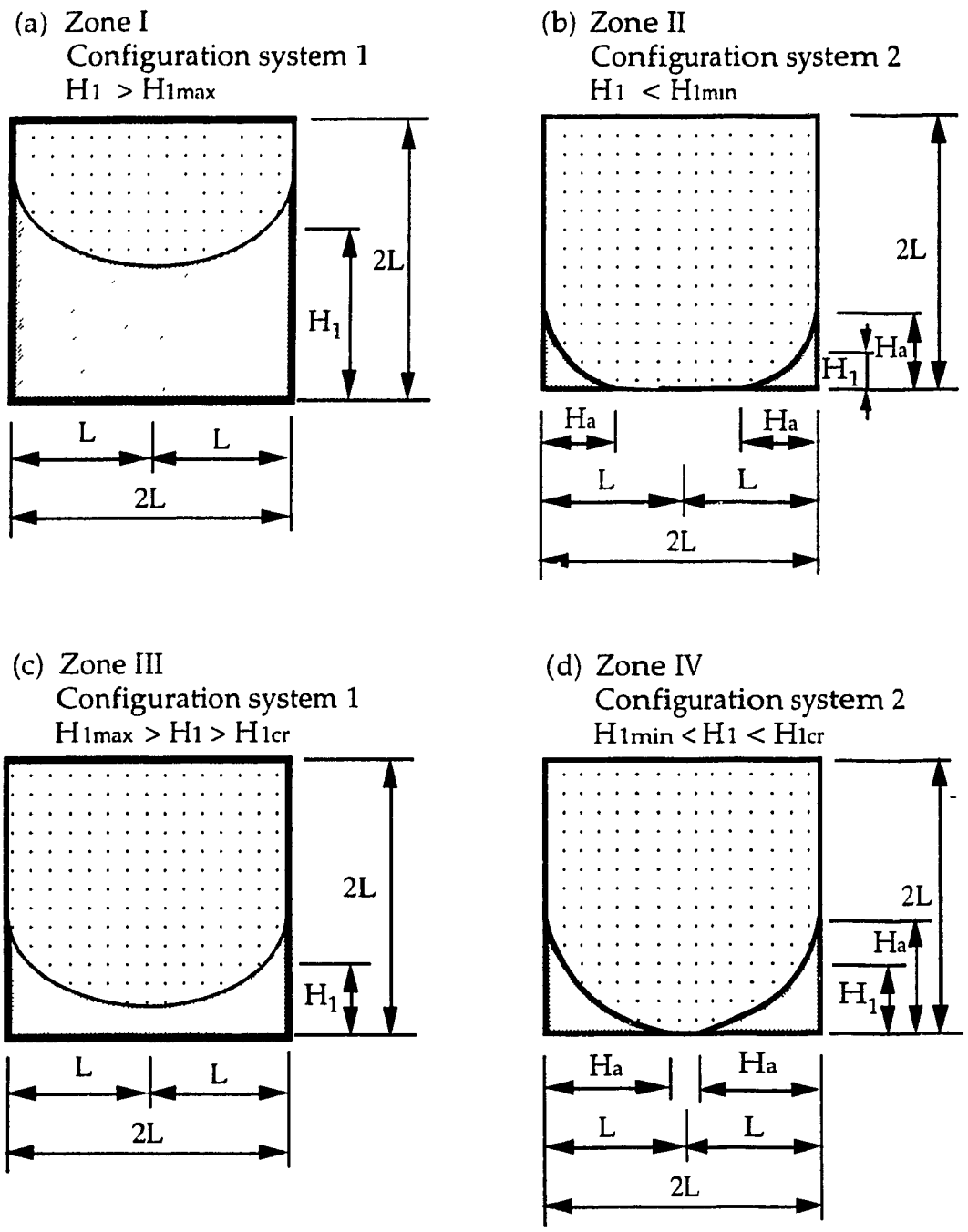


Fig.2.6.3 Schematic diagram of configuration with liquid height

1 has less energy than configuration 2. Configuration 2, however, could be the other solution though it would be less possible and unstable. This phenomenon might be considered as configuration 2 trapped in one of the metastable states. Small perturbations in configuration 2 will result in an increase in energy. If a sufficiently large disturbance is introduced, the system will go to the next more stable state or to the most stable state.

Configuration 2 becomes the most likely configuration if the system is located in the Zone IV while configuration 1 becomes impossible. The frames (c) and (d) in Fig.2.6.3 show configurations 1 and 2 in Zones III and IV, respectively. The range of multi-configuration is expanding with increasing contact angle.

Configuration corresponding to different zones is therefore summarized as:

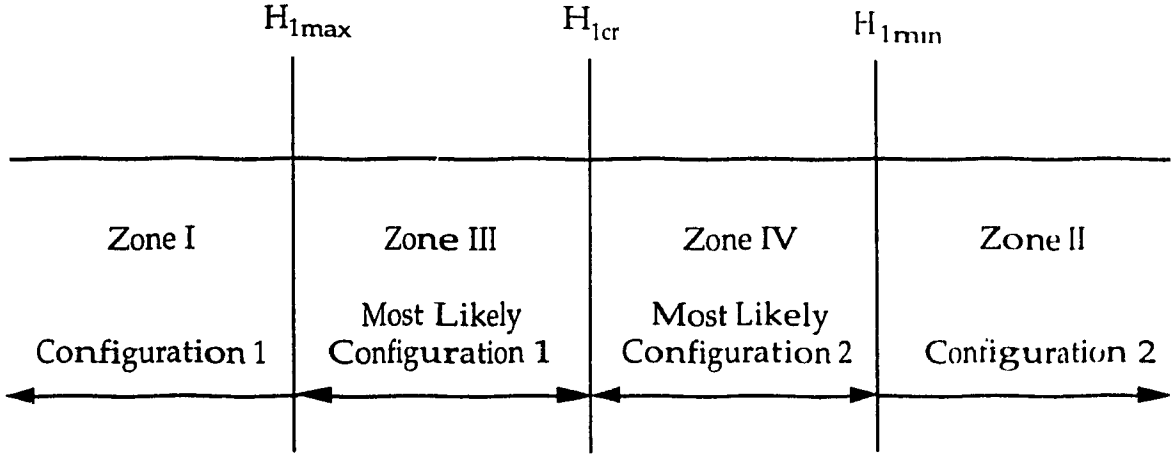


It is clear that the configuration is a function of the initial liquid height and the contact angle. The minimum and maximum liquid heights can be used to define the type of configuration a system will result by comparing the

initial liquid height to the minimum and maximum values if a contact angle is given. The critical liquid height can be used to predict the possible configuration by comparing the liquid height to the critical value. At the critical liquid height, the system can have either configuration system 1 or 2. The above analysis indicates that the minimum, maximum and critical heights have no relation to the height of the tank provided that the latter is higher than these heights. These discussion results can also be used for non-wetting liquid and for a cylindrical tank.

## 2.7 Non-wetting Liquid

Configurations in a rectangular tank partially filled with an non-wetting liquid while the system is exposed to weightlessness are to be investigated. Two important cases concerning configurations 1 and 2 at the zero equilibrium state, previously discussed for the wetting liquid, are still the subject.

### 2.7.1 *Configuration 1* $(90^\circ < \alpha < 145^\circ,\ 145^\circ < \alpha < 180^\circ)$

Configuration system 1 for non-wetting liquid is shown in Fig.2.7.1. As the result of the contact angle requirement in equilibrium, the surface radius is

$$R_1 = -\frac{L}{\cos(\alpha)} \tag{2.7.1.1}$$

Under the equilibrium condition the liquid-vapor interface curve passes through the point $(0, H_c)$, the height of the interface is given by

$$y = H_c - R_1 + \sqrt{R_1^2 - x^2} \tag{2.7.1.2}$$

where

$$H_c = H_1 + \delta \tag{2.7.1.3}$$

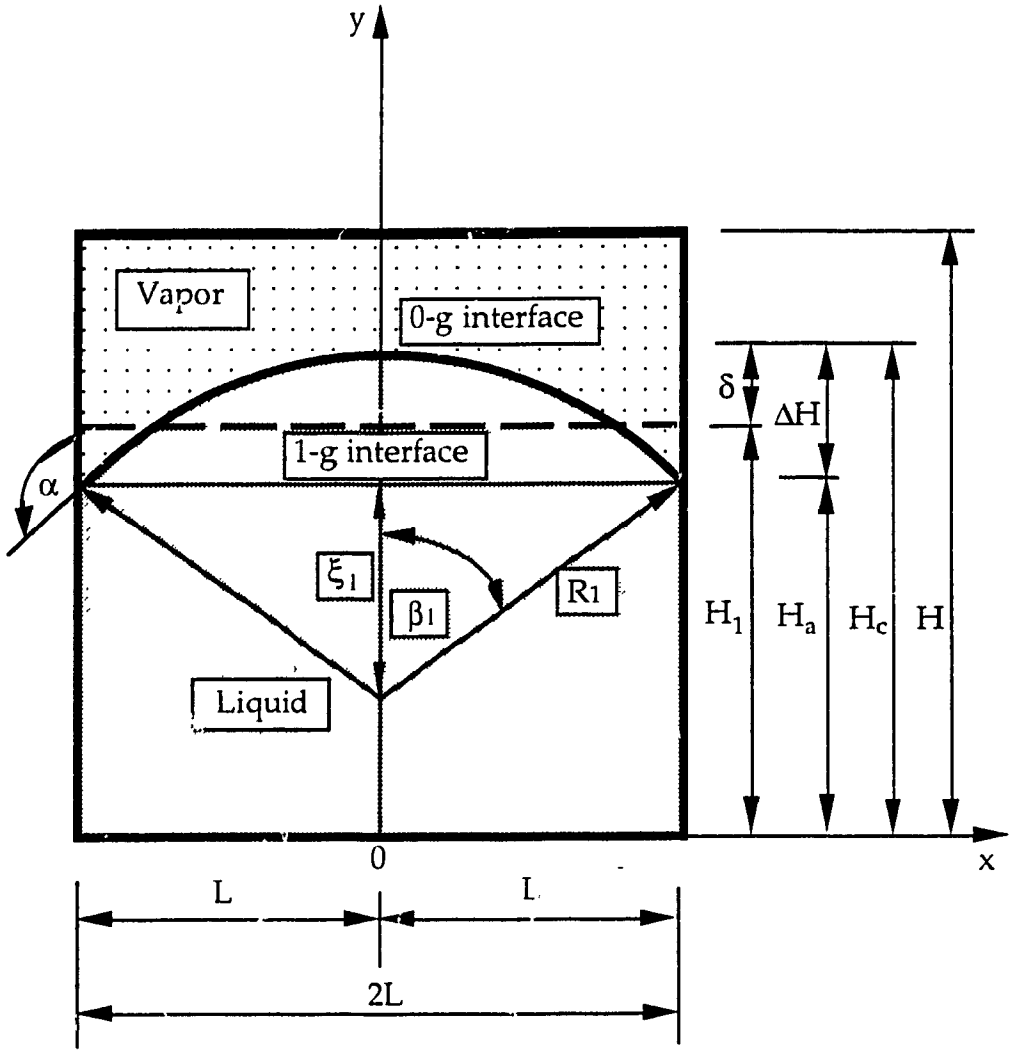


Fig. 2.7.1 Non-wetting liquid configuration system 1 in a rectangular tank

$$\delta = \Delta H - \frac{\beta_1 L}{2\cos^2\alpha} + \frac{L}{2}\tan\alpha \qquad (2.7.1.4)$$

$$\Delta H = H_c - H_a = R_1 - \sqrt{R_1^2 - L^2} \qquad (2.7.1.5)$$

$$\beta_1 = \alpha - \frac{\pi}{2} \qquad (2.7.1.6)$$

All length parameters are normalized by the half width of the tank, L. The liquid-vapor and liquid-solid interface areas are calculated (details see A.5 in Appendix), respectively

$$\overline{A}_{lv,1} = \frac{2\beta_1}{\sin\beta_1} \qquad (2.7.1.7)$$

$$\overline{A}_{ls,1} = 2\overline{H}_1 - \frac{\beta_1}{\sin^2\beta_1} + \cot\beta_1 + 2 \qquad (2.7.1.8)$$

The liquid volume calculation is detailed in A.5 of Appendix. The liquid height is

$$\overline{H}_1 = \overline{H}_a + \frac{1}{2}\left(\frac{\beta_1}{\sin^2\beta_1} - \cot\beta_1\right) \qquad (2.7.1.9)$$

$\overline{H}_1$ will be at minimum when $\overline{H}_a = 0$

$$\overline{H}_{1min} = \frac{1}{2}\left(\frac{\beta_1}{\sin^2\beta_1} - \cot\beta_1\right) \qquad (2.7.1.10)$$

### 2.7.2(a) *Configuration 2* $(90^{\circ} \le \alpha \le 145^{\circ})$

The dimensionless liquid-vapor interface area in configuration 2 shown in Fig.2.7.2 is

$$\bar{A}_{lv,2} = 4\beta_2 \sqrt{\frac{\bar{H}_1}{\eta_2}} \tag{2.7.2.1}$$

where

$$\eta_2 = \sin^2\beta_2 - \sin\beta_2 \cos\beta_2 + \beta_2 \tag{2.7.2.2}$$

$$\beta_2 = \alpha - \frac{\pi}{4} \tag{2.7.2.3}$$

The dimensionless liquid-solid interface area is also expressed as

$$\bar{A}_{ls,2} = \sin\beta_2 \sqrt{\frac{32}{\eta_2}}\ \sqrt{\bar{H}_1} \tag{2.7.2.4}$$

Consider the criteria of the minimum liquid height, the liquid volume remains unchanged, the minimum liquid height is

$$\bar{H}_{1min} = \frac{\beta_1}{2\sin^2\beta_1} - \frac{\cot\beta_1}{2} \tag{2.7.2.5}$$

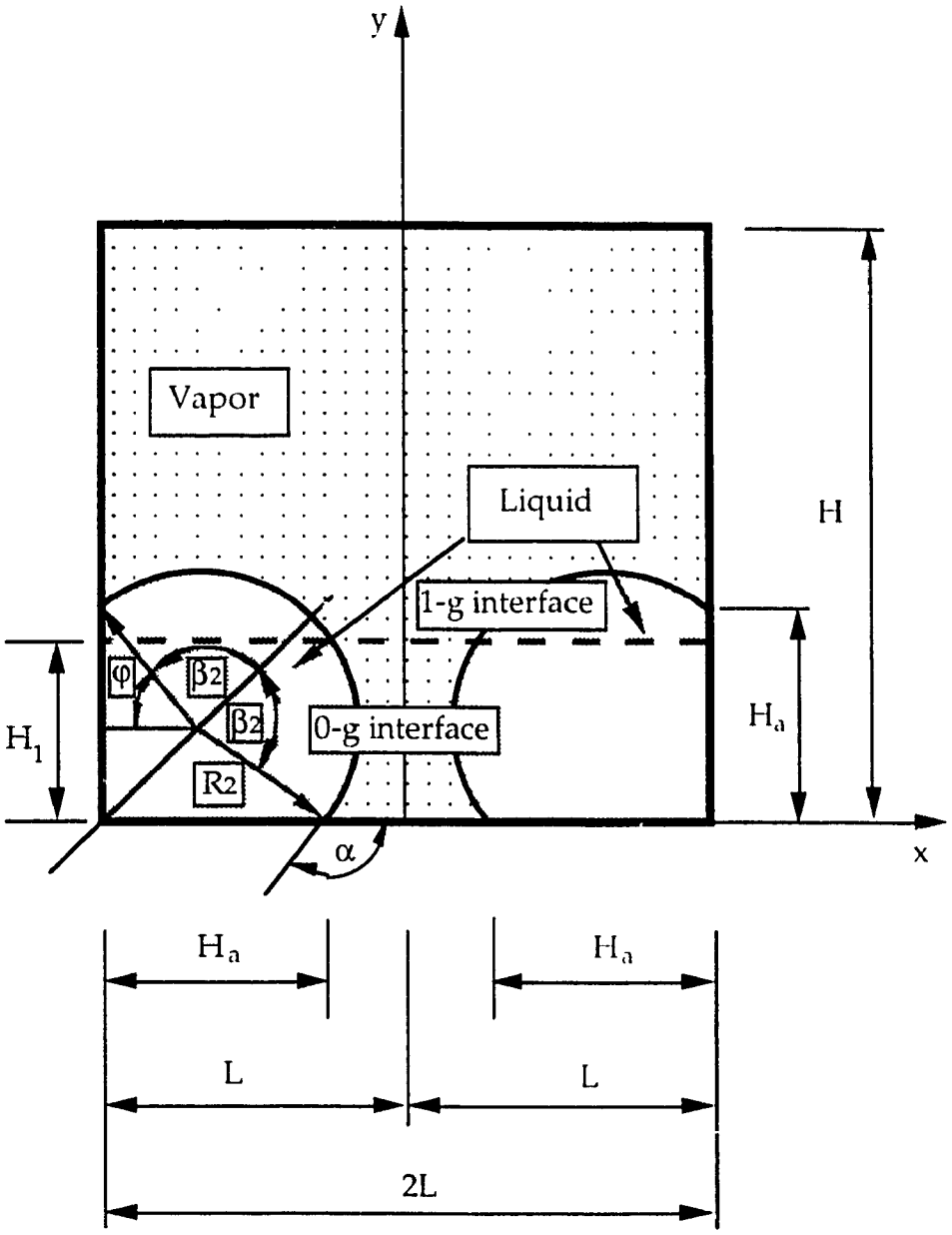


Fig. 2.7.2 Non-wetting liquid configuration system 2 in a rectangular tank

### 2.7.2(b) *Configuration 2* $(145^{o} \le \alpha \le 180^{o})$

The liquid-vapor and liquid-vapor interface areas can be expressed as

$$\overline{A}_{lv,2} = 4\,\beta_2 \sqrt{\frac{\overline{H}_1}{\eta_2}} \tag{2.7.2.6}$$

$$\overline{A}_{ls,2} = \sin\beta_2 \sqrt{\frac{32}{\eta_2}}\,\sqrt{\overline{H}_1} \tag{2.7.2.7}$$

where

$$\eta_2 = \beta_2 - \sin\beta_2 \cos\beta_2 + \sin^2\beta_2 \tag{2.7.2.8}$$

$$\beta_2 = \alpha - \frac{\pi}{4} \tag{2.7.2.9}$$

The maximum liquid height is calculated as:

$$\overline{H}_{1max} = \left(\frac{1}{1+\cos\varphi}\right)^2 \eta_2 \tag{2.7.2.10}$$

### 2.7.2(c) *Critical Liquid Height*

The dimensionless energy difference between configurations 1 and 2 can be calculated

$$\Delta\bar{E} = 4\beta_2\sqrt{\frac{\bar{H}_1}{\eta_2}} - \frac{2\beta_1}{\sin\beta_1}$$

$$-\cos\alpha\left\{\sqrt{\frac{32\bar{H}_1}{\eta_2}}\sin\beta_2 - 2\bar{H}_1 + \left(\frac{\beta_1}{\sin^2\beta_1} - \cot\beta_1\right) - 2\right\} \qquad (2.7.2.11)$$

The dimensionless critical liquid height is calculated as

$$\bar{H}_{1cr} = \left\{ \left(\sqrt{2}\sin\beta_2 - \frac{\beta_2}{\cos\alpha}\right)\frac{1}{\sqrt{\eta_2}} + \sqrt{\left[\frac{\beta_2}{\cos\alpha} - \sqrt{2}\sin\beta_2\right]^2\frac{1}{\eta_2} + \left(\frac{\beta_1}{2\sin^2\beta} + \frac{\beta_1}{\sin\beta\cos\alpha} - \frac{\cot\beta_1}{2} - 1\right)} \right\} \qquad (2.7.2.12)$$

## 2.8 Result Summary

The energy difference and liquid height limitation for the contact angles ranging from 0 to 180 degrees are calculated. The results are listed in the tabulate form, where Pa represents the parameters.

Table 2.8.1 (a) Energy differences $\left(0 < \alpha < \frac{\pi}{4} \text{ and } \frac{\pi}{4} < \alpha < \frac{\pi}{2}\right)$.

| Pa | Values | |
|---|---|---|
| $\alpha$ | $\left[0, \frac{\pi}{4}\right]$ | $\left[\frac{\pi}{4}, \frac{\pi}{2}\right]$ |
| $\beta_1$ | $\frac{\pi}{2} - \alpha$ | $\frac{\pi}{2} - \alpha$ |
| $\beta_2$ | $\frac{\pi}{4} - \alpha$ | $\alpha - \frac{\pi}{4}$ |
| $\eta_2$ | $\sin^2\beta_2 + \sin\beta_2 \cos\beta_2 - \beta_2$ | $\sin^2\beta_2 - \sin\beta_2 \cos\beta_2 + \beta_2$ |
| $\overline{A}_{lv,1}$ | $\frac{\pi - 2\alpha}{\cos\alpha}$ | $\frac{\pi - 2\alpha}{\cos\alpha}$ |
| $\overline{A}_{lv,2}$ | $\beta_2 \sqrt{\frac{\overline{H}_1}{\eta_2}}$ | $\beta_2 \sqrt{\frac{\overline{H}_1}{\eta_2}}$ |
| $\overline{A}_{ls,1}$ | $2 + 2\overline{H}_1 + \frac{\pi - 2\alpha}{2\cos^2\alpha} - \tan\alpha$ | $2 + 2\overline{H}_1 + \frac{\pi - 2\alpha}{2\cos^2\alpha} - \tan\alpha$ |
| $\overline{A}_{ls,2}$ | $\sqrt{\frac{32\overline{H}_1}{\eta_2}} \sin\beta_2$ | $\sqrt{\frac{32\overline{H}_1}{\eta_2}} \sin\beta_2$ |
| $\Delta\overline{E}$ | $4\beta_2\sqrt{\frac{\overline{H}_1}{\eta_2}} - \frac{\pi-2\alpha}{\cos\alpha}$<br>$- \cos\alpha \sqrt{\frac{32\overline{H}_1}{\eta_2}} \sin\beta_2$<br>$+ 2\cos\alpha\left(1 + \overline{H}_1 + \frac{\pi - 2\alpha}{4\cos^2\alpha} - \frac{\tan\alpha}{2}\right)$ | $4\beta_2\sqrt{\frac{\overline{H}_1}{\eta_2}} - \frac{\pi-2\alpha}{\cos\alpha}$<br>$- \cos\alpha \sqrt{\frac{32\overline{H}_1}{\eta_2}} \sin\beta_2$<br>$+ 2\cos\alpha\left(1 + \overline{H}_1 + \frac{\pi - 2\alpha}{4\cos^2\alpha} - \frac{\tan\alpha}{2}\right)$ |

Table 2.8.1 (b) Energy differences $\left(\frac{\pi}{2} < \alpha < \frac{3\pi}{4} \text{ and } \frac{3\pi}{4} < \alpha < \pi\right)$.

| Pa | Values | |
|---|---|---|
| $\alpha$ | $\left[\frac{\pi}{2}, \frac{3\pi}{4}\right]$ | $\left[\frac{3\pi}{4}, \pi\right]$ |
| $\beta_1$ | $\alpha - \frac{\pi}{2}$ | $\alpha - \frac{\pi}{2}$ |
| $\beta_2$ | $\alpha - \frac{\pi}{4}$ | $\alpha - \frac{\pi}{4}$ |
| $\eta_2$ | $\sin^2\beta_2 - \sin\beta_2\cos\beta_2 + \beta_2$ | $\sin^2\beta_2 + \sin\beta_2\cos\beta_2 + \beta_2$ |
| $\overline{A}_{lv,1}$ | $\frac{2\beta_1}{\sin\beta_1}$ | $\frac{2\beta_1}{\sin\beta_1}$ |
| $\overline{A}_{lv,2}$ | $4\beta_2\sqrt{\frac{\overline{\overline{H}}_1}{\eta_2}}$ | $4\beta_2\sqrt{\frac{\overline{\overline{H}}_1}{\eta_2}}$ |
| $\overline{A}_{ls,1}$ | $2\overline{H}_1 - \left(\frac{\beta_1}{\sin^2\beta_1} - \cot\beta_1\right) + 2$ | $2\overline{H}_1 - \left(\frac{\beta_1}{\sin^2\beta_1} - \cot\beta_1\right) + 2$ |
| $\overline{A}_{ls,2}$ | $\sin\beta_2\sqrt{\frac{32}{\eta_2}}\sqrt{\overline{H}_1}$ | $\sin\beta_2\sqrt{\frac{32}{\eta_2}}\sqrt{\overline{H}_1}$ |
| $\Delta\overline{E}$ | $4\beta_2\sqrt{\frac{\overline{\overline{H}}_1}{\eta_2}} - \frac{2\beta_1}{\sin\beta_1}$ | $4\beta_2\sqrt{\frac{\overline{\overline{H}}_1}{\eta_2}} - \frac{2\beta_1}{\sin\beta_1}$ |
| | $-\cos\alpha\sqrt{\frac{32\overline{\overline{H}}_1}{\eta_2}}\sin\beta_2$ | $-\cos\alpha\sqrt{\frac{32\overline{\overline{H}}_1}{\eta_2}}\sin\beta_2$ |
| | $+\cos\alpha\left(2\overline{H}_1 - \frac{\beta_1}{\sin^2\beta_1} + \cot\beta_1 + 2\right)$ | $+\cos\alpha\left(2\overline{H}_1 - \frac{\beta_1}{\sin^2\beta_1} + \cot\beta_1 + 2\right)$ |

Table 2.8.2 (a) Energy differences $\left(\alpha = 0, \frac{\pi}{4} \text{ and } \frac{\pi}{2}\right)$ .

| Pa | Values | | |
|---|---|---|---|
| $\alpha$ | $0$ | $\frac{\pi}{4}$ | $\frac{\pi}{2}$ |
| $\beta_1$ | $\frac{\pi}{2}$ | $\frac{\pi}{4}$ | $0$ |
| $\beta_2$ | $\frac{\pi}{4}$ | $0$ | $\frac{\pi}{4}$ |
| $\eta_2$ | $\frac{4-\pi}{4}$ | $0$ | $\frac{\pi}{4}$ |
| $\overline{A}_{lv,1}$ | $\pi$ | $\frac{\sqrt{2}}{2}\pi$ | $2$ |
| $\overline{A}_{lv,2}$ | $2\pi\sqrt{\frac{\overline{\overline{H}}_1}{4-\pi}}$ | $4\sqrt{\overline{\overline{H}}_1}$ | $2\sqrt{\pi\,\overline{\overline{H}}_1}$ |
| $\overline{A}_{ls,1}$ | $2\overline{H}_1 + \frac{\pi+4}{2}$ | $2\overline{H}_1 + \frac{\pi}{2} + 1$ | $2\left(\overline{H}_1 + 1\right)$ |
| $\overline{A}_{ls,2}$ | $8\sqrt{\frac{\overline{\overline{H}}_1}{4-\pi}}$ | $4\sqrt{2\,\overline{\overline{H}}_1}$ | $8\sqrt{\frac{\overline{\overline{H}}_1}{\pi}}$ |
| $\Delta\overline{\overline{E}}$ | $(2\pi - 8)\sqrt{\frac{\overline{\overline{H}}_1}{4-\pi}} + 2\overline{H}_1 - \frac{\pi}{2} + 2$ | $\sqrt{2}\,\overline{H}_1 - \frac{\sqrt{2}\,\pi}{4} + \frac{\sqrt{2}}{2}$ | $2\left(\sqrt{\pi\,\overline{H}_1} - 1\right)$ |

Table 2.8.2 (b) Energy differences $\left(\alpha = \frac{3\pi}{4} \text{ and } \pi\right)$.

| Pa | Values | |
|---|---|---|
| $\alpha$ | $\frac{3\pi}{4}$ | $\pi$ |
| $\beta_1$ | $\frac{\pi}{4}$ | $\frac{\pi}{2}$ |
| $\beta_2$ | $\frac{\pi}{2}$ | $\frac{3\pi}{4}$ |
| $\eta_2$ | $\frac{\pi+2}{2}$ | $\frac{3\pi}{4}$ |
| $\overline{A}_{lv,1}$ | $\frac{\sqrt{2}}{2}\pi$ | $\pi$ |
| $\overline{A}_{lv,2}$ | $\pi\sqrt{\frac{8\overline{\overline{H}}_1}{\pi+2}}$ | $2\sqrt{3\pi\overline{\overline{H}}_1}$ |
| $\overline{A}_{ls,1}$ | $2\left(\overline{H}_1 - \frac{\pi}{2} + 3\right)$ | $2\left(\overline{H}_1 + 1\right) - \frac{\pi}{2}$ |
| $\overline{A}_{ls,2}$ | $4\sqrt{\frac{2\overline{\overline{H}}_1}{\pi+2}}$ | $8\sqrt{\frac{\overline{\overline{H}}_1}{3\pi}}$ |
| $\Delta\overline{E}$ | $\left(2\sqrt{2}\pi+4\right)\sqrt{\frac{\overline{\overline{H}}_1}{\pi+2}} - \sqrt{2}\left(\overline{H}_1 + \frac{\pi}{4} + \frac{3}{2}\right)$ | $\left(6\pi+8\right)\sqrt{\frac{\overline{\overline{H}}_1}{3\pi}} - 2\overline{H}_1 - \frac{\pi}{2} - 2$ |

Table 2.8.3 (a) Limits of liquid height.

| Pa | Values | |
|---|---|---|
| $\alpha$ | $\left[0, \frac{\pi}{4}\right]$ | $\left[\frac{\pi}{4}, \frac{\pi}{2}\right]$ |
| $\beta_1$ | $\frac{\pi}{2} - \alpha$ | $\frac{\pi}{2} - \alpha$ |
| $\beta_2$ | $\frac{\pi}{4} - \alpha$ | $\alpha - \frac{\pi}{4}$ |
| $\eta_2$ | $\sin^2\beta_2 + \sin\beta_2 \cos\beta_2 - \beta_2$ | $\sin^2\beta_2 - \sin\beta_2 \cos\beta_2 + \beta_2$ |
| $\overline{H}_{1min}$ | $\frac{1 - \sin\alpha}{\cos\alpha} - \frac{\pi - 2\alpha}{4\cos^2\alpha} + \frac{\tan\alpha}{2}$ | |
| $\overline{H}_{1max}$ | $\frac{\eta_2}{2\sin^2\beta_2}$ | |
| $\overline{H}_{1cr}$ | $\left\{ \left(\sqrt{2}\sin\beta_2 - \frac{\beta_2}{\cos\alpha}\right)\frac{1}{\sqrt{\eta_2}} + \sqrt{\left[\frac{\beta_2}{\cos\alpha} - \sqrt{2}\sin\beta_2\right]^2 \frac{1}{\eta_2} - \left(1 - \frac{\pi - 2\alpha}{4\cos^2\alpha} - \frac{\tan\alpha}{2}\right)} \right\}^2$ | |

Table 2.8.3 (b) Limits of liquid heigh'.

| Pa | Values |
|---|---|
| $\alpha$ | $\left[\frac{\pi}{2}, \frac{3\pi}{2}\right]$ |
| $\beta_1$ | $\alpha - \frac{\pi}{2}$ |
| $\beta_2$ | $\alpha - \frac{\pi}{4}$ |
| $\theta$ | $\pi - \alpha$ |
| $\eta_2$ | $\sin^2\beta_2 - \sin\beta_2 \cos\beta_2 + \beta_2$ |
| $\overline{H}_{1min}$ | $\frac{\beta_1}{2\sin^2\beta_1} - \frac{\cot\beta_1}{2}$ |
| $\overline{H}_{1max}$ | $\left(\frac{1}{1+\cos\varphi}\right)^2 \eta_2$ |
| $\overline{H}_{1cr}$ | $\left\{ \left(\sqrt{2}\sin\beta_2 - \frac{\beta_2}{\cos\alpha}\right) \frac{1}{\sqrt{\eta_2}} + \sqrt{\left[\frac{\beta_2}{\cos\alpha} - \sqrt{2}\sin\beta_2\right]^2 \frac{1}{\eta} + \left(\frac{\beta_1}{2\sin 2\beta} + \frac{\beta_1}{\sin\beta\cos\alpha} - \frac{\cot\beta_1}{2} - 1\right)} \right\}^2$ |

## 2.9 Wetting Liquid in Cylindrical Tanks

Similar to the analysis of rectangular tanks, two configuration systems of wetting liquid placed in a flat-bottom circular cylindrical tank in the zero-gravity environment are introduced here. One of them is with the sufficient liquid volume, defined as configuration 3. The other is with not enough volume of liquid to cover the base of the tank under the conditions to be investigated, called as configuration 4.

### 2.9.1 *Interface Areas of Configuration 3*

Consider a liquid-vapor configuration system 3 of a cylindrical tank shown in Fig.2.9.1. The dimensionless liquid-vapor interface area is expressed as:

$$\overline{A}_{lv,3} = \frac{2\pi(1-\sin\alpha)}{\cos^2\alpha} \tag{2.9.1.1}$$

The dimensionless liquid-solid interface area (detail see B.1 in Appendix) is

$$\overline{A}_{ls,3} = 2\pi\left\{\overline{H}_1 + \frac{1-\sin(\alpha)}{\cos^2(\alpha)} - \frac{1}{\cos(\alpha)} + \frac{2}{3}\frac{\left[1-\sin^3(\alpha)\right]}{\cos^3(\alpha)}\right\} + \pi \tag{2.9.1.2}$$

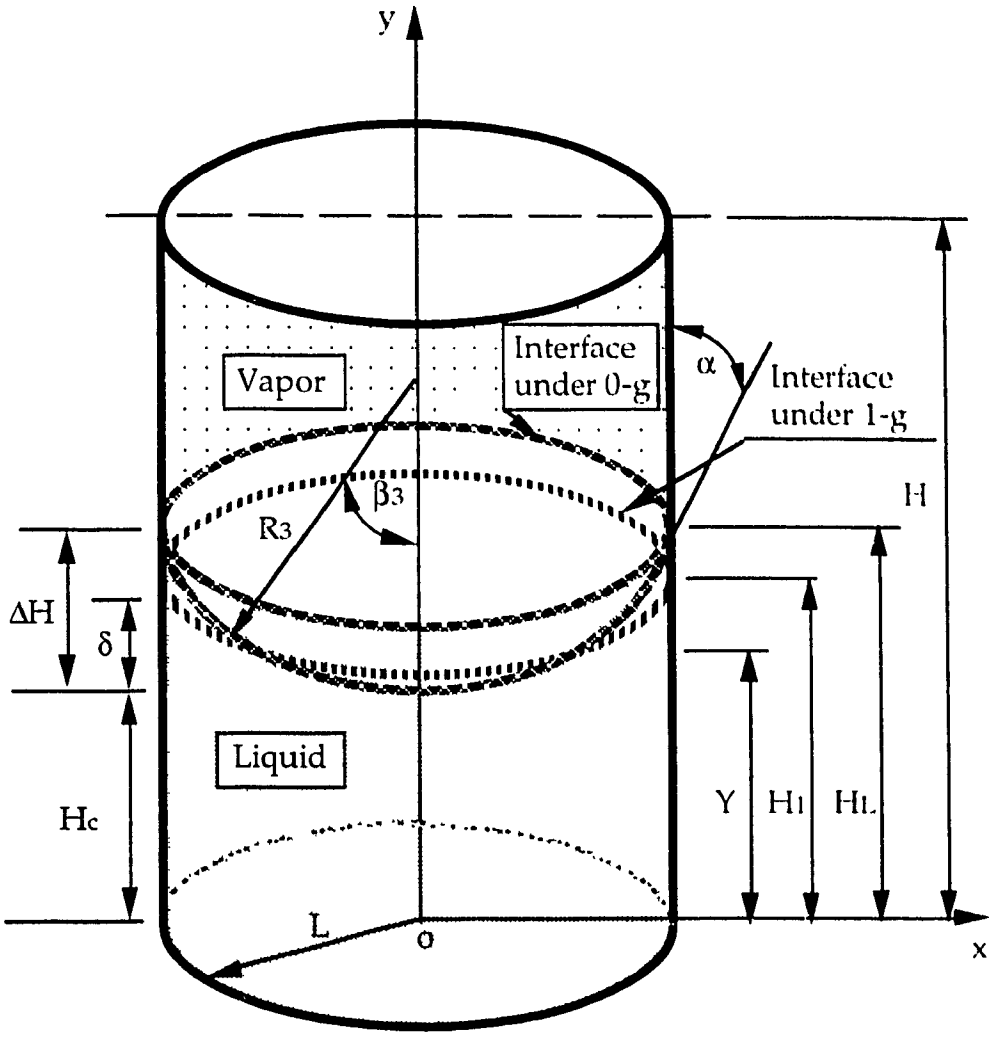


Fig.2.9.1 Configuration system 3 in a cylindrical tank

### 2.9.2 *Interface Areas of Configuration 4*

The alternate interface configuration 4 in a cylindrical tank is presented in Fig.2.9.2. The volume of the liquid is obtained by the integral disc method. The liquid-vapor interface area is calculated by revolving the liquid-vapor interface curve about the y axis. After integration (see B.2 in Appendix), the dimensionless liquid-vapor interface area is

$$\bar{A}_{lv,4} = 2\,\pi\,\bar{R}_4\left[1-\bar{H}_4\left(\frac{\pi}{2}-2\,\alpha\right)\right]^2 \tag{2.9.2.1}$$

where

$$\bar{R}_4 = \frac{\sqrt{2}\,\bar{H}_b}{2\sin\beta_4} \tag{2.9.2.2}$$

$$\bar{H}_4 = -\frac{1}{2}+\frac{\sqrt{H_b^2-\sin^2\beta_4}}{2\sin\beta_4} \tag{2.9.2.3}$$

$$\beta_4 = \frac{\pi}{4}-\alpha \tag{2.9.2.4}$$

$\bar{H}_b$ can be obtained from the conservation of the liquid volume (see B.2 in Appendix).

The liquid-solid interface area is

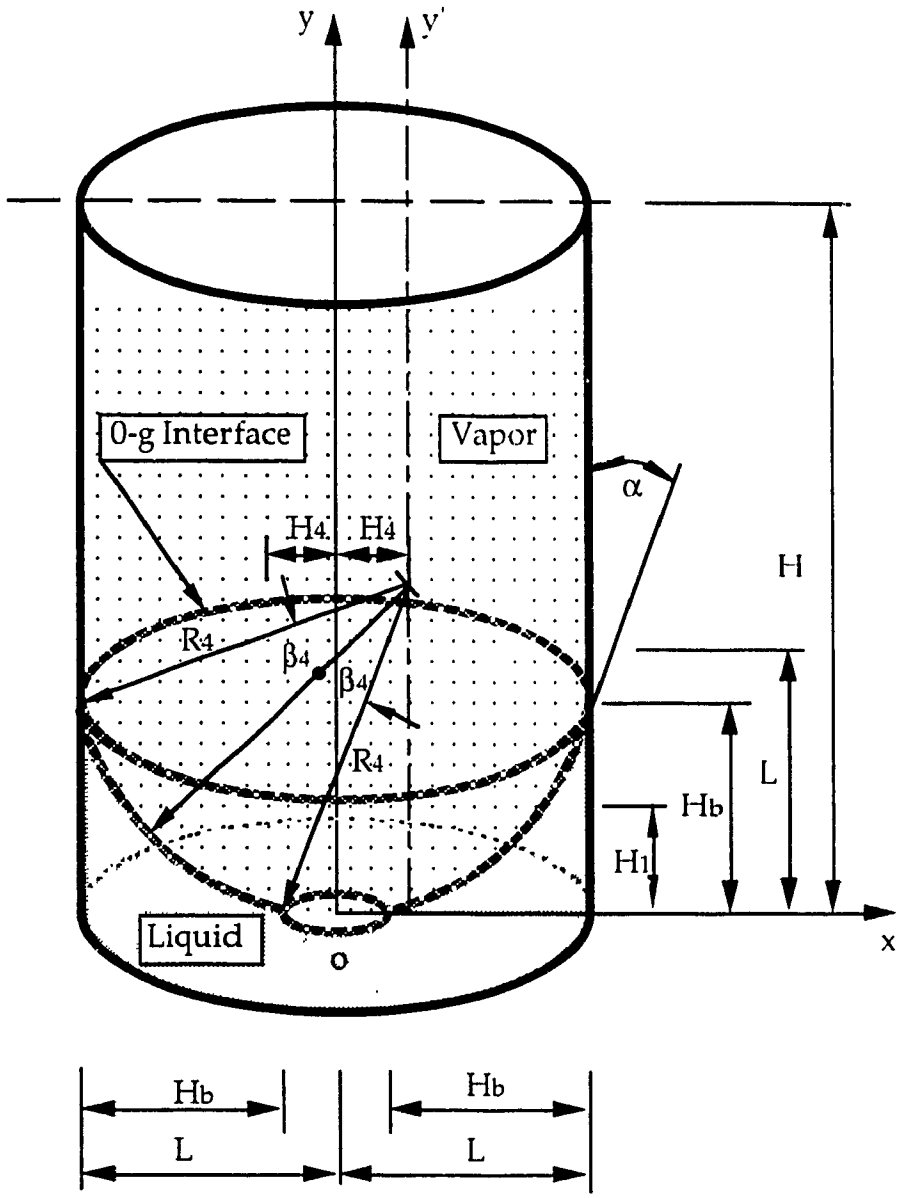


Fig.2.9.2 Configuration system 4 in a cylindrical tank

$$\overline{A}_{ls,4} = \pi \overline{H}_b \left(4 - \overline{H}_b\right) \tag{2.9.2.5}$$

### 2.9.3 *Minimum Liquid Height $H_{1min}$*

The minimum liquid height can be determined by the unaltered liquid volume in the tank throughout the transition of gravitational field.

The dimensionless liquid height in 1-g field is

$$\overline{H}_1 = \frac{(1 - \sin\alpha)}{3\cos\alpha}\left(\frac{2\cos^2\alpha - 1 + \sin\alpha}{\cos^2\alpha}\right) + \overline{H}_c \tag{2.9.3.1}$$

The liquid height will come to the minimum liquid height when the liquid-vapor interface hits the bottom of the tank where the configuration 3 cannot be maintained. The dimensionless minimum liquid height thus is written as

$$\overline{H}_{1min} = (1 - \sin\alpha)\left(\frac{2\cos^2\alpha + \sin\alpha - 1}{3\cos^3\alpha}\right) \tag{2.9.3.2}$$

### 2.9.4 *Maximum Liquid Height $H_{1max}$*

The maximum liquid height can be determined by the liquid volume unchanged throughout the transition of gravitational field. If the liquid wetting length along the side wall of a tank tends to be equal to the half width of the tank, which is $\overline{H}_b \rightarrow 1$, the liquid height in 1-g field is defined as the

dimensionless maximum liquid height $\overline{H}_{1max}$. If the liquid height higher than the maximum liquid height, configuration 3 is the only possible one. The maximum liquid volume corresponding to the maximum liquid height in 0-g environment is

$$V_{4,max} = \pi \left\{ \frac{4}{3} L^3 - R_4^2 L + H_4 L^2 + H_4 R_4^2 \beta_5 \right\} \tag{2.9.4.1}$$

where

$$\beta_5 = \frac{\pi}{2} - 2\alpha \tag{2.9.4.2}$$

The liquid volume in 1-g field is equal to the volume in 0-g condition. The liquid height thus can be calculated as

$$\overline{H}_{1max} = \frac{4}{3} - \overline{R}_4^2 + \overline{H}_4 + \overline{H}_4 \overline{R}_4^2 \beta_5 \tag{2.9.4.3}$$

where

$$\overline{R}_4 = \frac{\sqrt{2}}{2 \sin\beta_4} \tag{2.9.4.4}$$

$$\overline{H}_4 = \frac{\sqrt{1 - \sin^2\beta_4} - \sin\beta_4}{2 \sin\beta_4} \tag{2.9.4.5}$$

$$\beta_4 = \frac{\pi}{4} - \alpha \tag{2.9.4.6}$$

After manipulating, the dimensionless maximum liquid height can also be given as

$$\overline{H}_{1max} = \frac{4}{3} - \frac{1}{2\sin^2\beta_4} + \frac{\cos\beta_4 - \sin\beta_4}{2\sin\beta_4} + \left(\frac{\cos\beta_4 - \sin\beta_4}{4\sin^3\beta_4}\right)\left(\frac{\pi}{2} - 2\alpha\right) \qquad (2.9.4.7)$$

### 2.9.5 *Energy Difference*

The energy difference between configurations 3 and 4 in the cylindrical tank is calculated

$$\begin{aligned}\Delta\overline{E} = {} & 2\pi\overline{R}_4\left[1 - \overline{H}_4\left(\frac{\pi}{2} - 2\alpha\right)\right] - \frac{2\pi(1-\sin\alpha)}{\cos^2\alpha} \\ & - \cos\alpha\left[\pi\left(4\overline{H}_b - \overline{H}_b^2\right) - 2\pi\left\{\overline{H}_1 + \frac{1-\sin\alpha}{\cos^2\alpha} - \frac{1}{\cos\alpha} + \frac{2}{3}\frac{\left[1-\sin^3\alpha\right]}{\cos^3\alpha}\right\} - \pi\right]\end{aligned} \qquad (2.9.5.1)$$

The liquid height $\overline{H}_1$ becomes the critical liquid height when $\Delta\overline{E}$ in Equation (2.9.5.1) is equal to zero.

Similar to the previous discussion, a configuration in a cylindrical tank is a function of the initial liquid height and the contact angle. If a contact angle is given, the configuration can be predicted by comparing the initial liquid height to the minimum, maximum and critical heights.

## 2.10 Liquid Dynamics during Draining and Filling

If liquid draining and filling pass through an infinitesimal slow process, the dynamic behavior of liquid during the process may be assumed as if the system is experiencing an infinite number of equilibrium steps in a small time period. The interface is therefore not dynamically responding to the disturbances of the draining and filling. The configuration may change from one to the other. The principle of the interface configuration at the equilibrium state depending on the contact angle and the initial liquid height in the field of zero-gravity can be used for analysis.

Figure 2.10.1 shows the processes of filling and draining of a wetting liquid through the center outlet located at the bottom of a rectangular tank. The effect of the filling process on the configuration is shown schematically in Fig.2.10.2. Each frame is corresponding to a step in Fig.2.10.1 by the same number. At point 1 shown in Fig.2.10.1, no liquid enters the tank as the initial condition. After point 1, the liquid starts to fill in the tank, as shown in frame (1-2) of Fig.2.10.2. The solid bottom surface is wetted and a liquid droplet is formed between points 1 and 2. Once the drop reaches the corners of the tank (point 2), the drop of liquid separates into two symmetrically equal parts staying at the lower corners satisfying Young's equation, and configuration 2 is formed. Side walls are wetted and wetting length is rapidly extending. From points 3 to 4, another liquid droplet is formed by continuous filling. When the droplet becomes large enough to meet the liquid already in the tank (point 4), the drop is broken and the liquid volume in the tank is added up with the one from the broken droplet (point 5). Configuration 2 is still

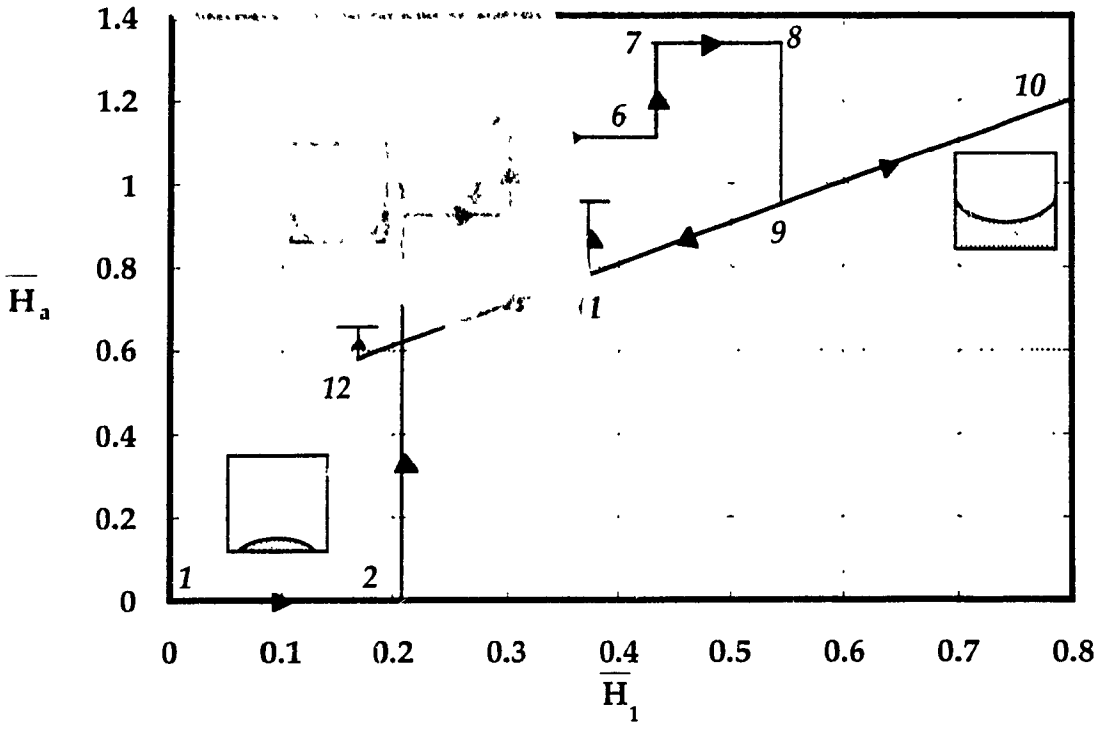


Fig. 2.10.1 Configuration change due to draining and filling from center outlets

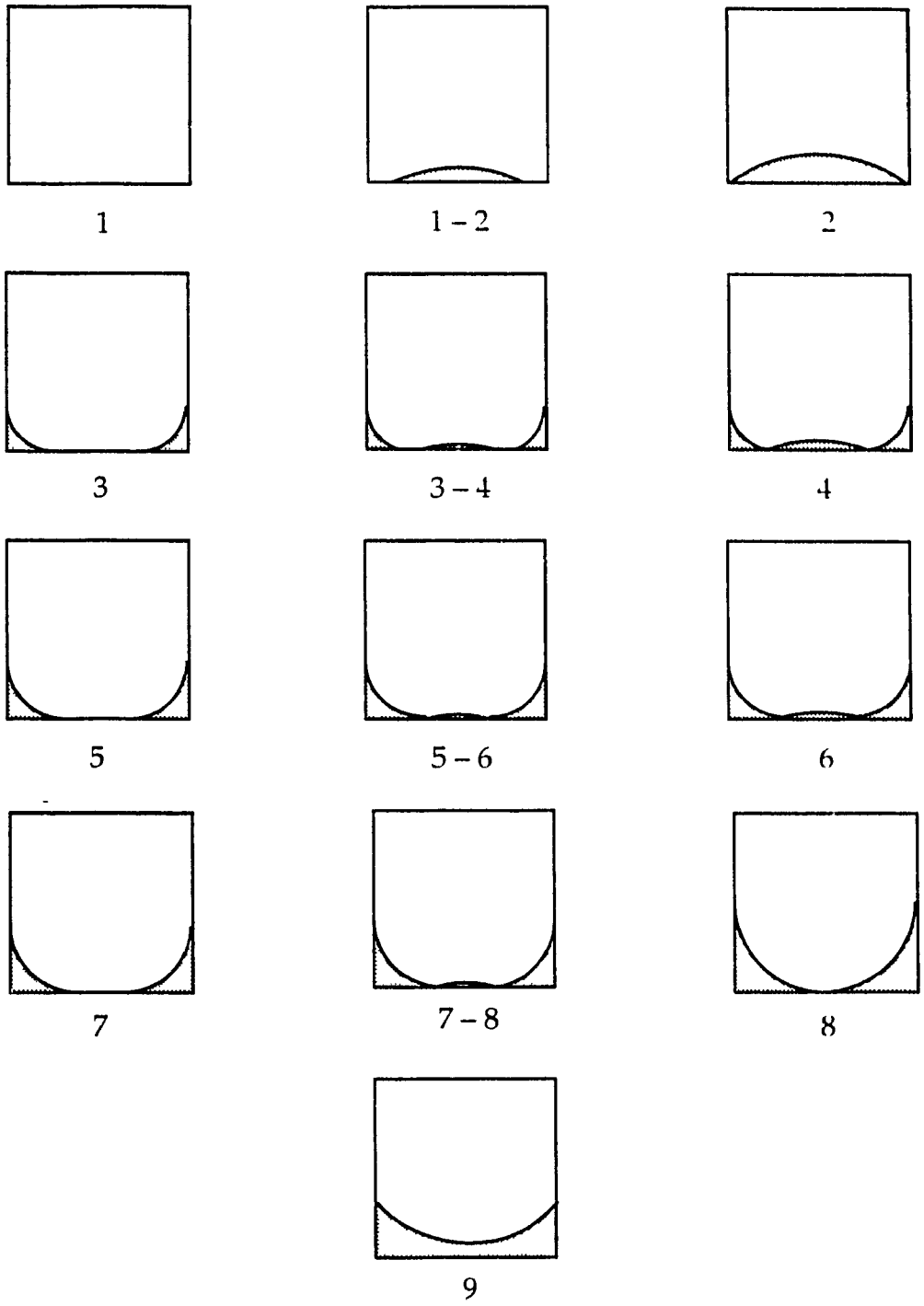


Fig.2.10.2 Schematic diagram of filling and draining a liquid through the center outlet

maintained at this moment. The same procedure is repeated until point 8 when the liquid volume is going to be so sufficient that the liquid from the two parts are met each other. Configuration 2 cannot be sustained any more since the liquid volume exceeds the maximum liquid volume, consequently, configuration changes from 2 to 1, as shown in frame 9. The liquid wetting height is suddenly dropping. The configuration 1 will remain for the rest of filling process.

Draining a liquid from the outlet located at the center of the same rectangular tank is different from filling. Draining starts with configuration 1 at point 9. The liquid wetting height is decreasing with the decrease of the liquid volume and the draining process will not alter the configuration 1 between points 9 and 11. However, if an external disturbance with an appropriate amount is given to the system between points 11 and 12, the configuration may change from 1 to 2 since the system tends to be at more stable state. As a result of liquid uncovering the outlet, the draining will stop. If no external disturbance is exerted, the draining will continue until point 12 where the draining is terminated due to the interface reaches the center outlet. The configuration will have to change to 2 since there is no sufficient amount liquid to keep configuration 1.

The filling and draining a liquid through the corner outlet of a rectangular tank are illustrated in Fig.2.10.3. The filling is going through the route 1-2-3-4 while maintaining configuration 2. However, the configuration could change from 2 to 1 after point 3 if a disturbance is introduced.

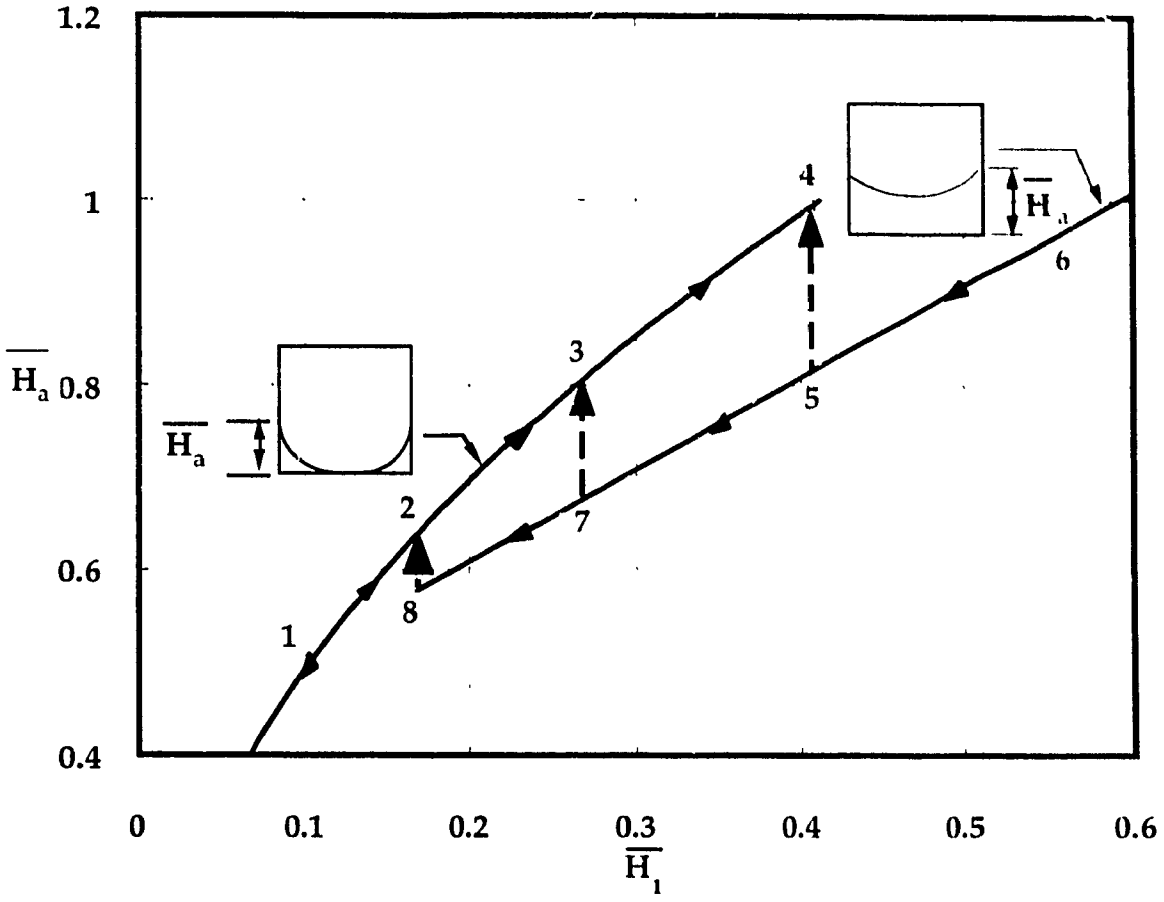


Fig.2.10.3 Configuration change due to draining and filling from corner outlets

Nevertheless, the configuration has to become 1 at points 4-5 since the liquid volume is greater than the maximum liquid volume. The draining is passing through the route 6-5-7-8. If an external force is exerted to the system when the draining has passed point 7, the configuration may change from 1 to 2. Otherwise, the configuration may remain 1 until point 8. An interesting phenomenon is observed that for corner outlet the draining can be an infinite process as long as the liquid is available in the tank, in other words, the liquid in tank can be completely expelled. This suggests that the corner location of the outlet has the advantage of no liquid residuals over the center location of the outlet. The liquid residuals will be further discussed in Chapter 6.

Liquid-vapor interface configuration varying with draining and filling of a liquid through center and corner outlets exhibits a hysteresis behavior. The configuration during draining may be different from the one during filling while other physical parameters are held constant.

# CHAPTER 3

# COMPUTATIONAL METHOD FOR LIQUID DYNAMICS

## 3.1 Numerical Solutions

An important subject of fluid science in a microgravity environment is the dynamic behavior of liquids in spacecrafts. The incompressible fluid behavior can be especially difficult to understand and quantify when the free surfaces have appreciable surface tension and are arbitrarily complex in topology. Many techniques have been developed to determine liquid dynamics in zero-gravity environment. To obtain an exact analytic solution to the general problem of liquid motion in a container on a spacecraft by solving the complete Navier-Stokes equations is extremely difficult. Only very small fraction of a wide range of problems can be solved by the classical methods. Since drastic simplifications with respect to the physics of the problem are required to achieve analytical solutions, the results are limited and often unrealistic. Earthbound experiments using drop towers or aircrafts suffer from a low period of microgravity which is not sufficient to evaluate fluid response to dynamic disturbances. Orbital experiments provide excellent means to evaluate low-gravity fluid dynamic behavior. However, at present, these are expensive and require a long lead time to carry out the tests.

The development of numerical methods and the availability of high speed computers has made it possible to simulate the fluid dynamics with the liquid free surface. Computational methods provide sufficiently accurate information concerning the physics of the problem with characteristics of fast results, lower cost and availability. The number of experiments that have to be performed in space can greatly be reduced. The computer code that will be presented here has been developed to predict liquid dynamic characteristics for rather general conditions. The present analysis focuses on the dynamic response of a liquid in rectangular and cylindrical containers to a step transition from terrestrial to weightlessness conditions and outflow disturbance.

A numerical algorithm for a time-dependent transient incompressible flow involving free surfaces where the surface tension forces are dominant is needed to conduct the investigation of the liquid dynamics in 0-g environment. Lagrangian methods cannot be used to solve fluid dynamics problems where free boundaries undergo large deformations. The MAC (Marker-and-cell) method (Welch et al, 1966) was the first method to successfully treat incompressible fluid problems involving free surface motions. This method was also the first one to use an Eulerian finite-difference formulation with velocity and pressure as the primary dependent variables. The MAC method used marker particles to define fluid region and set free surface pressures at the centers of cells defined to contain the surface. The SOLA code (Hirt et al, 1975) used a simplified version of the basic solution algorithm in MAC, which was the foundations of later development. Afterwards, many improvements were made and the basic technique matured through applications to a wide class of problems. The

SOLA-VOF code developed by Nichols et al (1980) and Hirt et al (1981) was based on the concept of a fractional volume of fluid (VOF) for treating arbitrary free boundaries. The NASA-VOF2D program contains several improvements over the SOLA-VOF program, such as curved boundaries, contained in literature (Torrey et al, 1985).

The SOLA–VOF Eulerian finite-difference solution algorithm has been modified to conduct the analysis. This method is for computing time-dependent, viscous, incompressible fluid flow in two-dimension. An important characteristic of this method is that it is strongly based on physical considerations, not just on mathematical manipulations. In addition to serving as an instructional tool, its purpose is to demonstrate that many useful and difficult problems can be solved. The employed numerical technique is able to successfully track the liquid-vapor interface configuration over a wide range of conditions using the VOF scheme and provide useful design data.

The liquid motions are calculated by solving the Navier-Stokes equations. This technique uses pressure and velocity as the primary variables. The calculation proceeds through a sequence of cycles, each advancing the entire fluid configuration through a small, but finite time increment. The results of each cycle act as an initial condition for the next one, and the calculation continues for as many cycles as the objective requires. This technique enables an instantaneous representation of the fluid for any particular time during the evolution of the dynamics. The concept of VOF uses the donor-acceptor differencing technique to track the free surface across an Eulerian grid. The function of the VOF is utilized to determine which cell

contains a liquid-vapor interface and where the fluid is located in these cells. In addition, the use of the values of F and its derivatives to construct a line cutting the cell that approximately draws the interface. Apart from obtaining the curvature of the interface, surface pressure can be computed from incorporating surface tension forces into the calculation.

In order to obtain meaningful results from numerical methods, a number of modifications must be made for microgravity applications. A number of improvements have been made to the original SOLA-VOF code, including the dynamic contact angle, obstacle boundaries and volume adjustment for F advection. These improvements will be detailed along with the relevant sections.

The fluid computation is advanced through a series of time cycles. Each time cycle at one time increment, $\Delta t$, consists of the followings: (i) finite difference approximations of the Navier-Stokes equations are used to compute the first guess for velocities at a new time level using the initial conditions or previous time cycle values for all advective, pressure, and viscous terms; (ii) pressures are adjusted in each cell through iterations and then the velocity changes induced by each pressure change are added to the previous velocities obtained from the last step in order to satisfy the continuity equation; (iii) the function of fractional volume of fluid defining fluid regions is calculated accordingly to give the new fluid configuration. Repetition of these steps will arrive at a solution through any desired time period.

The computational code is executed on the Alpha 2100 Model A500MP (Open VMS AXP) and Digital Equipment VAX-4000 Model 500 (VMS system); while the resulting data processes and vector plots are performed on SUN Workstations (UNIX system); microcomputers are also used to assist work. All computing facilities are located at Concordia University.

## 3.2 Governing Equations

Fluids to be investigated are assumed to be incompressible with constant kinematic viscosity. The differential equations to be solved are mass continuity and momentum equations, the equation of the fractional volume of fluid and Laplace's equation for surface tension effects.

An Eulerian method is used for modeling this two-dimensional incompressible fluid flow involving interfaces. The velocity field $\vec{q}$ is the function of fixed points $\vec{r}$ in the space and time:

$$\vec{q} = f(\vec{r}, t) \tag{3.2.1}$$

In two-dimensional Cartesian coordinates (x,y),

$$\vec{q}(\vec{r}, t) = u(x,y,t)\vec{i} + v(x,y,t)\vec{j} \tag{3.2.2}$$

For axisymmetric cylindrical coordinates, x is the radial coordinate (represented by r), y is the axial coordinate (represented by z).

The equation of mass conservation for an incompressible flow is

$$\nabla \cdot \vec{q} = 0 \tag{3.2.3}$$

The Navier-Stokes equation

$$\frac{\partial \vec{q}}{\partial t} + (\vec{q}\cdot\nabla)\vec{q} = -\frac{\nabla p}{\rho} + G + \nu\nabla^2\vec{q} \qquad (3.2.4)$$

where p is the pressure, G is the body or gravitational accelerations, ρ is the density and ν is the kinematic viscosity.

The fractional volume of fluid, F, consists of a step function defined for a mesh cell as follows:

$$\begin{cases} F(x,y,t) = 0, \text{ containing no fluid} \\ 0 < F(x,y,t) < 1, \text{ at liquid-vapor interface} \\ F(x,y,t) = 1, \text{ full of fluid} \end{cases} \qquad (3.2.5)$$

The average value of F is evaluated to equal to the fractional volume of the cell occupied by fluid. Fluid location in an interface cell can thus be determined by the F function. With known location of liquid and the value of F in an interface cell, a line cutting the cell can be constructed that approximates the interface. The transient transport equation of F is:

$$\frac{\partial F}{\partial t} + (\vec{q}\cdot\nabla)F = 0 \qquad (3.2.6)$$

If denoting $P_s$ as the surface pressure, σ as the surface tension and K as the curvature of liquid-vapor interface, Laplace's equation for surface tension effects after neglecting the viscous effects and assuming constant surface tension at the liquid-vapor interface is:

$$P_s = -\sigma K \tag{3.2.7}$$

In addition, a contact angle that is the angle between the tangential planes to the solid-liquid and liquid-vapor interfaces at the line of contact with the solid must be retained for all levels of gravitational field. In other words, the Young-Dupre equation is still valid in the zero-gravity environment.

## 3.3 Finite-Difference Approximations

A computational mesh and location of the variables in a mesh cell are shown in Fig.3.3.1. The finite-difference mesh used for numerically solving the differential equations consists of rectangular cells of width $\Delta x$ and height $\Delta y$. There is a single layer of fictitious cells (dashed area in Fig.3.3.1) around the fluid region. The finite-difference notation, subscripts i and j denote ith cell in the x-direction and jth cell in the y-direction at cell centers, $i+\frac{1}{2}$ denotes the right cell edge, and $j+\frac{1}{2}$ denotes the upper cell edge. Fluid velocities and pressures as well as the fractional volume of fluid are located at cell positions as shown in the magnifying part of Fig.3.3.1. The u-velocity component is at the middle of the vertical sides of a cell. The v-velocity component is located at the middle of the horizontal sides. Pressure and fractional volume of fluid are at the cell center.

As the first step of the calculation, the momentum equations are taken finite-difference approximations for computing the first guess for new time level velocities using the values obtained from the initial conditions or previous time cycle.

The momentum equation given by Equation (3.2.4) can be written in x-direction and y-direction, respectively:

$$\frac{\partial u}{\partial t} + u\frac{\partial u}{\partial x} + v\frac{\partial u}{\partial y} = -\frac{1}{\rho}\frac{\partial p}{\partial x} + G_x + \nu\left\{\frac{\partial^2 u}{\partial x^2} + \frac{\partial^2 u}{\partial y^2} + \varepsilon\left(\frac{1}{x}\frac{\partial u}{\partial x} - \frac{u}{x^2}\right)\right\} \qquad (3.3.1)$$

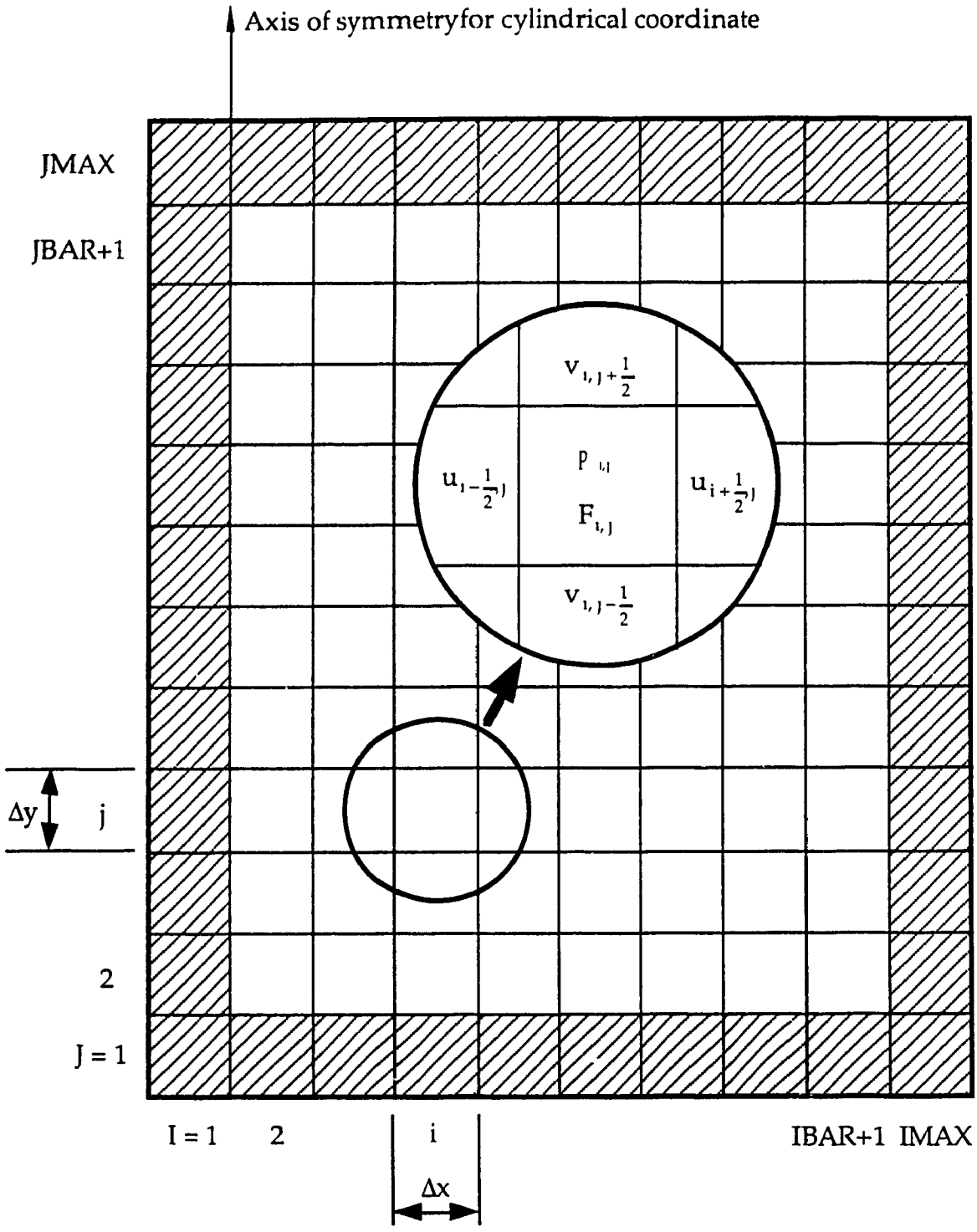


Fig.3.3.1 Mesh and cell arrangement

$$\frac{\partial v}{\partial t} + u\frac{\partial v}{\partial x} + v\frac{\partial v}{\partial y} = -\frac{1}{\rho}\frac{\partial p}{\partial y} + G_y + \nu\left\{\frac{\partial^2 v}{\partial x^2} + \frac{\partial^2 v}{\partial y^2} + \frac{\varepsilon}{x}\frac{\partial v}{\partial x}\right\} \tag{3.3.2}$$

where $\varepsilon$ is the coordinate control coefficient, which is defined as follows:

$$\varepsilon = \left\{\begin{array}{l} 0, \text{ Cartesian coordinate;} \\ \\ 1, \text{ cylindrical coordinate.} \end{array}\right\} \tag{3.3.3}$$

The derivatives of velocity component that are used in the finite-difference approximation for Equations (3.3.1) and (3.3.2) are:

$$\left(\frac{\partial u}{\partial x}\right)_{i,j} = \frac{u_{i+\frac{1}{2},j} - u_{i-\frac{1}{2},j}}{\Delta x} \tag{3.3.4}$$

$$\left(\frac{\partial u}{\partial y}\right)_{i+\frac{1}{2},j+\frac{1}{2}} = \frac{u_{i+\frac{1}{2},j+1} - u_{i+\frac{1}{2},j}}{\Delta y} \tag{3.3.5}$$

$$\left(\frac{\partial v}{\partial y}\right)_{i,j} = \frac{v_{i,j+\frac{1}{2}} - v_{i,j-\frac{1}{2}}}{\Delta y} \tag{3.3.6}$$

$$\left(\frac{\partial v}{\partial x}\right)_{i+\frac{1}{2},j+\frac{1}{2}} = \frac{v_{i+1,j+\frac{1}{2}} - v_{i,j+\frac{1}{2}}}{\Delta x} \tag{3.3.7}$$

The same treatment is applied to variables located at $(i+1, j)$ and $(i+\frac{1}{2}, j-\frac{1}{2})$. The convective terms in Equations (3.3.1) and (3.3.2) are approximated by a linear combination of donor cell and centered difference to

make a compromise between accuracy and stability. Given below illustrates the form of differencing:

$$\left(u\frac{\partial u}{\partial x}\right)_{i+\frac{1}{2},j}=\frac{u_{i+\frac{1}{2},j}}{2}\left\{\left(\frac{\partial u}{\partial x}\right)_{i+1,j}+\left(\frac{\partial u}{\partial x}\right)_{i,j}+\psi\left[\operatorname{sgn}\left(u_{i+\frac{1}{2},j}\right)\right]\left[\left(\frac{\partial u}{\partial x}\right)_{i,j}-\left(\frac{\partial u}{\partial x}\right)_{i+1,j}\right]\right\} \tag{3.3.8}$$

where $\operatorname{sgn}\left(u_{i+\frac{1}{2},j}\right)$ represents the sign of $u_{i+\frac{1}{2},j}$. The parameter $\Psi$ governs the choice of the donor-cell or centered-difference approximations. The second order centered-difference approximation is indicated by a zero value of $\Psi$. When $\Psi$ is equal to unity, the first order donor-cell (full upstream) form is obtained. A $\Psi$ value between zero and one corresponds to the approximation between first order and second order, which can be easily adjusted to satisfy both numerical stability and accuracy requirement.

After simple manipulating, all convective terms become:

$$\left(u\frac{\partial u}{\partial x}\right)_{i+\frac{1}{2},j}=\frac{u_{i+\frac{1}{2},j}}{2\,\Delta x}\left\{u_{i+\frac{3}{2},j}-u_{i-\frac{1}{2},j}+\psi\left[\operatorname{sgn}\left(u_{i+\frac{1}{2},j}\right)\right]\left(2\,u_{i+\frac{1}{2},j}-u_{i+\frac{3}{2},j}-u_{i-\frac{1}{2},j}\right)\right\} \tag{3.3.9}$$

$$\left(v\frac{\partial u}{\partial y}\right)_{i+\frac{1}{2},j}=\frac{v_{i+\frac{1}{2},j}}{2\Delta y}\left\{u_{i+\frac{1}{2},j+1}-u_{i+\frac{1}{2},j-1}+\psi\left[\operatorname{sgn}\left(v_{i+\frac{1}{2},j}\right)\right]\left(2\,u_{i+\frac{1}{2},j}-u_{i+\frac{1}{2},j-1}-u_{i+\frac{1}{2},j+1}\right)\right\} \tag{3.3.10}$$

where

$$v_{i+\frac{1}{2},j}=\frac{1}{4}\left(v_{i+1,j-\frac{1}{2}}+v_{i,j+\frac{1}{2}}+v_{i,j-\frac{1}{2}}+v_{i+1,j+\frac{1}{2}}\right) \tag{3.3.11}$$

$$\left(u\frac{\partial v}{\partial x}\right)_{i,\,j+\frac{1}{2}} = \frac{u_{i,\,j+\frac{1}{2}}}{2\Delta x}\left\{v_{i+1,j+\frac{1}{2}} - v_{i-1,j+\frac{1}{2}} + \psi\left[\mathrm{sgn}\left(u_{i,\,j+\frac{1}{2}}\right)\right]\left(2\,v_{i,j+\frac{1}{2}} - v_{i-1,j+\frac{1}{2}} - v_{i+1,j+\frac{1}{2}}\right)\right\} \tag{3.3.12}$$

$$\left(v\frac{\partial v}{\partial y}\right)_{i,\,j+\frac{1}{2}} = \frac{v_{i,j+\frac{1}{2}}}{2\,\Delta y}\left\{v_{i,j+\frac{1}{2}} - v_{i,j-\frac{1}{2}} + \psi\left[\mathrm{sgn}\left(v_{i,j+\frac{1}{2}}\right)\right]\left(2\,v_{i,j+\frac{1}{2}} - v_{i,j-\frac{1}{2}} - v_{i,j+\frac{1}{2}}\right)\right\} \tag{3.3.13}$$

where

$$u_{i,\,j+\frac{1}{2}} = \frac{1}{4}\left(u_{i-\frac{1}{2},j} + u_{i-\frac{1}{2},j+1} + u_{i+\frac{1}{2},j} + u_{i+\frac{1}{2},j+1}\right) \tag{3.3.14}$$

The centered approximations are used for computing the viscous terms in Equations (3.3.1) and ((3.3.2) using the same velocity derivatives.

$$\begin{aligned}\nu\left[\frac{\partial^2 u}{\partial x^2} + \frac{\partial^2 u}{\partial y^2} + \varepsilon\left(\frac{1}{x}\frac{\partial u}{\partial x} - \frac{u}{x^2}\right)\right]_{i+\frac{1}{2},\,j} &= \frac{\nu}{\Delta x}\left[\left(\frac{\partial u}{\partial x}\right)_{i+1,\,j} - \left(\frac{\partial u}{\partial x}\right)_{i,\,j}\right] \\ &+ \frac{2\nu}{\Delta y}\left[\left(\frac{\partial u}{\partial y}\right)_{i+\frac{1}{2},\,j+\frac{1}{2}} - \left(\frac{\partial u}{\partial y}\right)_{i+\frac{1}{2},\,j-\frac{1}{2}}\right] + \frac{\varepsilon\,\nu}{x_{i+\frac{1}{2}}}\left[\frac{\left(\frac{\partial u}{\partial x}\right)_{i,\,j} + \left(\frac{\partial u}{\partial x}\right)_{i+1,\,j}}{2} - \frac{u_{i+\frac{1}{2},\,j}}{x_{i+\frac{1}{2}}}\right]\end{aligned} \tag{3.3.15}$$

$$\begin{aligned}\nu\left[\frac{\partial^2 v}{\partial x^2} + \frac{\partial^2 v}{\partial y^2} + \frac{\varepsilon}{x}\frac{\partial v}{\partial x}\right]_{i,\,j+\frac{1}{2}} &= \frac{\nu}{\Delta y}\left[\left(\frac{\partial v}{\partial y}\right)_{i,\,j+1} - \left(\frac{\partial v}{\partial y}\right)_{i,\,j}\right] \\ &+ \frac{2\nu}{\Delta x}\left[\left(\frac{\partial v}{\partial x}\right)_{i+\frac{1}{2},\,j+\frac{1}{2}} - \left(\frac{\partial v}{\partial x}\right)_{i-\frac{1}{2},\,j+\frac{1}{2}}\right] + \frac{\varepsilon\,\nu}{2\,x_i}\left[\left(\frac{\partial v}{\partial x}\right)_{i+\frac{1}{2},\,j+\frac{1}{2}} + \left(\frac{\partial v}{\partial x}\right)_{i-\frac{1}{2},\,j+\frac{1}{2}}\right]\end{aligned} \tag{3.3.16}$$

By denoting VISCX and VISCY to be the right sides of Equations (3.3.15) and (3.3.16), thus they can be simplified as the followings:

$$VISCX = \frac{\nu}{\Delta x^2}\left(u_{i+\frac{3}{2},j} - 2\,u_{i+\frac{1}{2},j} + u_{i-\frac{1}{2},j}\right) + \frac{\nu}{\Delta y^2}\left(u_{i+\frac{1}{2},j+1} - 2\,u_{i+\frac{1}{2},j} + u_{i+\frac{1}{2},j-1}\right)$$
$$+ \nu\,\varepsilon\left[\frac{u_{i+\frac{3}{2},j} - u_{i-\frac{1}{2},j}}{2\,x_{i+\frac{1}{2}}\,\Delta x} - \frac{u_{i+\frac{1}{2},j}}{\left(x_{i+\frac{1}{2}}\right)^2}\right] \qquad (3.3.17)$$

$$VISCY = \frac{\nu}{\Delta x^2}\left(v_{i+1,j+\frac{1}{2}} - 2\,v_{i,j+\frac{1}{2}} + v_{i-1,j+\frac{1}{2}}\right) + \frac{\nu}{\Delta y^2}\left(v_{i,j+\frac{3}{2}} - 2\,v_{i,j+\frac{1}{2}} + v_{i,j-\frac{1}{2}}\right)$$
$$+ \nu\,\varepsilon\left[\frac{v_{i+1,j+\frac{1}{2}} - v_{i-1,j+\frac{1}{2}}}{2\,x_i\,\Delta x}\right] \qquad (3.3.18)$$

The finite-difference approximations of momentum equations for x-direction become

$$u^{n+1}_{i+\frac{1}{2},j} = u_{i+\frac{1}{2},j} + \Delta t\left\{\frac{2\left(p^{n+1}_{i,j} - p^{n+1}_{i+1,j}\right)}{\rho\Delta x\left(F_{i,j} + F_{i+1,j}\right)} + G_x - \left(u\frac{\partial u}{\partial x}\right)_{i+\frac{1}{2},j} - \left(v\frac{\partial u}{\partial y}\right)_{i+\frac{1}{2},j} + VISCX\right\} \qquad (3.3.19)$$

and for y-direction

$$v^{n+1}_{i,j+\frac{1}{2}} = v_{i,j+\frac{1}{2}} + \Delta t\left\{\frac{2\left(p^{n+1}_{i,j} - p^{n+1}_{i,j+1}\right)}{\rho\Delta y\left(F_{i,j} + F_{i,j+1}\right)} + G_y - \left(u\frac{\partial v}{\partial x}\right)_{i,j+\frac{1}{2}} - \left(v\frac{\partial v}{\partial y}\right)_{i,j+\frac{1}{2}} + VISCY\right\} \qquad (3.3.20)$$

where $\Delta t$ is the time increment. All terms in the right side of Equations (3.3.19) and (3.3.20) are evaluated at time level of $n\Delta t$. The superscript on quantities evaluated at time $n\Delta t$ are omitted, while n+1 means the next time step. At the beginning of the computation, the $p^{n+1}$ values in Equations

(3.3.19) and (3.3.20) are replaced by $p^n$. The pressure at new time level will be obtained through the iteration.

The next step is to obtain advanced time pressure and velocity that satisfy the continuity equation to within a convergence at the new time. The velocities computed from Equations (3.3.1) and (3.3.2) will not, however, satisfy the mass continuity equation, written in term of the two-dimensional differential equation:

$$\frac{\partial u}{\partial x} + \frac{\partial v}{\partial y} + \varepsilon \frac{u}{x} = 0 \tag{3.3.21}$$

Its finite-difference form is:

$$\frac{u^{n+1}_{i+\frac{1}{2},j} - u^{n+1}_{i-\frac{1}{2},j}}{\Delta x} + \frac{v^{n+1}_{i,j+\frac{1}{2}} - v^{n+1}_{i,j-\frac{1}{2}}}{\Delta y} + \varepsilon \frac{\left(u^{n+1}_{i+\frac{1}{2},j} + u^{n+1}_{i-\frac{1}{2},j}\right)}{2x_i} = 0 \tag{3.3.22}$$

If Equation (3.3.22) fails to vanish anywhere, there is a discrepancy in this conservation requirement. Thus, the left side of the above equation is denoted as a discrepancy term $D^{n+1}_{i,j}$. The pressure must be adjusted in each computational cell to arrive at the required values of velocities in order to meet the needs of the constraint of mass conservation. If the discrepancy of a cell, $D^{n+1}_{i,j}$, is positive, which indicates a net flow of mass out of the cell, the cell pressure is needed to be decreased to draw a flow back. Likewise, the pressure is increased to eliminate the inflow when there is the net flow into the cell. Since there is only one pressure variable for a cell, an appreciable value of the pressure can make the divergence equal to zero. For each cell encountered,

the divergence $D_{i,j}^{n+1}$ is evaluated using the most current velocity values available. The iterating procedure of the pressure adjustment throughout the mesh must be required since adjusting one cell will affect its surrounding cells.

Thus the new cell pressure is

$$p_{i,j}^{m+1} = p_{i,j} + \Delta p \tag{3.3.23}$$

where the superscript m+1 means the current step of iteration while the superscript m on pressure evaluated at last step is omitted. Consequently, the changes of the velocity component located at the sides of the cell are

$$u_{i+\frac{1}{2},j}^{m+1} = u_{i+\frac{1}{2},j} + \frac{\Delta t\, \Delta p}{\rho\, \Delta x} \tag{3.3.24}$$

$$u_{i-\frac{1}{2},j}^{m+1} = u_{i-\frac{1}{2},j} - \frac{\Delta t\, \Delta p}{\rho\, \Delta x} \tag{3.3.25}$$

$$v_{i,j+\frac{1}{2}}^{m+1} = v_{i,j+\frac{1}{2}} + \frac{\Delta t\, \Delta p}{\rho\, \Delta y} \tag{3.3.26}$$

$$v_{i,j-\frac{1}{2}}^{m+1} = v_{i,j-\frac{1}{2}} - \frac{\Delta t\, \Delta p}{\rho\, \Delta y} \tag{3.3.27}$$

The pressure change $\Delta p$ to drive divergence to zero is

$$\Delta p = -\frac{S}{\frac{\partial S}{\partial p}} \tag{3.3.28}$$

where S is denoted for an interior cell in fluid by the left side of the following equation

$$S = D_{i,j}^{n+1} + \frac{2\,\Delta t\,\Delta p}{\rho}\left[\frac{1}{(\Delta x)^2} + \frac{1}{(\Delta y)^2}\right] \tag{3.3.29}$$

Equation (3.3.29) is obtained by substituting the right sides of Equations (3.3.24) to (3.3.27) into the divergence condition. For a liquid-vapor interface cell the free surface cell pressure, $P_{i,j}$, is computed by a linear interpolation between the surface pressure, $P_s$, and an adjacent pressure inside the fluid, $P_n$, in a direction closest to the normal of the free surface. Thus, S for the interface cell is described by

$$S = (1-\eta)\,P_n + \eta P_s - P_{i,j} \tag{3.3.30}$$

where $\eta$ is the ratio of the distance between the cell centers and the distance between the free surface and the center of the interpolation cell.

The iteration of the pressure adjustment usually is required because its neighbors are affected when one cell is adjusted. The iteration proceeds by sweeping the computational mesh row by row starting with the bottom and working upward. For each cell, the divergence, $D_{i,j}^{n+1}$, is computed using the most current velocity values available. If values of S in all cells reach a very

small number, typically of order $10^{-3}$ or smaller, the iteration is considered to arrive at convergence when the velocity field is within accuracy requirements. The velocity and pressure from the last iteration are taken as the advanced time values. The accuracy of the representation depends strongly upon the fineness of the mesh composed to the macroscopic structure of the flow. Multiplication of $\Delta p$ by a coefficient $\omega$ can be used to accelerate the convergence of the iteration. The value of $\omega$ in this solution is set to 1.7.

## 3.4 Fractional Volume of Fluid

After calculation of velocities and pressure adjustment, the values of fractional volume of fluid are evaluated. By using the mass continuity equation,

$$F\left(\frac{\partial u}{\partial x}+\frac{\partial v}{\partial y}+\frac{\varepsilon\, u}{x}\right)=0 \tag{3.4.1}$$

the equation of the fractional volume of fluid becomes the conservation form:

$$\frac{\partial F}{\partial t}+\frac{\partial Fu}{\partial x}+\frac{\partial Fv}{\partial y}+\varepsilon\frac{Fu}{x}=0 \tag{3.4.2}$$

However, in numerical calculation, the divergence of velocity, $\nabla\cdot\vec{q}$, is not exactly zero owing to the finite number of pressure iteration and rounding errors. The convergence criterion of pressure iteration is set when the divergence in all cells is less than some small number, $\lambda$. The accumulation of this divergence through many cycle calculation would lead to erroneous results. This error may be offset by adding an additional term to Equation (3.4.2), the values of F in each cell are adjusted accordingly.

$$\frac{\partial F}{\partial t}+\frac{\partial Fu}{\partial x}+\frac{\partial Fv}{\partial y}+\varepsilon\frac{Fu}{x}-\lambda F=0 \tag{3.4.3}$$

This adjustment for volume conservation improves the accuracy of F flux.

A difference approximation which conserves fluid volume is:

$$F_{i,j}^{n+1} = (1+\lambda)\,F_{i,j} - \frac{\Delta t}{\Delta x}\left[(uF)_{i+\frac{1}{2},j}^{n+1} - (uF)_{i-\frac{1}{2},j}^{n+1}\right] \tag{3.4.4}$$

$$- \frac{\Delta t}{\Delta y}\left[(vF)_{i,j+\frac{1}{2}}^{n+1} - (vF)_{i,j-\frac{1}{2}}^{n+1}\right] - \frac{\varepsilon\,\Delta t}{2\,x_i}\left[(uF)_{i+\frac{1}{2},j}^{n+1} + (uF)_{i-\frac{1}{2},j}^{n+1}\right]$$

This equation serves as the basis for the convection of F.

The SOLA-VOF technique uses a type of donor-acceptor flux approximation to insure the sharp definition of free surface, without negative diffusion truncation errors and the exact amount of F across the cell boundaries. The essential idea is to use information about F downstream as well as upstream of a flux boundary to establish a crude interface shape, and then to use this shape in computing the flux.

At each boundary of each computing cell, the two cells immediately adjacent to the interface boundary are distinguished, one becoming a donor (D) cell and the other an acceptor (A) cell; and F values are given by $F_D$ and $F_A$. The algebraic sign of the fluid velocity normal to the boundary determines the type of the cell; the donor cell is always upstream and the acceptor cell downstream of the boundary. Assuming an amount of F to be fluxed through the right-hand cell boundary during a time step of duration $\Delta t$, the value of F, which will not remove more fluid, nor more void, is

$$F_{i+\frac{1}{2},j}^{n+1}\,V_x = \mathrm{sgn}\left(u_{i+\frac{1}{2},j}^{n+1}\right)\mathrm{MIN}\left(F_{AD}\,|V_x| + CF,\; F_D\,\Delta x_D\right) \tag{3.4.5}$$

where

$$V_x = u^{n+1}_{i+\frac{1}{2},j}\,\Delta t \tag{3.4.6}$$

and

$$CF = MAX\left[\left(\widetilde{F} - F_{AD}\right)|V_x| - \left(\widetilde{F} - F_D\right)\Delta x_D,\ 0.0\right] \tag{3.4.7}$$

where

$$\widetilde{F} = MAX\left(F_D,\ F_{DM},\ \phi\right) \tag{3.4.8}$$

The MIN statement in Equation (3.4.5) prevents the fluxing of more F than the donor cell contains, while the MAX feature prevents the fluxing of more void from the donor cell than it has. Equation (3.4.7) was used in NASA-VOF2D, which is the modified version to restrict the amount of void fluxed by the operation of the CF term. This is for improving the accuracy of the fluid convection and suppressing the appearance of spurious wisps of fluid in the void cells of the computing mesh. The DM cell is the one upstream of the donor cell. The value of $\phi$ is set as 0.1 in NASA-VOF2D. This prevents the advection of fluid by the CF term until either the D or the DM cell becomes at least 0.1 full of fluid, which suppresses the spurious small wisps of fluid.

## 3.5 Interface Determination and Interfacial Tensions

The function of fractional volume of fluid is governed by Equation (3.4.3). A straight line cutting through a cell can be assumed as an approximate interface. The interface slope is determined using a function $Y(x)$ or $X(y)$, depending on its orientation. When the interface is described by $Y(x)$, it is approximated to

$$Y_i = Y(x_i) = \left(F_{i,j-1} + F_{i,j} + F_{i,j+1}\right)\Delta y \tag{3.5.1}$$

then

$$\left(\frac{dY}{dx}\right)_i = \frac{Y_{i+1} - Y_{i-1}}{2\Delta x} \tag{3.5.2}$$

$dX/dy$ can also be obtained in the same way.

The smaller value between the $\left|\frac{dY}{dx}\right|$ and $\left|\frac{dX}{dy}\right|$ is chosen to be the approximation of the slope. For example, if $\left|\frac{dY}{dx}\right|$ is smaller, the interface is horizontal. After determining the slope of this line, it can then be constructed in the cell with the known amount of F volume lying on the F fluid side. Fluid lies below the interface when $\frac{dX}{dy}$ is negative. This line provides the information for the application of free surface pressure boundary conditions. Once the curvature K in each free surface cell is obtained from the function $Y(x)$ or $X(y)$, the liquid-vapor surface tension pressure can be found. This pressure is calculated by Equation (3.2.7). The surface pressure due to surface

tension forces is used in Equation (3.3.30). The curvature of the liquid-vapor is

$$K = \frac{1}{R_1} + \frac{\varepsilon}{R_2} \tag{3.5.3}$$

where $R_1$ is the principal radius of curvature in the x-y plane and $R_2$ is the principal radius of curvature associated with the azimuthal direction in case of cylindrical coordinates. Thus, Laplace's equation for surface tension effects when the interface is mostly horizontal is:

$$P_s = -\sigma \left\{ \frac{d}{dx} \left[ \frac{\frac{dy}{dx}}{\sqrt{1 + \left(\frac{dy}{dx}\right)^2}} \right] + \frac{\varepsilon}{x} \left[ \frac{\frac{dy}{dx}}{\sqrt{1 + \left(\frac{dy}{dx}\right)^2}} \right] \right\} \tag{3.5.4}$$

The effects of liquid-solid and vapor-solid interfacial tension forces must be accounted for if the interface near the container walls. A contact angle $\alpha$ is assigned to model the effects. If no interfacial forces involved this angle is set to zero. To impose this angle condition, the values of $Y(x)$ or $X(y)$ at walls must be adjusted. For example, suppose F fluid assumes to be below the surface in the boundary cell (i,j) of the right wall, the surface is assumed to make an contact angle with the wall by adjusting the i+1 value of $Y(x)$ and the j+1 value of $X(y)$ as

$$Y_{i+1} = Y_i + \frac{\Delta x}{\tan\alpha} \tag{3.5.5}$$

and

$$X_{j+1} = X_i - \frac{\Delta y}{\tan\alpha} \qquad (3.5.6)$$

Similar adjustments are made to the appropriate variables for all other orientations of walls and interfaces.

## 3.6 Dynamic Contact Angle

A static contact angle is used in the SOLA-VOF and other software mentioned above. The recent studies arising from the surface science indicate that the use of the constant value of the static contact angle may lead to erroneous results. From the experimental observation, it is found that advancing and receding contact angles may be very different (Adamson, 1982). The reason is that if a viscous fluid is rapidly moving across a solid wall surface, the liquid near the surface cannot keep up with the advancing front. This results that the equilibrium contact angle has smaller value than the dynamic contact angle, $\alpha_d$. The contact angle is known to depend on the velocity of the advancing liquid-vapor interface, surface tension and viscosity. The dynamic contact angle, $\alpha_d$, is used to be an adjustment for better description of the process. For certain liquids, the dynamic contact angle is expressed by the Fritz equation (Kinloch, 1987):

$$\tan \alpha_d = m \left(\frac{\mu v}{\sigma}\right)^n \tag{3.6.1}$$

where $\mu$ is the viscosity, $\sigma$ is the surface tension of liquid-vapor interface, v is the velocity of the meniscus, and m and n are constants.

Newman (1968) presented an expression of dynamic angle which is depending on the system under consideration, based on the experimental investigation. His work assumed Poiseuille's law for the flow of Newtonian liquids through horizontal capillaries where the gravitational effects are neglected, and no slip boundary conditions at the wall. The velocity of the fluid, u, is

$$u = \frac{R_t^2 p}{4 \mu l}\left[1 - \left(\frac{r}{R_t}\right)^2\right] \tag{3.6.2}$$

where $R_t$ is the radius of the tube, r the radial distance from the center, l the tube length, $\mu$ the viscosity and p the pressure. By defining the average fluid velocity

$$u_{av} = \frac{R_t^2 p}{8 \mu l} \tag{3.6.3}$$

and the p value from Equation (3.2.7), the average velocity of a liquid flowing under surface tension forces becomes:

$$\frac{dl}{dt} = \frac{R_t \sigma \cos \alpha}{4 \mu l} \tag{3.6.4}$$

In the past the rate of wetting or the development of equilibrium contact angles was assumed to be sufficiently rapid relative to the rate of movement of liquid, thus $\cos \alpha$ is taken as a constant. Recent investigations have shown that there is a strong time dependence of the contact angle and that $\cos \alpha$ adjusts itself at the interface without regard to the mass of the fluid involved. It is now of interest to consider the implication of replacing constant $\cos \alpha$ by a function as

$$\cos \alpha_d = (\cos \alpha)\left(1 - ae^{-ct}\right) \tag{3.6.5}$$

where a and c are constant. The plot of the Equation (3.6.5) fits with the experimental data over the entire time range. There was a deviation between the results of using the $\cos \alpha$ and $\cos \alpha_d$. Obviously, neglect of the effects of $\cos \alpha_d$ would lead to erroneous results.

Joos et al (1990) used the similar analysis to that of Newman and conducted capillary experimental studies. They introduced the dynamic contact angle in simple and completed form

$$\cos \alpha_d = \cos \alpha - 2 (1 + \cos \alpha) \sqrt{\frac{\rho v v}{\sigma}} \qquad (3.6.6)$$

where $\alpha$ is the static contact angle, $v$ is the kinematic viscosity of the liquid, $\rho$ is the density. Equation (3.6.6) has the advantage of containing no adjustable parameters over the Equation (3.6.5). Since the Equation (3.6.6) incorporates the liquid properties and dynamics which encounter with the fluid problems in the present studies, the dynamic contact angle is adopted instead of the static contact angle. This makes more sense in physical science and leads to more accurate results.

## 3.7 Boundary Conditions

Boundary conditions are satisfied by setting appropriate velocities in the fictitious cells surrounding the mesh. The left boundary will be discussed while the boundary conditions at other walls are analogous. If the left boundary is a no-slip rigid wall, for all jth row, the normal velocity component must vanish and the tangential velocity component should be zero, i.e.,

$$u_{1,j} = 0 \tag{3.7.1}$$

$$v_{1,j} = -v_{2,j} \tag{3.7.2}$$

If it is a rigid free-slip wall, the normal velocity component must vanish and the tangential velocity should have no normal gradient. The conditions imposed for all jth row are:

$$u_{1,j} = 0 \tag{3.7.3}$$

$$v_{1,j} = v_{2,j} \tag{3.7.4}$$

The outflow boundary conditions used at the left wall for all jth row are:

$$u_{1,j} = u_{2,j} \tag{3.7.5}$$

$$v_{1,j} = v_{2,j} \tag{3.7.6}$$

No-slip and free-slip conditions are imposed on the velocities calculated from applying the momentum equations and after each cycle of pressure iteration through the mesh. These outflow boundary conditions, however, are only imposed after solving the momentum equations and not after each pass through the pressure iteration. Pressure and fractional volume given in the following equations are imposed to no-slip, free-slip and outflow conditions.

$$P_{1,j} = P_{2,j} \tag{3.7.7}$$

$$F_{1,j} = F_{2,j} \tag{3.7.8}$$

For the free surface boundary conditions, velocities are set to vanish the divergence on every cell boundary between a surface cell and an empty one. Zero values for $\frac{\partial u}{\partial y}$ or $\frac{\partial v}{\partial x}$ are also used to set exterior tangent velocities to a free surface on boundaries between empty cells adjacent to a surface cell. The free surface boundary condition for normal stress is also satisfied by the Equation (3.3.30).

For obstacle boundary conditions, the flags for these cells are used to block out the cells. In SOLA-VOF, no velocities or pressure are calculated in obstacle cells, and all velocity components on faces of obstacle cells are set to zero. It should be noted that tangential velocities being zero at locations shifted into the obstacles one-half of a cell width from the actual boundary location. Thus the no-slip tangential velocity conditions at obstacle boundaries are only first-order accurate since all velocity components within

obstacle cells are set to zero. This treatment will result in errors. The error would be noticeable, especially in the region of containing few fluid cells. To improve accuracy, no-slip conditions are set in all obstacle cells bordering fluid cells and the other obstacle cells have zero values for velocities.

# CHAPTER 4

# DYNAMIC MOTION OF LIQUID DURING WEIGHTLESSNESS

## 4.1 Responses of Liquid Systems to Step Change of Gravity

The computational method is used to simulate the dynamic behavior of the liquid-vapor during a step transition from terrestrial conditions to weightlessness, and its 0-g equilibrium configuration when all the transient effects have dissipated. The solution from the simulation provides a history of free surface motion in addition to a final value. The computational code further feathers a graphical interpretation of this history in addition to the detailed numerical results at any desired instant of time. Part of the study will focus on determining the time required for the liquid-vapor interface to reach its equilibrium in rectangular and cylindrical tanks.

A closed rigid container partially filled with a wetting liquid is considered to undertake a step transition from terrestrial conditions to weightlessness. The system is initially under the 1-g influence. At time $t = 0^+$, the system is exposed to a weightless environment. During the transition period, the system is assumed to preserve the contact angle. The equations of momentum, continuity, fractional volume and surface tension pressure are marched in time using the previously presented numerical technique. The velocity components, liquid-vapor interface etc... are recorded at a chosen time level.

It is seen that liquid motions result from a variety of vehicle disturbances. These motions may result in dislocation of the liquid from the outlet end of the tank, formation of vapor bubbles and disturbances to vehicle attitude owing to movement of the liquid mass. When a liquid-vapor-solid system enters a zero-gravity environment, the liquid-vapor interface undergoes a transition in which it moves from a nearly flat configuration in a gravitational field to a curved configuration in zero-gravity. The potential energy of the system is considerably in excess of its zero-gravity equilibrium value at initiating the transition process. The liquid mass then oscillates about the 0-g equilibrium liquid configuration until viscous forces in the liquid damp out the oscillation and bring the liquid to rest.

These stable interface configurations are expected when no kinetic energy exists in the liquid. The equilibrium configurations are conditions of minimum surface energy. Any disturbance, causing some other shape of the interface, results in an increase in surface energy at the expense of kinetic energy. If the total energy input is comparable to the equilibrium surface energy, then a periodic oscillation might result. This motion could be in the form of a first-mode periodic wave or a more complex motion. As the kinetic energy is dissipated by viscous forces, the liquid may settle in one or both ends with periodic wave motion, eventually reverting to one of the equilibrium configurations.

In general, the liquid-vapor-solid systems exhibit characteristics of under-damped systems. Typically, the interface oscillates about its 0-g

equilibrium configuration for a period of time that depends on liquid property parameters and system dimensions.

Reynolds et al (1961) and Benedikt (1959) studied analytically the time response of a deformed liquid drop (a liquid-vapor system) under the influence of surface tension forces. In general, however, a solid-liquid-vapor system is the most desirable one in a spacecraft. The time, T, required for the interface to reach its 0-g equilibrium configuration was derived from the Weber number that is basically the ratio of inertia to capillary forces.

$$T = \sqrt{\frac{\rho L^3}{\sigma We}} \tag{4.1.1}$$

where $\rho$ is density of the fluid, L is the half width or radius of a container, $\sigma$ is surface tension and

$$We = \frac{\rho v_c^2 L}{\sigma} \tag{4.1.2}$$

$v_c$ is the characteristic velocity. It is necessary to indicate that Equation (4.1.1) does not take into account the retaining effect of viscosity and all three interfacial surface forces on the time required to reach equilibrium.

Siegert et al (1964 1965) experimentally investigated the liquid-vapor interface formation time of a liquid-vapor-solid system in a drop tower. The Equation (4.1.1) was retained and the Weber number was replaced by a scaling

parameter, K, determined from the experimental data. The empirical constant K, was found to be a function of the geometry of the system.

Due to the limited 0-g experimental test time available in the drop tower, results obtained were insufficient. Even for the relatively small tanks, to observe the complete decay of the oscillations of the liquid-vapor interface is very difficult since the zero-gravity time attainable in the test is relatively short (2.25 second). The interface formation time, however, was not the exact time required for the system reaching the equilibrium configuration, owing to the limited 0-g experimental test time. The time required for the interface to reach its 0-g equilibrium configuration in the drop tower experiment was, consequently, defined as the time for the first pass of the center point on the 1-g interface to traverse the straight-line distance to its perpendicular projection on the 0-g steady-state theoretical interface. When this center point reached its specified location on the 0-g steady-state analytical interface, however, the entire liquid-vapor interface was generally not in its 0-g steady-state configuration. Experimental observations confirmed that the liquid-vapor interface at the time of measurement of the time to reach equilibrium was somewhat different from the analytical configuration at the steady state. Significant difference in spherical tanks was observed since the entire wall of the tank had not as yet become totally wetted though these differences were not as prominent in cylindrical tanks.

To assess the effect of viscosity on interface formation time, computations were made to simulate thc liquids with a ratio in kinematic viscosity of 100:1. Figure 4.1.1 clearly illustrates the problem by the history of

interface motion with viscosity, where the dimensionless time $\bar{t}$ (Vatistas et al, 1994), is used in the transition process and

$$\overline{H} = \frac{H}{L} \tag{4.1.3}$$

The frequencies of the first couple of cycles for different values of kinematic viscosity ν are almost identical. The viscosity does not have an effect on the time for the first pass of the interface through its steady-state position. If the entire interface formation period is taken into consideration, the magnitude of the interface oscillation and the interface formation time are significantly affected by the viscous force, which indicates that the true time for the whole interface to reach its 0-g equilibrium configuration is dependent on the viscosity. If the viscosity is small, the time of the interface to reach the 0-g equilibrium interface is long. For the high viscous force, the rate of decay is high, which results in short interface formation time. As seen from Fig.4.1.1, the effect of viscosity is very clear. This illustration implies it is impractical for the expression given in Equation (4.1.1) since that did not take into account the effect of viscosity on the time required to reach equilibrium in the past. Hence, viscosity must be taken into consideration for different fluids.

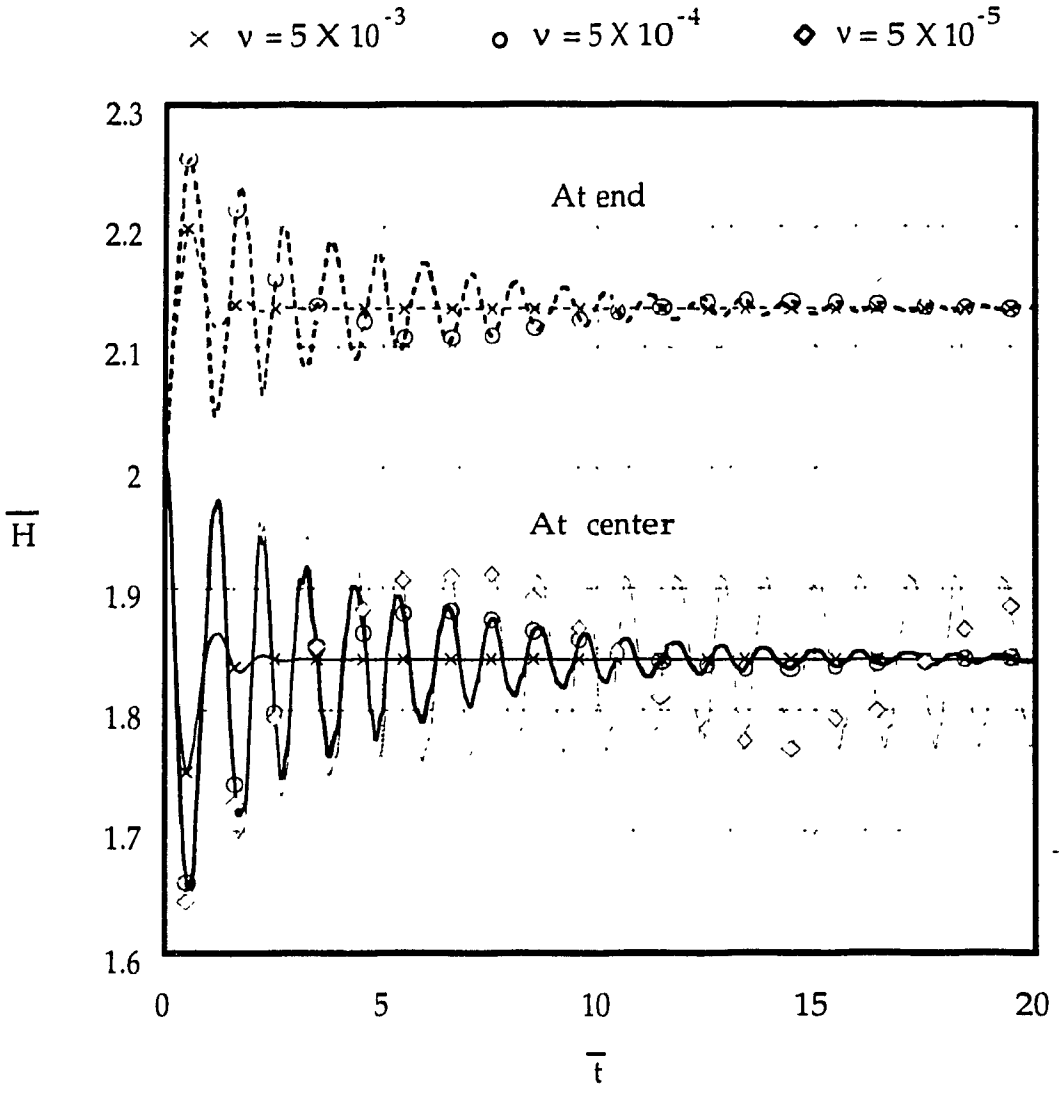


Fig.4.1.1 Interface oscillations versus different viscosity

The dynamic motion of the interface during the gravity transition can be simulated at any desired time period to ensure that the system reaches the zero-gravity equilibrium state. The time required for the whole liquid-vapor interface to reach its zero-gravity equilibrium state after the system has been exposed to weightlessness is defined as the liquid-vapor interface formation time $\tau$. The interface formation time is the important measuring parameter, which can be approximately represented by the time required for the liquid-vapor interface oscillations to decay to 0.1% of the original amplitude in the first half cycle of the oscillation, $t_{0.1\%}$. It is anticipated that such an approximation would only result in a negligible error.

The dimensional analysis is conducted to investigate the important parameters including the time $t_{0.1\%}$, fluid density $\rho$, surface tension $\sigma$, viscosity $\nu$, the half width or radius of a container L, and the contact angle $\alpha$. A functional relationship is found,

$$f_n\left(t_{0.1}, \rho, \sigma, \nu, L, \alpha\right) = 0 \tag{4.1.4}$$

From the dimensional analysis, the dimensionless interface formation time $\tau$, is found to be the function of surface tension, density, tank width, viscosity and contact angle (Vatistas et al, 1994).

$$\tau = f_n\left(\pi_2, \pi_3\right) = f_n\left(\sqrt{\frac{\sigma L}{\rho \nu^2}}, \alpha\right) \tag{4.1.5}$$

for a given contact angle

$$\tau = f_n(\pi_2) = f_n\left(\sqrt{\frac{\sigma L}{\rho \nu^2}}\right) \qquad (4.1.6)$$

The results establish a functional dependence of the time to reach equilibrium state on the pertinent liquid parameters and container geometry expected to influence the time response of the interface. It is expected that the dimensionless parameter $\pi_2$, will be of significance in describing dynamic behavior because it incorporates the effects of viscosity, container geometry, density and surface tension forces. $\pi_2$ expresses the ratio of surface tension forces to viscous forces. The order of magnitude for the time required to resume the equilibrium state of the liquids can be estimated using Equation (4.1.6). If surface tension is constant, the interface formation time is determined by viscous forces. Thus, the interface formation time is affected by viscosity.

These effective factors are examined using the dimensionless interface formation time $\tau$, as a function of the $\pi_2$ in a rectangular tank and a cylindrical tank, as given in Figs.4.1.2 and 4.1.3. Both figures show a similar tendency, which indicates that the transition time required for the interface under 1-g to reach 0-g steady state conditions increases as the effective damping forces decrease. The slope of the curve at the beginning is steep, then it tends to be nearly horizontal, which means that the required time increases steeply at considerably small $\pi_2$ while the time increases quite slowly at large $\pi_2$. The correlations between the interface formation time and $\pi_2$ might be expressed by a formula which is numerically calculated from the data of these figures.

$$\tau = b\,(\pi_2)^d \qquad (4.1.7)$$

where b and d are constant, which is dependent on tank geometry and contact angle. These values are:

b = 0.55968 and d = 0.833512 for cylindrical tanks;

b = 2.0298, d = 0.56036 for rectangle tanks.

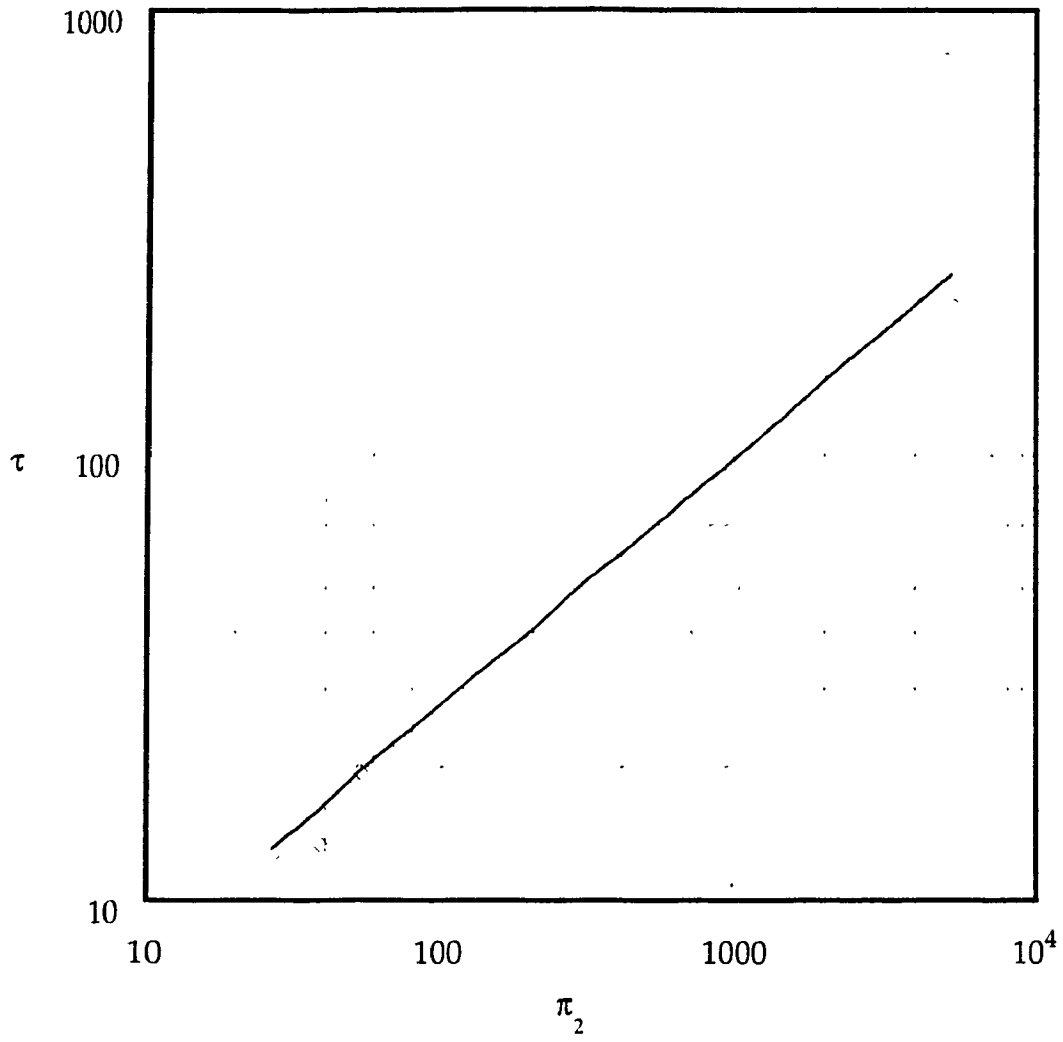


Fig.4.1.2 Interface formation time versus dimensionless parameter $\pi_2$ in rectangular tanks

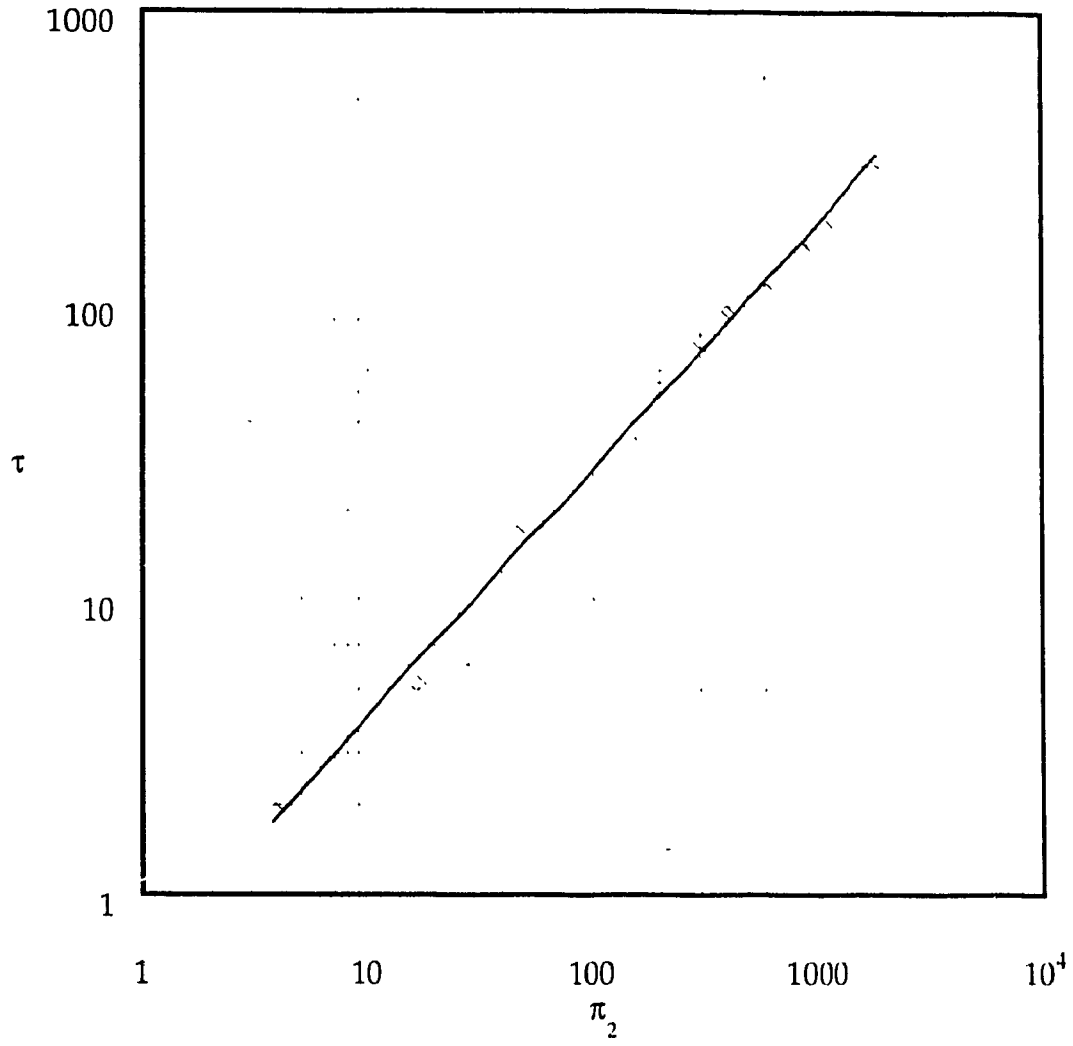


Fig.4.1.3 Interface formation time versus dimensionless parameter $\pi_2$ in cylindrical tanks

## 4.2 Prediction of Configurations at Equilibrium State

The liquid-vapor interface is expected to reach the steady state, after certain time, when all the transient effects have disappeared. The liquid-vapor interface tends towards a configuration of constant surface curvature meeting the tank walls at the contact angle as the condition of the equilibrium due to surface tensions and contact angles The interface shape of the zero-gravity equilibrium state can be obtained numerically when sufficient time is allowed so that most of the fluid motion decays. The hypothesis concerning the most probable liquid-vapor interface configuration will be also verified by numerical solutions. Since only limited experimental data in microgravity environment from the literature are available, they are used as reference for verifying the reliability of the numerical method and studying the deviation of the dynamic behavior obtained from the numerical analysis.

The equilibrium interface in response to the gravity conditions of terrestrial to weightlessness in a rectangular tank when the initial liquid depth is high or low is demonstrated in the two phases, as shown in Fig.4.2.1.

Phase (a) in Fig.4.2.1 indicates that for liquid depth at high initial height at one-gravity field, the pressure is hydrostatic and liquid-vapor interface is flat due to initial forces. At zero-gravity, the surface tension forces are a dominant factor when the liquid system reaches the equilibrium state. The liquid-vapor interface becomes a curved surface of constant curvature intersecting the wall at the contact angle. The steady state configuration of system 1 indicated by the analytic approach is presented.

Phase (b) in Fig.4.2.1 shows liquid behavior under 1-g and 0-g when the initial liquid depth is low. Liquid-vapor interface is flat under 1-g condition. The liquid is separated into two parts left in corners of the container at the steady state in 0-g environment. This plot is as expected by the analytic method to be configuration of system 2.

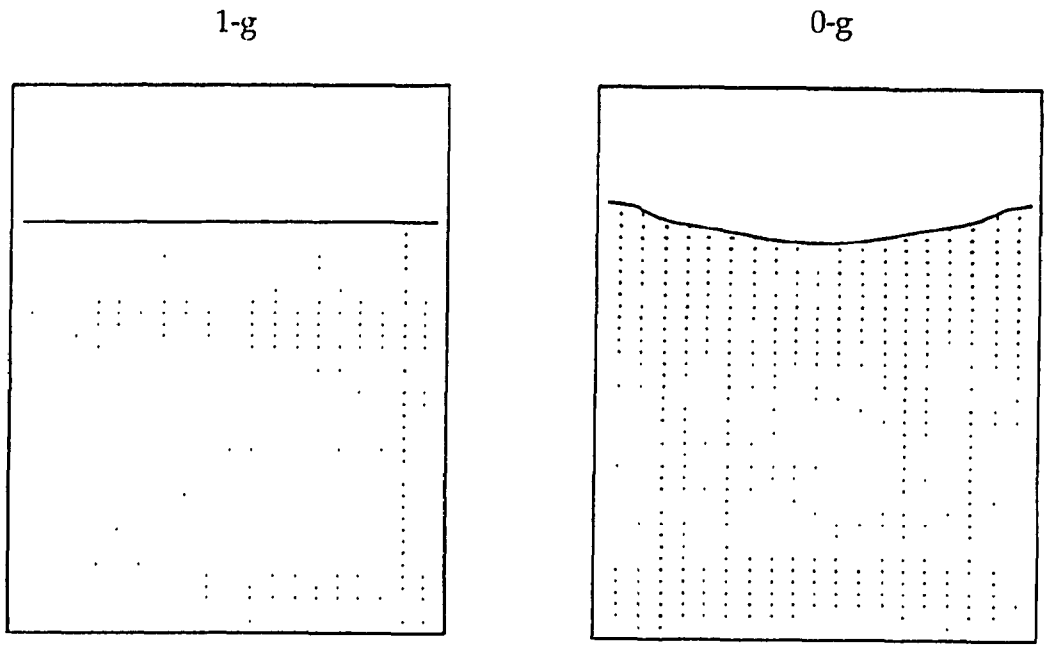


(a) Liquid depth at high initial height

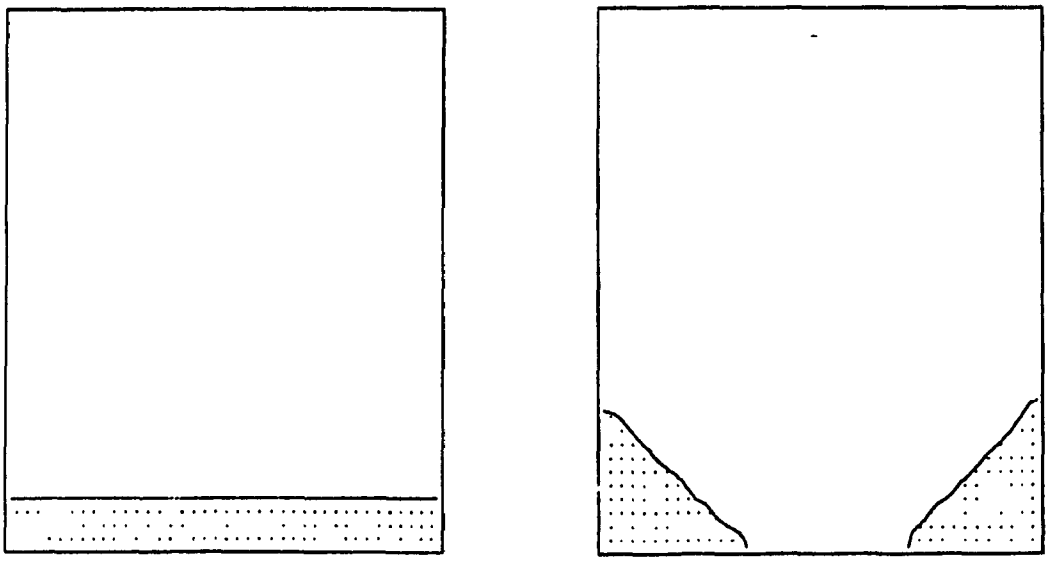

(b) Liquid depth at low initial height

Fig.4.2.1 Liquid configurations at different initial liquid heights under 1-g and 0-g equilibrium conditions

## 4.3 Interface Configuration Validation

The liquid-vapor interface configuration at its zero-gravity state is subjected to surface tensions and contact angles. The comparison of interface shapes for high initial liquid depth at 0-g equilibrium state from the results of numerical and analytical solutions were made for different contact angles. Figure 4.3.1 shows that the results are very close.

In order to verify the numerical result, a previously photographic experiment conducted at the Lewis Research Center of National Aeronautics and Space Administration (NASA), Cleveland, Ohio, U.S.A. (Petrash et al, 1963) is used for comparison. The experimental data were obtained in the 100-foot drop tower. The actual free-fall distance of the drop tower is 85 feet, yielding a 2.3-second period of zero-gravity time. In this particular facility, air drag on the experimental package is kept below $10^{-5}$ g by allowing the experiment to free fall inside an air drag shield. The test fluid was placed in a cylinder of dimensions of 40 mm diameter and 80mm height, mounted and illuminated to allow a high-speed motion picture camera to photograph the entire tank during free fall. The description of the facility and operation procedure of the experiment were presented in detail by Petrash et al (1963). The same cylinder dimensions, the initial liquid filling and the fluid material properties were used as the input data for the computational simulation. The zero gravity liquid-vapor interface configuration for the tetrabromoethane with the filling of 50 and 10 percent full are shown in Figs 4.3.2 and 4.3.3, respectively. It is clear from these figures that the predicted results are in good

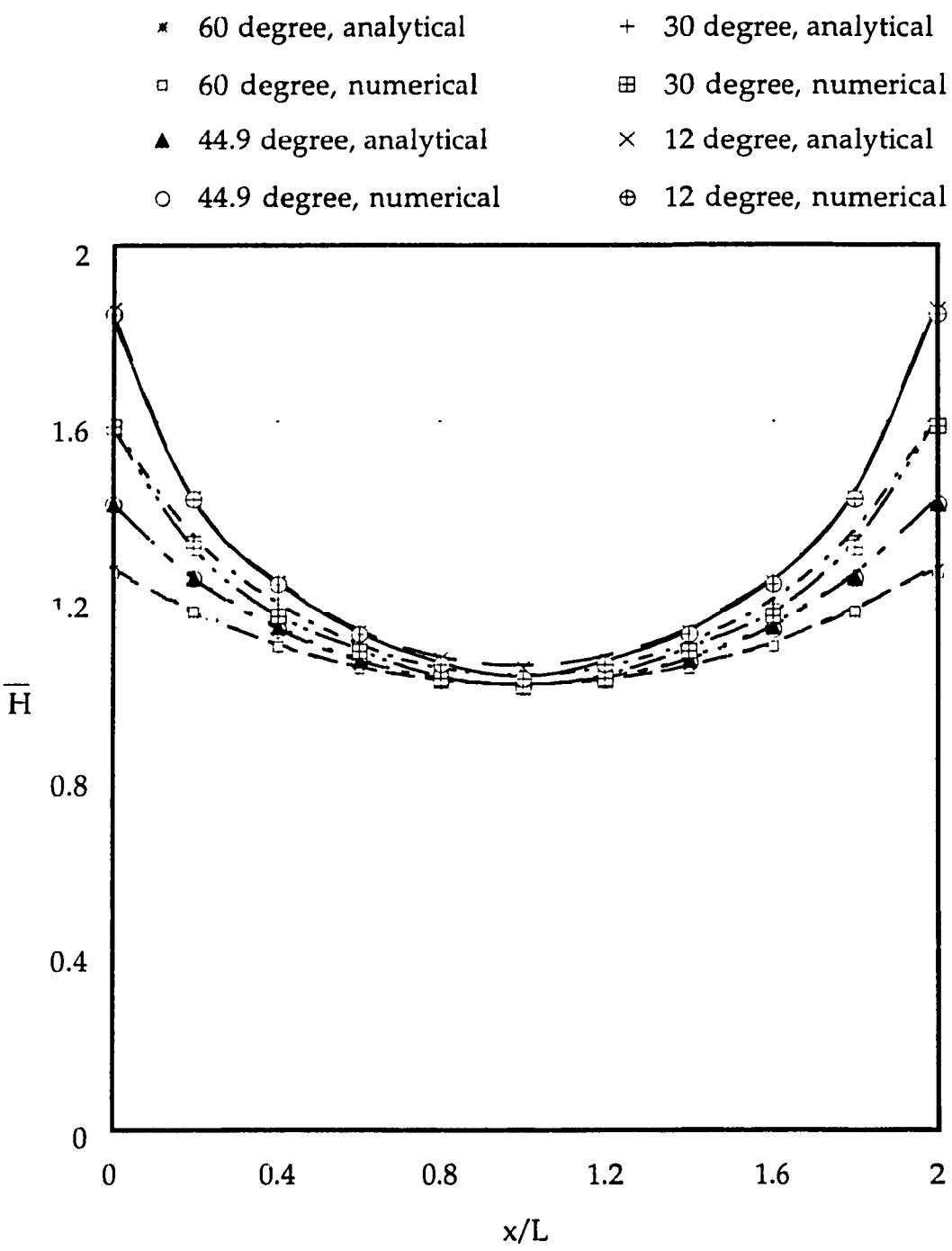


Fig.4.3.1 Interface configurations for different contact angles

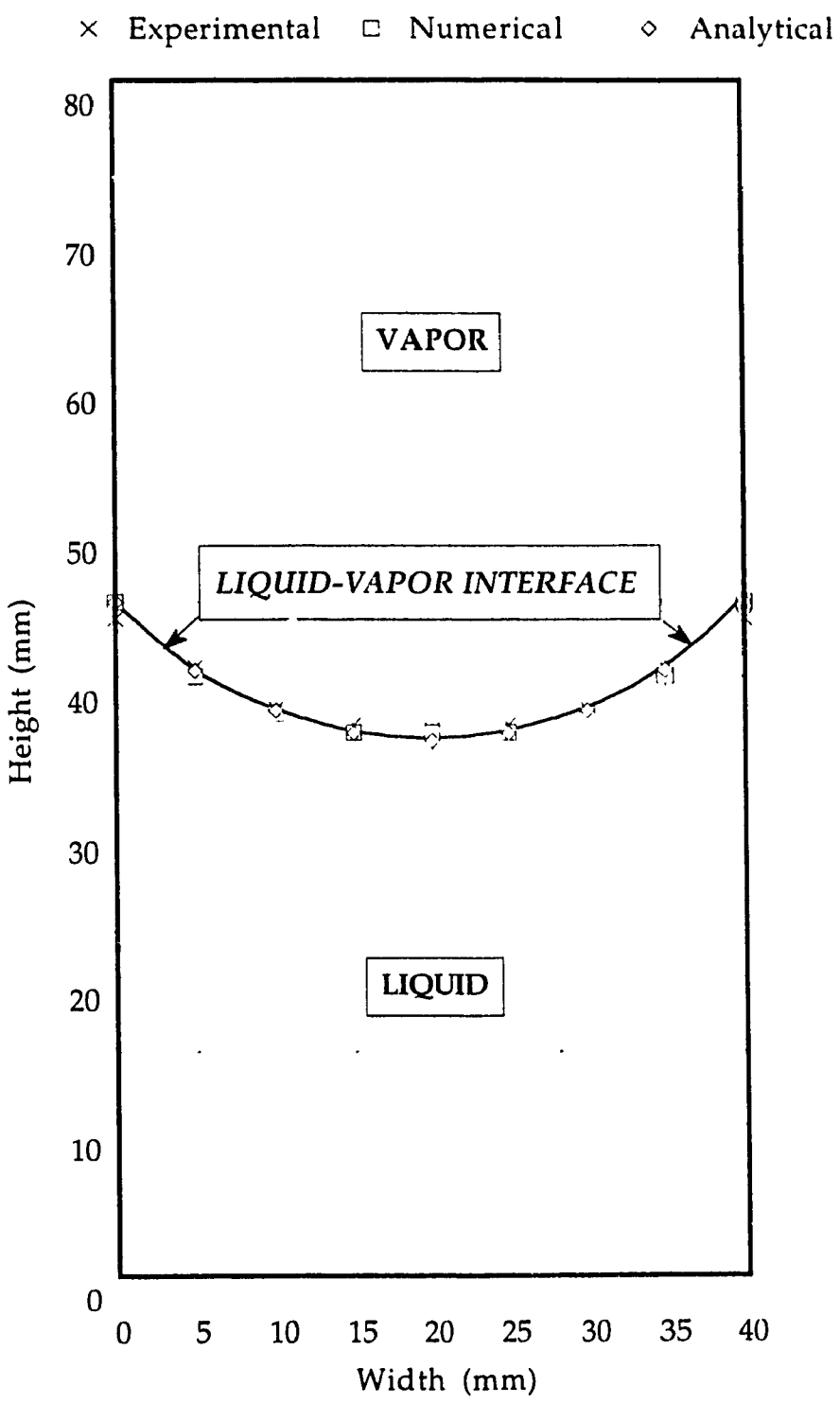


Fig.4.3.2 Interface configuration for tebrabromoethane with 50% full ($\alpha = 40^{o}$).

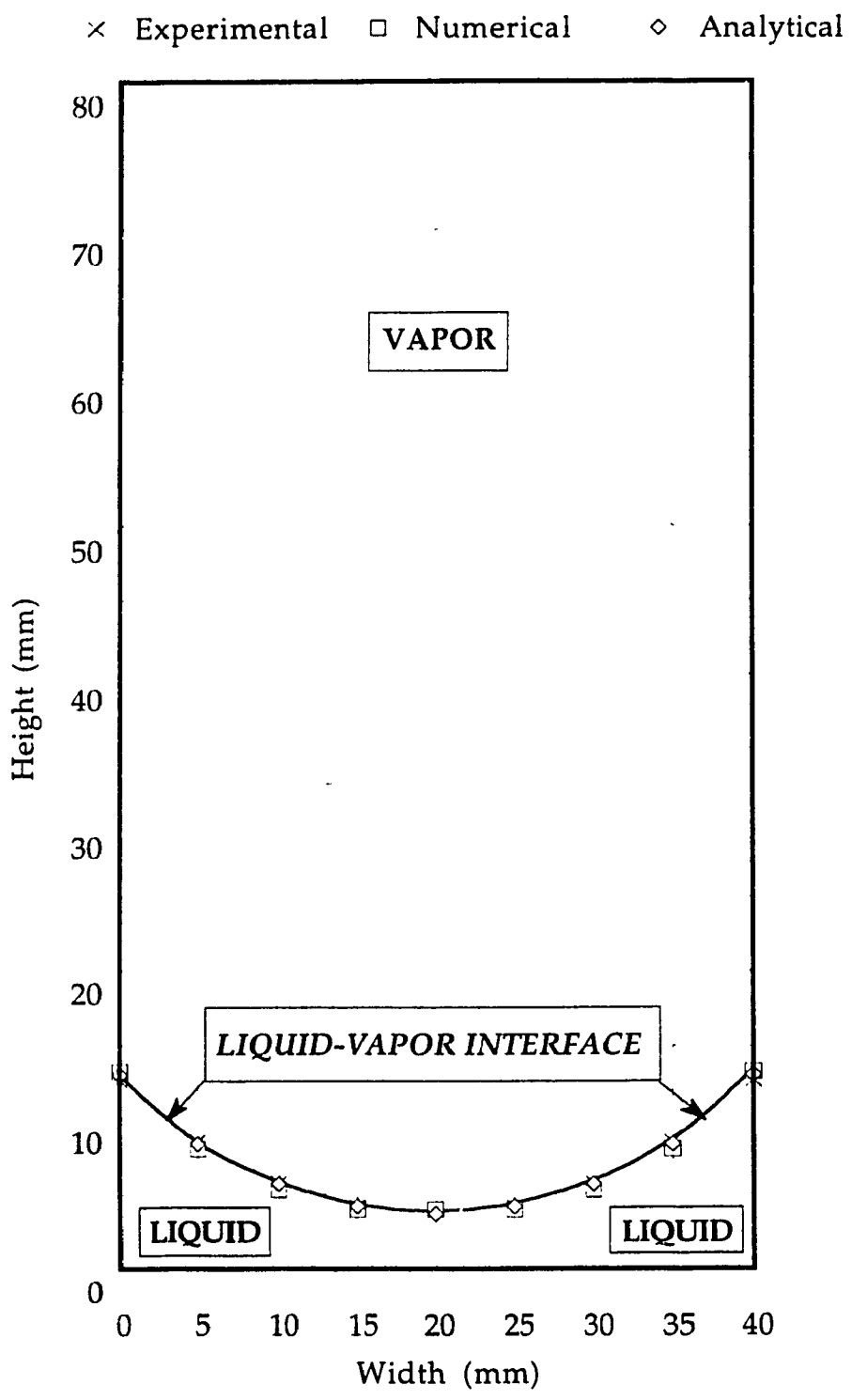


Fig. 4.3.3 Interface configuration for tebrabromoethane with 10% full ($\alpha$= 40$^{o}$)

agreement with the experimental data and the analytical solutions. The liquid-vapor interface configuration consists of a constant-curvature interface meeting the container walls at a contact angle of 40°. For this contact angle, the configuration 1 is maintained for both high and low initial liquid height.

Figure 4.3.4 shows the 0-g equilibrium interface configuration for alcohol ($\alpha = 0°$) at an initial filling of 50 % full. In general, the difference among results are quite small. A deviation at the wall is presented since it is difficult to observe the liquid height at the wall in experiment. Both numerical and experimental results for the interface configuration for alcohol ($\alpha = 0°$) at the initial filling of 10 % full at the 0-g equilibrium state agree well, as shown in Fig.4.3.5. The numerical data indicate that a small amount of liquid did adhere to the tank walls. This quantity of liquid, in general, is quite small. The liquid is separated staying at the corners of the container reflecting the effect of the contact angle, which also supports the hypothesis of configuration system 2 by the analytical method.

The validation of the configuration of liquid-vapor interface for non-wetting liquid in zero-gravity environment has also been made by these methods. Figures 4.3.6 and 4.3.7 indicate that the excellent agreement for the interface configuration of mercury (contact angle = 125°) at 50 % and 10 % full, respectively.

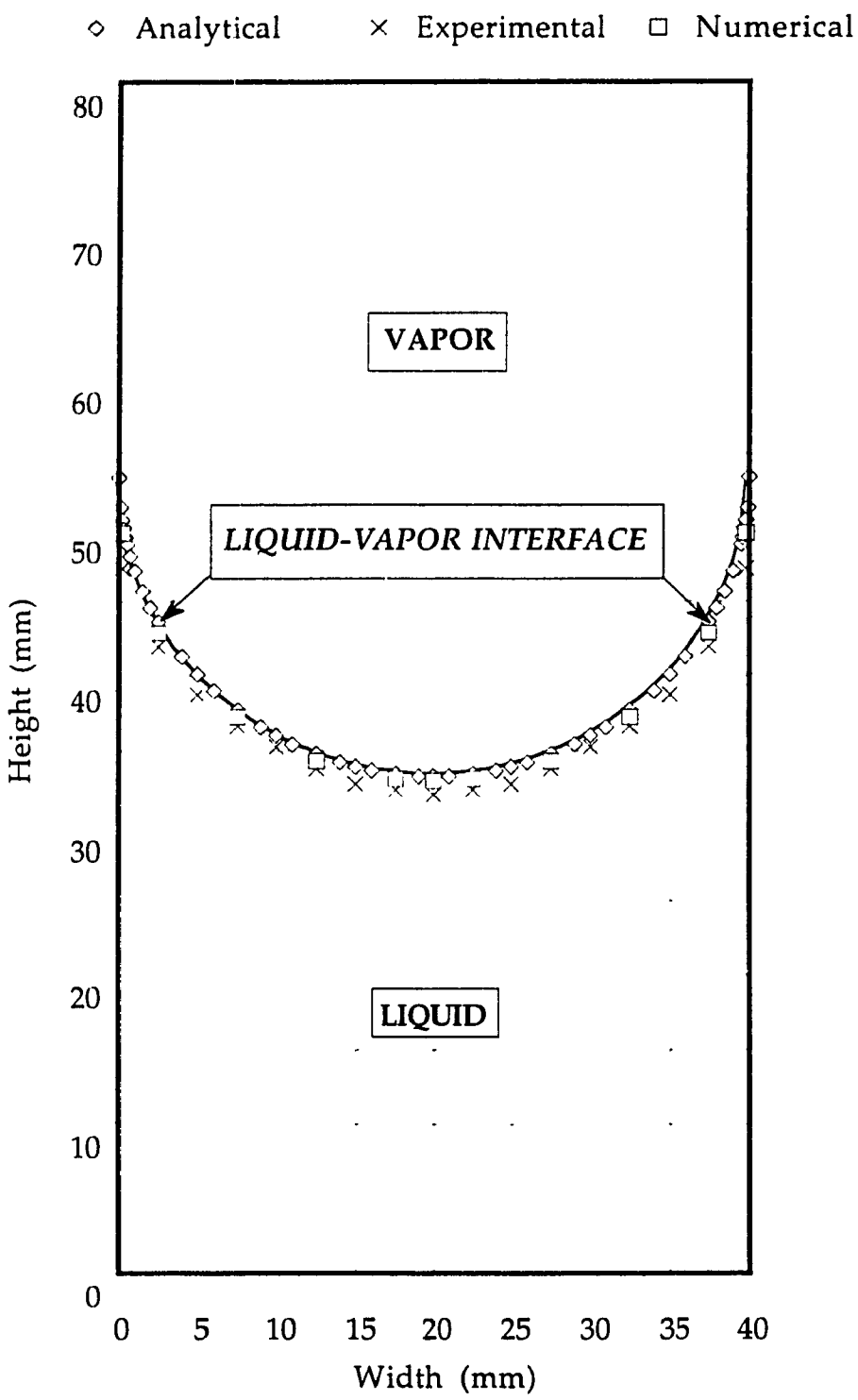


Fig.4.3.4 Interface configuration for alcohol with 50% full ($\alpha = 0^{o}$)

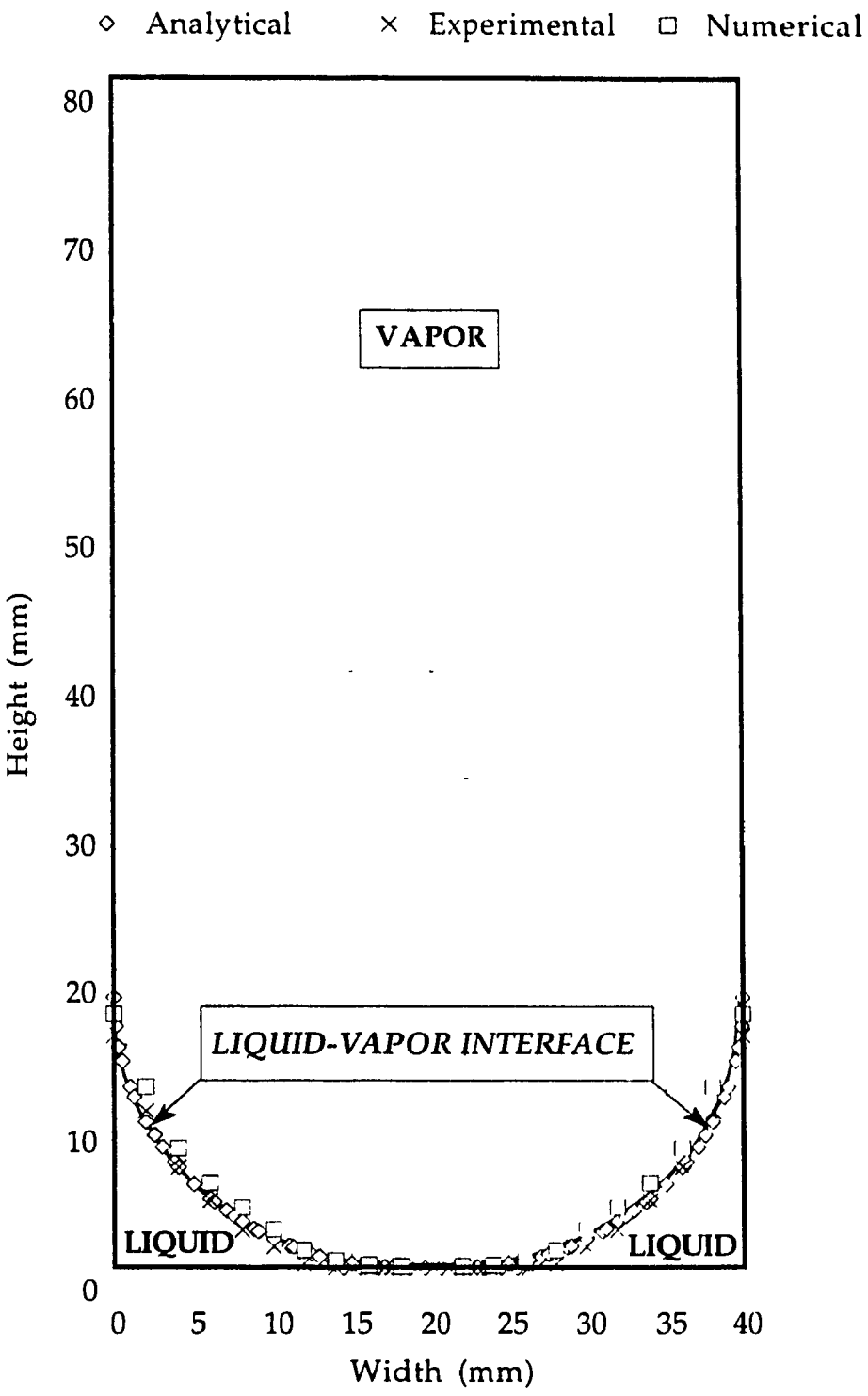


Fig.4.3.5 Interface configuration for alcohol with 10% full ($\alpha = 0^{o}$)

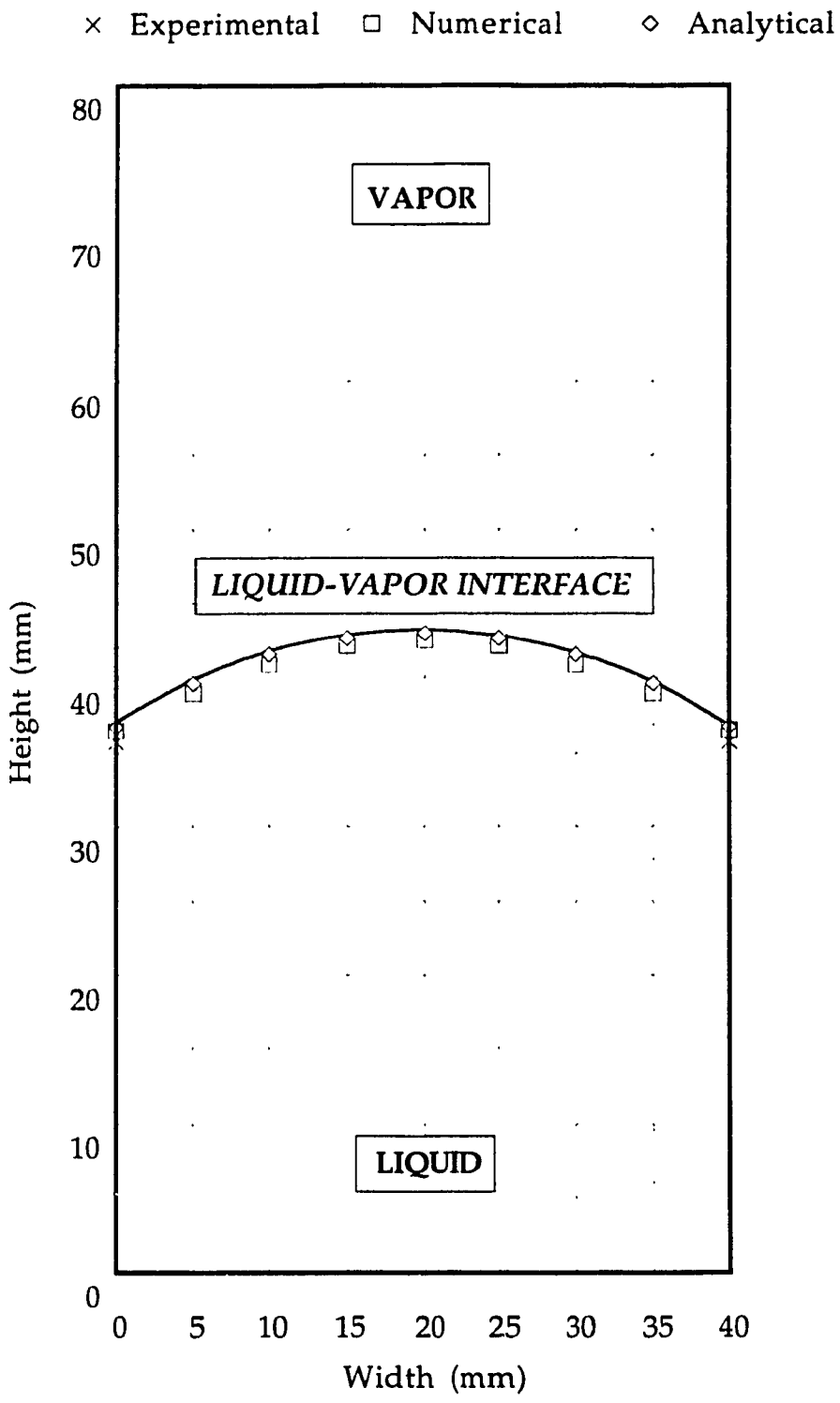


Fig.4.3.6 Interface configuration for mercury with 50% full ($\alpha = 125^{o}$)

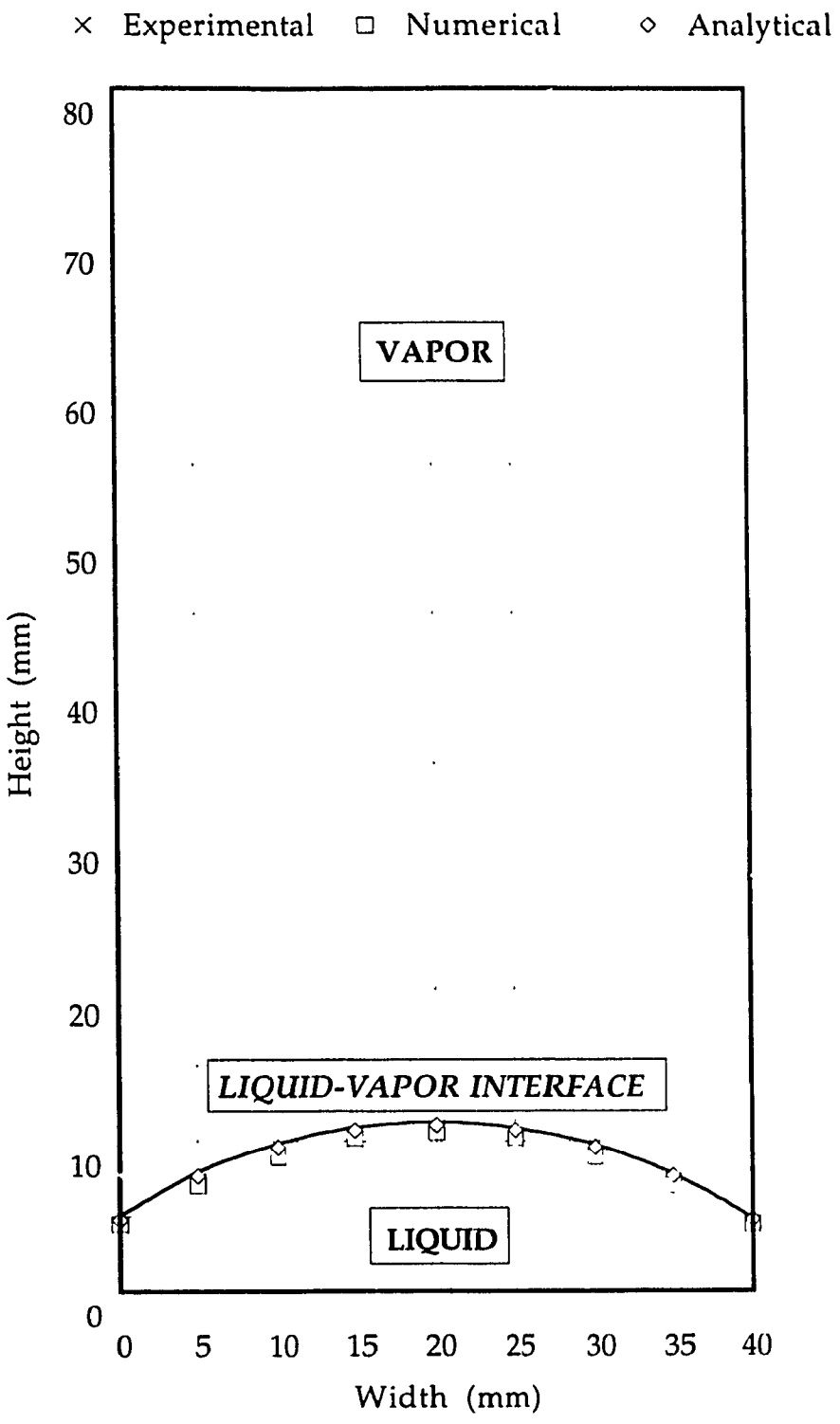


Fig.4.3.7 Interface configuration for mercury with 10% full ($\alpha = 125^{0}$)

The results of this investigation further reveal that, the geometry of the system can significantly alter the interface configuration since the contact angle is preserved, and that end effects can be present at dimensionless liquid height. A number of interface configurations may occur depending on the contact angle of the liquid at low liquid height.

These satisfactory correlations with experiments inspire confidence in the use of the computational model to predict the liquid response in spacecraft tanks due to gravity change.

# CHAPTER 5

# LIQUID MOTION DURING OUTFLOW IN WEIGHTLESSNESS

## 5.1 Interface Dynamics during Outflow

Various phenomena occurring when liquid outflow from tanks in a zero-gravity environment will be studied. The scope of this investigation includes tank geometry, liquid properties and flow conditions.

The liquid-vapor interface will be affected by liquid outflow. The draining phenomenon is illustrated in the time sequences in Fig.5.1.1. The vector plots indicate the interface shape and liquid motion during draining of a liquid from a rectangular tank through a center opening in the bottom of the tank with an outflow velocity of 8 m/s. Outflow was simulated to be initiated at 10 seconds after exposing the system to weightlessness, when the interface reached its equilibrium conically shaped configuration. The interface distorts from its initially curved surface. A considerable amount of liquid remains on the tank walls as the interface moves in the direction of the tank outlet shortly after outflow begins, as seen at 0.0156 seconds. It is clear from the frame at 0.0404 seconds that the interface velocity at the center was higher than that near the tank wall, so that the interface was distorted. The distortion of the interface persisted until a time of 0.09 seconds after initiation of outflow, when the draining was terminated. The remaining outlet flow was a

mixture of liquid and vapor. This severe interface distortion liquid residuals remaining in the corners of the tank.

Consider the same situation but this time, the outflow velocity is low. When outflow at the relatively low outlet velocity of 4m/s begins, the interface is initially distorted, as seen at t = 0.01271 seconds in Fig.5.1.2. As outflow continues, the interface at the centerline remains nearly stationary as liquid is removed from the tank wall until the liquid-vapor interface has nearly returned to its 0-g equilibrium configuration. The entire interface then progresses towards the tank outlet until the inception of vapor ingestion. The interface distortion is reduced when the outflow velocity is decreased, resulting in less liquid residual.

Further reduction of interface distortion can be obtained by placing the outlet location at the corner of the tank. The phenomenon is illustrated in the time sequences in Fig.5.1.3 for typical draining cases. The outflow draws the interface above the outlet opening downwards to compensate the velocity difference among the centerline and outlet line. The results of interface distortion during corner draining can be seen in Fig.5.1.4 in the form of a time-distortion factor, where distortion factor is defined as the difference of the normalized liquid heights at center and at wall. The value of the distortion factor is smaller for corner draining than for center draining. The distorted interface was observed during the whole period of draining. The distortion due to outflow was larger than that without draining at $v_0$ = 8 m/s, see Fig.5.1.5.

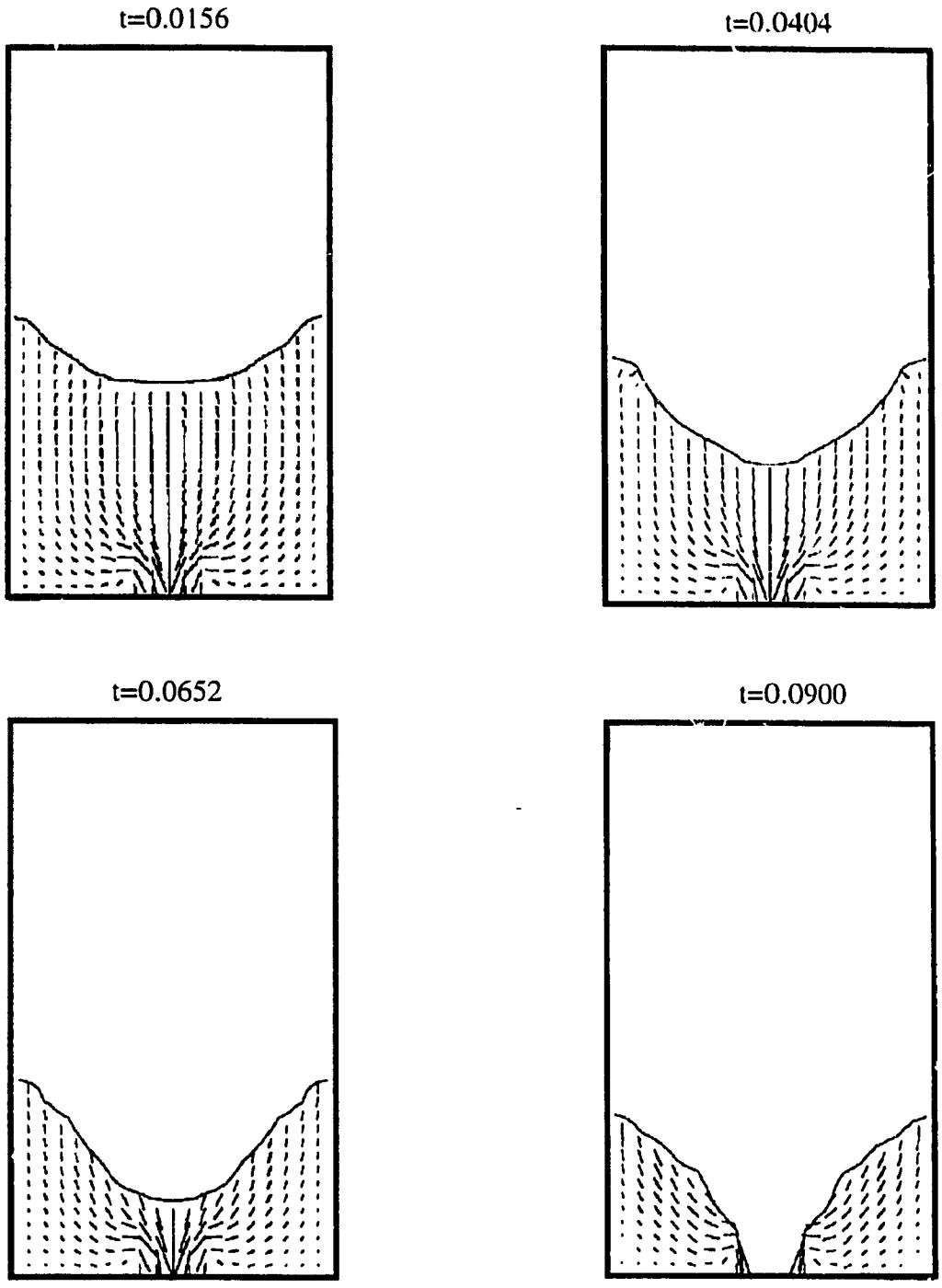


Fig.5.1.1 Liquid outflow initiated at 10 seconds after entering 0-g with 8 m/s outflow velocity

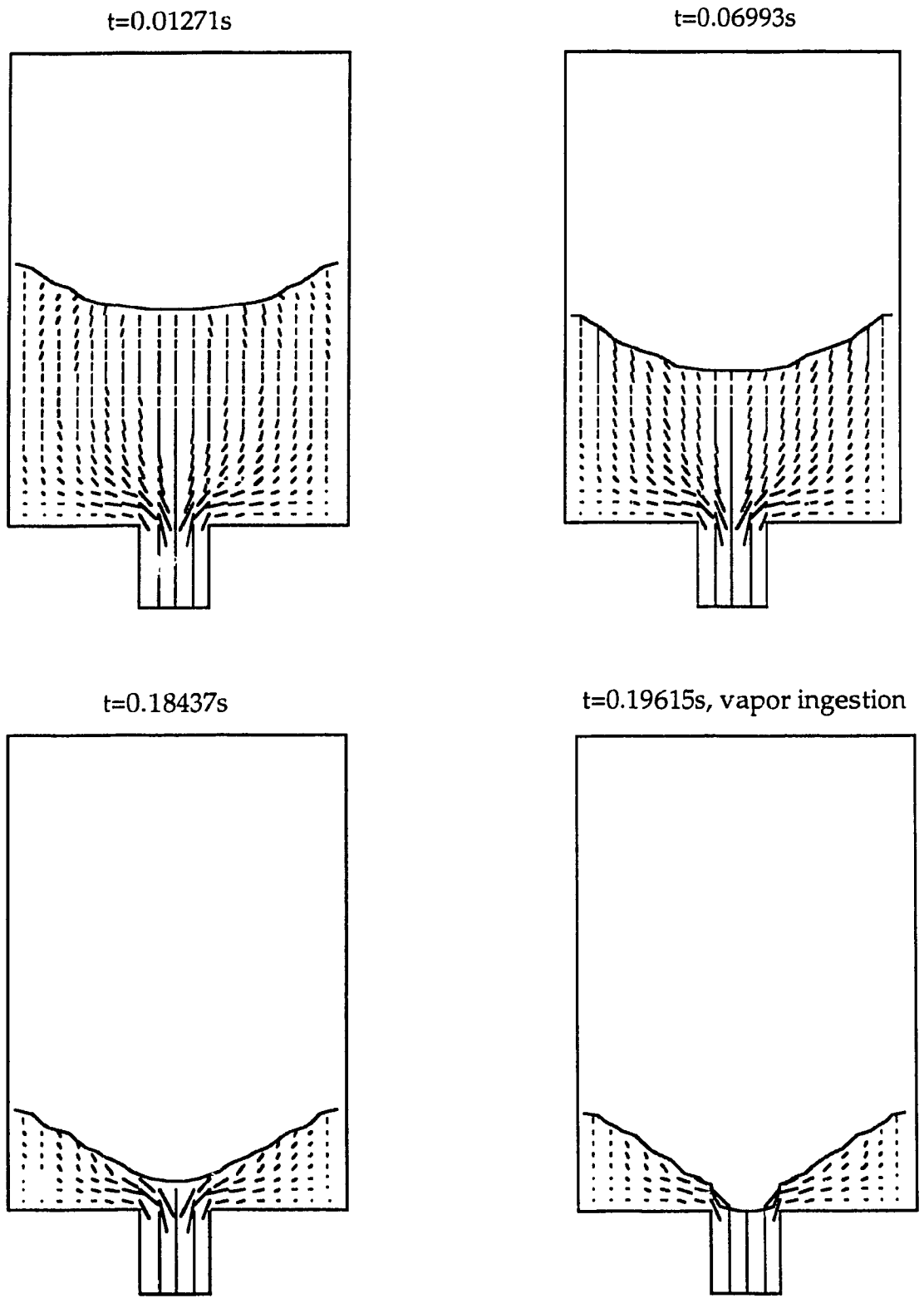


Fig.5.1.2 Outflow from center outlet initiated at 10 seconds after entering 0-g with 4 m/s outflow velocity

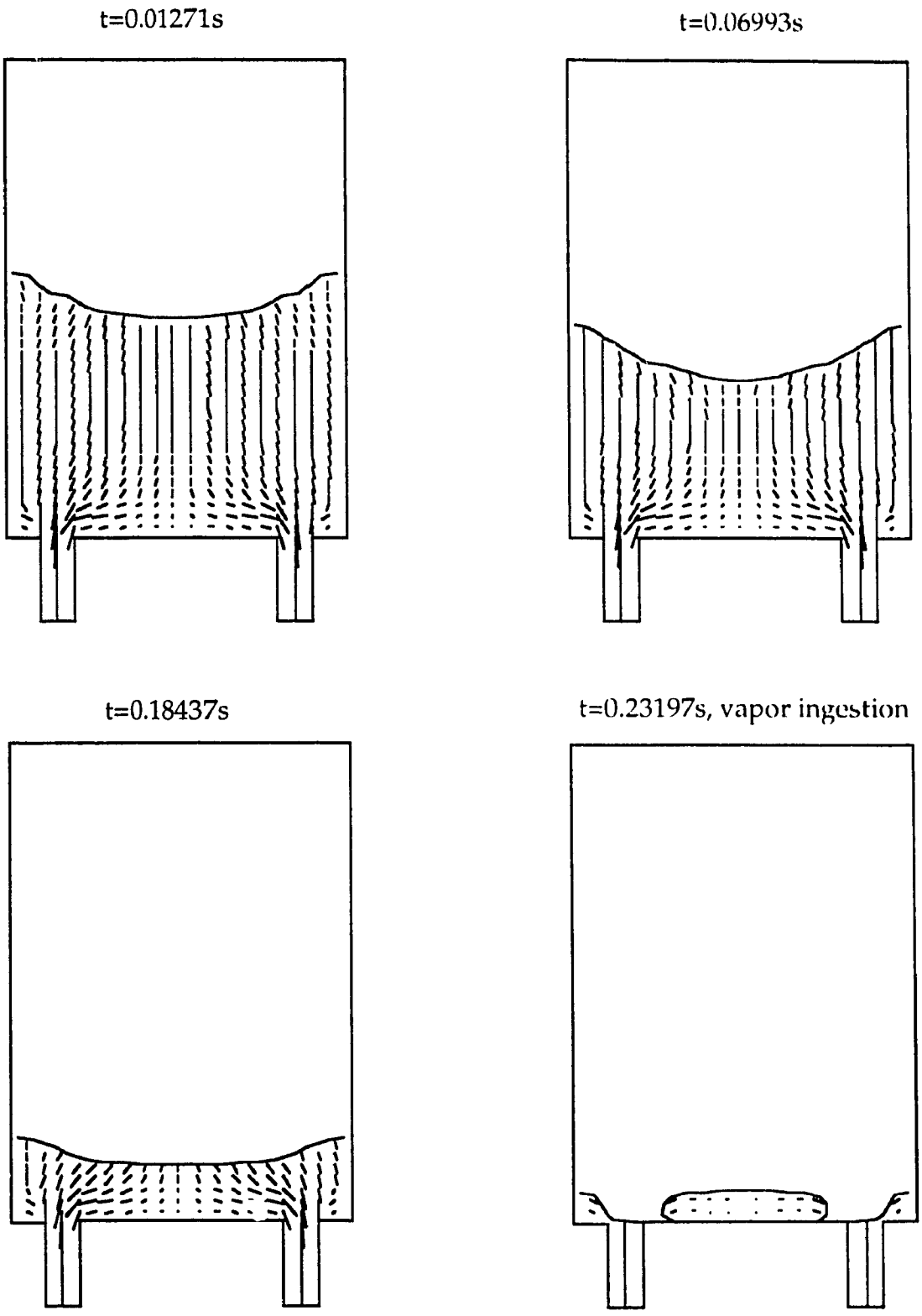


Fig.5.1.3 Outflow from corner initiated at 10 seconds after entering 0-g with 4m/s outflow velocity

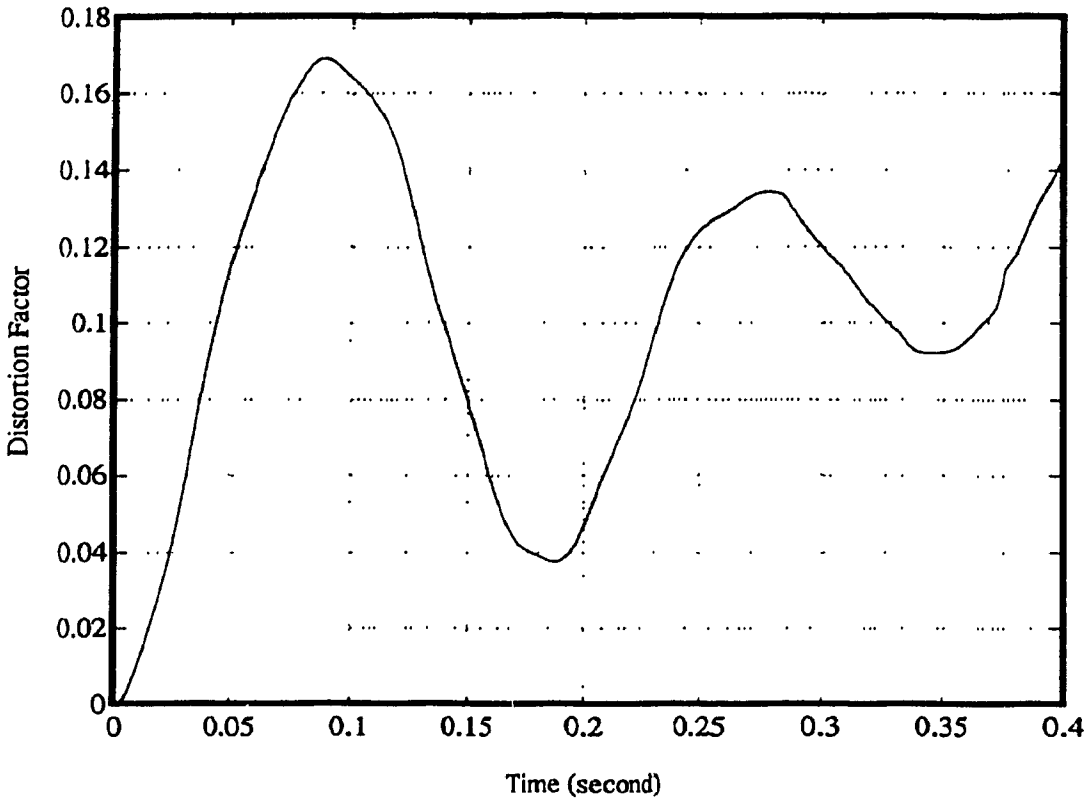


Fig.5.1.4 Distortion factor for draining from corner outlet starting at 0 second and $v_o$ = 2m/s

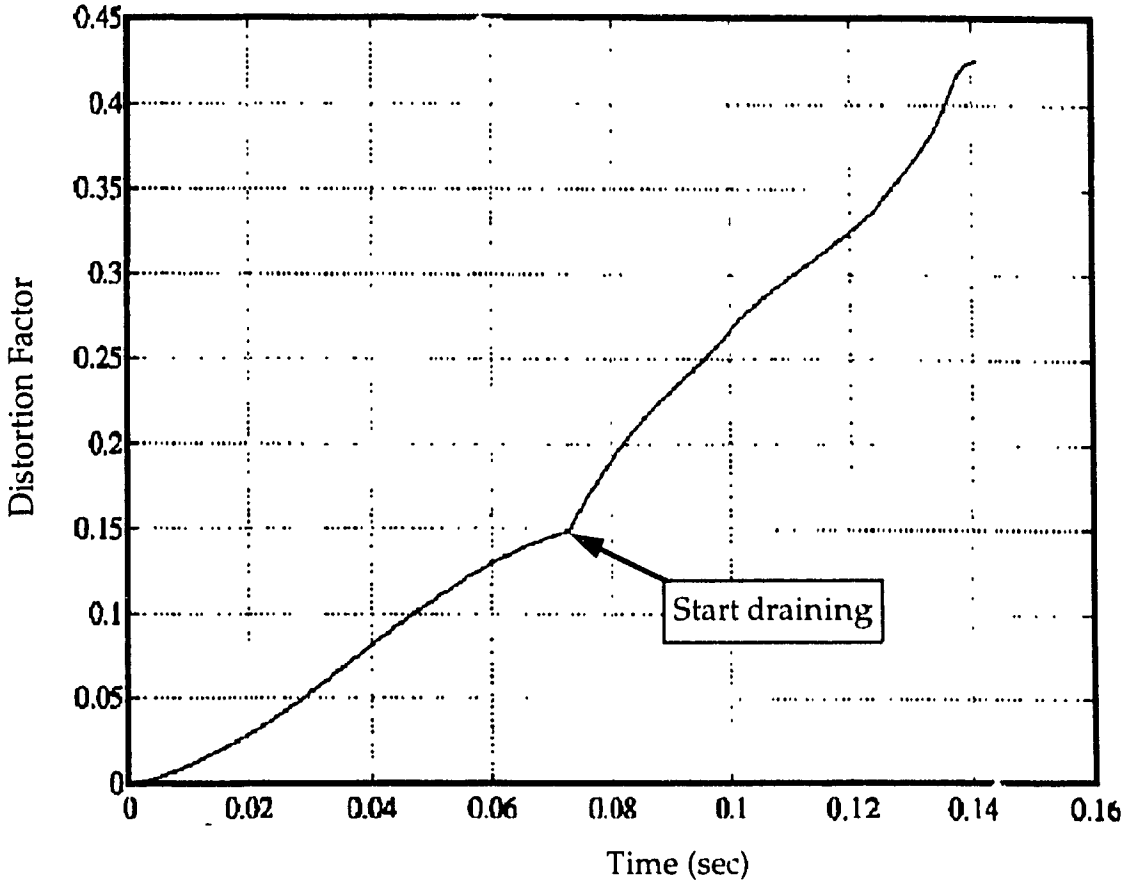


Fig.5.1.5 Distortion factor versus draining time

## 5.2 Interface Dynamics in Gravity Transition and Outflow

When entering a weightless environment, the system holds excessive energy, which may result in a periodic oscillation of liquid-vapor interface. When the outflow rate is very low, the interface is moving so slowly that the motion of the interface due to gravity transient effects may still be observed. The motion of a liquid-vapor interface as a function of draining time can be described by a time-displacement draining curve, as shown in Fig.5.2.1. For the outflow velocity of 0.5 m/s, the interface exhibits an oscillatory behavior since the transient effect is comparably larger than the draining effect. Thus, the interface motion is not dominated by inertia force. The interface oscillations continue throughout the draining. When compared to the one without draining, the frequency of the oscillations is decreased while the amplitude of the oscillations are fast decayed with the draining time due to the effects of both inertial forces and viscous dissipation. The inertia forces dominate the interface motion as the outflow rate is sufficiently large. Figure 5.2.2 is in illustration of its effect. The 16 m/s outflow velocity was so large that no interface oscillation was observed. It is clear that such large outflow rate is sufficient for the inertia forces to dominate the interface motion. The liquid-vapor interface proceeded to move smoothly after the beginning of the outflow. The interface velocity at the centerline was constant over most of the period of the draining time following the initial startup transient. An acceleration was observed when the interface approached the outlet.

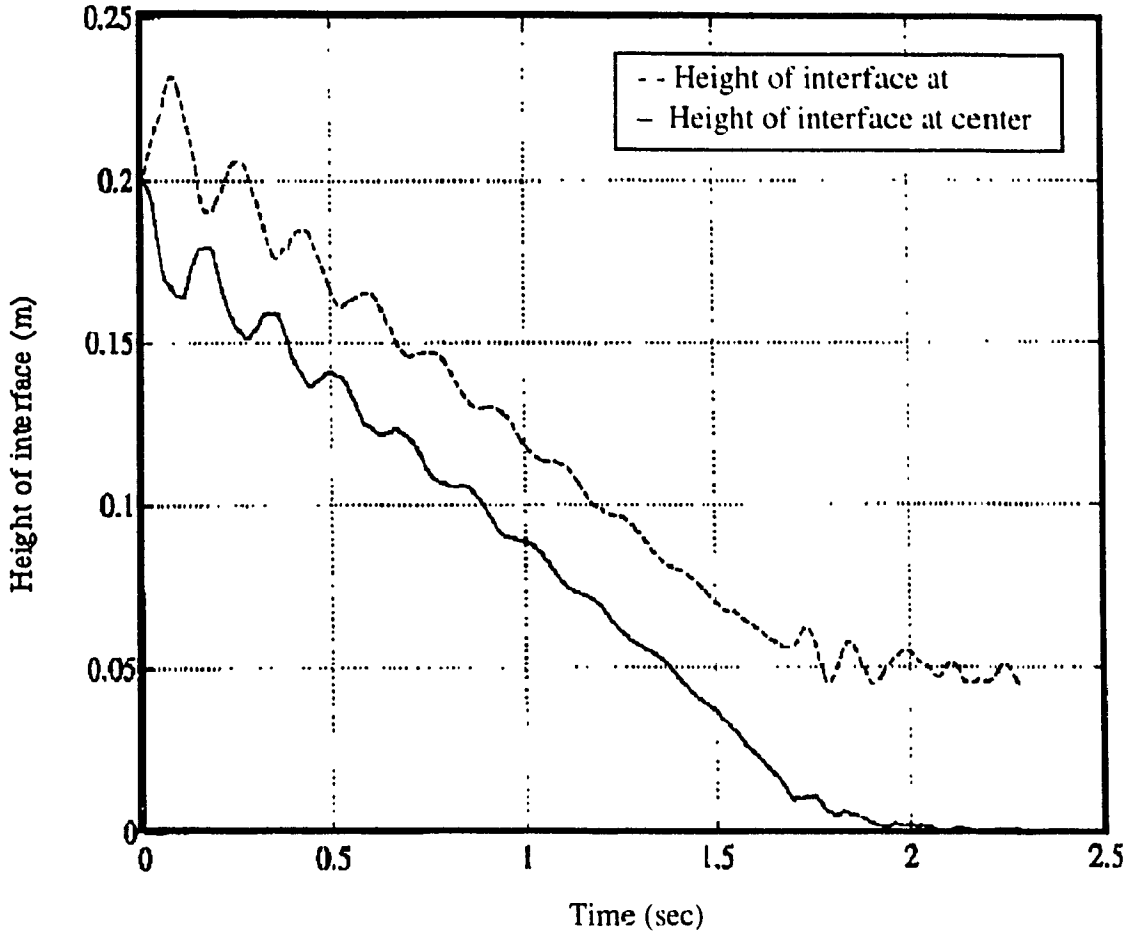


Fig.5.2.1 Centerline interface profiles for draining at center starting at 0 second and $v_o = 0.5$ m/s

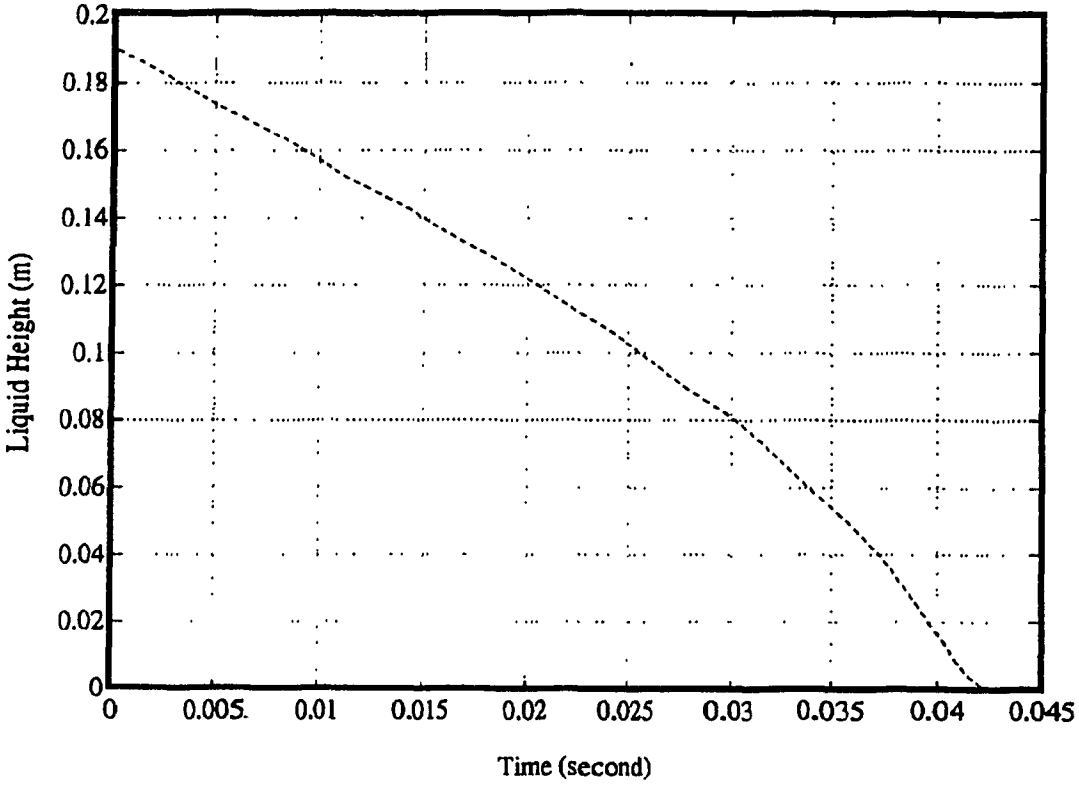


Fig.5.2.2 Draining at center starting at 0 second and $v_o = 16m/s$

The interface behavior is strongly dependent on the ratio of outflow velocity to the step gravity change. Figure 5.2.3 shows the number of interface oscillation cycles during the period of draining with outflow velocity. The higher the outflow velocity, the less the oscillation cycles, which means a comparably greater inertia influence and the less influence of the gravity transient. The representative draining curve of the simulation of a typical outflow test ($v_o$ = 8m/s) during weightlessness is presented in Fig.5.2.4 for a tank with center location of the outlet. The draining was initiated at 0.0725 seconds after the system entered a weightless environment, at which time the interface was at its lowest position of the first oscillation cycle. This initial draining start time is often used in experiments (Symons, 1979; Derdul et al, 1966; Berenyi et al, 1969), since the time required for the interface to come to 0-g equilibrium was too long to permit a draining test to follow. A constant velocity of the interface was reached following a very short transient period. This velocity was maintained constantly across most of the draining period until the interface approaches the outlet, after which the vapor enters the outlet.

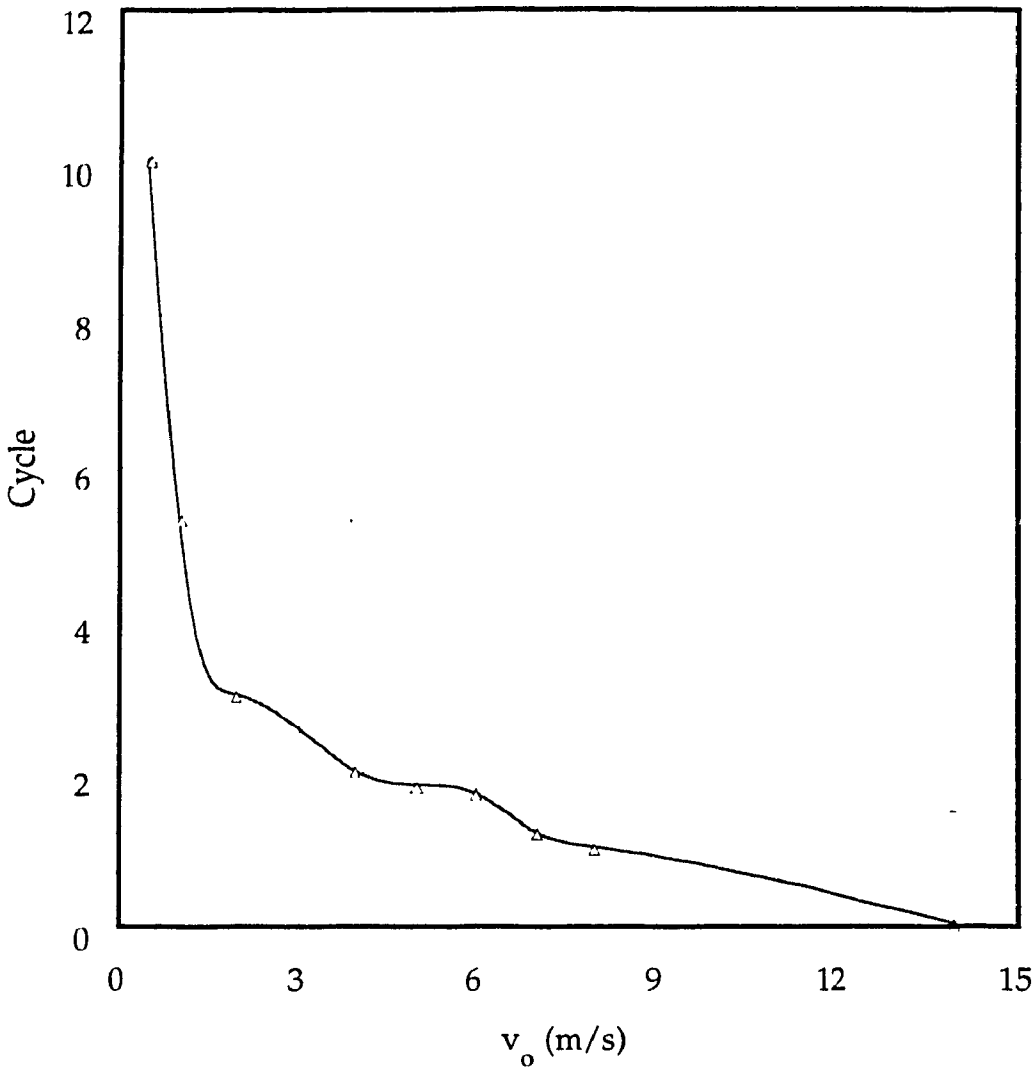


Fig.5.2.3 Interface oscillation versus outflow velocity when initiating draining upon entering 0-g environment

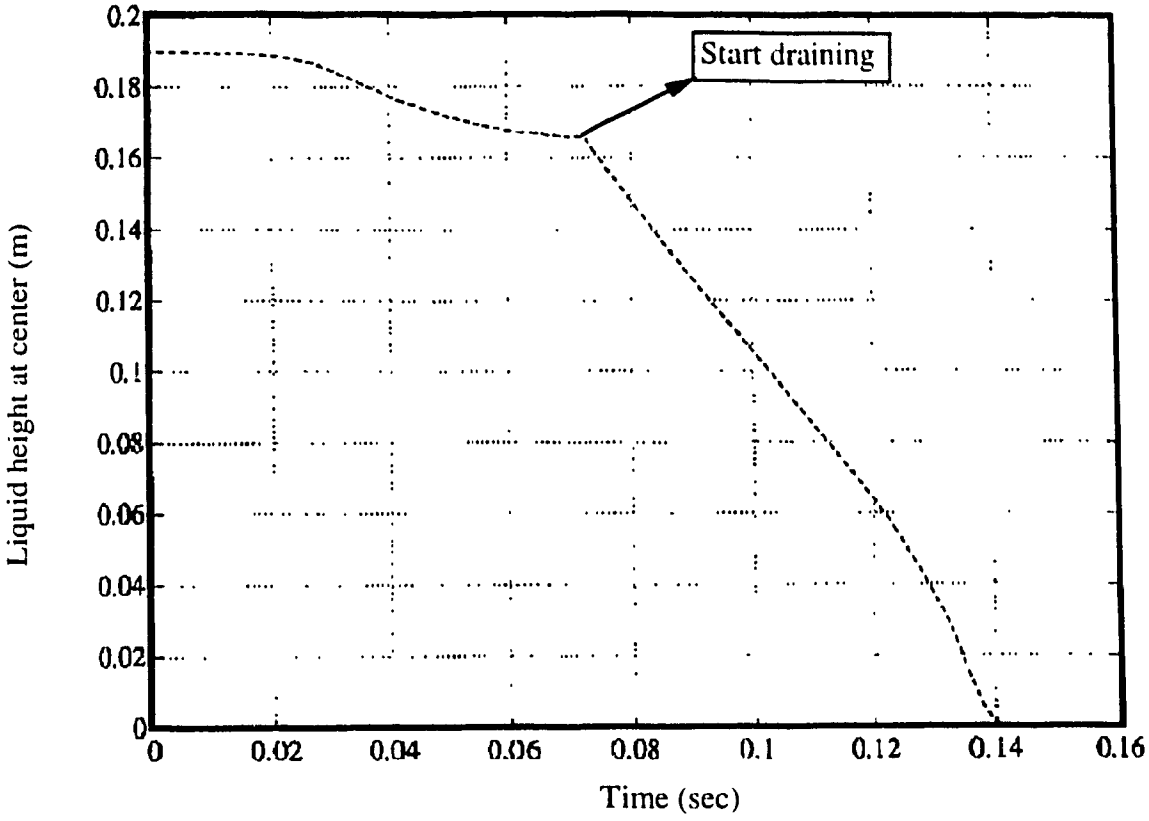


Fig.5.2.4 Interface height versus draining time

# CHAPTER 6

# LIQUID RESIDUALS DURING DRAINING

## 6.1 Liquid Residuals

The efficient use of stored liquids onboard a spacecraft requires the predetermined knowledge of the liquid behavior during draining in weightlessness. The liquid residuals in the tank at the termination of draining are very important since it represents the effective tank volume and unavailable liquid amount. In spacecrafts and their missions, vapor reaching a tank outlet must be avoided. The instant that vapor reaches the tank outlet, draining is considered terminated although the mixture of liquid and vapor may be continually drawn from the tank until the liquid is depleted. Thus, the liquid residuals are the amount of liquid remaining in the tank at the instant of vapor ingestion in the outlet of the tank.

Liquid residuals are determined by subtracting the drained liquid volume from the initial liquid volume $V_I$, in the tank. The total amount of drained liquid is the production of the draining time and the outflow rate. Therefore, the longer the draining time, the less the liquid residuals will be, provided the constant flow rate is maintained. The draining time is widely used in the zero-gravity experimental tests. The liquid residuals are also expressed in dimensionless form as the residual ratio of residual liquid volume at the time of draining termination to the initial liquid volume. The

dimensionless liquid residuals $\overline{V}_R$, are the ratio of the liquid residual volume to the initial liquid volume in the tank. Both draining time and dimensionless liquid residuals are used as the criteria to evaluate the effects on liquid residuals.

The behavior of the liquid residuals $V_R$, during outflow in weightlessness is discussed in relation to the variables of outflow velocity, draining start time, outlet location, outlet pipe, viscosity, contact angle, initial height and critical height. The results can be used to assist the design of a liquid tank that is capable of reducing the liquid residuals.

## 6.2 Effect of Outflow Velocity

The results of the numerical simulation presented in Fig.6.2.1 show the liquid inside the tank just before and after draining termination. The visual observation clearly illustrates the effects of the magnitude of different outflow velocity. The significant distortion of the liquid-vapor interface due to high outflow velocity results in an appreciable amount of liquid remaining on the tank walls when vapor enters the outlet as compared to that observed at the low value of outlet velocity. The liquid residual is much greater for 16 m/s than for 2 m/s, due to the fact that when the outflow velocity is decreased, the interface distortion is thus reduced. The reduction of outflow velocity lowers the liquid height at which vapor ingestion occurs, resulting in less liquid residuals.

The liquid residuals are found to be the function of outflow velocity. The larger the outflow velocity the more the residuals. These findings agree with the observations from an experimental study, conducted by Nussle et al (1965) in a 2.3-second drop tower although the experiment was limited to one test liquid in a cylindrical tank, and outflow velocities of 2.91 m/s and 14.08 m/s. The results of the other experimental investigation conducted by Abdalla et al (1969) are compared with the numerical prediction. Experimentally, the flat-bottom cylindrical tanks were initially filled with liquid to a height of 2 tank radii L. A 2-centimeter-radius tank with a 0.1-centimeter-radius outlet forms the ratio of the outlet radius to the tank radius being 1:20. Figure 6.2.2 shows that the compared results generally agree very well with respect to high outflow velocities. An exceptional deviation was expected at the velocity of 10.08m/s. As explained in the experimental data by Abdalla et al (1969), the interface centerline remained at a constant height for a considerable length of time while liquid drained from the tank. The interface away from the centerline was moving downward when the center of the interface remained stationary. Since draining was initiated at a preset time for each zero-gravity test, the interface at the instant of outflow may not have been precisely at the low point. The gravity transient exerts the great effect on interface motion, as shown in Fig.6.2.3. When outflow is at low velocity, the motion of the interface is partially due to interface formation. The interface oscillation for low outflow velocities was clearly observed. With the increment of outflow velocity, the effect of gravity transient was less significant.

Reducing outflow velocity at the proper time during draining may delay the ingestion of vapor into the outlet line. A reduction in outflow

velocity decreases the Weber number in zero-gravity, which, in turn, lowers the height at which vapor ingestion occurs. If the outflow velocity keeps sufficiently low, the interface will retain essentially its equilibrium shape and the maximum amount of liquid will be expelled.

Figure 6.2.4 shows that in the center draining the residuals are closely related to outflow velocity, where residuals are expressed as the ratio of residual liquid volume at the time of vapor ingestion to the initial liquid volume. It is observed that the liquid residuals in the tank increase with the velocity. The increment of liquid residuals is larger at low velocities than at high velocities. However, the liquid residuals become constant at high velocity since a constant value of distortion is reached. This phenomena confirms the experimental results (Abdalla et al, 1969).

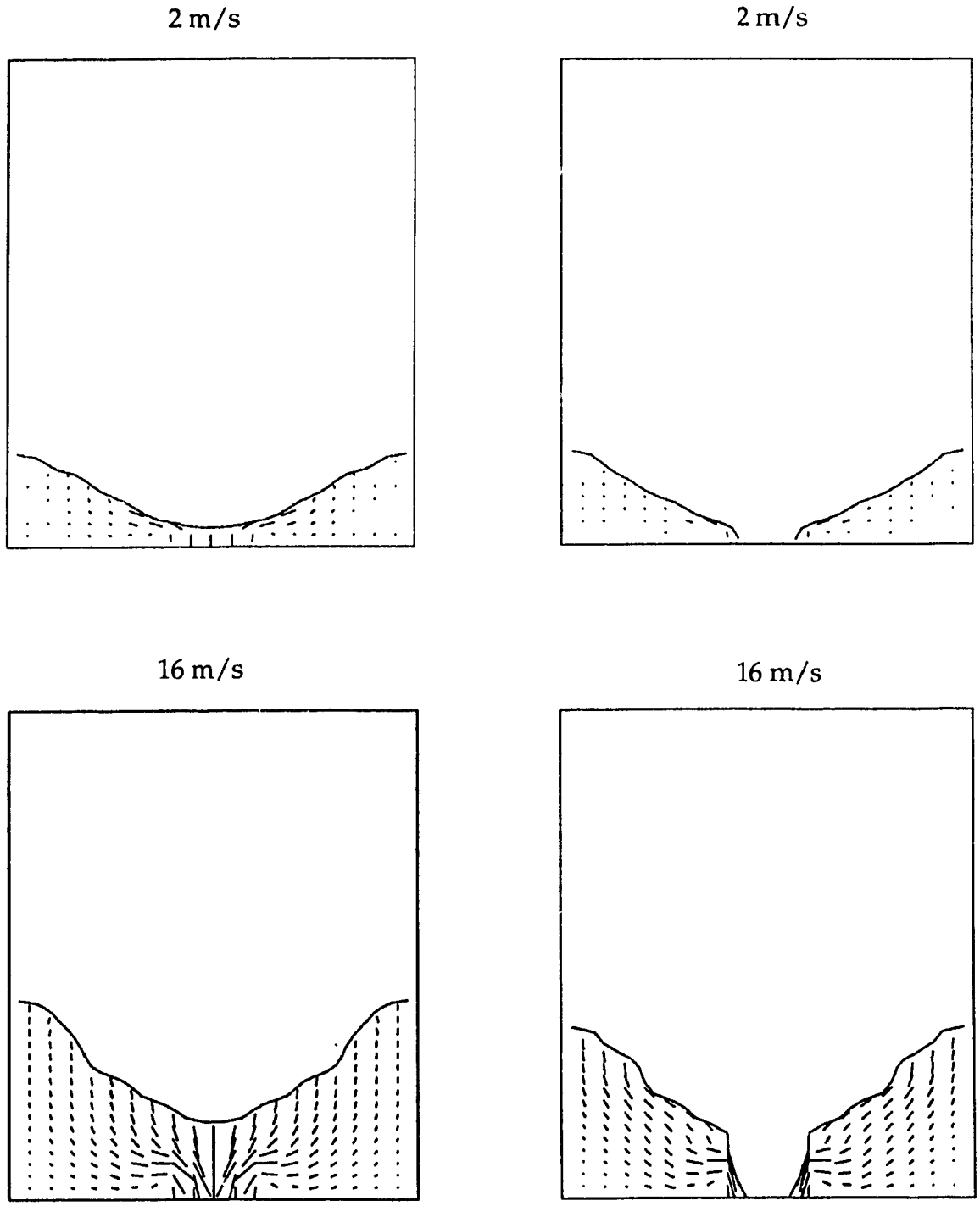


Fig.6.2.1 Draining with outflow velocities of 2 and 16 m/s

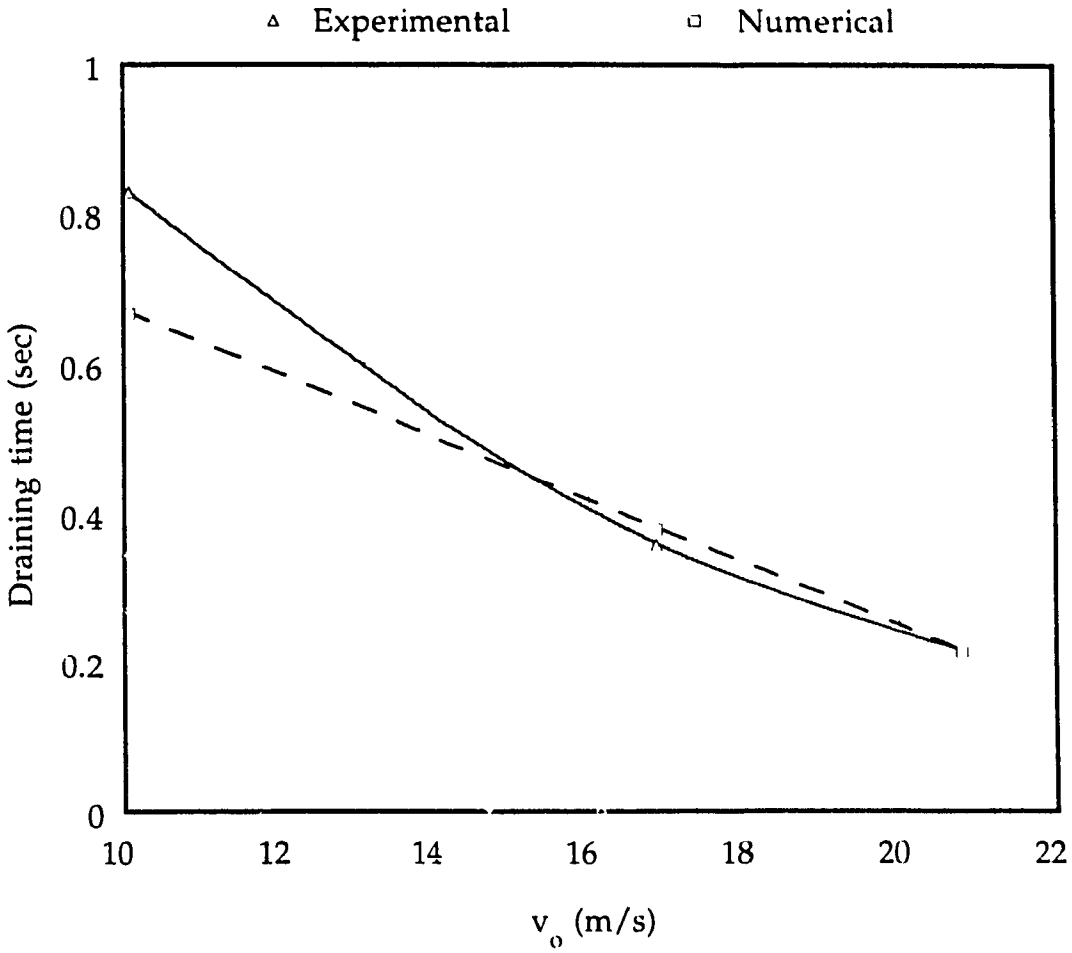


Fig.6.2.2 Draining time versus outflow velocity

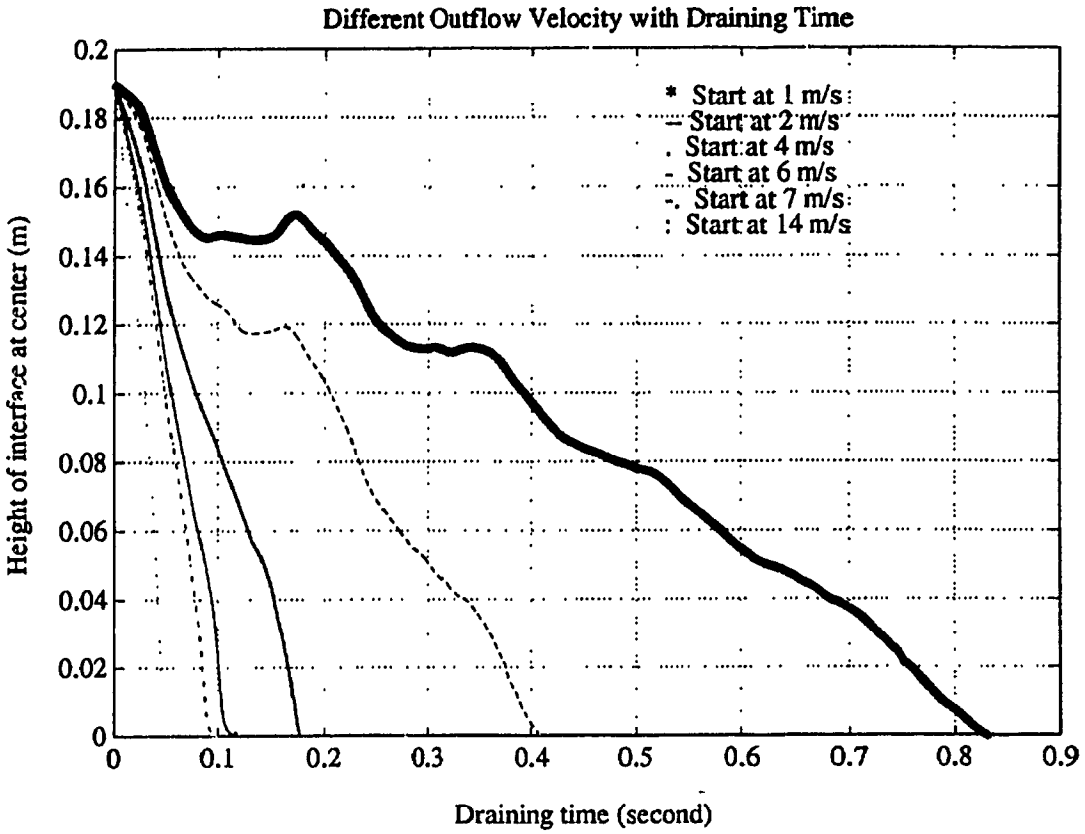


Fig.6.2.3 Different outflow velocity versus draining time

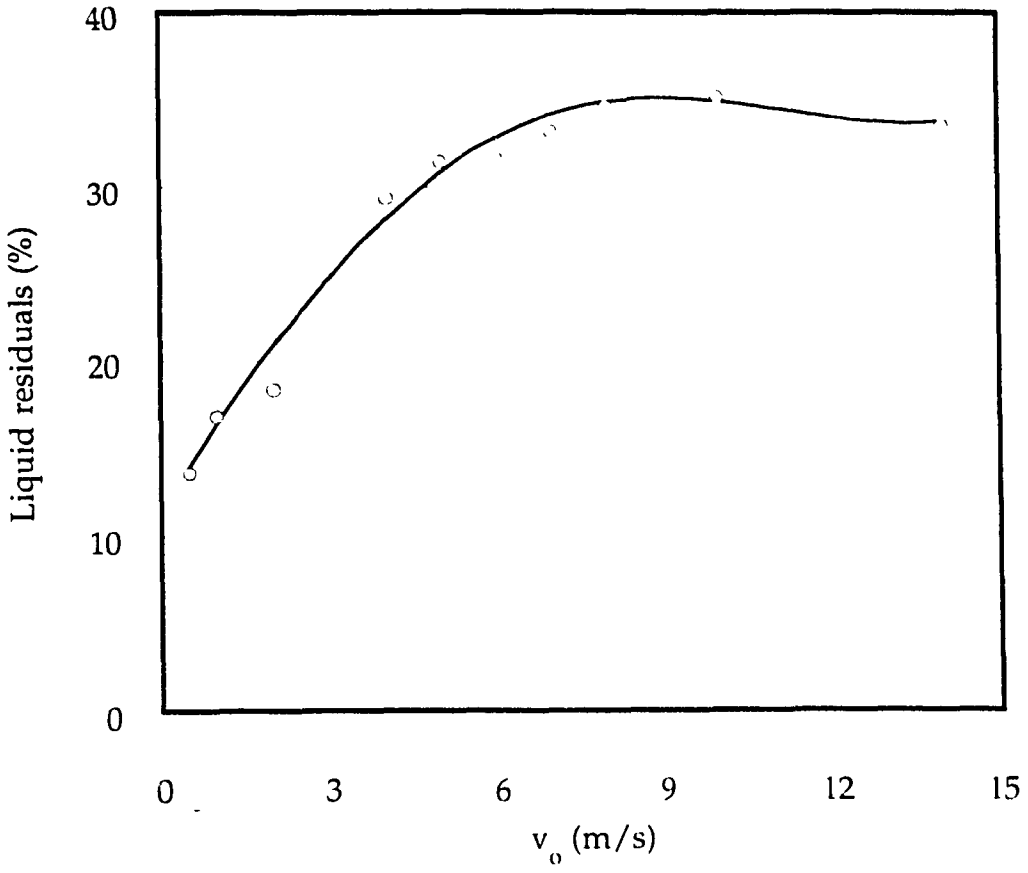


Fig.6.2.4 Liquid residuals versus outflow velocity at center draining

## 6.3 Effect of Gravity Transient

As previously mentioned, the liquid-vapor interface oscillates about its 0-g steady state configuration for a period of time after the system enters a zero-gravity environment. Owing to the limitation of the experiment, which is the time to reach its 0-g equilibrium usually exceeding the time available in drop towers, draining was initiated shortly upon entering into weightlessness, such that the draining was begun when the interface had reached the lowest point in its first pass through equilibrium. By that time, however, the interface had not in effect reached its 0-g equilibrium configuration. This may lead to inaccurate experimental data since the gravity transient had considerable effect on the liquid. Fortunately, the outflow can be simulated at any desired time period to ensure that the outflow is initiated when the system is at the 0-g equilibrium state. The computational method has overcome this difficulty and enable the long test time available, which can also be used to show the transient effects on the results.

The effect of transient residuals is evaluated in terms of liquid residuals. Figure 6.3.1 shows a draining curve of the interface motion for a draining was initiated at 10 seconds at which time, the system has reached its 0-g equilibrium state. The interface oscillation at center and walls were very noticeable. The effects of draining start time were examined. Draining start time is the time when the outflow is initiated after the system exposed to 0-g environment. Several draining start times commonly used in the drop tower experiments (Nussle et al, 1965; Derdul et al, 1966; Symons, 1979; Berenyi et al, 1969; Abdalla et al, 1969) and a start time of 10 seconds when the interface has reached the 0-g equilibrium condition were used in the simulations. Figure

6.3.2 shows the results of the draining time as a function of the start time at 8 m/s outflow velocity in the center outlet. It is evident that the draining time varied considerably with start time. The profile of the draining time curve is similar to the profile of the interface oscillation curve when the system entering 0-g environment without draining. Upon entering a zero-gravity environment, the interface oscillates, as already discussed, the initial interface heights are different corresponding to the draining start time. The draining curves for different start time are presented in Fig.6.3.3. The interfaces for different start time go downwards through the similar paths except one starting at 0.134 seconds which has the longest draining time. Both center and corner draining exhibit very similar behavior: the liquid residuals appear varied with draining start time as shown in Fig.6.3.4. The time and the position of the interface when the outflow is initiated affect the liquid residuals.

The results of liquid residuals related to the draining start time are in conflict with the contention that the draining start time had no effect since the previous experiment tests did not have sufficient low-gravity time to investigate the residual gravity effects. Hence one can not assume that start time has no effect on the draining and the behavior of the interface was not influenced by residual transient effects, were previously assumed in a variety of drop tower experiments. Gravity residual transient effects may be less noticeable when the outflow velocity is large since a comparable large inertia force exists.

The longest draining time corresponds to the least interface distortion, as shown in Fig.6.3.5. It shows the difference of the interface heights at the

centerline and the end during the corner draining. The interface displays a rather smooth distortion for different draining start time. In general, the smaller interface distortion in the form of the smaller height difference results in the longer draining time or less liquid residuals.

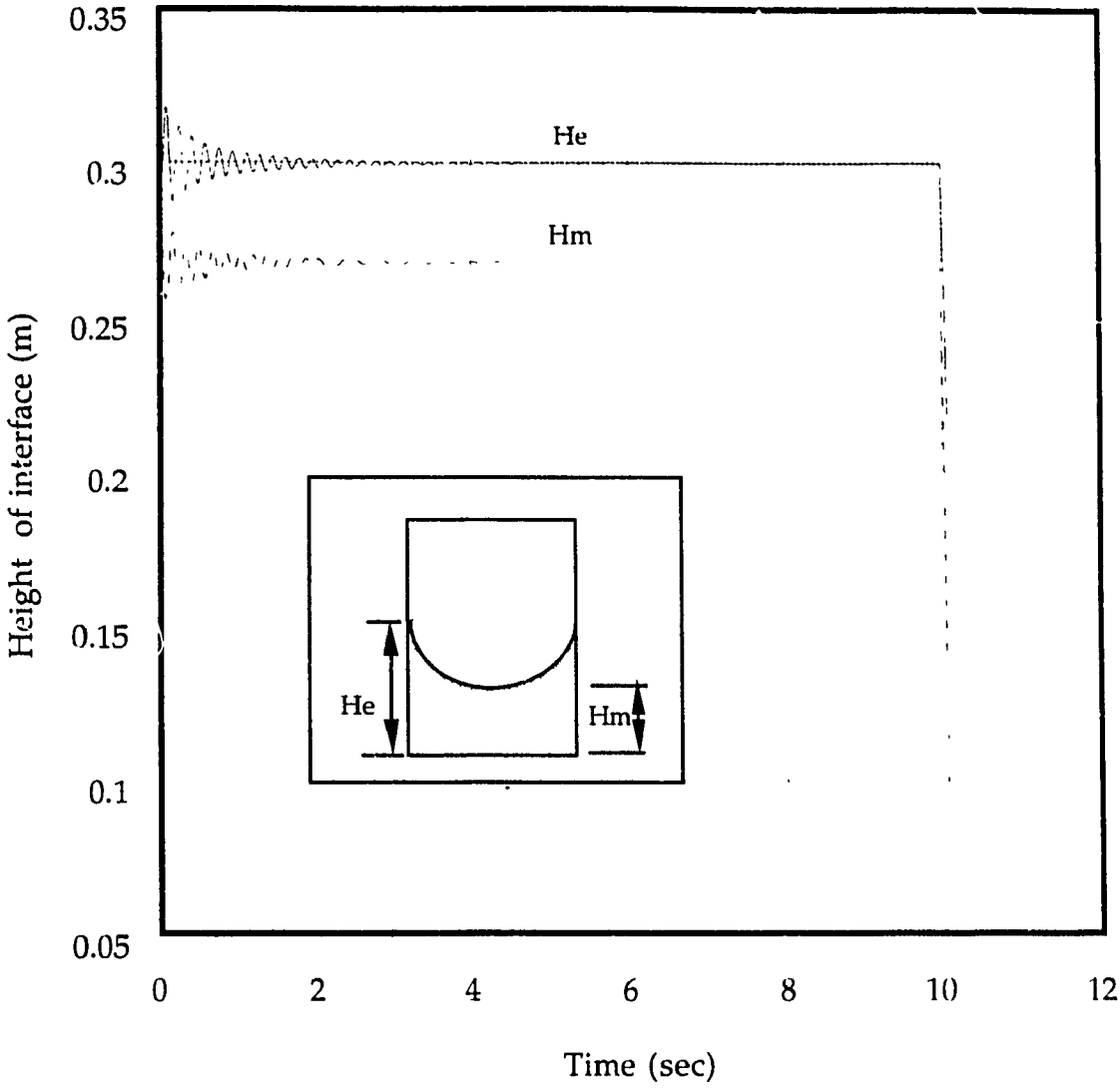


Fig.6.3.1 Outflow initiated at 10 seconds upon entering 0-g environment, 8m/s outflow velocity, center draining with outlet pipe

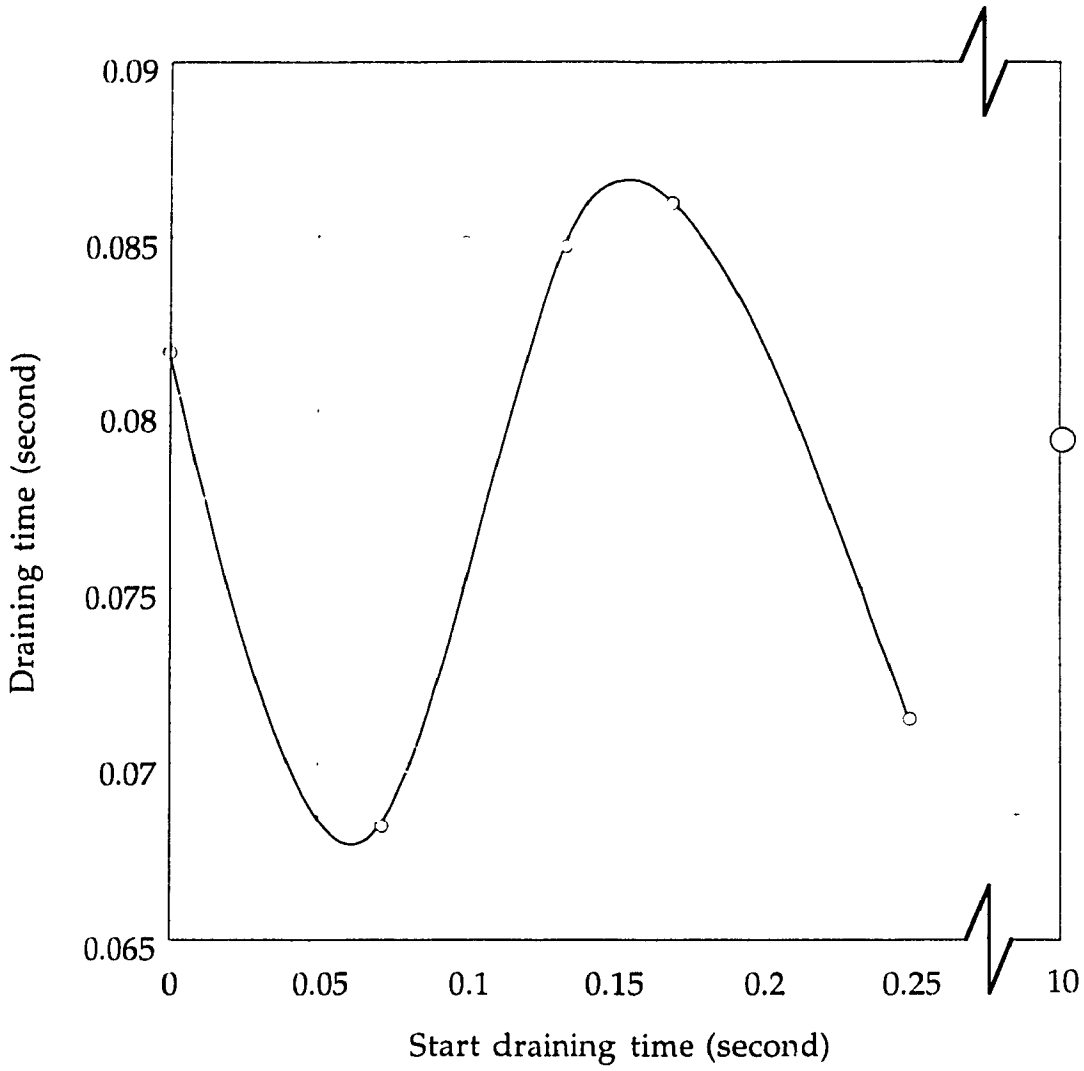


Fig.6.3.2 Draining time versus draining start time after entering 0-g environment

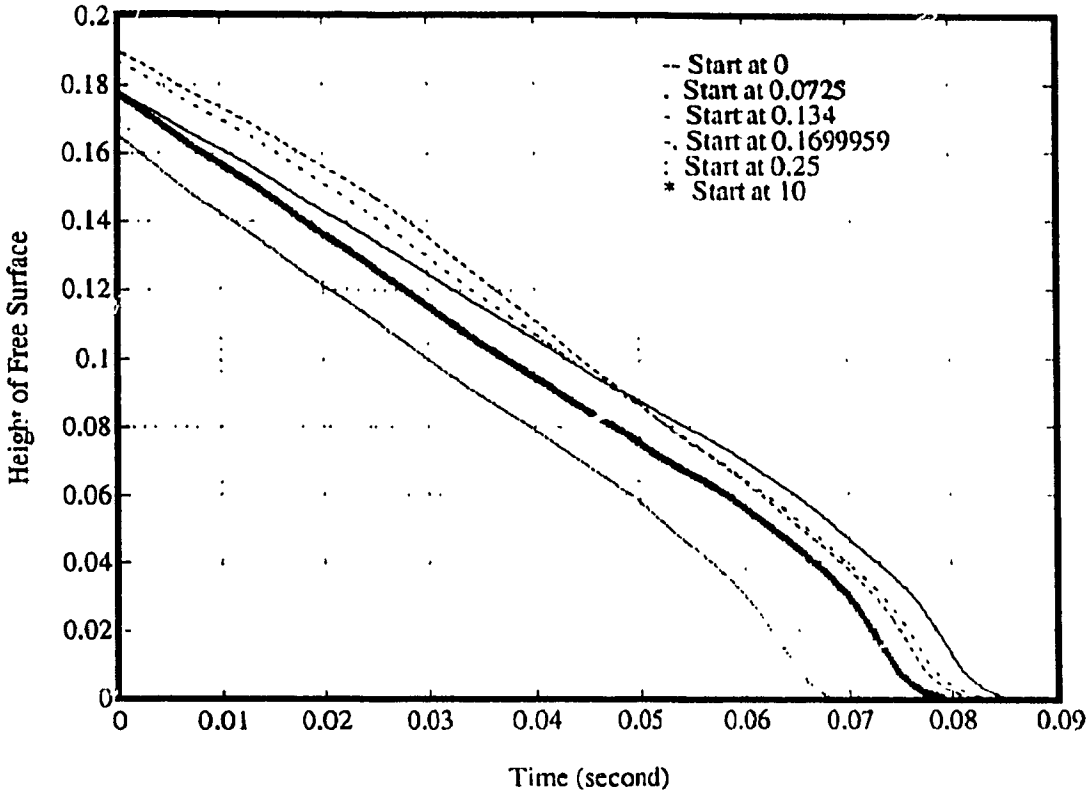


Fig.6.3.3 Different draining start time versus vapor ingestion time

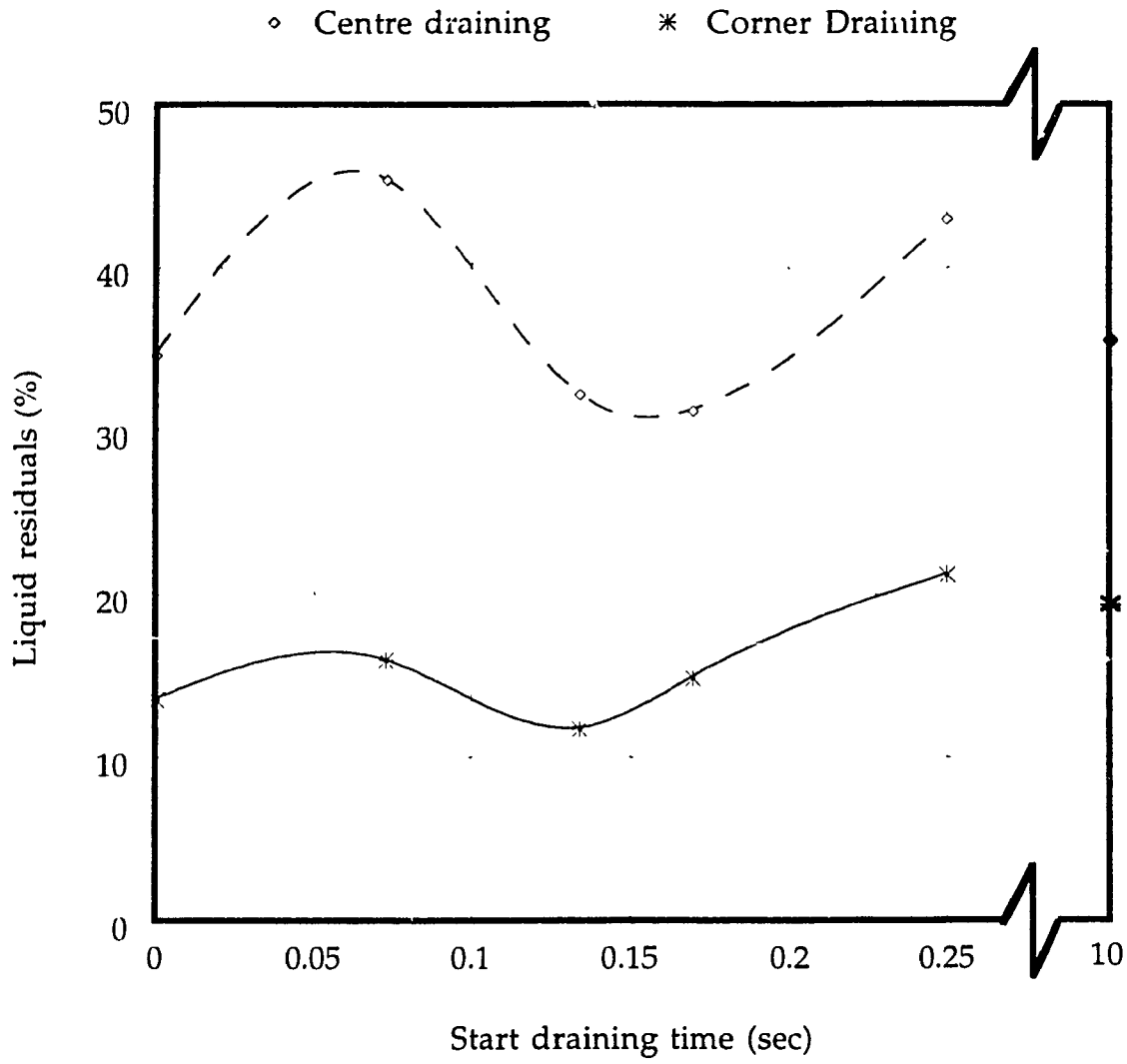


Fig.6.3.4 Liquid residuals versus draining start time at $v_o = 8m/s$

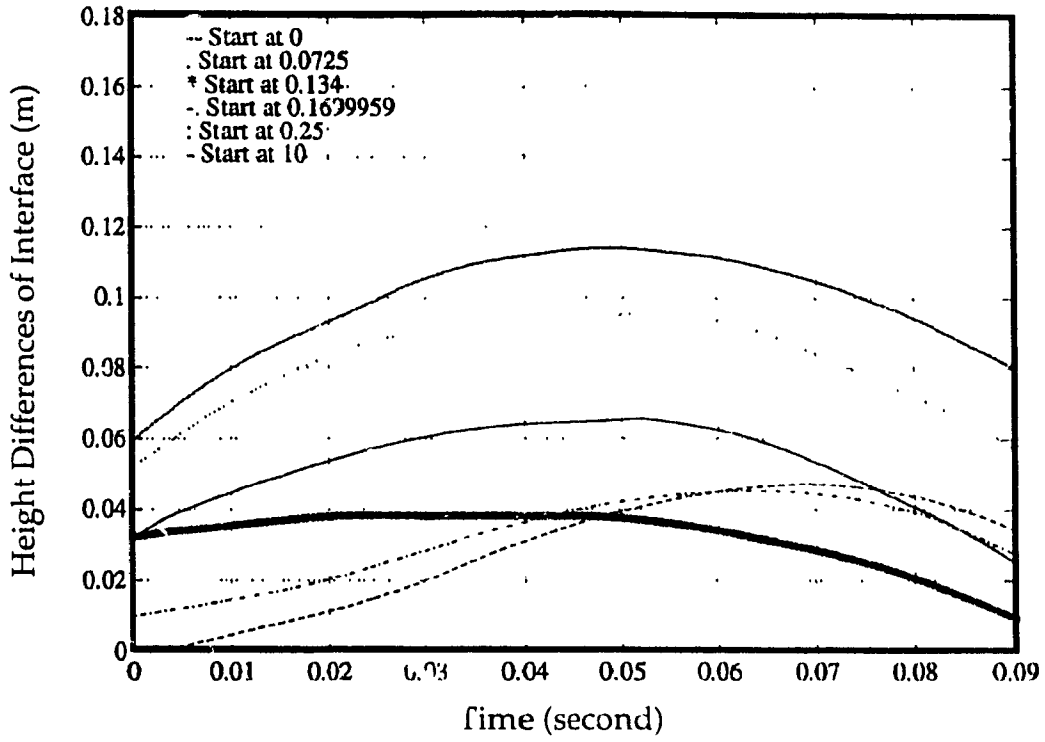


Fig.6.3.5 Effects of different draining start time to interface height differences between center and end

## 6.4 Effect of Viscosity

From the computational results of viscosity effect on the interface formation time, it is envisioned that any change in viscosity would necessitate that the amplitude of interface oscillation be significantly altered. Since the interface motion is closely related to liquid residuals, the effect from any change in viscosity needs being assessed. The effects of the viscosity on the liquid residuals are evaluated for 8 m/s outflow velocity, as shown in Fig.6.4.1. It is found that the viscosity has the influential effect on the draining time only during the transient period after the system was placed in zero-gravity environment. The more residual transient results, the more influence of the viscosity. The draining time is greatly affected by varying the kinematic viscosity ν, when draining is initiated upon entering zero-gravity environment. The quantity of the liquid residuals increases with increasing the kinematic viscosity although the kinematic viscosity in the range of smaller values does not lead to a significant increase in liquid residuals. The variation in kinematic viscosity at draining start time of 0.25 seconds had little effect on the draining time. The additional investigations are conducted at the 1 m/s and 4 m/s at the start time of 10 seconds after entering zero-gravity, when the interface is at its 0-g equilibrium state prior to draining. Of significance from the results shown in Fig.6.4.2, is the fact that no effect of the viscosity is noticeable over the ranges examined. From these figures, it is anticipated that the viscosity effects on liquid residuals would not be significantly changed if gravity transient were not involved. Thus, without the presence of residual effect of gravity transient, the liquid residuals are irrelevant to the viscosity. In other words, the gravity transient and viscosity can be considered as a joint effect on liquid residuals.

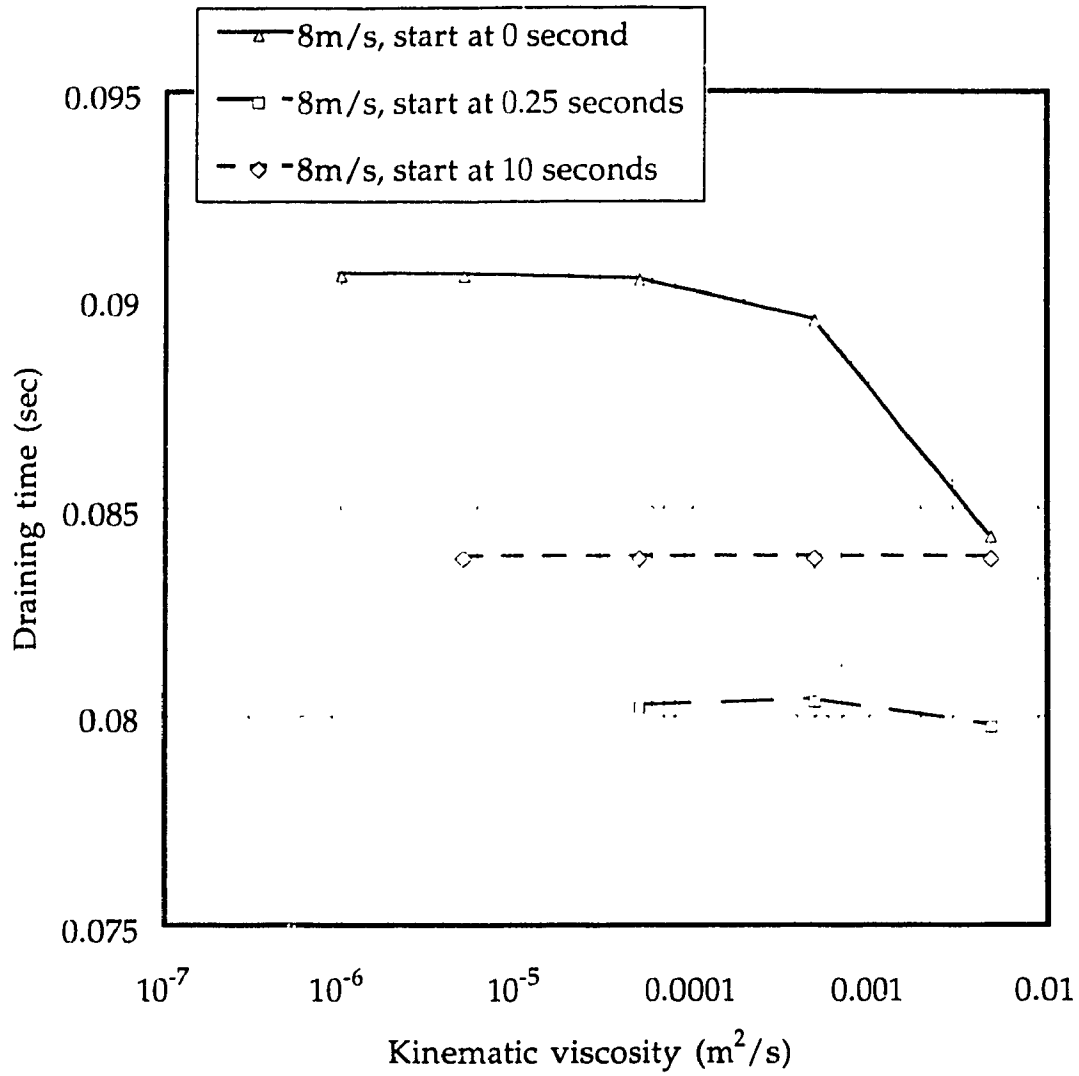


Fig 6.4.1 Viscosity effect on draining time
(draining started from 0 to 10 seconds)

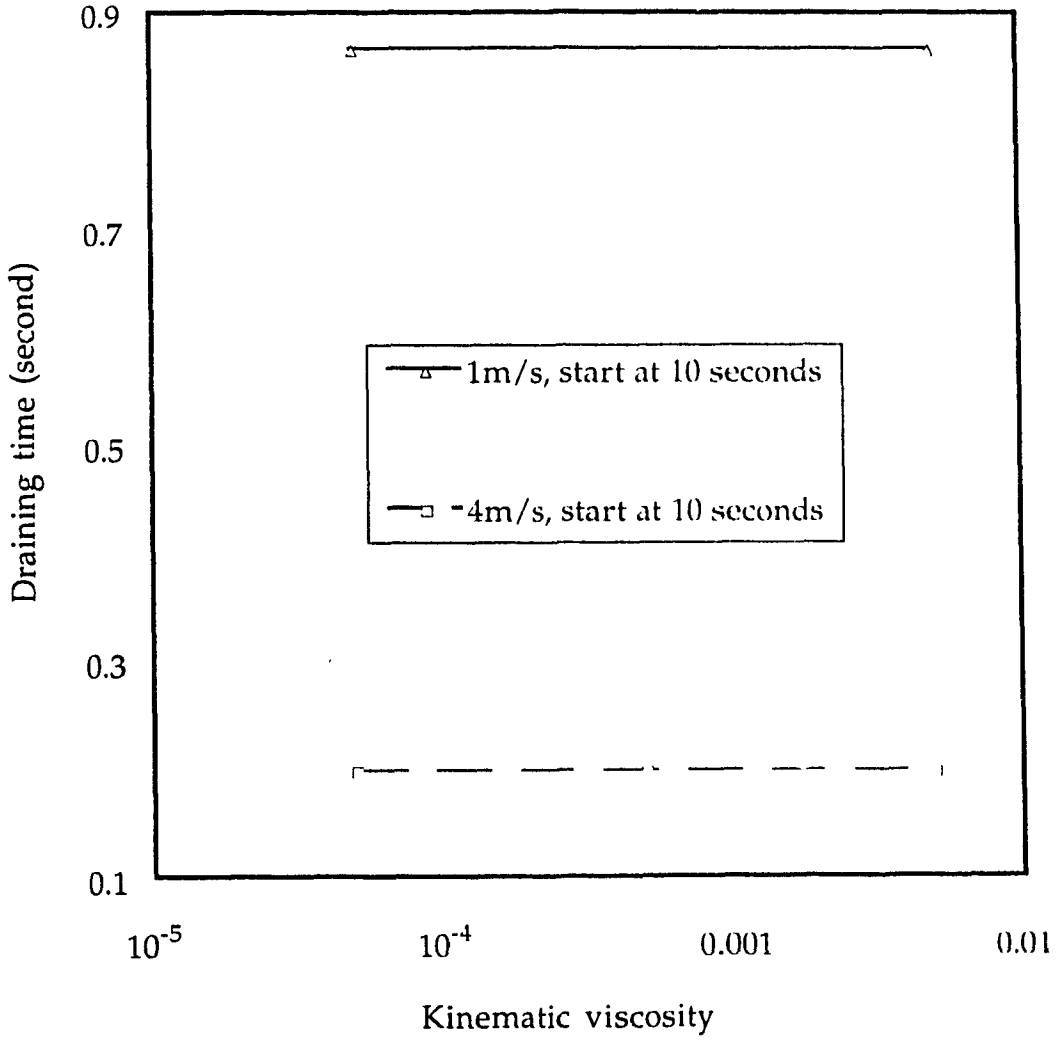


Fig.6.4.2 Viscosity effect on draining time (draining started at 10 seconds)

## 6.5 Effect of Outlet Pipe

The outlet pipe may exert effects during outflow. The ratio of length to width or diameter of an outlet pipe, the draining start time, outlet location and with or without outlet pipe are taken as variable parameters. The ratio of length to width, $L_o/D_o$, of an outlet pipe, versus draining time, is given in Fig.6.5.1. The curve shows the effects of an outlet pipe on draining time with 10 m/s outflow coming out through the center of a tank. For a $L_o/D_o$ ratio less than 1, the effect of outlet length is very pronounced. However, a negligible effect of outlet length on draining time is observable, provided the $L_o/D_o$ ratio is greater than 1. For a $L_o/D_o$ ratio greater than 2, the draining time becomes constant, thus the liquid residuals are independent of the outlet pipe length if the pipe length is longer than two times the pipe radius. It is not necessary to design or install very long outlet pipes to improve the draining condition.

With the outlet pipe, the draining from the center had less elapsed time than the corner, when the draining was initiated upon the system entering a weightless environment, as shown in Fig.6.5.2. It is found that the liquid residuals for corner outlets are consistently less than predicted for the same condition if the outlet is at center. This behavior is illustrated in Fig.6.5.3.

The effect of outlet pipe on the draining for the same corner outlet location is displayed in Fig.6.5.4. The draining time is longer with outlet pipe than without. The same phenomena holds true for the center draining, as shown in Fig.6.5.5. Examination of draining time in Figs.6.5.4 and 6.5.5

indicates that in both the corner and center draining, the residuals are less than predicted to occur at the same conditions without an outlet pipe.

The dependence of draining time on the draining start time is also significant in the draining with an outlet pipe. For comparison purpose, between start time at 0 and 10 seconds, the difference of draining time can be expressed in terms of a percentage form where draining time without outlet pipe is 100 %. The graph in Fig.6.5.6 indicates that an outlet pipe has a similar effect on liquid residuals for all cases without an outlet pipe. Hence, liquid residuals, regardless of outlet pipe, should be comparable if the other parameters were held constant. Since the draining time with the outlet pipe for both center and corner locations exhibits very similar increases, the investigations on the behavior of liquid residuals without outlet pipe give the accurate results.

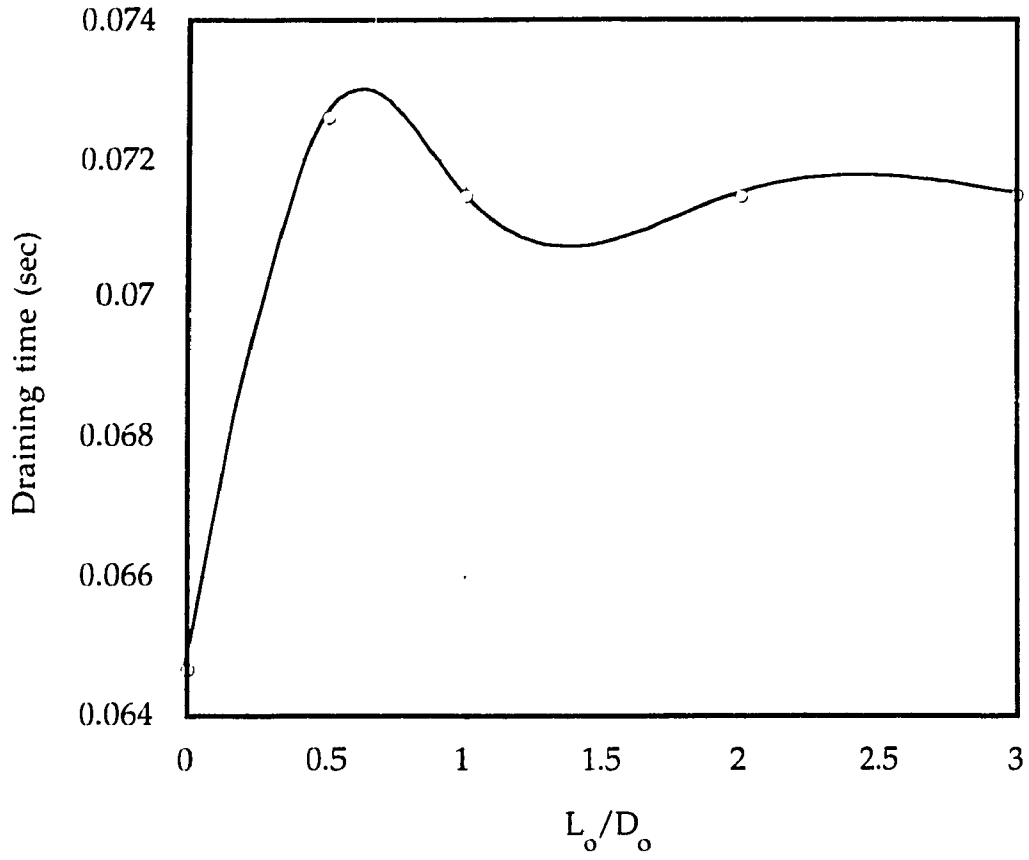


Fig.6.5.1 Outlet pipe effects on draining time at $v_o = 8m/s$ and draining at center

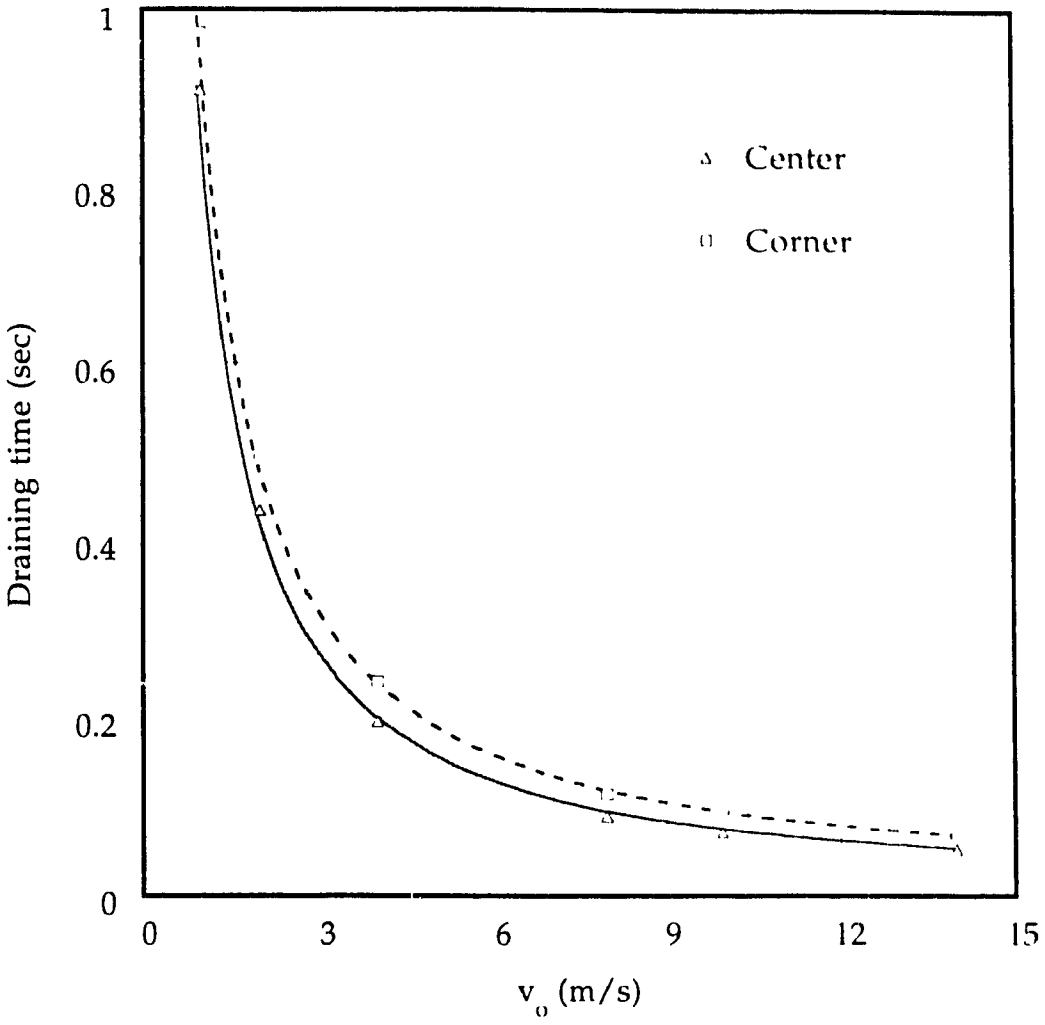


Fig. 6.5.2 Draining with outlet pipe starting at 0 second

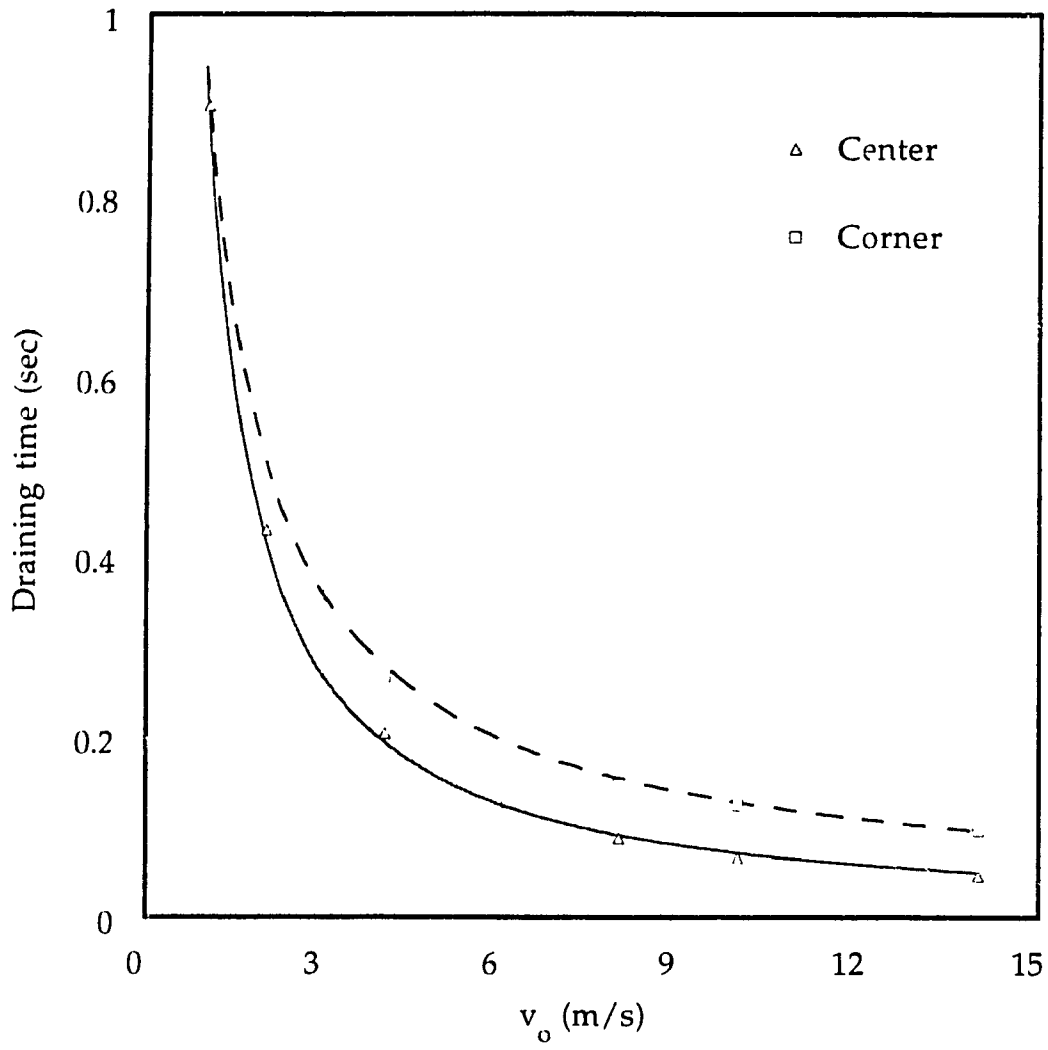


Fig.6.5.3 Draining with outlet pipe starting at 10 seconds

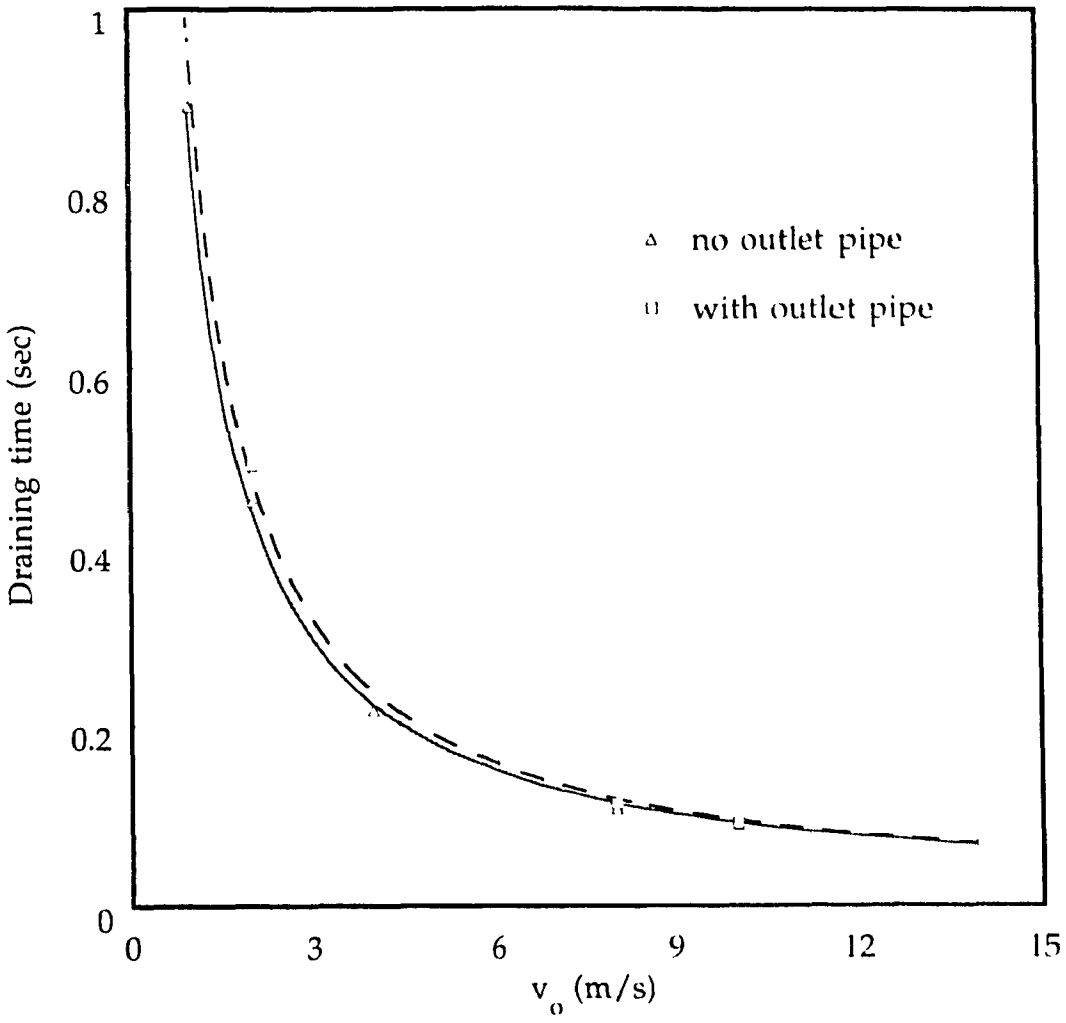


Fig.6.5.4 Outlet pipe effects on draining time starting at 0 second (draining from corner outlet)

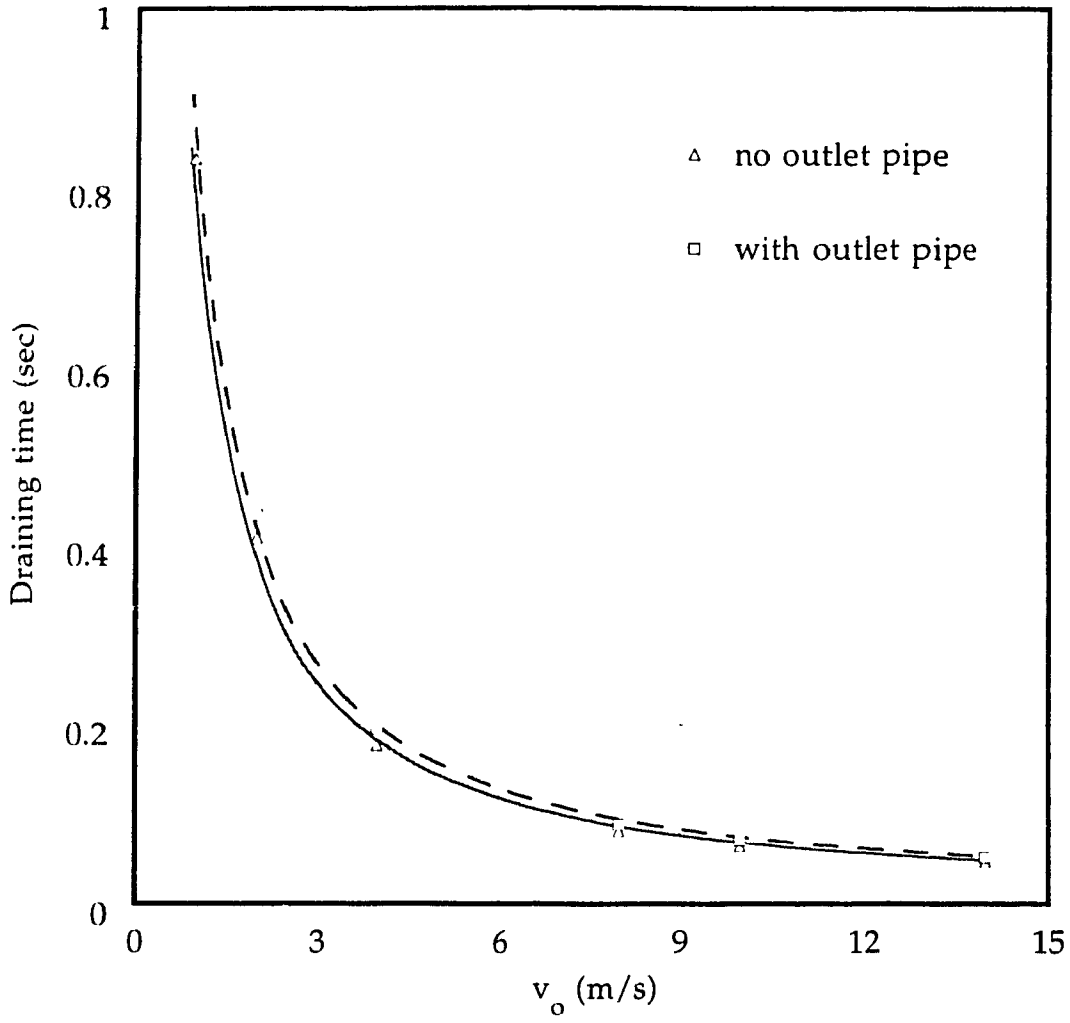


Fig.6.5.5 Outlet pipe effects on draining time starting at 0 second (draining from center outlet)

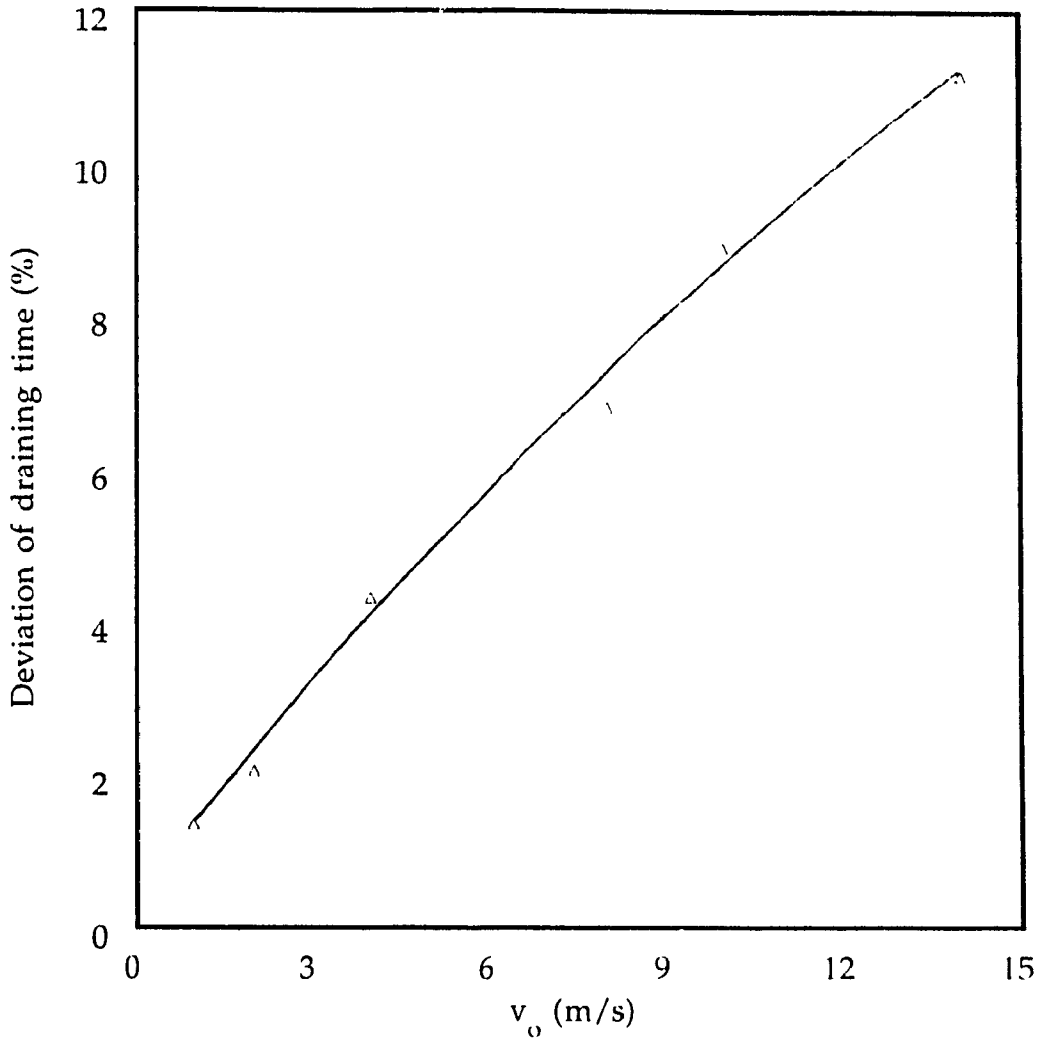


Fig.6.5.6 Draining at center with outlet pipe starting at 0 and 10 seconds

## 6.6 Effect of Outlet Location

An outlet location has significant influence on the liquid residual (Yan et al, 1994). As shown before, the visual illustration presented in Fig.6.3.4 indicates that for the same outlet, draining time from a corner outlet location lasts longer than that from a center outlet. The latter means that liquid residuals from the corner draining are less than that from the center. At the draining start time of 10 seconds after placing the system in a weightless environment, the liquid residual of 19.24% at the corner outlets was a considerable improvement over the 36.7% obtained in the center outlet. Further comparison of liquid utilized from center and corner outlets is shown in Fig.6.6.1. Liquid outflow from the tank is considered to be utilized in spacecrafts, and is taken as the percentage of the initial liquid volume in the tank. It is noticed that the utilized liquid volume for center is significantly influenced by the outflow velocity, thus the utilized liquid volume is greatly reduced when the velocity is large. For the outflow from the corner draining, the liquid utilized volume is almost constant with the outflow velocity. It is apparent that the corner outlets significantly reduce the liquid residuals near the wall. The visualization of outflow time history of corner and center draining with outflow velocity of 16 m/s, as shown in Fig.6.6.2, shows the liquid residuals before and after draining termination. There is significant difference for the different outlet locations. The outflow from corner outlet presents less severe interface distortion and liquid residuals.

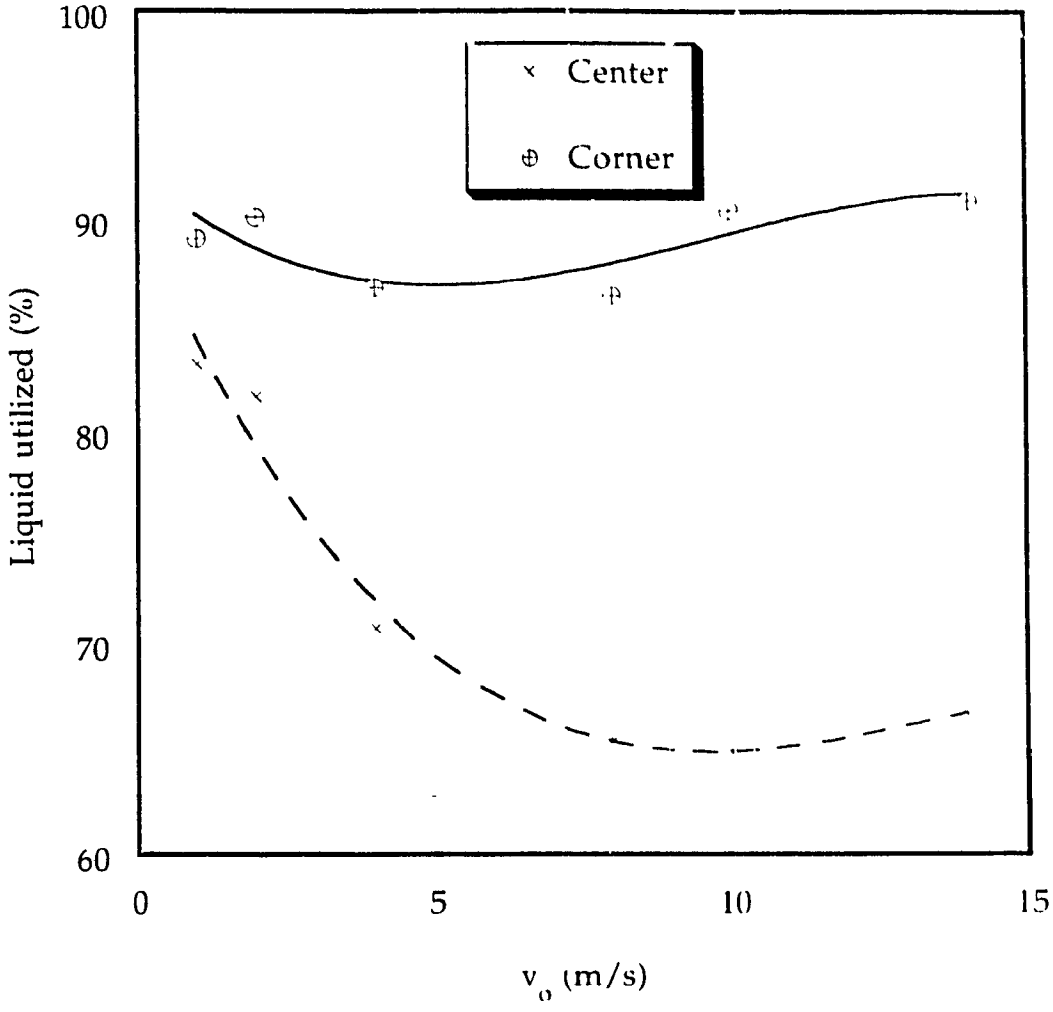


Fig.6.6.1 Comparison of liquid utilized from center and corner outlets

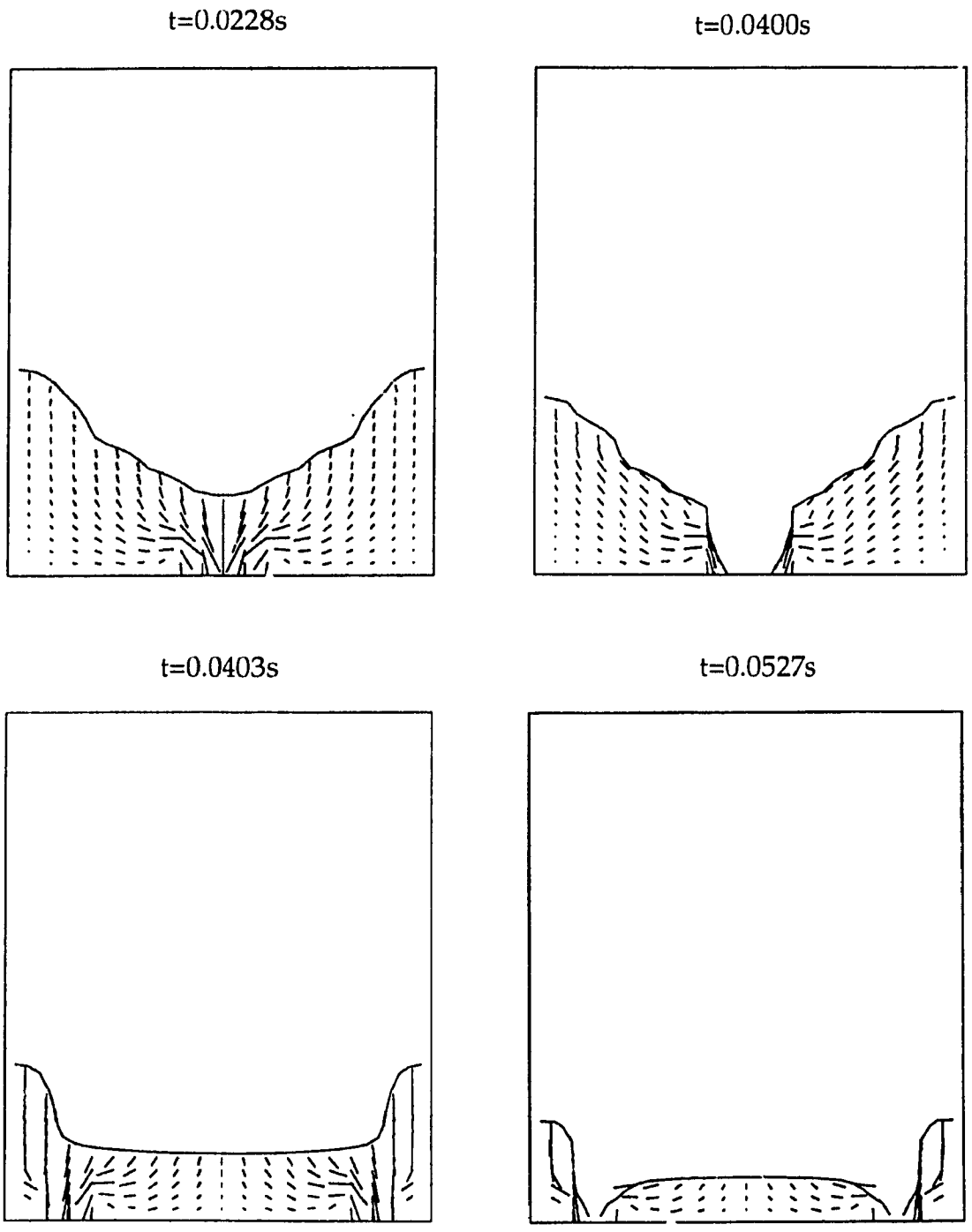


Fig.6.6.2 Draining from corner and center outlets at $v_o$ = 16 m/s

To further review the effect of the outlet location, the tank is tested at each outlet location starting from the center to the corners. For the same outlet, draining time is increasing when the outlet location is moved towards the walls. The liquid residuals at vapor ingestion for several outlet locations are given in Figs.6.6.3, 6.6.4 and 6.6.5 for outflow velocities of 4, 8 and 10 m/s, respectively. Draining from center outlets (frames <A>) produces the largest residuals while ones from the corner outlets (frames <C> and <D>) result in the least residual. Although the outlets near the walls (frames <D>) may sometimes have the least residual, taking into account the structure difficulty, the corner outlets (frames <C>) next to the ones near the walls are the optimum choice. The liquid residuals $V_R$ are found to be a function of the outlet location represented by the ratio of the distance between the center of the tank and the outlet center to the half width of the tank, $R_d/L$, see Fig.6.6.6. The liquid residuals are decreasing with the outlet location moving away from the center for these three outflow velocities. The greater improvement of reducing liquid residuals occurs at $R_d/L$ between 0.2 to 0.5. The corner location of outlet can be considered as a potential method of reducing or even eliminating liquid residuals. Tanks equipped with corner outlets could offer an advantage over the system with additional equipment. Structure and operation of the tanks could be simplified since no baffles, throttling or additional devices would be required. Overall tank size and weight could be reduced because less liquid could be carried since there would be a little or no residuals. Locating outlet at the appreciate position of the tank seems to be an attractive means for reducing or eliminating liquid residuals when draining liquid from a tank in zero-gravity environment.

<A> Vapor ingestion at t=0.19615s

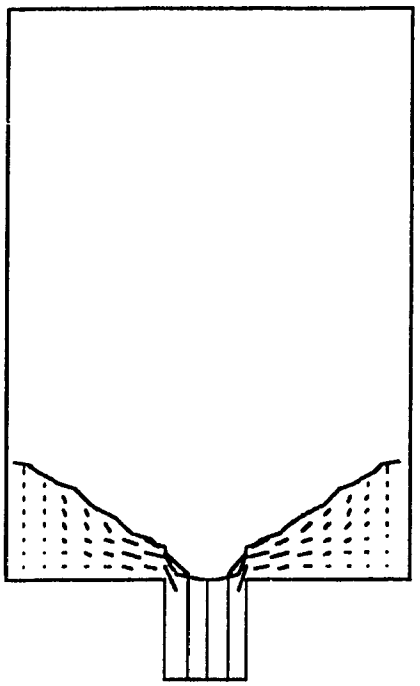

<B> Vapor ingestion at t=0.230195s

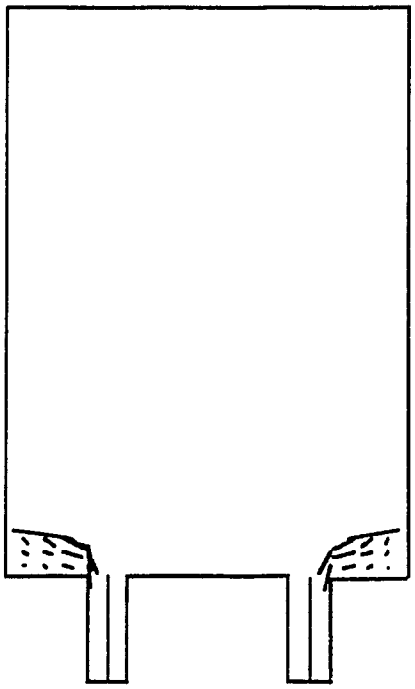

<C> Vapor ingestion at t=0.23980s

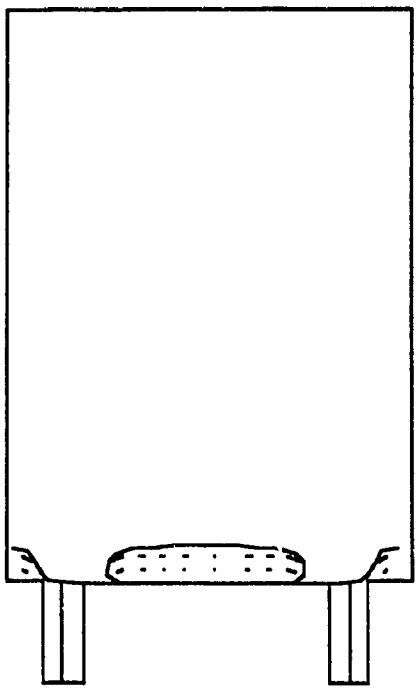

<D> Vapor ingestion at t=0.23949s

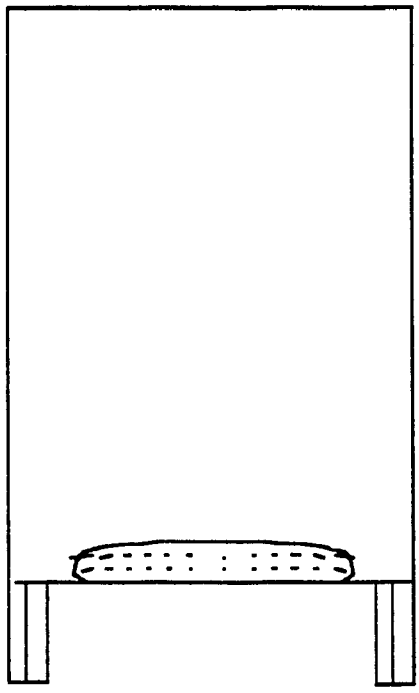

Fig.6.6.3 Outlet location effect on liquid residuals at $v_o$ = 4 m/s

<A> Vapor ingestion at 0.0.08379s

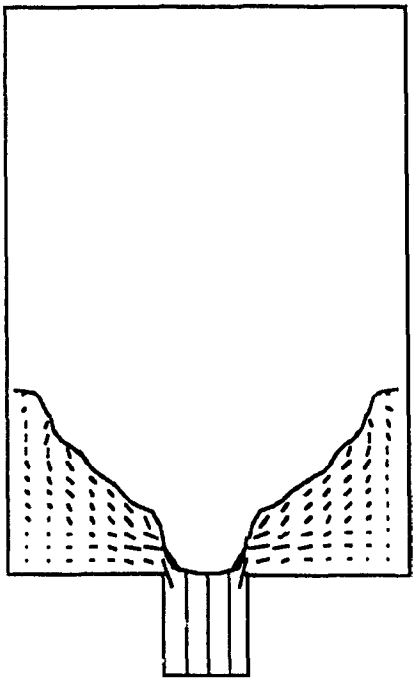

<B> Vapor ingestion at 0.11221s

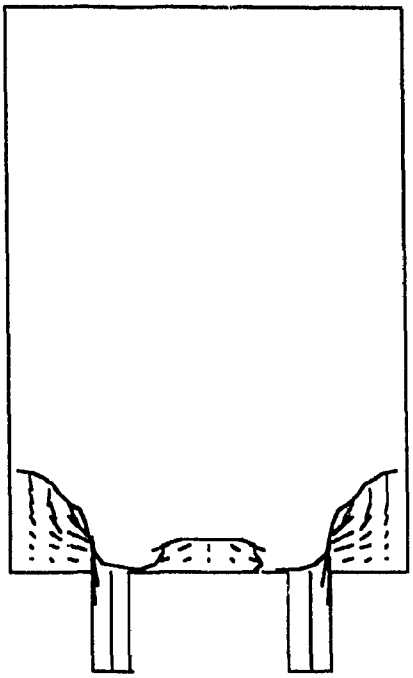

<C> Vapor ingestion at 0.11460s

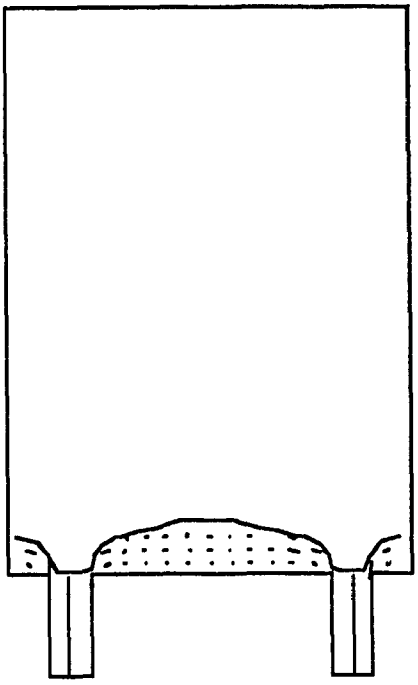

<D> Vapor ingestion at 0.11607s

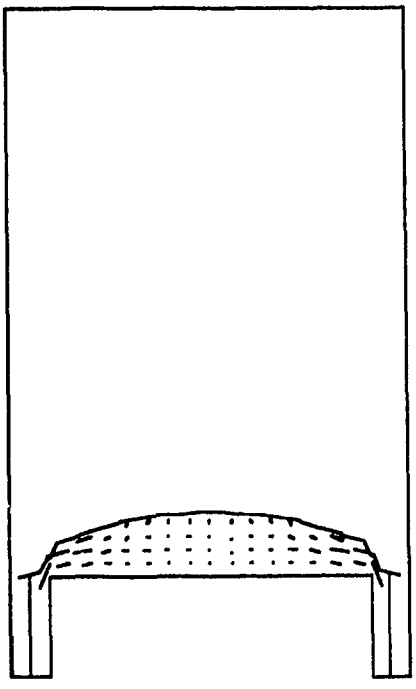

Fig.6.6.4 Outlet location effect on liquid residuals at $v_o = 8$ m/s

<A> Vapor ingestion at 0.06371s

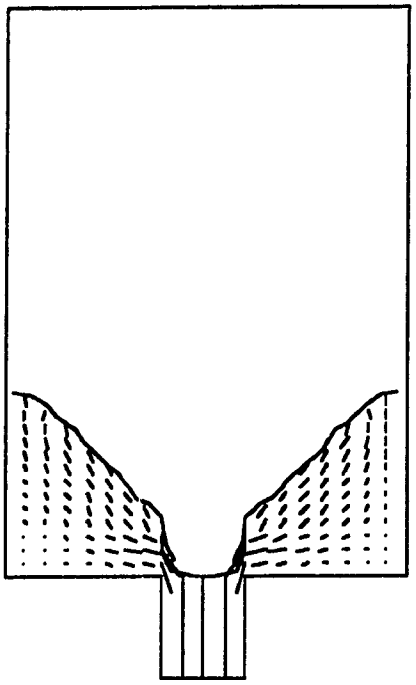

<B> Vapor ingestion at 0.08870s

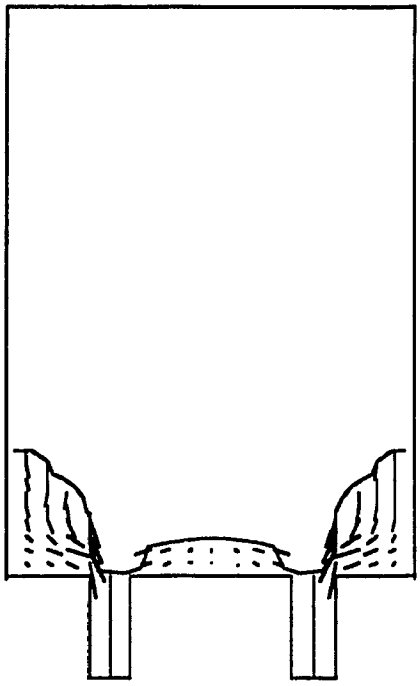

<C> Vapor ingestion at 0.09160s

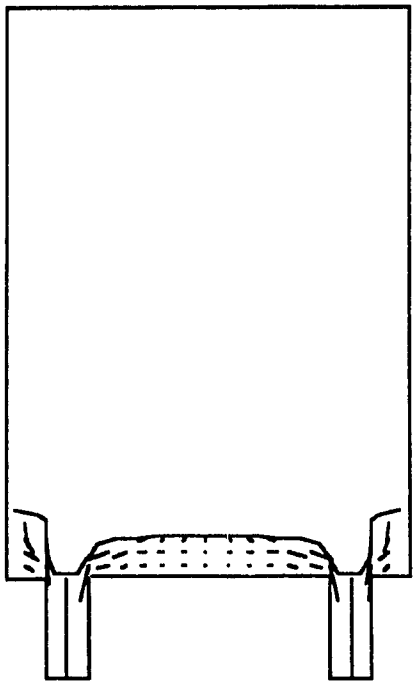

<D> Vapor ingestion at 0.09303s

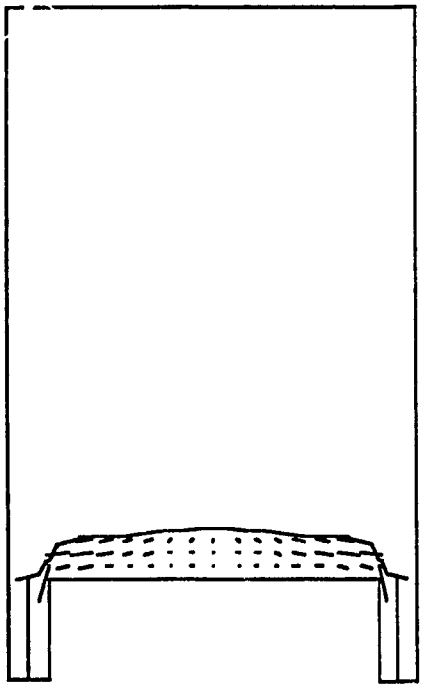

Fig.6.6.5 Outlet location effect on liquid residuals at $v_o = 10$ m/s

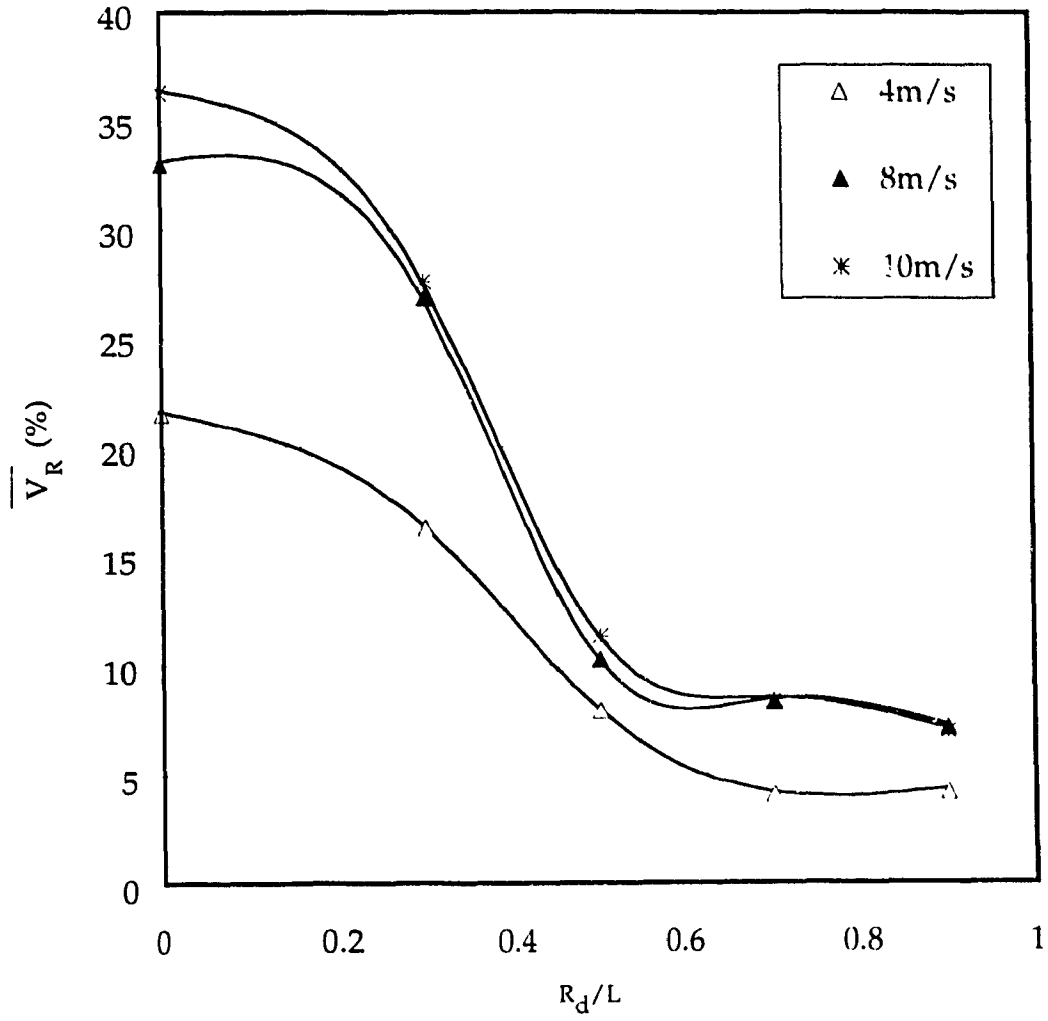


Fig.6.6.6 Outlet location versus draining time, starting at 10 seconds

## 6.7 Dimensional Analysis

The dimensional analysis is conducted to study the important parameters involved during draining in weightlessness. From the numerical computation, the outflow during weightlessness is related to liquid properties, geometry condition and initial condition. It is found that the outflow is greatly affected by the liquid density, surface tension, contact angle, viscosity, outflow velocity, tank width or radius, outlet width or radius, outlet location, draining start time and initial liquid height. There is a functional relationship among these parameters, mathematically,

$$f_n\left(\rho, \sigma, \nu, \alpha, v_o, v_t, L, R_o, R_1, t_d, t_s, V_R, V_I, H_I\right) = 0 \qquad (6.7.1)$$

where $\rho$ is the density, $\sigma$ is the surface tension, $\nu$ is the viscosity, $\alpha$ is the contact angle, $v_o$ is the outflow velocity, $v_t$ is the mean outflow velocity of the tank, L is the half width or radius of the tank, $R_o$ is the half width or radius of the outlet pipe, $R_d$ is the distance of the outlet location from the center, $t_d$ is the draining time, $t_s$ is the draining start time, $V_R$ is the liquid residual volume, $V_I$ is the initial liquid volume and $H_I$ is the initial liquid height.

By dimensional analysis, the dimensionless draining time, and dimensionless liquid residuals expressed as a ratio of the liquid residual volume to the initial liquid volume, are found to have the following function:

$$\bar{t}_d = f_n\left(\frac{\rho L v_t^2}{\sigma}, \frac{v_t L}{\nu}, \frac{t_s v_t}{L}, \frac{R_o}{L}, \frac{R_d}{L}, \frac{H_I}{L}, \alpha\right) \qquad (6.7.2)$$

and

$$\bar{V}_R = f_n\left(\frac{\rho L v_t^2}{\sigma}, \frac{v_t L}{\nu}, \frac{t_s v_t}{L}, \frac{R_o}{L}, \frac{R_d}{L}, \frac{H_I}{L}, \alpha\right) \tag{6.7.3}$$

Replacing the first two terms of the right hand side of Equations (6.7.2) and (6.7.3) by We number and Re number, respectively,

$$\bar{t}_d = f_n\left(We, Re, \frac{t_s v_t}{L}, \frac{R_o}{L}, \frac{R_d}{L}, \frac{H_I}{L}, \alpha\right) \tag{6.7.4}$$

$$\bar{V}_R = f_n\left(We, Re, \frac{t_s v_t}{L}, \frac{R_o}{L}, \frac{R_d}{L}, \frac{H_I}{L}, \alpha\right) \tag{6.7.5}$$

The viscous effect is related to the transient period. If the draining start time is fixed, the second and third terms in Equations (6.7.4) and (6.7.5) would be neglected. The tank and outlet sizes and outlet location are generally defined at the design stage, which can be taken as constants. Thus, for the zero-gravity experimental tests, the liquid residuals are tied to We number, initial height and contact angle:

$$\bar{t}_d = f_n\left(We, \frac{H_I}{L}, \alpha\right) \tag{6.7.6}$$

and

$$\bar{V}_R = f_n\left(We, \frac{H_I}{L}, \alpha\right) \tag{6.7.7}$$

Equations (6.7.6) and (6.7.7) establish a functional dependence of liquid residuals on We number, initial height and contact angle. Velocity is a main component of We number. The effect of velocity has been previously discussed.

## 6.8 Effect of Contact Angle

From dimensional analysis, contact angle affects the liquid residuals. Since space missions become increasingly ambitious, different liquids available on Earth could be used in permanently manned spacecrafts and stations. The studies of liquids with contact angle of 0 degree (most liquid propellants have $0^o$ contact angle) during weightlessness are not sufficient as the various liquids may have different contact angles other than $0^o$. In order to determine whether the contact angle affects the vapor ingestion phenomenon, the draining simulation is subjected to a series of computations. The effect of varying contact angle on the liquid draining for constant outflow rate and constant fluid properties is shown in Fig.6.8.1. As the contact angle is increasing, the corresponding calculated draining time also increases. The effect of change in contact angle on liquid residuals may be attributed primarily to the configuration of the liquid-vapor interface.

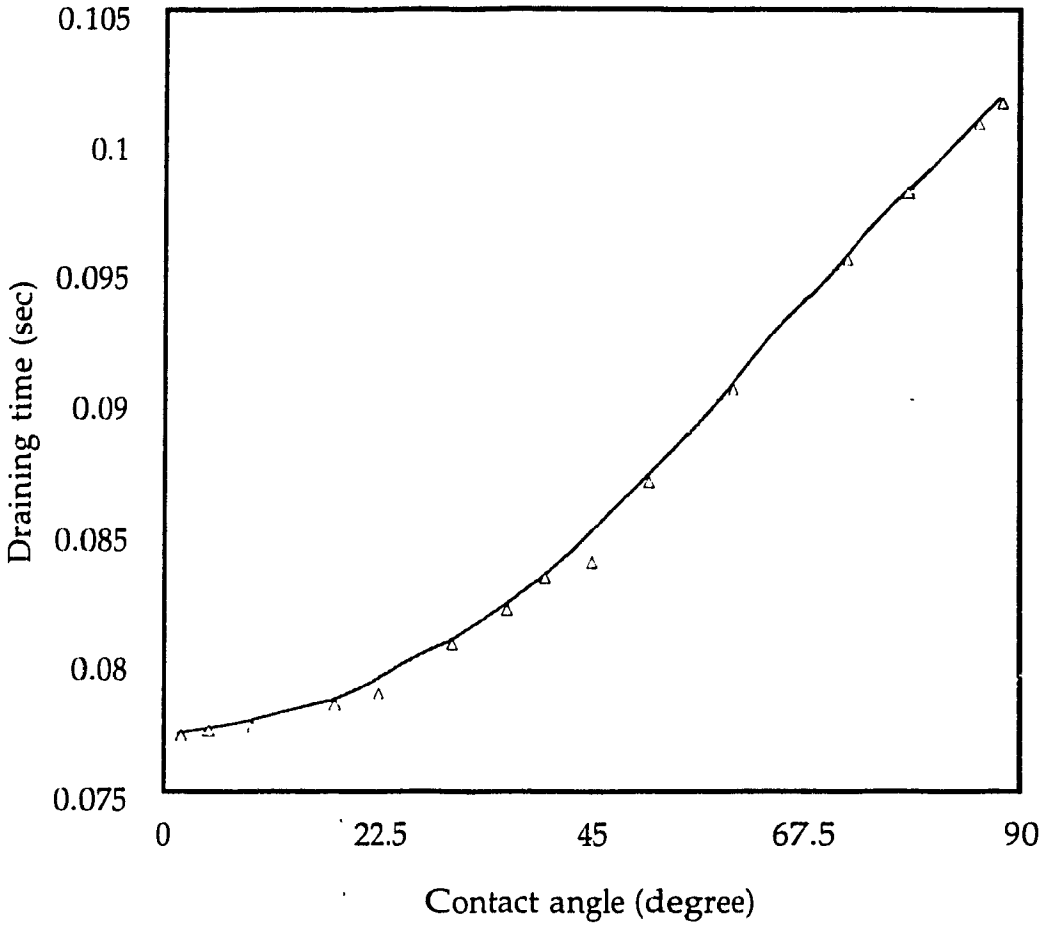


Fig.6.8.1 Contact angle effect on draining time

## 6.9 Effect of Initial Liquid Height

A series of computation runs are carried out to study the effect of initial liquid height. The effect of initial height on liquid residuals at outflow velocity of 14 m/s is significant, as shown in Fig.6.9.1. The liquid residuals are increasing when the initial liquid height is decreasing. This phenomenon is better understood in relation to the interface distortion, based on the correlation of liquid residuals with the liquid-vapor interface distortion. This agrees with the experimental investigation of interface distortion (Derdul et al, 1966) in which the interface distortion was increased with the decrease of initial liquid height. Abdalla et al (1969) showed that the draining test curves have an apparent effect of initial height on the interface centerline velocity.

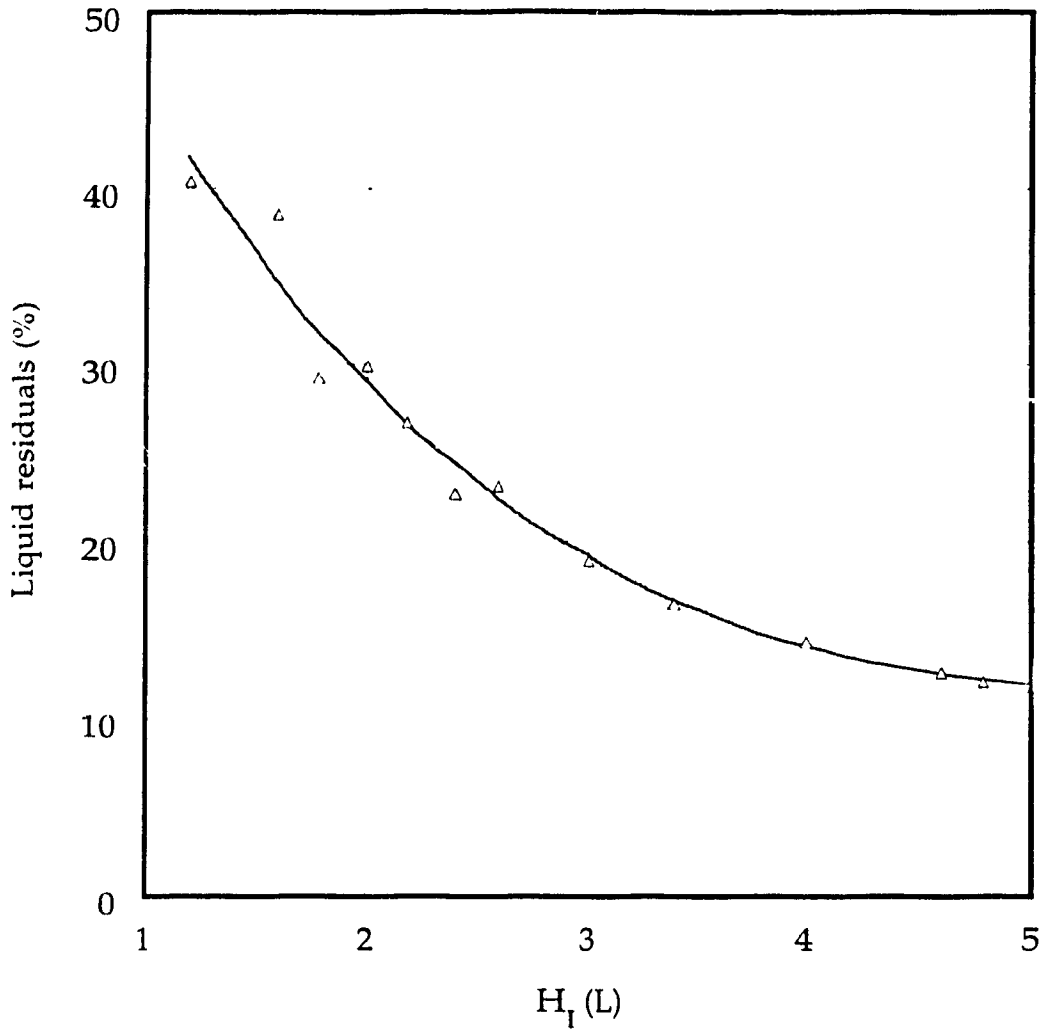


Fig.6.9.1 Initial liquid height effect on liquid residuals

## 6.10 Liquid Critical Height in Outflow

The interface prior to draining in zero-gravity is a curved surface whose shape is determined by surface tensions and contact angle. During outflow, the interface distorts from its equilibrium configuration. As draining proceeds, a dip in the interface forms above the draining outlet and rapidly accelerates toward the outlet quickly followed by vapor ingestion into the outlet line. The height of the liquid-vapor interface at the incipience of vapor ingestion is defined as the critical height. The critical height occurs at the time when the interface centerline deviates from the constant velocity period. The critical height is used to describe the vapor ingestion phenomenon in zero-gravity environment. Figure 6.10.1 presents the critical heights plotted as a function of the outflow velocity. The critical height is increasing with increasing draining rate.

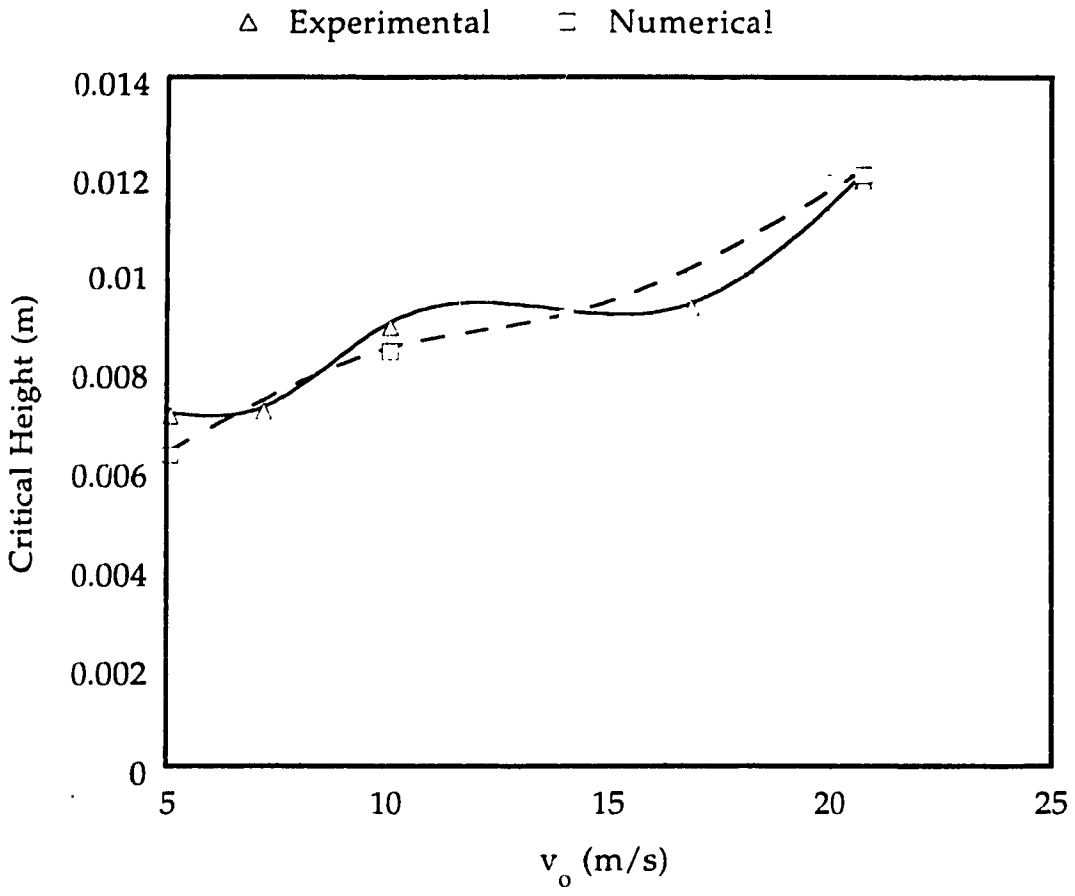


Fig.6.10.1 Critical heights versus outflow velocity

# CHAPTER 7

# CONCLUSIONS

Computational and analytical studies concerning liquid dynamic behavior during transition from terrestrial gravitation to weightlessness and outflow in weightlessness in rectangular and cylindrical tanks have been presented. In addition, the liquid-vapor interface configuration at a zero-gravity equilibrium state is also investigated

The liquid dynamic behavior in a liquid-vapor-solid system in spacecrafts is studied numerically. The effects of various system parameters are evaluated. The investigations of the transient numerical simulations reveal that the dimensionless interface formation time increases with the decrease of the viscous forces. The results indicate that the liquid-vapor interface configuration during outflow can be significantly affected by outflow velocity, outlet location and draining start time. An increased distortion of the interface and liquid residuals can be caused by an increased outlet velocity. Liquid residuals are affected by the fluid properties, the geometry of the tank and other physical parameters. The liquid residuals vary with draining start time. The center outlet results in the less amount of liquid expelled from the tank. However, when the outlet is located away from center, it would prevent premature vapor ingestion during tank draining. The corner location of outlet can be considered as a potential method of reducing or even eliminating liquid residuals. Hysteresis behavior of interface configuration

during draining and filling of a liquid through an infinitesimal slow process is found.

Liquid-vapor interface configuration at 0-g equilibrium depends on an initial liquid height, tank geometry and a contact angle. Configuration and stability can be predicted by analytical method using minimum, maximum and critical liquid heights. Computational results confirm the analytical prediction findings.

Both numerical and analytical results compare favorably with the published experimental data. The results can be used for guidance and aid to design liquid management devices in spacecrafts without the need of extensive experimental studies. Further experimental investigations in proper microgravity facilities to evaluate liquid dynamic behavior will be part of the future work.

# REFERENCES


Abdalla, K.L. and Berenyi, S.G., Vapor Ingestion Phenomenon in Weightlessness, NASA Technical Note, NASA TN D-5210, Washington, D.C., May 1969.

Abramson, H.N. (editor), The Dynamic Behavior of Liquids in Moving Containers, NASA SP-106, 1966.

Adamson, A.W., Physical Chemistry of Surfaces, 4th edition, John Wiley & Sons, 1982.

Agafonov, M.S., Levtov, V.L., Leskov, V.L., Romanov, V.V., Experimental Researches on Fluid Physics, Proceedings, AIAA/IKI Microgravity Science Symposium, Moscow, USSR, AIAA, May, 1991.

Avduyevsky, V.S., Microgravity Science Activity in USSR, Proceedings, AIAA/IKI Microgravity Science Symposium, Moscow, USSR, AIAA, May, 1991.

Benedikt, E.T., Scale of Separation Phenomena in Liquids under Conditions of Nearly Free Fall, ARS Journal, 29, 150, 1959.

Benedikt, E.T., General Behavior of a Liquid in a Zero or Near-zero Gravity Environment, Weightlessness-Physical Phenomena and Biological Effects, edited by E.T. Benedikt, Plenum Press, New York, pp. 3-32, 1961.

Berenyi, S.G. and Abdalla, K.L., The Liquid-Vapor Interface during Outflow in Weightlessness, NASA TM X-1811, 1969.

Berenyi, S.G. and Abdalla, K.L., Vapor Ingestion Phenomenon in Hemispherically Bottomed Tanks in Normal Gravity and in Weightlessness, NASA report NASA TN D-5704, April, 1970.

Berenyi, S.G., Effect of Outlet Baffling on Liquid residuals for Outflow from Cylinders in Weightlessness, NASA TM X-2018, 1970.

Clodfelter, R.G., Rept. ASD-TDR-63-506, Air Force System Command, Wright-Patterson Air Force Base, Ohio, September, 1963.

Crouch, R.K. and Kicza, M.E., Microgravity Science and Applications Overview: Research, Facility and Instrumentation Development, Space Station Freedom Operations and Utilization Planning, Proceedings, AIAA/IKI Microgravity Science Symposium, Moscow, USSR, American Institute of Aeronautics and Astronautics, May 13-17, 1991.

Davis, N.W., Japan Sizes Up an Opportunity, Aerospace America, February 1987.

Defay, R., Prigogine, I. and Bellemans, A., translated by Everett, D.H., Surface Tension and Adsorption, Longmans, 1966.

Derdul, J.D., Grubb, L.S. and Petrash, D.A., Experimental Investigation of Liquid Outflow from Cylindrical Tanks during Weightlessness, NASA Technical Note D-3746, 1966.

Eckhart, K. and Netter, G., Experiment for Investigation of the Dynamic Behaviour of Fluid in a Surface Tension Tank under Microgravity Condition, Acta Astronautica, Vol.9, No.9, 1982.

Ford, L.R., Calculus, McGraw-Hill Book Company, Inc., 1963.

Gluck, D.F. and Gille, J.P., Fluid Mechanics of Zero-G Propellant Transfer in Spacecraft Propulsion Systems, Journal of Engineering for Industry, February, 1965.

Grubb, L.S. and Petrash, D.A., Experimental Investigation of Interfacial Behavior Following Termination of Outflow in Weightlessness, NASA TN D-3897, April 1967.

Halpern, Richard E., Facilities and Programs for Research in a Low-Gravity Environment, Opportunities for Academic Research in a Low-Gravity Environment, edited by George A. Hazelrgg and Joseph M. Reynolds, , Volume 108, PROGRESS IN ASTRONAUTICS AND AERONAUTCS, American Institute of Aeronautics and Astronautics, Inc., 1986.

Hedgepeth, L.L.M., Zero Gravity Boiling and Condensing, Energy Conversion for Space Power, Edited by Snyder, N.W., Academic Press, 1961.

Hirt, C.W., Nichols, B.D. and Romero, N.C., SOLA – A Numerical Solution Algorithm for Transient Flows, Los Alamos Scientific Laboratory Report LA-5852, 1975.

Hirt, C.W. and Nichols, B.D., Volume of Fluid (VOF) Method for the Dynamics for Free Boundaries, Journal of Computational Physics, Vol.39, 1981.

Ishida, K., Outline of the Japanese Space Activities in the Field of Microgravity, Hydromechanics and Heat/Mass Transfer in Microgravity, Gordon and Breach Science Publishers, 1992.

Johnson, W.E., Development and Application of Computer Programs Related to Hypervelocity Impact, System, Science and Software report 3SR-335, 1970

Joos, P., Remoortere, P.V. and Brace, M., The Kinetics of Wetting in a Capillary, Journal of Colloid and Interface Science, Vol.136, No.1, April, 1990.

Kinloch, A.J., Adhesion and Adhesives Science and Technology, Chapman and Hall, 1987.

Li, T., Preliminary Studies of Liquid Behavior in a Low-g Field, Rept. ERR-AN-036, Convair Astronautics, March, 1961.

Li, T., Hydrostatics in Various Gravitational Fields, The Journal of Chemical Physics, Vol. 36, No. 9, May, 1962.

Masica, W.J., Petrash, D.A. and Otto, E.W., Hydrostatic Stability of the Liquid-Vapor Interface in a Gravitational Field, NASA TN D-2267, 1964

Masica, W.J., Derdul, J.D. and Petrash, D.A., Hydrostatic Stability of the Liquid-Vapor Interface in a Low-acceleration Field, NASA TN D-2444, 1964.

Myshkis, A.D., Babskii,V.G., Kopachevskii, N.D., SlobozhaninL, L.A. and Tyuptsov,A.D., translated by Wadhwa,R.S., Low-gravity Fluid Mechanics, Springer-Verlag, 1987.

Myshkis, A.D., Zero-gravity Hydromechanics: Some Results and Problems, Hydromechanics and Heat/Mass Transfer in Microgravity, Gordon and Breach Science Publishers, 1992.

Newman, S., Kinetics of Wetting of Surfaces by Polymers: Capillary Flow, Journal of Colloid and Interface Science, Vol.26, 1968.

Nichols, D.B., Hirt, C.W. and Hotchkiss, R.S., SOLA-VOF: A Solution Algorithm for Transient Fluid Flow with Multiple Free Boundaries, Los Alamos Scientific Laboratory Report LA-8355, August, 1980.

Nussle, R.C., Derdul, J.D. and Petrash, D.A., Photographic Study of Propellant Outflow from a Cylindrical Tank during Weightlessness, NASA TN D-2572, 1965.

Ostrach, S., Low-Gravity Fluid Flows, Ann. Rev. Fluid Mech., Vol.14, 1982.

Otto, E.W., Static and Dynamic Behavior of the Liquid-Vapor Interface during Weightlessness, Aerospace Chemical Engineering, No.61, Vol.62, 1966.

Paynter, H.L., Time for a Totally Wetting Liquid to Deform from a Gravity-Dominated to a Nulled-Gravity Equilibrium State, AIAA Journal, September 1964.

Petrach, D.A., Zappa, R.F. and Otto, E. W. Experimental Study of the Effects of Weightlessness on the Configuration of Mercury and Alcohol in Spherical Tanks, NASA TN D-1197, April 1962.

Petrach, D.A., Nussle, R.C. and Otto, E. W., Effect of the Acceleration Disturbances Encountered in the MA-7 Spacecraft on the Liquid-vapor Interface in a Baffled Tank during Weightlessness, NASA TN D-1577, January 1963.

Petrach, D.A., Nussle, R.C. and Otto, E. W., Effect of Contact Angle and Tank Geometry on the Configuration of the Liquid-vapor Interface During Weightlessness, Natl. Aeronaut. Space Admin. Tech. Note D-2075, October 1963.

Petrach, D.A., Nelson, T.M. and Otto, E. W., Effect of Surface Energy on the Liquid-vapor Interface Configuration During Weightlessness, NASA TN D-1582, January 1963.

Rath, H.J., and Kuhlmann, H.C., Fluid Dynamics at ZARM: An Overview, Hydromechanics and Heat/Mass Transfer in Microgravity, Gordon and Breach Science Publishers, 1992.

Reynolds, W.C., Behavior of Liquids in Free Fall, J. Aerospace Sci., 26, 847, 1959.

Reynolds, W.C., Hydrodynamic Considerations for the Design of Systems for Very Low Gravity Environments, TR LG-1, Dept. Mech. Eng., Stanford University, Sept., 1961.

Saghir,M.Z. and Wetter, B., Microgravity Science Activities in Canada, Proceedings, AIAA/IKI Microgravity Science Symposium, Moscow, USSR, American Institute of Aeronautics and Astronautics, May 13-17, 1991.

Seibert, G., The Microgravity Research Program of the European Space Agency, International Symposium on Microgravity Science and Application, Chinese Academy of Sciences, Beijing, China, May, 1993.

Siegert, C.E., Petrash, D.A. and Otto, E.W., Time Response of Liquid-vapor Interface after Entering Weightlessness, NASA TN D-2458, August, 1964.

Siegert, C.E., Petrash, D.A. and Otto, E.W., Behavior of Liquid-Vapor Interface of Cryogenic Liquids during Weightlessness, NASA Technical Note D-2658, 1965

Sutton, G.P., Rocket Propulsion Elements, An Introduction to the Engineering of Rockets, sixth edition, John Wiley & Sons, Inc., 1992.

Symons, E.P., Outlet Baffles–Effect on Liquid Residuals from Zero Gravity Draining of Hemispherically Ended Cylinders, NASA TM X-2631, 1972.

Symons, E.P., Effect of Throttling on Interface Behavior and Liquid Residuals in Weightlessness, NASA TM X-3034, 1974.

Symons, E.P., Contoured Tank Outlets for Draining of Cylindrical Tanks in Low-Gravity Environment, NASA Technical Paper 1492, July 1979.

Torrey, M.D., Cloutman, L.D., Mjolsness, R.C. and Hirt, C.W., NASA-VOF2D: A Computer Program for Incompressible Flows with Free Surfaces, Los Alamos National Laboratory Report LA-10612-MS, Los Alamos, New Mexico, December 1985.

Unterberg, W. and Conggelliere, J., Zero Gravity Problems in Space Powerplants: A Status Survey, ARS Journal, June, 1962.

Vatistas, G. H., Yan, W. and Sankar, T.S., Dynamic Behavior of Liquids in Cylindrical Containers under Zero Gravity Conditions, Canadian Aeronautics and Space Journal, Volume 40, No.3, 1994.

Vatistas, G. H. and Yan, W., Dynamics of Liquids during and after Transition to Zero-gravity, Symposium on Microgravity Science, Chongqing, China, May 24-27, 1995.

Walter, H.U., Scientific Cooperation, Hydromechanics and Heat/Mass Transfer in Microgravity, Reviewed Proceedings of the First International Symposium on Hydromechanics and Heat/Mass Transfer in Microgravity, Perm-Moscow, Russia, 6-14 July, 1991, Gordon and Breach Science Publishers, 1992.

Welch, J.E., Harlow, F.H., Shannon, J.P. and Daly, B.J., THE MAC METHOD: A Computing Technique for Solving Viscous, Incompressible, Transient Fluid-Flow Problems Involving Free Surfaces, Los Alamos Scientific Laboratory report LA-3425, 1966.

Yan, W., Vatistas, G. H. and Sankar, T.S., Liquid Configurations in Rectangular Containers in Zero Gravity Environment, proceedings of the Second International Conference on Fluid Mechanics (ICFM)-II), Beijing, China, July 7-10, 1993.

Yan, W. and Vatistas, G. H., Dynamic Characteristics of Liquid Draining from a Tank in Weightlessness, Computers in Engineering 1995, proceedings of the 1995 ASME International Computers in Engineering Conference and Exhibition, Boston, U.S.A., August 1995.

Yan, W., Vatistas, G. H. and Sankar, T.S., Behavior of Liquid-Vapor Interface in Solid Containers during Weightlessness, proceedings of the CFD 94 – Second Annual Conference of the CFD Society of Canada, 1-3 June 1994, Toronto, Ontario, Canada.

Yan, W. and Vatistas, G. H., Computational Simulation of Liquid Dynamics of Liquid-Vapor-Solid Systems in Space Vehicles, 1st International Conference on Engineering Computation and Computer Simulation, ECCS-1, Changsha, China, November 27-29, 1995.

# APPENDIX

## I. CALCULATIONS IN A RECTANGULAR TANK

### A.1 Configuration System 1

#### A.1.1 Volume in Configuration System 1 $(0 \le \alpha < 90^o)$

From Fig.A.1, for a unit thickness in the z-direction perpendicular to the x-y plan, the liquid volume $V_1$ in configuration 1 at 0-g field is defined by

$$V_1 = V_{a1} + V_{b1} \tag{A.1.1.1}$$

where

$$V_{a1} = 2\,L\,H_c \tag{A.1.1.2}$$

$$V_{b1} = 2L\,\Delta H - \beta_1 R_1^2 + L\xi \tag{A.1.1.3}$$

The liquid volume $V_1$ thus is

$$V_1 = 2\,L\,H_c + 2\,L^2\left(\frac{1-\sin\alpha}{\cos\alpha} - \frac{\beta_1}{2\cos^2\alpha} + -\frac{\tan\alpha}{2}\right) \tag{A.1.1.4}$$

The liquid volume $V_1$ in 1-g condition is

$$V_1 = 2LH_1 \tag{A.1.1.5}$$

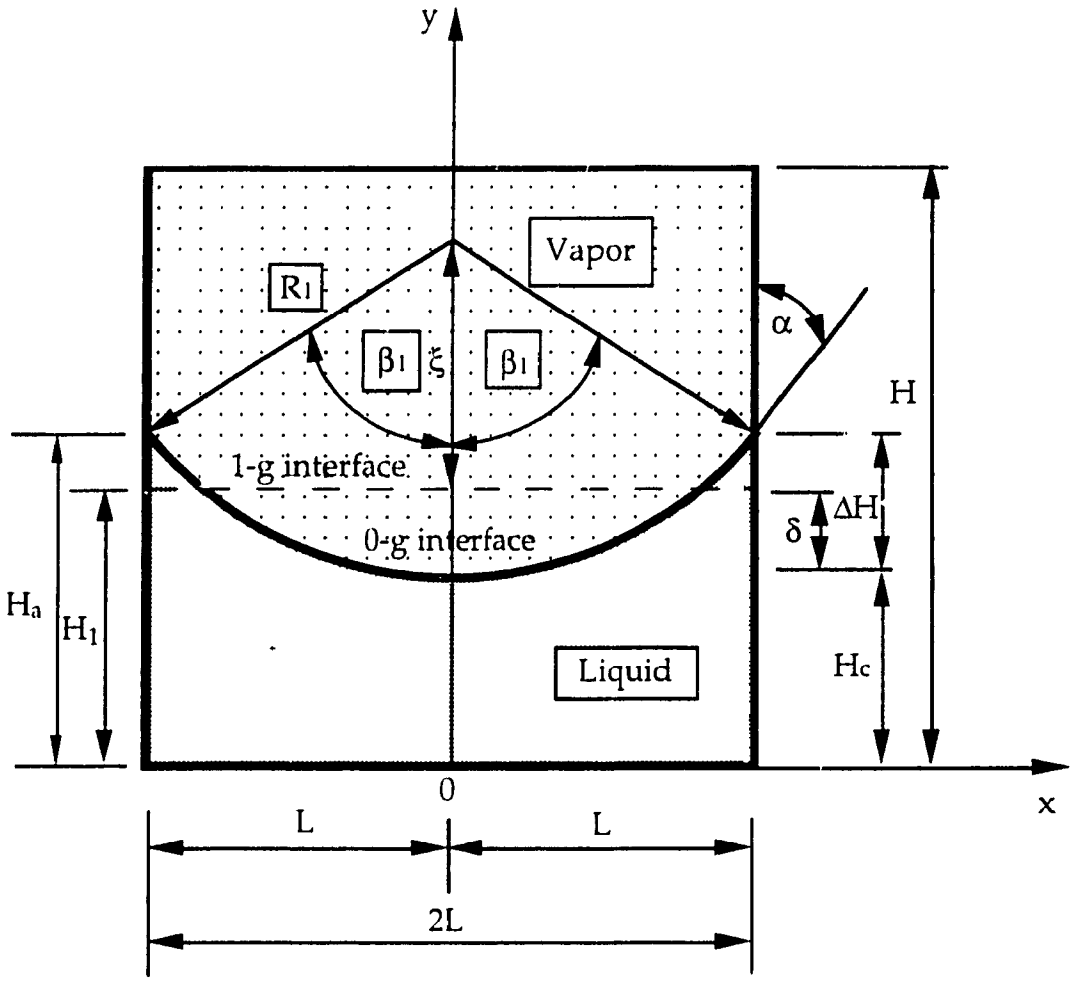


Fig.A.1 Configuration system 1 in a rectangular tank

Combing equations (A.1.1.4) and (A.1.1.5), and denoting $\overline{H}_1 = \frac{H_1}{L}$. liquid height in 1-g is

$$\overline{H}_1 = \overline{H}_c + \frac{1}{2\cos^2\alpha}\left\{\cos\alpha(2-\sin\alpha) - \left(\frac{\pi}{2}-\alpha\right)\right\} \qquad \text{(A.1.1.6)}$$

### A.1.2 Interface Areas in Configuration System 1 $(0 \le \alpha < 90^o)$

The liquid-vapor interface area $A_{lv,1}$ in configuration 1 is defined by

$$A_{lv,1} = 2\,\beta_1\,R \qquad \text{(A.1.2.1)}$$

where

$$\beta_1 = \frac{\pi}{2} - \alpha \qquad \text{(A.1.2.2)}$$

$$R_1 = \frac{L}{\cos\alpha} \qquad \text{(A.1.2.3)}$$

Interface areas are normalized by the half width of the tank, L. Thus, equation (A.1.2.1) becomes:

$$\overline{A}_{lv,1} = 2\left(\frac{\pi}{2}-\alpha\right)\frac{1}{\cos\alpha} \qquad \text{(A.1.2.4)}$$

The liquid-solid interface area is expressed by

$$A_{ls,1} = 2\,L + 2\,H_c + 2\,\Delta H \qquad \text{(A.1.2.5)}$$

where

$$H_c = H_1 - L\left(\frac{1-\sin\alpha}{\cos\alpha} - \frac{\beta_1}{2\cos^2\alpha} + \frac{\tan\alpha}{2}\right) \qquad \text{(A.1.2.6)}$$

$$\Delta H = \frac{L\,(1-\sin\alpha)}{\cos\alpha} \qquad \text{(A.1.2.7)}$$

Equation (A.1.2.5) may thus be written in dimensionless form as:

$$\overline{A}_{ls,1} = 2 + 2\,\overline{H}_1 + \frac{\pi - 2\alpha}{2\cos^2\alpha} - \tan\alpha \qquad \text{(A.1.2.8)}$$

## A.2 Configuration System 2

### A.2.1 Volume in Configuration System 2 $(0 \le \alpha < 45^o)$

From Fig.A.2 $(0 \le \alpha < 45^o)$, for a unit thickness in z-direction which is perpendicular to x-y plan, the liquid volume in 0-g field is calculated by

$$V_2 = 2\left(X_2^2 + X_2\,\zeta_2 - \beta_2\,R_2^2\right) \qquad \text{(A.2.1.1)}$$

where

$$R_2 = \frac{\sqrt{2}}{2\sin\beta_2}\,H_a \qquad \text{(A.2.1.2)}$$

$$\beta_2 = \frac{\pi}{4} - \alpha \qquad \text{(A.2.1.3)}$$

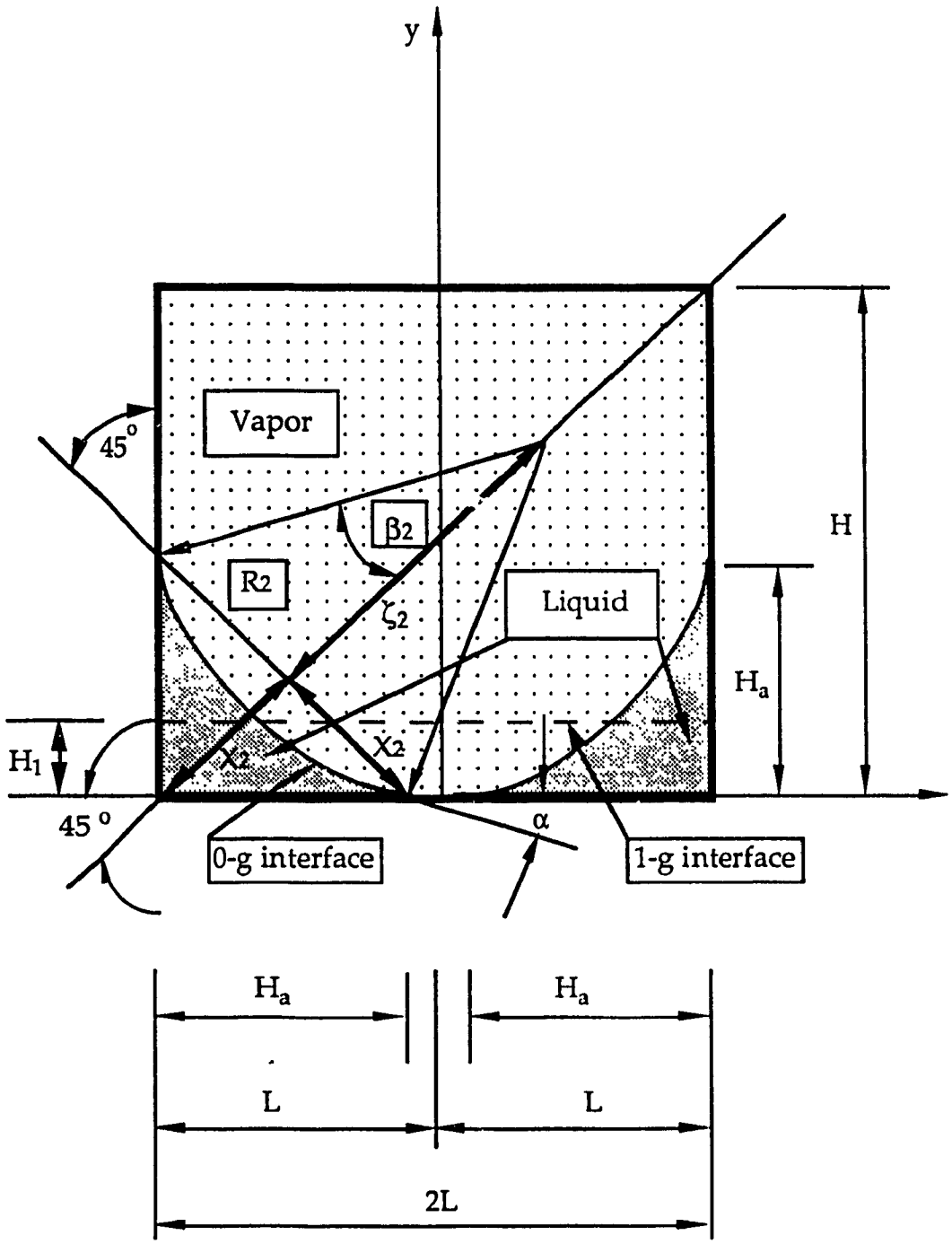


Fig.A.2 Configuration system 2 in a rectangular tank ($0^o < \alpha < 45^o$)

$$V_2 = \frac{H_a^2\left(\sin^2\beta_2 + \sin\beta_2\cos\beta_2 - \beta_2\right)}{\sin^2\beta_2} \qquad \text{(A.2.1.4)}$$

Let

$$\eta_2 = \sin^2\beta_2 + \sin\beta_2\cos\beta_2 - \beta_2 \qquad \text{(A.2.1.5)}$$

$$V_2 = \frac{\eta_2 H_a^2}{\sin^2\beta_2} \qquad \text{(A.2.1.6)}$$

The liquid volume $V_2$ in 1-g condition is

$$V_2 = 2LH_1 \qquad \text{(A.2.1.7)}$$

By equaling equations (A.2.1.6) and (A.2.1.7), and let $\overline{H}_a = \frac{H_a}{L}$

$$\overline{H}_1 = \frac{\overline{H}_a^2}{2\sin^2\beta_2}\eta_2 \qquad \text{(A.2.1.8)}$$

or

$$H_a = \sqrt{\frac{2LH_1}{\eta_2}}\sin\beta_2 \qquad \text{(A.2.1.9)}$$

### A.2.2 Interface Areas in Configuration System 2 $(0 \le \alpha < 45^o)$

The liquid-vapor interface area $A_{lv,2}$ is defined as

$$A_{lv,2} = 4\,\beta_2\,R_2 \tag{A.2.2.1}$$

or

$$A_{lv,2} = 2\sqrt{2}\left(\frac{\pi}{4} - \alpha\right)\frac{H_a}{\sin\beta_2} \tag{A.2.2.2}$$

The dimensionless liquid-vapor interface area is

$$\overline{A}_{lv,2} = (\pi - 4\,\alpha)\sqrt{\frac{\overline{H}_1}{\eta_2}} \tag{A.2.2.3}$$

The liquid-solid interface area is

$$A_{ls,2} = 4\,H_a \tag{A.2.2.4}$$

$$\overline{A}_{ls,2} = \sqrt{\frac{32\,\overline{H}_1}{\eta_2}}\,\sin\beta_2 \tag{A.2.2.5}$$

### A.2.3 Volume in Configuration 2 $(45^o < \alpha < 90^o)$

From Fig.A.3, for a unit thickness in z-direction, the liquid volume of configuration system 2 in 0-g field is calculated by

$$V_2 = \frac{\eta_2 H_a^2}{\sin^2\beta_2} \qquad \text{(A.2.3.1)}$$

where

$$\eta_2 = \sin^2\beta_2 - \sin\beta_2 \cos\beta_2 + \beta_2 \qquad \text{(A.2.3.2)}$$

$$\beta_2 = \alpha - \frac{\pi}{4} \qquad \text{(A.2.3.3)}$$

The liquid volume $V_2$ in 1-g condition is the same as in 0-g environment. Therefore,

$$H_a = \sqrt{\frac{2 L H_1}{\eta_2}}\ \sin\beta_2 \qquad \text{(A.2.3.4)}$$

### A.2.4 Interface Areas in Configuration System 2 ($45^\circ < \alpha < 90^\circ$)

The liquid-vapor interface area $A_{lv,2}$ is defined by

$$A_{lv,2} = 4\,\beta_2\,R_2 \qquad \text{(A.2.4.1)}$$

where

$$R_2 = \frac{\sqrt{2}}{2\sin\beta_2} H_a \qquad \text{(A.2.4.2)}$$

Thus

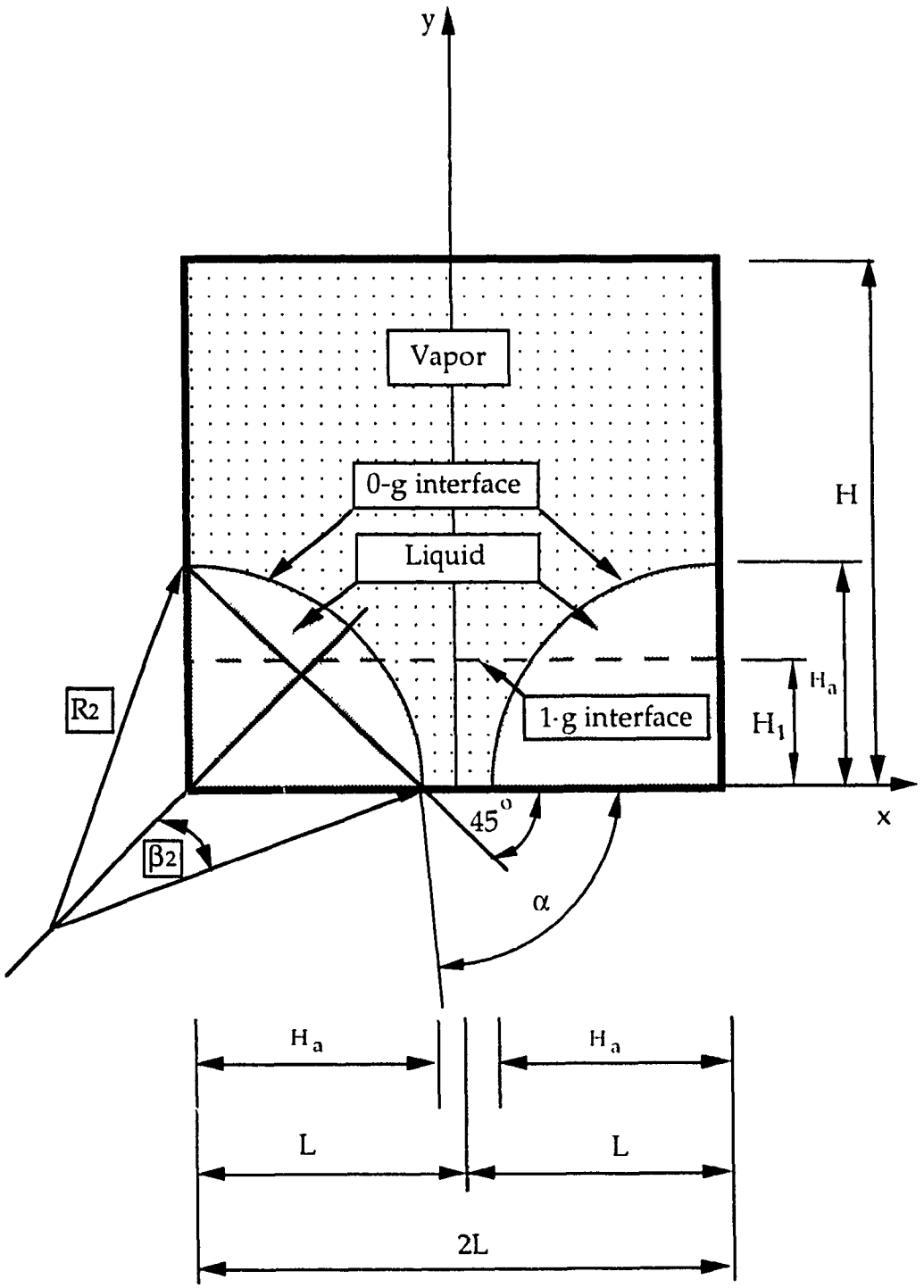


Fig.A.3 Configuration system 2 in a rectangular tank ($45^o < \alpha < 90^o$)

$$A_{lv,2} = 2\sqrt{2}\left(\alpha - \frac{\pi}{4}\right)\frac{H_a}{\sin\beta_2} \tag{A.2.4.3}$$

Making use of $H_a$ in equation (A.2.3.4), the dimensionless liquid-vapor interface is

$$\overline{A}_{lv,2} = (4\alpha - \pi)\sqrt{\frac{\overline{\overline{H}}_1}{\eta_2}} \tag{A.2.4.4}$$

$$A_{ls,2} = 4\,H_a \tag{A.2.4.5}$$

$$\overline{A}_{ls,2} = \sqrt{\frac{32\,\overline{\overline{H}}_1}{\eta_2}}\,\sin\beta_2 \tag{A.2.4.6}$$

## A.3 Critical Liquid Height $H_1 (H_{1min} \le H_1 \le H_{1max})$

### A.3.1 Energy Difference $(0 \le \alpha < 45^\circ)$

$$\Delta\left|\overline{A}_{lv}\right| = \frac{\Delta\left|A_{lv}\right|}{L} = \frac{A_{lv,2} - A_{lv,1}}{L}$$
$$= 4\left(\frac{\pi}{4} - \alpha\right)\sqrt{\frac{\overline{\overline{H}}_1}{\eta_2}} - \frac{\pi - 2\alpha}{\cos\alpha} \tag{A.3.1.1}$$

$$\Delta\left|\overline{A}_{ls}\right| = \frac{\Delta\left|A_{ls}\right|}{L} = \frac{A_{ls,2} - A_{ls,1}}{L}$$
$$= \sqrt{\frac{32\,\overline{\overline{H}}_1}{\eta_2}}\,\sin\beta_2 - 2\left(1 + \overline{\overline{H}}_1 + \frac{\beta_1}{2\cos^2\alpha} - \frac{\tan\alpha}{2}\right) \tag{A.3.1.2}$$

$$\Delta\bar{E} = \frac{\Delta E}{L\,\sigma_{lv}} = \Delta\left|\bar{A}_{lv}\right| - \cos\alpha\ \Delta\left|\bar{A}_{ls}\right|$$

$$= 4\left(\frac{\pi}{4} - \alpha\right)\sqrt{\frac{\bar{\bar{H}}_1}{\eta_2}} - \frac{\pi - 2\alpha}{\cos\alpha} \qquad \text{(A.3.1.3)}$$

$$- \cos\alpha\left\{\sqrt{\frac{32\,\bar{\bar{H}}_1}{\eta_2}}\ \sin\beta_2 - 2\left(1 + \bar{\bar{H}}_1 + \frac{\pi - 2\alpha}{4\cos^2\alpha} - \frac{\tan\alpha}{2}\right)\right\}$$

## A.3.2 Critical Liquid Height $H_1$ $(0 \le \alpha < 45^o)$

$$\Delta\bar{E} = 0 \qquad \text{(A.3.2.1)}$$

$$\left(\pi - 4\,\alpha\right)\sqrt{\frac{\bar{\bar{H}}_{1cr}}{\eta_2}}$$

$$-\frac{\pi - 2\alpha}{\cos\alpha} - \cos\alpha\left\{\sqrt{\frac{32\,\bar{\bar{H}}_{1cr}}{\eta_2}}\ \sin\beta_2 - 2\left(1 + \bar{\bar{H}}_{1cr} + \frac{\pi - 2\alpha}{4\cos^2\alpha} - \frac{\tan\alpha}{2}\right)\right\} = 0 \qquad \text{(A.3.2.2)}$$

$$\bar{\bar{H}}_{1cr} + \left\{\frac{(\pi - 4\,\alpha)}{2\cos\alpha}\sqrt{\frac{1}{\eta_2}} - \sin\beta_2\sqrt{\frac{8}{\eta_2}}\right\}\sqrt{\bar{\bar{H}}_{1cr}}$$

$$+ 1 - \frac{\pi - 2\,\alpha}{4\cos 2\alpha} - \frac{\tan\alpha}{2} = 0 \qquad \text{(A.3.2.3)}$$

which is a quadratic equation solved for $x = \sqrt{\bar{\bar{H}}_{1cr}}$

$$x^2 + \left\{\frac{(\pi - 4\,\alpha)}{2\cos\alpha}\sqrt{\frac{1}{\eta_2}} - \sin\beta_2\sqrt{\frac{8}{\eta_2}}\right\}x + 1 - \frac{\pi - 2\,\alpha}{4\cos 2\alpha} - \frac{\tan\alpha}{2} = 0 \qquad \text{(A.3.2.4)}$$

$$a\,x^2 + b\,x + c = 0 \qquad \text{(A.3.2.5)}$$

where

$$a = 1 \tag{A.3.2.6}$$

$$b = \frac{(\pi - 4\alpha)}{2\cos\alpha}\sqrt{\frac{1}{\eta_2}} - \sin\beta_2\sqrt{\frac{8}{\eta_2}} \tag{A.3.2.7}$$

$$c = 1 - \frac{\pi - 2\alpha}{4\cos^2\alpha} - \frac{\tan\alpha}{2} \tag{A.3.2.8}$$

$$x_{1,2} = \frac{-b \pm \sqrt{b^2 - 4ac}}{2a} \tag{A.3.2.9}$$

The solution of $x_2$ is not realistic. After eliminating the nonrealistic root, the solution for critical liquid height is

$$x = \frac{1}{2}\left[\sin\beta_2\sqrt{\frac{8}{\eta_2}} - \frac{(\pi - 4\alpha)}{2\cos^2\alpha}\sqrt{\frac{1}{\eta_2}}\right] + \frac{1}{2}\sqrt{\left[\frac{(\pi - 4\alpha)}{2\cos\alpha}\sqrt{\frac{1}{\eta_2}} - \sin\beta_2\sqrt{\frac{8}{\eta_2}}\right]^2 - 4\left(1 - \frac{\pi - \alpha}{4\cos^2\alpha} - \frac{\tan\alpha}{2}\right)} \tag{A.3.2.10}$$

$$\overline{H}_{1cr} = \left\{\left(\sqrt{2}\sin\beta_2 - \frac{\beta_2}{\cos\alpha}\right)\frac{1}{\sqrt{\eta_2}} + \sqrt{\left[\frac{\beta_2}{\cos\alpha} - \sqrt{2}\sin\beta_2\right]^2\frac{1}{\eta_2} - \left(1 - \frac{\pi - 2\alpha}{4\cos^2\alpha} - \frac{\tan\alpha}{2}\right)}\right\}^2 \tag{A.3.2.11}$$

### A.3.3 Energy Difference ($45° < \alpha < 90°$)

$$\Delta\left|\overline{A}_{lv}\right| = \frac{\Delta\left|A_{lv}\right|}{L} = 4\left(\alpha - \frac{\pi}{4}\right)\sqrt{\frac{\overline{\overline{H}}_1}{\eta_2}} - \frac{\pi - 2\alpha}{\cos\alpha} \qquad \text{(A.3.3.1)}$$

$$\Delta\left|\overline{A}_{ls}\right| = \frac{\Delta\left|A_{ls}\right|}{L} = \sqrt{\frac{32\,\overline{\overline{H}}_1}{\eta_2}}\sin\beta_2 - 2\left(1 + \overline{H}_1 + \frac{\beta_1}{2\cos^2\alpha} - \frac{\tan\alpha}{2}\right) \qquad \text{(A.3.3.2)}$$

$$\begin{aligned}\Delta\overline{E} = \frac{\Delta E}{\sigma_{lv}} &= 4\left(\alpha - \frac{\pi}{4}\right)\sqrt{\frac{\overline{\overline{H}}_1}{\eta_2}} - \frac{\pi - 2\alpha}{\cos\alpha} \\ &- \cos\alpha\left\{\sqrt{\frac{32\,\overline{\overline{H}}_1}{\eta_2}}\sin\beta_2 - 2\left(1 + \overline{H}_1 + \frac{\pi - 2\alpha}{4\cos^2\alpha} - \frac{\tan\alpha}{2}\right)\right\}\end{aligned} \qquad \text{(A.3.3.3)}$$

### A.3.4 Critical Liquid Height $H_{1cr}$ $(45^\circ < \alpha < 90^\circ)$

$$\Delta\overline{E} = 0 \qquad \text{(A.3.4.1)}$$

$$\begin{aligned}&4\left(\alpha - \frac{\pi}{4}\right)\sqrt{\frac{\overline{\overline{H}}_{1cr}}{\eta_2}} - \frac{\pi - 2\alpha}{\cos\alpha} \\ &- \cos\alpha\left\{\sqrt{\frac{32\,\overline{\overline{H}}_{1cr}}{\eta_2}}\sin\beta_2 - 2\left(1 + \overline{H}_{1cr} + \frac{\pi - 2\alpha}{4\cos^2\alpha} - \frac{\tan\alpha}{2}\right)\right\} = 0\end{aligned} \qquad \text{(A.3.4.2)}$$

$$\overline{H}_{1cr} + \left\{\frac{(4\alpha - \pi)}{2\cos\alpha}\sqrt{\frac{1}{\eta_2}} - \sin\beta_2\sqrt{\frac{8}{\eta_2}}\right\}\sqrt{\overline{\overline{H}}_{1cr}} + 1 - \frac{\pi - 2\alpha}{4\cos^2\alpha} - \frac{\tan\alpha}{2} = 0 \qquad \text{(A.3.4.3)}$$

$$\begin{aligned}\sqrt{\overline{\overline{H}}_{1cr}} &= \frac{1}{2}\left[\sin\beta_2\sqrt{\frac{8}{\eta_2}} - \frac{(4\alpha - \pi)}{2\cos\alpha}\sqrt{\frac{1}{\eta_2}}\right] \\ &+ \frac{1}{2}\sqrt{\left[\frac{(4\alpha - \pi)}{2\cos\alpha}\sqrt{\frac{1}{\eta_2}} - \sin\beta_2\sqrt{\frac{8}{\eta_2}}\right]^2 - 4\left(1 - \frac{\pi - 2\alpha}{4\cos^2\alpha} - \frac{\tan\alpha}{2}\right)}\end{aligned} \qquad \text{(A.3.4.4)}$$

$$\overline{H}_{1cr} = \left\{ \left( \sqrt{2}\,\sin\beta_2 - \frac{(4\alpha - \pi)}{4\cos\alpha} \right) \frac{1}{\sqrt{\eta_2}} + \sqrt{\left[ \frac{(4\alpha - \pi)}{4\cos\alpha} - \sqrt{2}\,\sin\beta_2 \right]^2 \frac{1}{\eta_2} - \left( 1 - \frac{\pi - 2\alpha}{4\cos^2\alpha} - \frac{\tan\alpha}{2} \right)} \right\}^2 \qquad \text{(A.3.4.5)}$$

## A.4 Limiting Cases

### A.4.1 Configuration System 2 ($\alpha = 45^o$)

L' Hopital's rule (Ford, 1963) shows: if f(a) = g(a) = 0,

$$\lim_{x \to a} \frac{f(x)}{g(x)} = \lim_{x \to a} \frac{f'(x)}{g'(x)} \qquad \text{(A.4.1.1)}$$

Applying to Equations (2.4.2.6) and (2.3.2.18)

$$\begin{aligned} \lim_{\beta_2 \to 0} \overline{H}_{1max} &= \lim_{\beta_2 \to 0} \frac{\sin^2\beta_2 + \sin\beta_2 \cos\beta_2 - \beta_2}{2\sin^2\beta_2} \\ &= \lim_{\beta_2 \to 0} \frac{2\sin\beta_2\cos\beta_2 + \cos^2\beta_2 - \sin^2\beta_2 - 1}{4\sin\beta_2\cos\beta_2} \\ &= \lim_{\beta_2 \to 0} \frac{\cos\beta_2 - \sin\beta_2}{2\cos\beta_2} \\ &= \frac{1}{2} \end{aligned} \qquad \text{(A.4.1.2)}$$

$$\overline{A}_{lv,2} = (4\alpha - \pi)\sqrt{\frac{\overline{H}_1}{\eta_2}} \qquad \text{(A.4.1.3)}$$

$$\lim_{\beta_2 \to 0} \overline{A}_{lv,2} = \lim_{\beta_2 \to 0} \left[ (4\alpha - \pi) \sqrt{\frac{\overline{H}_1}{\eta_2}} \right]$$
$$= 4\sqrt{\overline{H}_1} \lim_{\beta_2 \to 0} \left( \sqrt{\frac{\beta_2^2}{\eta_2}} \right) \qquad \text{(A.4.1.4)}$$

$$\lim_{\beta_2 \to 0} \frac{\eta_2}{\beta_2^2} = \lim_{\beta_2 \to 0} \left( \frac{\sin^2\beta_2 - \sin\beta_2 \cos\beta_2 + \beta_2}{\beta_2^2} \right)$$
$$= \lim_{\beta_2 \to 0} \left( \frac{2 \sin\beta_2 \cos\beta_2}{2\beta_2} - \frac{\cos^2\beta_2}{2\beta_2} + \frac{\sin^2\beta_2}{2\beta_2} \right) \qquad \text{(A.4.1.5)}$$
$$= \lim_{\beta_2 \to 0} \left[ \frac{1}{2} \left( 2\cos^2\beta_2 - 2\sin^2\beta_2 + 4 \sin\beta_2 \cos\beta_2 \right) \right]$$
$$= 1$$

$$\overline{A}_{lv,2} = \lim_{\beta_2 \to 0} \left( 4\sqrt{\overline{H}_1} \sqrt{\frac{\beta_2^2}{\eta_2}} \right) \qquad \text{(A.4.1.6)}$$

Thus

$$\overline{A}_{lv,2} = 4\sqrt{\overline{H}_1} \qquad \text{(A.4.1.7)}$$

The same treatment is applied to $\overline{A}_{ls,2}$

$$\overline{A}_{ls,2} = \lim_{\beta_2 \to 0} \left( \sqrt{\frac{32\overline{H}_1}{\eta_2}} \sin\beta_2 \right) = \sqrt{32\overline{H}_1} \lim_{\beta_2 \to 0} \left( \sqrt{\frac{\sin^2\beta_2}{\eta_2}} \right) \qquad \text{(A.4.1.8)}$$

$$\lim_{\beta_2 \to 0} \frac{\sin^2\beta_2}{\eta_2} = \lim_{\beta_2 \to 0} \left( \frac{\cos\beta_2}{\cos\beta_2 + \sin\beta_2} \right) = 1 \qquad \text{(A.4.1.9)}$$

Therefore

$$\overline{A}_{ls,2} = \sqrt{32\,\overline{H}_1} \tag{A.4.1.10}$$

$$\begin{aligned}\Delta\overline{E}_{45^o} &= 4\sqrt{\overline{H}_1} - \frac{2\left(\frac{\pi}{2}-\frac{\pi}{4}\right)}{\sin 45^o} \\ &\quad - \cos 45^o\left[\sqrt{32\overline{H}_1} - 2\left(1 + \overline{H}_1 + \frac{\frac{\pi}{2}-\frac{\pi}{4}}{2\cos^2 45^o} - \frac{\tan 45^o}{2}\right)\right] \\ &= \sqrt{2}\ \overline{H}_1 + \sqrt{2}\left(\frac{1}{2}-\frac{\pi}{4}\right)\end{aligned} \tag{A.4.1.11}$$

$$\overline{H}_{1cr,\,45^o} = \frac{\pi - 2}{4} \tag{A.4.1.12}$$

### A.4.2 Configuration System 1 ($\alpha = 90^o$)

The contact angle of 90 degree is the limit of configuration 1. As $\alpha$ approaches $90^o$, cos $\alpha$ intends to be 0. To overcome this difficulty, L' Hopital's rule is used.

$$\overline{A}_{lv,1,\,90^o} = \lim_{\alpha \to 90^o} \frac{\pi - 2\alpha}{\cos\alpha} = 2 \tag{A.4.2.1}$$

$$\cos\alpha\,\Delta\left|\bar{A}_{ls}\right| = \lim_{\alpha\to 90^0}\left\{\cos\alpha\left(8\sqrt{\frac{\bar{\bar{H}}_1}{\pi}} - 2 - 2\bar{H}_1 - \frac{\pi - 2\alpha}{2\cos^2\alpha} + \tan\alpha\right)\right\}$$

$$= 8\cos\alpha\sqrt{\frac{\bar{\bar{H}}_1}{\pi}} - 2\cos\alpha\,\bar{H}_1 - \frac{\pi - 2\alpha}{2\cos\alpha} + \sin\alpha \qquad \text{(A.4.2.2)}$$

$$=0$$

$$\Delta\bar{E}_{90^o} = 2\sqrt{\pi\,\bar{\bar{H}}_1} - 2 \qquad \text{(A.4.2.3)}$$

$$\bar{H}_{1cr,\ 90^o} = \frac{1}{\pi} \qquad \text{(A.4.2.4)}$$

## A.5 Non-wetting Liquid

### A.5.1 Configuration 1 $\left(90^o < \alpha < 180^o\right)$

From Fig A.4, the configuration 1 in zero-gravity presents:

$$H_1 = H_c - \delta \qquad \text{(A.5.1.1)}$$

where

$$\delta = \Delta H - \frac{\beta_1 L}{2\cos^2\alpha} + \frac{L}{2}\tan\alpha \qquad \text{(A.5.1.2)}$$

$$\Delta H = H_c - H_L = R_1 - \sqrt{R_1^2 - L^2} \qquad \text{(A.5.1.3)}$$

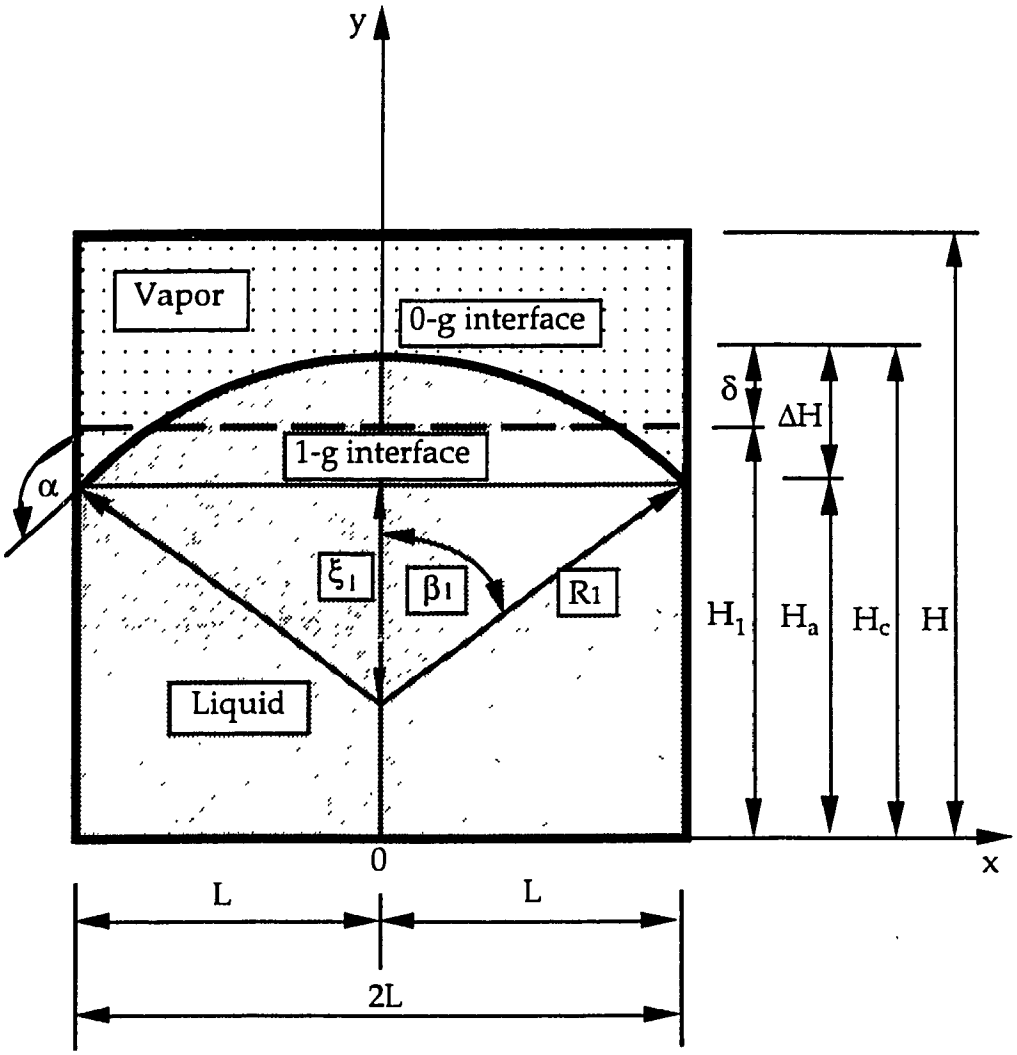


Fig. A.4 Non-wetting liquid configuration system 1 in a rectangular tank

$$\beta_1 = \alpha - \frac{\pi}{2} \tag{A.5.1.4}$$

$$\xi_1^2 + L^2 = R_1^2 \tag{A.5.1.5}$$

All length parameters are normalized by the half width of the tank, L.

$$\bar{\xi}_1^2 + 1 = \bar{R}_1^2 \tag{A.5.1.6}$$

$$\bar{R}_1^2 = \frac{1}{1-\cos^2\beta_1} = \frac{1}{\sin^2\beta_1} \tag{A.5.1.7}$$

$$\bar{V}_{a1} = \beta_1 \bar{R}_1^2 - \bar{\xi}\,\bar{R}_1 \sin\beta_1 = \beta_1 \bar{R}_1^2 - \bar{R}_1^2 \sin\beta_1 \cos\beta_1 \tag{A.5.1.8}$$

From above two equations,

$$\bar{V}_{a1} = \frac{\beta_1}{\sin^2\beta_1} - \frac{\sin\beta_1 \cos\beta_1}{\sin^2\beta_1} = \frac{\beta_1}{\sin^2\beta_1} - \cot\beta_1 \tag{A.5.1.9}$$

$$\bar{V}_{b1} = 2\bar{H}_L \tag{A.5.1.10}$$

$$\bar{V}_1 = \bar{V}_{a1} + \bar{V}_{b1} = 2\bar{H}_L + \frac{\beta_1}{\sin^2\beta_1} - \cot\beta \tag{A.5.1.11}$$

The liquid volume in zero-gravity is:

$$\bar{V}_1 = 2\bar{H}_1 \tag{A.5.1.12}$$

By equating Equation (A.5.1.11) to Equation (A.5.1.12)

$$\overline{H}_1 = \overline{H}_a + \frac{1}{2}\left(\frac{\beta_1}{\sin^2\beta_1} - \cot\beta_1\right) \tag{A.5.1.13}$$

$$\overline{A}_{lv,1} = 2\,\beta_1\,\overline{R}_1 = \frac{2\,\beta_1}{\sin\beta} \tag{A.5.1.14}$$

$$\begin{aligned}\overline{A}_{ls,1} &= 2\left(\overline{H}_a + 1\right) = 2\left[\overline{H}_1 - \frac{1}{2}\left(\frac{\beta_1}{\sin^2\beta_1} - \cot\beta_1\right) + 1\right] \\ &= 2\,\overline{H}_1 - \left(\frac{\beta_1}{\sin^2\beta_1} - \cot\beta_1\right) + 2\end{aligned} \tag{A.5.1.15}$$

## A.5.2 Configuration 2 $\left(90^\circ \le \alpha \le 145^\circ\right)$

See Fig.A.5, liquid volume in zero-gravity is calculated as

$$\overline{V}_{a2} = 2\left(\beta_2\,\overline{R}_2^2 - \overline{R}_2^2 \sin\beta_1 \cos\beta_1\right) \tag{A.5.2.1}$$

$$\begin{aligned}\overline{V}_2 &= \overline{V}_{a2} + \overline{V}_{b2} \\ &= 2\left(\beta_2\,\overline{R}_2^2 - \overline{R}_2^2 \sin\beta_2 \cos\beta_2 + \overline{R}_2^2 \sin^2\beta_2\right)\end{aligned} \tag{A.5.2.2}$$

since

$$\overline{V}_2 = 2\,\overline{H}_1 \tag{A.5.2.3}$$

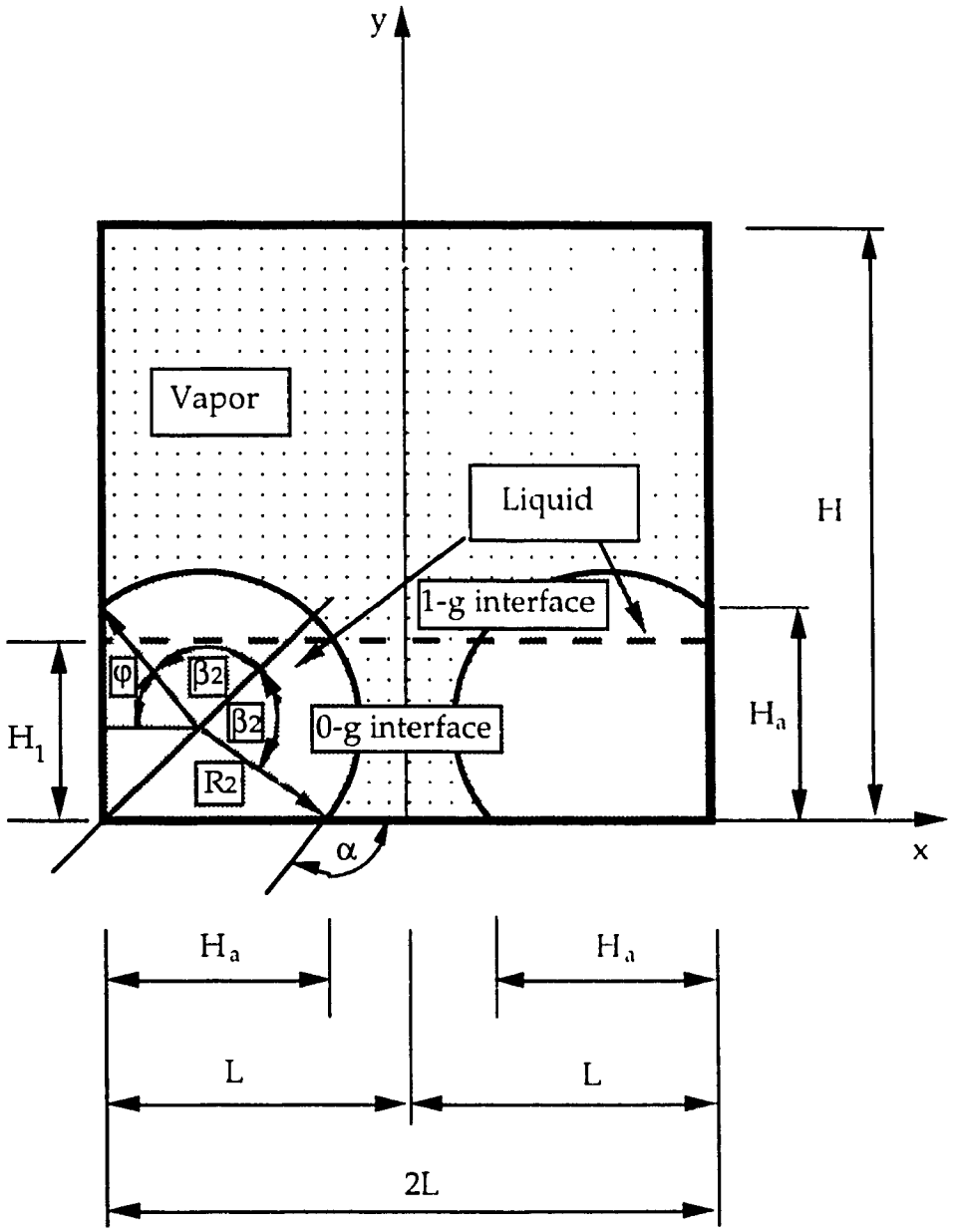


Fig. A.5 Non-wetting liquid configuration system 2 in a rectangular tank

$$\bar{H}_1 = \beta_2 \bar{R}_2^2 - \bar{R}_2^2 \sin\beta_2 \cos\beta_2 + \bar{R}_2^2 \sin^2\beta_2 \qquad \text{(A.5.2.4)}$$

$$\bar{R}_2 = \sqrt{\frac{\bar{H}_1}{\eta_2}} \qquad \text{(A.5.2.5)}$$

where

$$\eta_2 = \sin^2\beta_2 - \sin\beta_2 \cos\beta_2 + \beta_2 \qquad \text{(A.5.2.6)}$$

$$\beta_2 = \alpha - \frac{\pi}{4} \qquad \text{(A.5.2.7)}$$

$$\bar{A}_{lv,2} = 4\,\beta_2\,\bar{R}_2 = 4\,\beta_2 \sqrt{\frac{\bar{H}_1}{\eta_2}} \qquad \text{(A.5.2.8)}$$

$$\begin{aligned} \bar{A}_{ls,2} &= 4\,\bar{H}_a = \sqrt{32}\,\bar{R}_2 \sin\beta_2 \\ &= \sin\beta_2 \sqrt{\frac{32}{\eta_2}}\,\sqrt{\bar{H}_1} \end{aligned} \qquad \text{(A.5.2.9)}$$

If

$$R_2 + R_2 \cos\varphi = L \qquad \text{(A.5.2.10)}$$

where

$$\varphi = \frac{3\pi}{2} - \beta_2 = \pi - \alpha \qquad \text{(A.5.2.11)}$$

The maximum liquid height is:

$$\overline{H}_{1max} = \left(\frac{1}{1+\cos\varphi}\right)^2 \eta_2 \qquad \text{(A.5.2.12)}$$

### A.5.3 Energy Difference $(90^o \le \alpha \le 145^o)$

$$\Delta\overline{E} = \frac{\Delta E}{\sigma_{lv}} = \Delta\left|\,\overline{A}_{lv}\,\right| - \cos\alpha\ \Delta\left|\,\overline{A}_{ls}\,\right|$$

$$= 4\beta_2\sqrt{\frac{\overline{H}_1}{\eta_2}} - \frac{2\beta_1}{\sin\beta_1} \qquad \text{(A.5.3.1)}$$

$$-\cos\alpha\left\{\sqrt{\frac{32\,\overline{H}_1}{\eta_2}}\,\sin\beta_2 - 2\,\overline{H}_1 + \frac{\beta_1}{\sin^2\beta_1} - \cot\beta_1 - 2\right.$$

### A.5.4 Configuration 2 $(145^o \le \alpha \le 180^o)$

$$\overline{H}_1 = \beta_2\,\overline{R}_2^2 + \overline{R}_2^2\sin\beta_2\cos\beta_2 + \overline{R}_2^2\sin^2\beta_2 \qquad \text{(A.5.4.1)}$$

$$\overline{R}_2 = \sqrt{\frac{\overline{H}_1}{\eta_2}} \qquad \text{(A.5.4.2)}$$

where

$$\eta_2 = \beta_2 + \sin\beta_2\cos\beta_2 + \sin^2\beta_2 \qquad \text{(A.5.4.3)}$$

$$\beta_2 = \alpha - \frac{\pi}{4} \qquad \text{(A.5.4.4)}$$

$$\overline{A}_{lv,2} = 4\,\beta_2 \sqrt{\frac{\overline{\overline{H}_1}}{\eta_2}} \tag{A.5.4.5}$$

$$\overline{A}_{ls,2} = \sin\beta_2 \sqrt{\frac{32}{\eta_2}}\,\sqrt{\overline{H}_1} \tag{A.5.4.6}$$

$$\begin{aligned}\Delta\overline{E} = {} & 4\,\beta_2 \sqrt{\frac{\overline{\overline{H}_1}}{\eta_2}} - \frac{2\,\beta_1}{\sin\beta_1} \\ & - \cos\alpha \left\{ \sqrt{\frac{32\,\overline{\overline{H}_1}}{\eta_2}}\,\sin\beta_2 - 2\,\overline{H}_1 + \left( \frac{\beta_1}{\sin^2\beta_1} - \cot\beta_1 \right) - 2 \right\}\end{aligned} \tag{A.5.4.7}$$

# II. CALCULATIONS OF WETTING LIQUID IN A CYLINDRICAL TANK

## B.1 Interface Areas of Configuration 3

The dimensionless liquid-vapor interface area shown in Fig.B.1 is calculated as:

$$\overline{A}_{lv,3} = \frac{2\pi(1-\sin\alpha)}{\cos^2\alpha} \tag{B.1.1}$$

The dimensionless liquid-solid interface area is

$$\overline{A}_{ls,3} = \pi + 2\pi\overline{\overline{H}}_L \tag{B.1.2}$$

where

$$\overline{\overline{H}}_L = \overline{\overline{H}}_1 + \Delta\overline{\overline{H}} - \bar{\delta} \tag{B.1.3}$$

$$\Delta\overline{\overline{H}} = \frac{1-\sin(\alpha)}{\cos(\alpha)} \tag{B.1.4}$$

$$\bar{\delta} = \frac{1}{\cos(\alpha)} - \frac{2}{3}\frac{\left[1-\sin^3(\alpha)\right]}{\cos^3(\alpha)} \tag{B.1.5}$$

$$\overline{A}_{ls,3} = 2\pi\left\{\overline{\overline{H}}_1 + \frac{1-\sin(\alpha)}{\cos^2(\alpha)} - \frac{1}{\cos(\alpha)} + \frac{2}{3}\frac{\left[1-\sin^3(\alpha)\right]}{\cos^3(\alpha)}\right\} + \pi \tag{B.1.6}$$

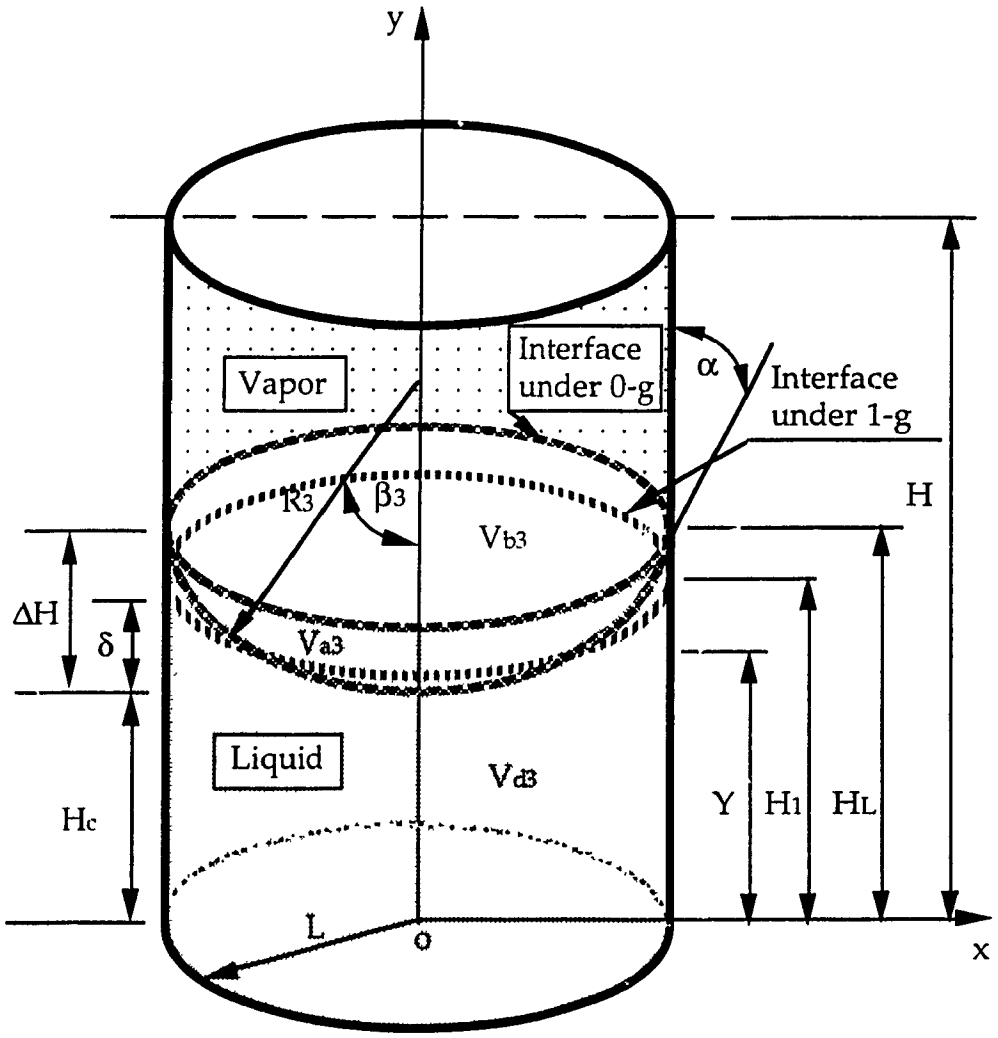


Fig.B.1 Configuration system 3 in a cylindrical tank

## B.2 Interface Areas of Configuration 4

Configuration system 4 is shown in Fig.B.2. The liquid-vapor interface area can be defined by the following equation

$$A_{lv,4} = \int_0^L 2\pi f(y)\sqrt{1+[f'(y)]^2}\,dy \tag{B.2.1}$$

where

$$f(y) = x = \sqrt{R_4^2 - (y + H_4)^2} - H_4 \tag{B.2.2}$$

Substituting $f(y)$ in equation (B.2.1) with equation (B.2.2), then integrate

The liquid-vapor interface area is

$$\overline{A}_{lv,4} = 2\pi \overline{R}_4\left[1 - \overline{H}_4\left(\frac{\pi}{2} - 2\alpha\right)\right] \tag{B.2.3}$$

where

$$\overline{R}_4 = \frac{\sqrt{2}\,\overline{H}_b}{2\sin\beta_4} \tag{B.2.4}$$

From

$$(L + H_4)^2 + H_4^2 = R_4^2 \tag{B.2.5}$$

$$\overline{H}_4 = \frac{\sqrt{\overline{H}_b^2 - \sin^2\beta_4} - \sin\beta_4}{2\sin\beta_4} \tag{B.2.6}$$

$$\beta_4 = \frac{\pi}{4} - \alpha \tag{B.2.7}$$

The liquid-solid interface area is

$$A_{ls,4} = \pi L^2 - \pi (L - H_b)^2 + 2\pi L H_b \tag{B.2.8}$$

$$\overline{A}_{ls,4} = \pi \overline{H}_b (4 - \overline{H}_b) \tag{B.2.9}$$

$\overline{H}_b$ may be obtained form the conservation of the liquid volume. The liquid volume in 0-g can be calculated by

$$V_4 = V_{b4} - V_{a4} \tag{B.2.10}$$

where

$$V_{b4} = \pi L^2 L = \pi L^3 \tag{B.2.11}$$

and

$$V_{a4} = \int_0^t \pi x^2 dy \tag{B.2.12}$$

where

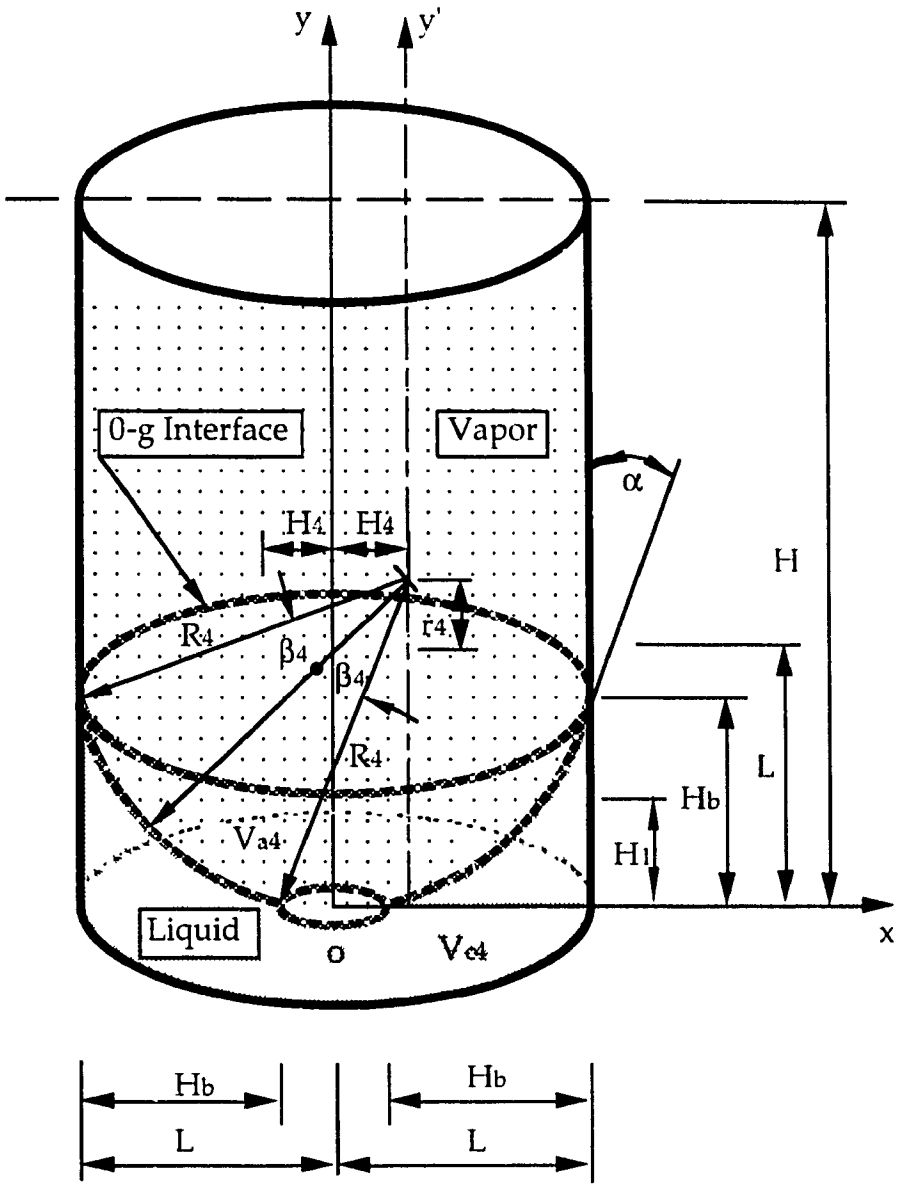


Fig.B.2 Configuration system 4 in a cylindrical tank

$$x = \sqrt{R_4^2 - (y + H_4)^2} - H_4 \tag{B.2.13}$$

After integration of equation (B.2.12)

$$V_{a4} = \pi\left[R_4^2 L - H_4 L^2 - \frac{1}{3}L^3 - H_4 R_4^2\left(\frac{\pi}{2} - 2\alpha\right)\right] \tag{B.2.14}$$

$$V_4 = \pi\left\{\frac{4}{3}L^3 - R_4^2 L + H_4 L^2 + H_4 R_4^2\left(\frac{\pi}{2} - 2\alpha\right)\right\} \tag{B.2.15}$$

The liquid volume in 1-g field is equal to the volume in 0-g condition. Thus, liquid height $H_1$ is

$$\overline{H}_1 = \frac{4}{3} - \overline{R}_4^2 + \overline{H}_4 + \overline{H}_4\,\overline{R}_4^2\,\beta_5 \tag{B.2.16}$$

or

$$\overline{H}_1 = \frac{4}{3} - \frac{\overline{H}_b^2}{2\sin^2\beta_4} + \frac{\sqrt{\overline{H}_b^2 - \sin^2\beta_4} - \sin\beta_4}{2\sin\beta_4} + \left(\frac{\sqrt{\overline{H}_b^2 - \sin^2\beta_4} - \sin\beta_4}{2\sin\beta_4}\right)\left(\frac{\overline{H}_b^2}{2\sin^2\beta_4}\right)\left(\frac{\pi}{2} - 2\alpha\right) \tag{B.2.17}$$

By solving Equation (B.2.17), $H_b$ can be obtained. Thus the energy difference is

$$\Delta\overline{E} = 2r\,\overline{R}_4\left[1 - \overline{H}_4\left(\frac{\pi}{2} - 2\alpha\right)\right] - \frac{2\pi(1 - \sin\alpha)}{\cos^2\alpha} - \cos\alpha\left[\pi\left(4\overline{H}_b - \overline{H}_b^2\right) - 2\pi\left\{\overline{H}_1 + \frac{1 - \sin\alpha}{\cos^2\alpha} - \frac{1}{\cos\alpha} + \frac{2}{3}\frac{\left[1 - \sin^3\alpha\right]}{\cos^3\alpha}\right\} - \pi\right] \tag{B.2.18}$$